VOLUME 86 NO. EM5
OCTOBER 1960

JOURNAL of the

Engineering Mechanics Division

PROCEEDINGS OF THE
AMERICAN SOCIETY
OF CIVIL ENGINEERS

Journal of the

ENGINEERING MECHANICS DIVISION

Proceedings of the American Society of Civil Engineers

ENGINEERING MECHANICS DIVISION
EXECUTIVE COMMITTEE
Dan H. Pletta, Chairman; Egor P. Popov, Vice Chairman; Bruce G. Johnston
Merit P. White; Edward Wenk, Jr., Secretary

COMMITTEE ON PUBLICATIONS
Egor P. Popov, Chairman; Hans H. Bleich; Jack E. Cermak;
Albert G. H. Deitz; William J. Hall; John D. Haltiwanger; Ernest F. Masur;
Herbert S. Suer

CONTENTS

October, 1960

Papers

	Page
Restrained Columns by Morris Ojalvo	1
Wind Stresses in Domes by P. Gondikas and M. G. Salvadori	13
Bending of Plates on a Viscoelastic Foundation by K. S. Pister and M. L. Williams	31
Electrical Energy Analogs of Vibrating Beams by Frederick L. Ryder	45
Elastic-Plastic Analysis of Transversely Loaded Plates by John F. Brotchie	57
Dynamic Response of Beams Traversed by Two-Axle Loads by Robert K. Wen	91
Bearing Capacity of Floating Ice Sheets by G. G. Meyerhof	113
Membrane Stresses in Hyperboloid Shells of Revolution by Placido Cicala	147

(over)

Copyright 1960 by the American Society of Civil Engineers.

Page

DISCUSSION

Behavior of Structures During Earthquakes, by George W. Housner. (October, 1959. Prior discussion: April, June, 1960. Discussion closed.)
by George W. Housner (closure) 163

Behavior of Buckled Rectangular Plates, by Manuel Stein. (April, 1960. Prior discussion: None. Discussion closed.)
by Morris Ojalvo and Ahmet Cakmak 169

Commentary on Plastic Design in Steel: Connections: Progress Report No. 6 of the Joint WRC-ASCE Committee on Plasticity Related to Design. (April, 1960. Prior discussion: None. Discussion closed.)
by Hashim H. Hamzawi 171

Commentary on Plastic Design in Steel: Deflections: Progress Report No. 7 of the Joint WRC-ASCE Committee on Plasticity Related to Design. (April, 1960. Prior discussion: None. Discussion closed.)
by R. J. P. Garden 175

Behavior of Viscoelastic Plates in Bending, by George E. Mase. (June, 1960. Prior discussion: None. Discussion closes November 1, 1960.)
by O. C. Zienkiewicz 181

Errata 185

Journal of the
ENGINEERING MECHANICS DIVISION
Proceedings of the American Society of Civil Engineers

RESTRAINED COLUMNS

By Morris Ojalvo,[1] M. ASCE

SYNOPSIS

A method for determining the carrying capacity of restrained columns of constant cross section is described. The type of column failure considered is that due to bending about one of the principal axes of the cross section. The plane of bending is also the plane of the thrust, applied moments, and the restraining moments. The method is applicable when the loads are applied to the columns with equal or unequal end eccentricities and can be used for cases where the restraining moments are not linear functions of the end rotations of the column. It also takes into account the inelastic action of the column and thus leads to a solution of the true ultimate carrying capacity of such members. It is shown how convenient nomographs may be developed for columns with one end hinged and for columns with equal applied end moments and with equal rotational restraints at the ends. The availability of nomographs for the latter two cases reduces the effort involved in designing restrained columns to a point where such a design would be appropriate for design office use.

INTRODUCTION

Columns in framed structures are not, as a rule, pin-ended. They are connected at their ends to beams, tension members, and other columns that provide translational and rotational restraints. The beams of an ordinary tier building, for example, serve primarily to carry the loads to the columns. In doing so they

Note.—Discussion open until March 1, 1961. To extend the closing date one month, a written request must be filed with the Executive Secretary, ASCE. This paper is part of the copyrighted Journal of the Engineering Mechanics Division, Proceedings of the American Society of Civil Engineers, Vol. 86, No. EM 5, October, 1960.

[1] Assoc. Prof., Dept. of Civil Engineering, Ohio State Univ., Columbus, Ohio.

also transmit bending moments because of the rigidity of the beam-to-column connections. These bending moments, together with the axial loads in the columns, cause the columns to flex from the very beginning of loading. Eventually if the axial load in a column becomes large enough, the sign of the bending moments at the column ends may change and the beams take over the role of restraining the end rotations of the column and thereby limit its deflections. It is thus seen that the restrained column must be studied in order to arrive at a more accurate estimate of the strength of columns in a continuous structure. Such knowledge is necessary in order that further progress may be made in the application of plastic design to multi-story frames.

Various aspects of the restrained column problem have been investigated by E. Chwalla,[2] P. P. Bijlaard, G. P. Fisher, and G. Winter,[3] T. C. Kavanagh,[4] Bijlaard,[5] J. F. Baker, M. R. Horne, and J. W. Roderick,[6,7], and J. S. Ellis.[8]

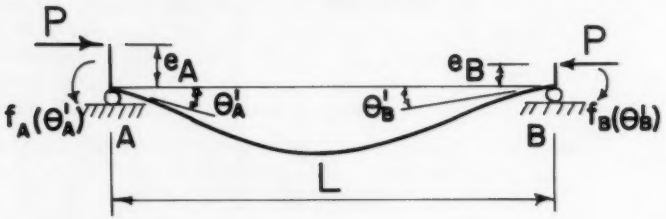

FIG. 1

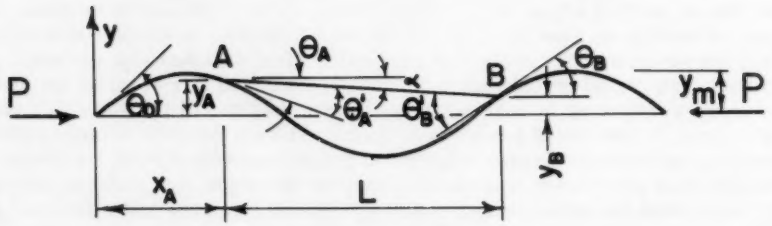

FIG. 2

---

2 "Aussermittig Gedruckte Baustahlstabe mit Eingespannten Enden und verschieden grossen Angriffshebeln," by E. Chwalla, Die Bautechnik, 10. Jahrgang, 1937, pp. 49 and 57.

3 "Eccentrically Loaded End-Restrained Columns," by P. P. Bijlaard, G. P. Fisher, and G. Winter, Transactions, ASCE, Vol. 120, 1955.

4 "Rational Simplification for the Buckling Length of Columns," by T. C. Kavanagh, Proceedings of the Seventh Tech. Session, Column Research Council of the Engrg. Foundation, 1957.

5 "Buckling of Columns with Equal and Unequal End Eccentricities and Equal and Unequal End Restraints," by P. P. Bijlaard, Proceedings of the Second U. S. Natl. Congress of Applied Mechanics,,1954.

6 "The Behavior of Continuous Stanchions," by J. F. Baker, M. R. Horne, and J. W. Roderick, Proceedings, Royal Soc., Vol. 198, 1949.

7 "The Elastic-Plastic Theory of Compression Members," by M. R. Horne, Journal of the Mechanics and Physics of Solids, Vol. 4, 1956.

8 "Plastic Behaviour of Compression Members," by J. S. Ellis, Journal of the Mechanics and Physics of Solids, Vol. 6, 1958.

The present work systematizes the approach used by Chwalla and extends its applicability to cases where the rotational restraints at the ends of the column are not elastic.

The type of column that will be considered is illustrated in Fig. 1. The ends are fully restrained against translation. The loads consist of the forces P applied with eccentricities e_A and e_B. The ends of the column are also subject to restraining moments that are denoted by $f_A(\theta'_A)$ and $f_B(\theta'_B)$ to indicate their dependency upon end rotations θ'_A and θ'_B. It will be assumed that the stress-strain diagram and the column cross section are specified so that moment-curvature curves at several values of the average column stress may be constructed by the methods described elsewhere.[9, 10, 11, 12] It will be further assumed that the shearing force is small compared to the axial force in a column.

Notation.—The letter symbols adopted for use in this paper are defined where they first appear, in the illustrations or in the text, and are arranged alphabetically, for convenience of reference, in the Appendix.

THEORY

A column in equilibrium with end moments and end rotations, as shown in Fig. 1, may be thought of as a segment of a column deflection curve such as the one shown[5] in Fig. 2. A column deflection curve is defined as the shape that a compressed member will take when the axial load and its maximum deflection y_m are specified. If unloading of the fibers stressed into the plastic range is ignored, as will be the case in the present analysis, then the moment-curvature relationship will be such that for every moment there will be but one value of the curvature.[12] For this condition the shape and wave length of a column deflection curve will be unique. It also follows, from the preceeding, that the column deflection curve is symmetrical about a line perpendicular to the thrust line and passing through a point of maximum deflection on the curve. This means that the entire column deflection curve may be constructed from a known quarter wave length.

A particular column deflection curve for a given section may also be identified by the load P and θ_o (the roation at y = O) or the load P and the curvature at the point where the deflection is a maximum. In this analysis it was found convenient to use θ_o to identify the column deflection curve. The column deflection curve for a given value of θ_o may be constructed with the aid of the appropriate moment-curvature curve by a numerical integration procedure described by S. Timoshenko.[11] Computations were carried out for an 8WF31 rolled steel column. When the stresses were entirely in the elastic range, checks with theoretically computed column deflection curves showed that errors in the wave length and in the maximum deflection were of the order of 0.1%. The length of increments used in the numerical integration was 13.88 in., or four times the radius of gyration about the axis of bending.

---

9 "Untersuchungen uber Knickfestigkeit," by T. v. Karman, Forschungsarbeiten, No. 81, Berlin, 1910.

10 "Theorie des Aussermittig Gedruckten Stabes aus Baustahl," by E. Chwalla, Die Bautechnik, 7. Jahrgang, 1934, pp. 161, 173, and 180.

11 "Theory of Elastic Stability," by S. Timoshenko, McGraw-Hill Book Co., New York, 1936.

12 "Plastic Deformation of Wide-Flange Beam Columns," by R. L. Ketter, E. L. Kaminsky, and L. S. Beedle, Transactions, ASCE, Vol. 120, 1955.

The solution to an actual restrained column problem involves the quantities e_A, e_B, P, L, $f_A(\theta)$, $f_B(\theta)$, the stress-strain diagram of the material, and the shape of the cross section. The approach consists of fixing all but one of the variables and then examining a number of columns that satisfy the conditions of equilibrium so as to arrive at the one that yields the greatest value for the open parameter. Since each of these columns may be considered as a segment of a column deflection curve, it is necessary, as a preliminary step, to compute several column deflection curves for each value of P.

GENERAL CASE

In considering the solution of the stability of Fig. 1, the eccentricity e_A will be the variable and L, e_A/e_B, $f_B(\theta')$, $f_A(\theta')$, and P will be specified. Each column deflection curve available from the previous computations for the given load and the given column cross section will be examined to determine the location of the segment of length L which makes e_A/e_B equal to the prescribed value. Fig. 2 illustrates the procedure for the location of the correct segment on a column deflection curve. End A is located at a trial distance x_A from the end of a column deflection curve and end B is found on the curve at a horizontal distance L from A. The angles θ_A and θ_B are known at any section of the column deflection curve from the numerical integration used to determine the curve. The angles θ'_A, θ'_B and the eccentricities e_A, e_B are given by the following equations:

$$\theta'_A = \theta_A - \alpha \quad \ldots\ldots\ldots\ldots\ldots\ldots (1)$$

$$\theta'_B = \theta_B + \alpha \quad \ldots\ldots\ldots\ldots\ldots\ldots (2)$$

$$\alpha = \frac{y_A - y_B}{L} \quad \ldots\ldots\ldots\ldots\ldots\ldots (3)$$

$$e_A = \frac{f_A(\theta'_A) - P\,y_A}{P} \quad \ldots\ldots\ldots\ldots\ldots\ldots (4)$$

$$e_B = \frac{f_B(\theta'_B) - P\,y_B}{P} \quad \ldots\ldots\ldots\ldots\ldots\ldots (5)$$

and

$$e_A/e_B = \frac{f_A(\theta'_A) - P\,y_A}{f_B(\theta'_B) - P\,y_B} \quad \ldots\ldots\ldots\ldots\ldots\ldots (6)$$

Values for θ'_A, θ'_B, α, y_A, y_B, e_A and e_B are positive when they are as shown in Fig. 2.

Eqs. 4 and 5 stem from the requirement that at A and B the external moment must equal the internal moment. The internal moments at A and B are equal to P y_A and P y_B respectively, as can be seen by a consideration of the column deflection curve (Fig. 2). By plotting e_A/e_B versus x_A as in Fig. 3, it is possible to arrive, graphically, at a value of x_A which locates the segment of the

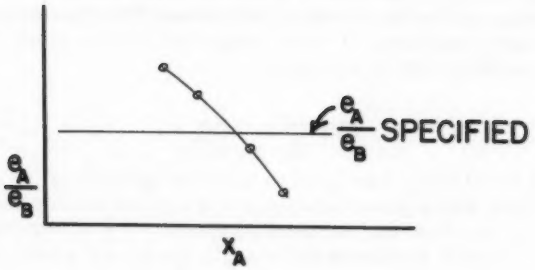

FIG. 3

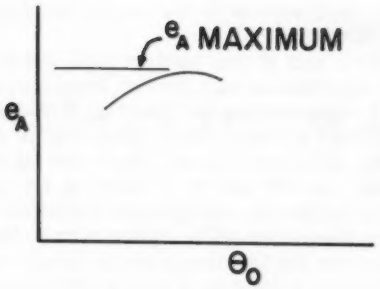

FIG. 4

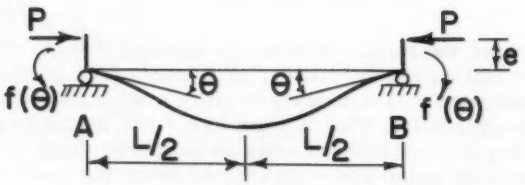

FIG. 5

column deflection curve representing an equilibrium shape for the specified ratio of eccentricities.

This segment yields a certain value for e_A. When values of e_A are plotted against the end rotation of the column deflection curve that gave rise to the value of e_A, a curve such as the one in Fig. 4 is obtained. This curve is characteristic of column stability problems.[11] The horizontal tangent gives the maximum value of e_A consistent with equilibrium.

SPECIAL CASE - I

When e_A is equal to e_B and $f_A(\theta)$ is equal to $f_B(\theta)$ (Fig. 5) the solution is greatly simplified. For a given value of P and a given column deflection curve identified by θ_o, the slope and the bending moment P y, are known at any distance from the point of maximum deflection. The three quantities are plotted for a number of column deflection curves to give curves that are shown diagrammatically in the nomograph of Fig. 6. Each column deflection curve supplies one pair of curves for the nomograph. In the upper portion the internal moment is plotted against the slope θ at the corresponding point of the column deflection curve. In the lower portion, the distance L/2 is plotted against θ. The distance L/2 is measured from the low point on the column deflection curve to the point where the slope is measured.

For this case, e, $f(\theta)$, and P may be specified and the maximum column length consistent with equilibrium can then be found. Equilibrium at the ends of the column in Fig. 5 requires that the internal moment of the column equal the restraining moment $f(\theta)$ minus the applied moment, P e. In the upper portion of the nomograph of Fig. 6, curve A is drawn for the equation $M = f(\theta) - P e$. The intersection of this line with the M-θ curve of a column deflection curve gives the value of θ for which the equilibrium condition will be satisfied. A vertical line is carried down from each intersection to the corresponding L/2 versus θ curve. This gives the half length of the column in equilibrium for an end rotation of θ. By joining a number of points in the lower diagram, curve B is obtained. The point of horizontal tangency on this curve gives the half-length of the longest column which will support the load P at the given eccentricity.

SPECIAL CASE - II

When one end of the column is simply supported and the other end is restrained (Fig. 7 (a)) an equally convenient nomograph is possible. Instead of using θ as an abscissa it is necessary to plot θ' which corresponds to the rotation at the restrained end. This is equal to $\theta - y/L$ as can be seen from Fig. 7 (b). The bending moment is determined as in Special Case-I while the length is measured from the point where the column deflection curve has a zero deflection and therefore a zero bending moment. This point of zero bending moment corresponds to the hinged end of the column. The equilibrium of moments at the restrained end requires:

$$M = f_B(\theta'_B) - P e_B \quad \ldots\ldots\ldots\ldots\ldots\ldots (7)$$

A nomograph for Special Case-II was constructed for an 8WF31 rolled steel column with a yield stress of 33,000 psi and a maximum residual stress of 9,900

psi. The residual stress pattern assumed was identical to the one assumed by T. V. Galambos and R. L. Ketter.[13] This nomograph is shown in Fig. 8. The length and moment ordinates were non-dimensionalized so that the nomograph could be used with little error for all wide flange sections.[13] Fig. 7 of the Galambos-Ketter paper gives values for the collapse load of beam columns. These

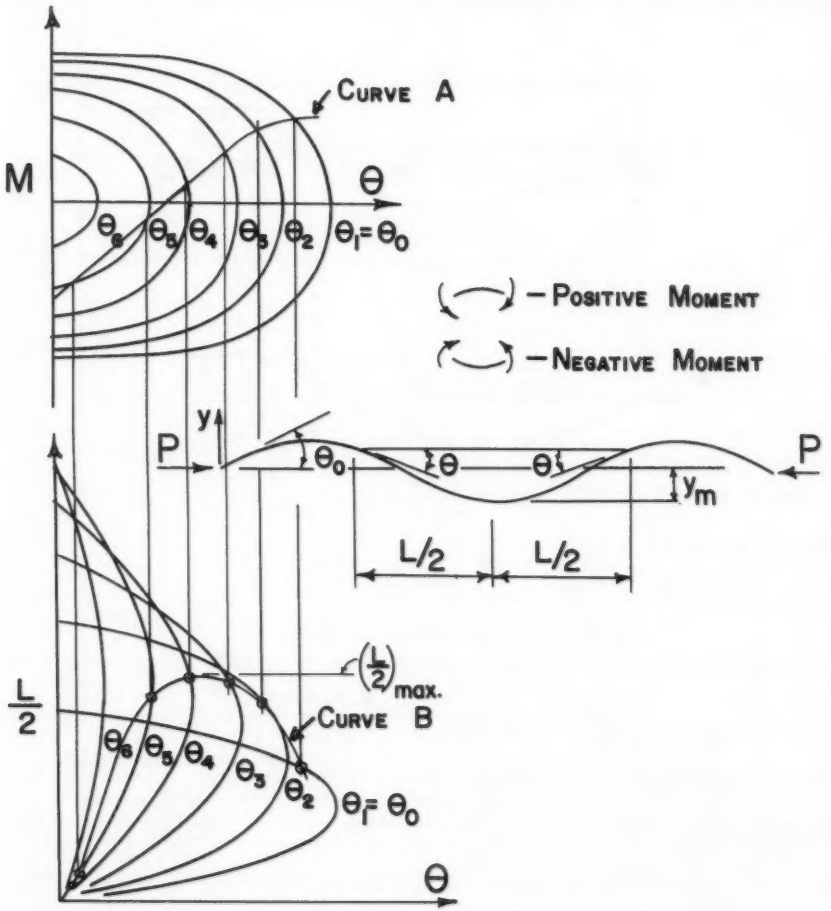

FIG. 6

columns correspond to those of Special Case-II when the restraining function $f_B(\theta')$ is identically equal to zero. For this case $M_o = P\, e_B$. The construction

13 "Columns under Combined Bending and Thrust," by T. V. Galambos and R. L. Ketter, Proceedings, ASCE, Vol. 85, No. EM 2, April, 1959.

in Fig. 8 shows how M_o may be obtained when the slenderness ratio of the column is specified. Table I shows a comparison of the results obtained by this method with those of Galambos and Ketter.[13] As can be seen, both methods give substantially the same results.

For the more general case when a restraining moment exists at B, the quantities e_B, $f_B(\theta)$, and P may be taken as the independent variables. The maximum length consistent with equilibrium remains to be determined. The use of

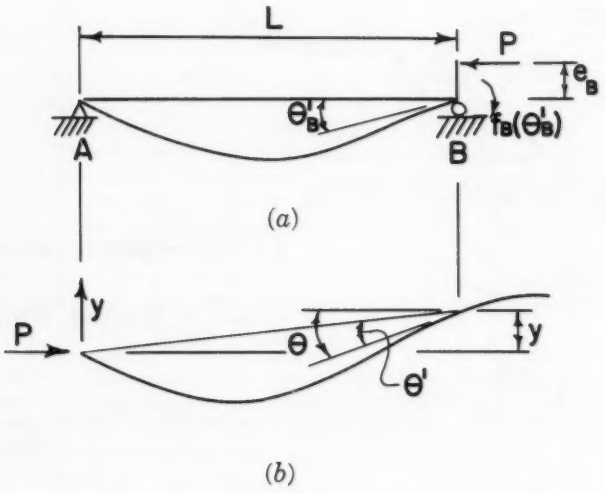

FIG. 7

TABLE 1.—COMPARISON OF RESULTS

L/r	$P/P_y = 0.3$	
	M_o/M_p	M_o/M_p from Galambos-Ketter
120	0.49	0.49
100	0.63	0.65
80	0.73	0.74
60	0.76	0.78

nomographs for this case follows the description given for the case of equal end eccentricities and end restraints.

ACKNOWLEDGMENTS

This study is part of the general investigation entitled, "Welded Continuous Frames and Their Components" currently being carried out at Fritz Engineering Laboratory, Lehigh University, under the direction of Lynn S. Beedle, F.

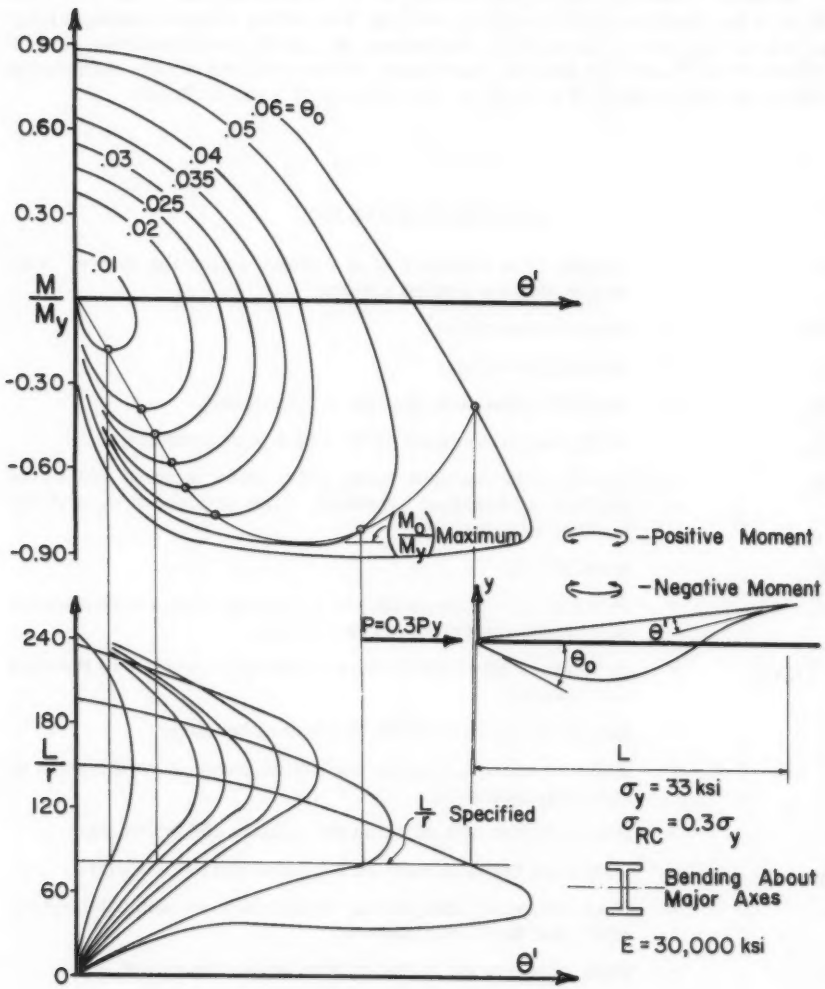
0.90
0.60
0.30
-0.30
-0.60
-0.90
M/My
θ'
.06=θo
.05
.04
.035
.03
.025
.02
.01
(Mo/My) Maximum
⟷ -Positive Moment
⟷ -Negative Moment
P=0.3Py
y
θ'1
θo
240
180
120
60
0
L/r
L/r Specified
L
σy = 33 ksi
σRC = 0.3σy
Bending About Major Axes
E = 30,000 ksi

FIG. 8

ASCE. This investigation is sponsored jointly by the Welding Research Council and the Department of the Navy with funds furnished by the American Iron and Steel Institute, American Institute of Steel Construction, Office of Naval Research, Bureau of Ships, and Bureau of Yards and Docks.

William J. Eney, F. ASCE, is Director of Fritz Engineering Laboratory and Head of the Department of Civil Engineering. The author wishes to acknowledge gratefully the aid of Theodore V. Galambos, M. ASCE, in translating several references[2,10] and the helpful comments and suggestions on the manuscript offered by Akira Nitta, Theodore V. Galambos, and Lynn S. Beedle.

APPENDIX. NOTATION

L	=	Length of a segment of a column deflection curve. Also length of a restrained column;
L/r	=	Slenderness ratio;
M	=	Bending moment;
M_o	=	Applied moment at the end of a member;
M_p	=	Fully plastic moment value under pure moment;
M_y	=	Initial yield moment value under pure moment and in the absence of residual stresses. (The product of σ_y and the section modulus);
P	=	Axial thrust;
P_y	=	Axial thrust corresponding to a constant compressive stress of σ_y over the entire cross section;
e, e_A, e_B	=	Eccentricities at which the axial thrust is applied to the ends of a column;
r	=	Radius of gyration about the axis of bending;
x	=	Distance along a column deflection curve from the point of zero displacement;
y	=	Displacement of a point on the column deflection curve;
y_m	=	Maximum displacement on a column deflection curve;
α	=	Angle between a line joining two points on a column deflection curve and the line of thrust;
θ	=	Slope of a tangent to the column deflection curve;
θ_o	=	Slope of the tangent to a column deflection curve where its deflection is zero;
θ'	=	Angle between a line joining two points on a column deflection curve and the tangent to the column deflection curve at the end point of the line;
σ_y	=	Yield stress (assumed to be 33 ksi for A7 steel);

σ_{RC} = Maximum compressive residual stress; and

$f(\theta)$, $f(\theta')$ = Expressions giving the restraining moment at the ends of a column as a function of the end rotation of the column.

Journal of the
ENGINEERING MECHANICS DIVISION
Proceedings of the American Society of Civil Engineers

WIND STRESSES IN DOMES

By P. Gondikas,[1] J. M. ASCE, and M. G. Salvadori,[2] F. ASCE

SYNOPSIS

The bending stresses due to antisymmetrical wind pressures in a hemispherical dome elastically built-in into a cylinder are determined by means of a Geckeler approach extended to non-symmetrical loads. The simple form of the results allows their use by the designer. A numerical comparison with the asymptotic solution of Schwerin indicates the satisfactory accuracy of this approximate solution for all cases of practical interest. The methods used in the solution of the present problem are easily extended to spherical sector shells stiffened by rings at the boundary and to other types of non-symmetrical loads.

INTRODUCTION

The membrane stresses in spherical domes and circular cylinders due to antisymmetrical wind forces are well known,[3] or can easily be computed from the equilibrium equations of membrane theory.[4] The corresponding displacements are easily obtained by integration of the differential equations of membrane theory,[5] but when the dome is built-in into the cylinder, the membrane displacements do not allow a complete statement of the continuity between dome

Note.—Discussion open until March 1, 1961. To extend the closing date one month, a written request must be filed with the Executive Secretary, ASCE. This paper is part of the copyrighted Journal of the Engineering Mechanics Division, Proceedings of the American Society of Civil Engineers, Vol. 86, No. EM 5, October, 1960.

[1] Parther, Gondikas, and Righidis, Athens, Greece.

[2] Prof. of Civ. Engrg., Columbia Univ., and Assoc., Paul Weidlinger, Cons. Engr., New York, N. Y.

[3] "Theory of Plates and Shells," by S. Timoshenko, McGraw-Hill Book Co., New York, 1940, p. 377.

[4] Ibid, pp. 373-374, and p. 384.

[5] "Statik und Dynamik der Schalen," by W. Flügge, Springer, Berlin, 1947, p. 147 and pp. 73, 74.

and cylinder at their intersection for lack of a suitable number of arbitrary constants. Thus, bending disturbances must be added at the intersection of dome and cylinder, requiring for their rigorous evaluation the solution of the bending differential equations of the cylinder and dome. This solution has been obtained in asymptotic form[6,7] and requires lengthy calculations. The only problem evaluated by this procedure known in literature is the case of a hemispherical dome rigidly built-in around its edge.[8]

For the case of symmetrically loaded and supported domes, however, J. W. Geckeler has shown[9] that whenever the thickness to radius ratio is small (less than 1/50), satisfactory approximate solutions can be obtained by substituting for the dome the tangent cone (or cylinder) and by evaluating the bending stresses in the cone. The symmetrical case is thus reduced to the elementary problem of beams on elastic foundations.[10]

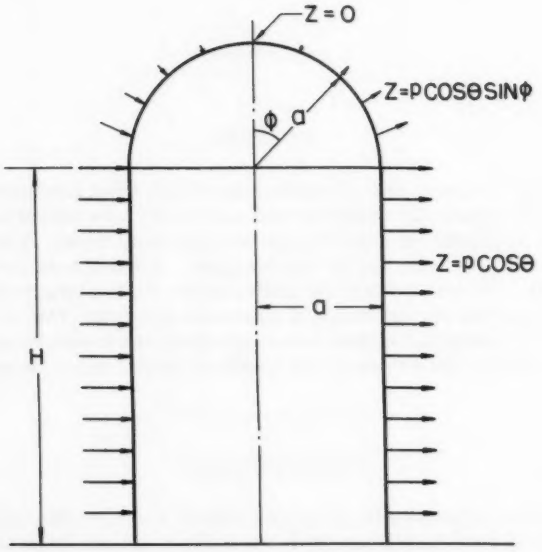

FIG. 1.—WIND FORCES

The same approach may be applied to the antisymmetrical case of wind forces. The membrane displacements at the intersection of cylinder and dome due to wind forces are first evaluated. The complete differential equations for

6 "Theory of Plates and Shells," by S. Timoshenko, McGraw-Hill Book Co., New York, 1940, p. 467.

7 "Statik und Dynamik der Schalen," by W. Flügge, Springer, Berlin, 1947, p. 180.

8 "Uber Spannungen in Symmetrisch und Unsymmetrisch Belasteten Kugelschalen (Kuppeln) insbesondere bei Belastung durch Winddruck," by E. Schwerin, Armierter Beton, 1919.

9 "Uber die Fiestigkeit Achsensymmetrischer Schalen," by J. W. Geckeler, Forschungsarbeiten auf dem Gebiete des Eisenbetons, Berlin, 1921, Heft 24.

10 "Beams on Elastic Foundations," by M. Hetenyi, The Univ. of Michigan Press, 1946, p. 163.

the anti-symmetrical displacements in the unloaded, semi-infinite cylinder are then solved, and their rigid body membrane and bending components analyzed. The bending displacements are expressed in terms of the transverse shear and bending moments at the cylinder boundary. Continuity between cylinder and dome is finally restored by means of boundary shears and moments, using cylindrical theory for the dome as well as for the cylinder, and the values of the

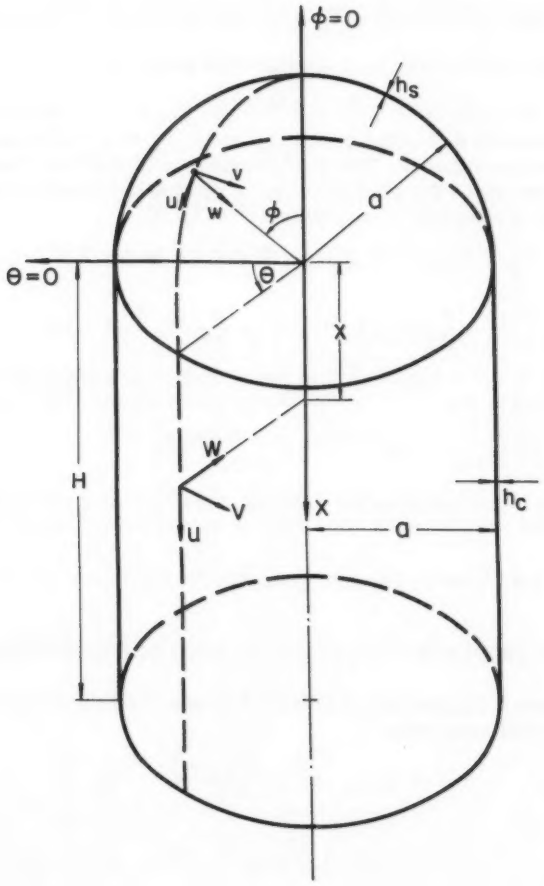

FIG. 2

shears and moments at the dome and cylinder boundary are thus explicitly evaluated in finite terms. The approximate solution obtained by this procedure is accurate for small values of the thickness to radius ratio. A comparison with the fairly thick dome (h/a - 1/40) used in the example of E. Schwerin[8] indicates

that the accuracy of the present solution is sufficient in all practical cases encountered in construction, where thickness to radius ratios are of the order of 1/100 or less. The method used to solve the present problem can be extended to evaluate bending stresses in spherical domes under other types of antisymmetrical loads, with opening angles $\pi/4 \leq \phi_0 \leq \pi/2$ and taking into account the effect of a stiffening ring at the dome base.

MEMBRANE STRESSES DUE TO WIND IN CYLINDRICAL SHELLS

With the symbols of Fig. 1, a normal wind pressure:

$$Z = p \cos \theta \quad \ldots\ldots\ldots\ldots\ldots\ldots (1)$$

varying sinusoidally and with a maximum value of p at $\theta = 0$, is assumed to act on a semi-infinite cylinder. The wind pressure p is one-half the pressure required by codes, since Eq. 1 indicates that a suction of intensity p acts at $\theta = \pi$. The equations of membrane equilibrium[11] (Fig. 2).

$$N'_{\xi} + N'_{\xi\theta} = X; \; N'_{\xi\theta} + N^{\cdot}_{\theta} = Y; \; N_{\theta} = -Z\,a \quad \ldots\ldots\ldots (2)$$

where:

$$(\ldots)' = \frac{\partial}{\partial \xi}(\ldots); \; (\ldots)^{\cdot} = \frac{\partial}{\partial \theta}(\ldots), \; \xi = x/a \quad \ldots\ldots\ldots (3)$$

integrated for X = Y = 0 and the Z of Eq. 1, under the assumption of a traction less boundary ($\xi = 0$);

$$N_{\xi}\Big]_{\xi=0} = N_{O\xi} = 0; \; N_{\xi\theta}\Big]_{\xi=0} = N_{O\xi\theta} = 0 \quad \ldots\ldots\ldots\ldots (4)$$

(the subscript zero indicates the value of a quantity at $\xi = 0$) give the membrane stresses:

$$N_{\xi} = \frac{1}{2} p\,a\,\xi^2 \cos\theta; \; N_{\xi\theta} = -p\,a\,\xi \sin\theta; \; N_{\theta} = -p\,a\cos\theta \quad \ldots\ldots (5)$$

MEMBRANE DISPLACEMENTS DUE TO WIND IN CYLINDRICAL SHELLS

The membrane displacements (Fig. 2) are related to the membrane stresses by the differential equations:[12]

$$u' + \nu v^{\cdot} - \nu w = \frac{a(1-\nu^2)}{E\,h_c} N_{\xi} \quad \ldots\ldots\ldots (6a)$$

$$u^{\cdot} - v' = \frac{2a(1+\nu)}{E\,h_c} N_{\xi\theta} \quad \ldots\ldots\ldots\ldots (6b)$$

and

$$v^{\cdot} - w + \nu u' = \frac{a(1-\nu^2)}{E\,h_c} N_{\theta} \quad \ldots\ldots\ldots\ldots (6c)$$

in which h_c is the cylinder thickness and a its radius.

---

11 "Theory of Plates and Shells," by S. Timoshenko, McGraw-Hill Book Co., New York, 1940, p. 384.

12 "Statik und Dynamik der Schalen," by W. Flügge, Springer, Berlin, 1957, p. 147, Eqs. 96(a-h) with K = 0.

Assuming, in view of the load of Eq. 2:

$$N_\xi = \overline{N}_\xi \cos\theta \quad \ldots\ldots (7a)$$

$$N_{\xi\theta} = \overline{N}_{\xi\theta} \sin\theta \quad \ldots\ldots (7b)$$

$$N_\theta = \overline{N}_\theta \cos\theta \quad \ldots\ldots (7c)$$

$$u = \overline{u} \cos\theta \quad \ldots\ldots (7d)$$

$$v = \overline{v} \sin\theta \quad \ldots\ldots (7e)$$

and

$$w = \overline{w} \cos\theta \quad \ldots\ldots (7f)$$

where the amplitudes $\overline{N}, \ldots, \overline{u}, \ldots$ are functions of ξ only, Eqs. 5, 6, and 7 give:

$$\overline{u}' + \nu\,\overline{v} - \nu\,\overline{w} = P(1-\nu^2)\,\xi^2 \quad \ldots\ldots (8a)$$

$$\nu\,\overline{u}' + \overline{v} - \overline{w} = -2P(1-\nu^2)\,\xi \quad \ldots\ldots (8b)$$

and

$$-\overline{u} + \overline{v}' = -4P(1+\nu)\,\xi \quad \ldots\ldots (8c)$$

with:

$$P = \frac{p\,a^2}{2\,E\,h_c} \quad \ldots\ldots (9)$$

Integrating Eqs. 8 with the boundary conditions:

$$u_o = 0 \quad \ldots\ldots (10a)$$

and

$$w_o = 0 \quad \ldots\ldots (10b)$$

the membrane displacements within a rigid body displacement take the form:

$$u = P\,\xi\left(\frac{\xi^2}{3} + 2\nu\right)\cos\theta \quad \ldots\ldots (11a)$$

$$v = P\left[\frac{\xi^4}{12} - (2-\nu)\,\xi^2 - 2\right]\sin\theta \quad \ldots\ldots (11b)$$

$$w = P\xi^2\left(\frac{\xi^2}{12} - 2\right)\cos\theta \quad \ldots\ldots (11c)$$

and

$$w' = P\xi\left(\frac{\xi^2}{3} - 4\right)\cos\theta \quad \ldots\ldots (11d)$$

At the cylinder boundary ($\xi = 0$) Eqs. 5 and 11 give:

$$N_{o_\xi} = 0,\ N_{o_{\xi\theta}} = 0,\ N_{o\theta} = -p\,a\cos\theta \quad \ldots\ldots (12)$$

and

$$u_o = 0,\ v_o = 2P\sin\theta,\ w_o = 0,\ w_o' = 0 \quad \ldots\ldots (13)$$

MEMBRANE STRESSES DUE TO WIND IN SPHERICAL DOME

With the symbols of Fig. 1, a normal wind pressure;

$$Z = p\sin\phi\cos\theta \quad \ldots\ldots (14)$$

of maximum intensity p, induces in the dome the membrane stresses:[3]

$$N_\phi = -\frac{p\,a}{3}\,\frac{2\cos\phi - 3\cos^2\phi + \cos^4\phi}{\sin^3\phi}\cos\theta \quad \ldots\ldots \quad (15a)$$

$$N_{\phi\theta} = -\frac{p\,a}{3}\,\frac{2-3\cos\phi + \cos^3\phi}{\sin^3\phi}\sin\theta \quad \ldots\ldots \quad (15b)$$

and

$$N_\theta = +\frac{p\,a}{3}\,\frac{-3 + 2\cos\phi + 3\cos^2\phi - 2\cos^4\phi}{\sin^3\phi}\cos\theta \quad \ldots\ldots \quad (15c)$$

At the boundary $(\phi - \pi/2)$ the membrane tractions are:

$$N_{o\phi} = 0,\ N_{o\theta\phi} = -\frac{2}{3}\,p\,a\sin\theta,\ N_{o\theta} = -\,p\,a\cos\theta \quad \ldots\ldots \quad (16)$$

The subscript zero indicates the value of a quantity at the dome boundary $\phi - \pi/2$. The membrane displacements in the dome are related to the membrane stresses by equations:[5]

$$u' - w = \frac{a}{E\,h_s}\left(N_\phi = \nu\,N_\theta\right) \quad \ldots\ldots \quad (17a)$$

$$v'\,\frac{1}{\sin\phi} + u\cot\phi - w = \frac{a}{E\,h_s}\left(N_\theta - \nu\,N_\phi\right) \quad \ldots\ldots \quad (17b)$$

and

$$v' - v\cot\phi + u'\,\frac{1}{\sin\phi} = \frac{2\,a(1+\nu)}{E\,h_s}\,N_{\theta\phi} \quad \ldots\ldots \quad (17c)$$

where:

$$(\ldots)' = \frac{\partial}{\partial\phi}(\ldots);\ (\ldots)^{\cdot} = \frac{\partial}{\partial\theta}(\ldots) \quad \ldots\ldots \quad (18)$$

Letting again:

$$u = \bar{u}\cos\theta \quad \ldots\ldots \quad (19a)$$

$$v = \bar{v}\sin\theta \quad \ldots\ldots \quad (19b)$$

$$w = \bar{w}\cos\theta \quad \ldots\ldots \quad (19c)$$

$$N_\phi = \bar{N}_\phi\cos\theta \quad \ldots\ldots \quad (19d)$$

$$N_{\phi\theta} = \bar{N}_{\phi\theta}\sin\theta \quad \ldots\ldots \quad (19e)$$

and

$$N_\theta = \bar{N}_\theta\cos\theta \quad \ldots\ldots \quad (19f)$$

where the amplitudes $\bar{u}, \ldots, \bar{N}_\phi, \ldots,$ are functions of ϕ only, the integration of Eqs. 17 with the condition that the displacements be finite at the top of the dome gives, within a rigid body displacement:

$$u = B\left[-\cos\phi\,\log(1+\cos\phi) + 1 + \cos\phi + \frac{1}{1+\cos\phi}\right]\cos\theta \quad \ldots\ldots \quad (20a)$$

$$v = B\left[\log(1+\cos\phi) - 2 - \frac{1}{1+\cos\phi}\right]\sin\theta \quad \ldots\ldots \quad (20b)$$

$$w = B\left[\sin\phi\,\log(1+\cos\phi) + \frac{1-2\nu}{1+\nu}\sin\phi - \frac{1-\cos\phi}{\sin\phi}\right]\cos\theta \quad \ldots\ldots \quad (20c)$$

and

$$w' = B\left[\cos\phi\,\log(1+\cos\phi) + \frac{2-\nu}{1+\nu}\cos\phi - 1 - \frac{1}{1+\cos\phi}\right]\cos\theta \quad \ldots\ldots \quad (20d)$$

where:

$$B = \frac{1+\nu}{3\,E\,h_s}\, p\,a^2 \quad \ldots\ldots\ldots\ldots\ldots \quad (21)$$

At the dome boundary ($\phi = \pi/2$) the displacements are:

$$u_o = 2\,B\cos\theta \quad \ldots\ldots\ldots\ldots\ldots \quad (22a)$$

$$v_o = 3\,B\sin\theta \quad \ldots\ldots\ldots\ldots\ldots \quad (22b)$$

$$w_o = \frac{3\,\nu}{1+\nu}\,B\cos\theta \quad \ldots\ldots\ldots\ldots\ldots \quad (22c)$$

and

$$w'_o = 2\,B\cos\theta \quad \ldots\ldots\ldots\ldots\ldots \quad (22d)$$

GENERAL ANALYSIS OF THE UNLOADED SEMI-INFINITE CYLINDER

Once boundary tractions and displacements are known from membrane analysis, a general state of stress must be superimposed on the unloaded cylinder in order to satisfy continuity boundary conditions. The bending stiffness of the shell must be considered in order to obtain meaningful results, but the bending stresses vanish rapidly away from the boundary, so that the general displacements may be taken in the form:

$$u = U\,e^{\mu\xi}\cos\theta \quad \ldots\ldots\ldots\ldots\ldots (23a)$$

$$v = V\,e^{\mu\xi}\sin\theta \quad \ldots\ldots\ldots\ldots\ldots \quad (23b)$$

and

$$w = W\,e^{\mu\xi}\cos\theta \quad \ldots\ldots\ldots\ldots\ldots \quad (23c)$$

where the amplitudes U, V, W are constants.

Flügge has shown[13] that if the displacements of Eqs. 23 are substituted in the corresponding homogeneous differential equations of equilibrium:

$$u'' + \frac{1-\nu}{2}\ddot{u} + \frac{1+\nu}{2}\dot{v}' - \nu\,w' + k_c\left(\frac{1-\nu}{2}\ddot{u} + w''' - \frac{1-\nu}{2}\ddot{w}'\right) = 0 \ldots\ldots \quad (24a)$$

$$-\frac{1+\nu}{2}\dot{u}' - \ddot{v} - \frac{1-\nu}{2}v'' + \dot{w} + k_c\left(-\frac{3(1-\nu)}{2}v'' - \frac{3-\nu}{2}\dot{w}''\right) = 0 \ldots \quad (24b)$$

and

$$\nu u' + \dot{v} - w + k_c\left(\frac{1-\nu}{2}\ddot{u}' - u''' - \frac{3-\nu}{3}\dot{v}'' - w'''' - 2\ddot{w}'' - \ddot{\ddot{w}} - 2\ddot{w} - w\right) = 0 \ldots \quad (24c)$$

and the determinant of the resulting algebraic equations in U, V, W is set equal to zero, the 8th degree determinantal equation for μ splits into the following two 4th degree equations:

$$I_1\,\mu^4 + I_2\,\mu^2 + I_3 = 0 \ldots\ldots\ldots\ldots\ldots \quad (25a)$$

and

$$\mu^4 = 0 \quad \ldots\ldots\ldots\ldots\ldots \quad (25b)$$

---

13 "Statik und Dynamik der Schalen," by W. Flügge, Springer, Berlin, 1957, pp. 141–156.

The coefficients I of Eq. 25a are polynomials in the thickness ratio parameter:

$$k_c = \frac{1}{12}\left(\frac{h_c}{a}\right)^2 \quad \ldots\ldots\ldots\ldots\ldots\ldots \quad (26)$$

Bending Terms of General Solution.—The asymptotic solution of Eqs. 24 for small values of $k_c (k_c \ll 1)$[14] shows that satisfactory approximations to the

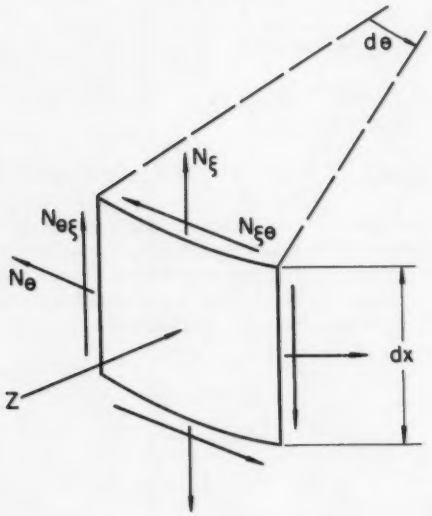

FIG. 3

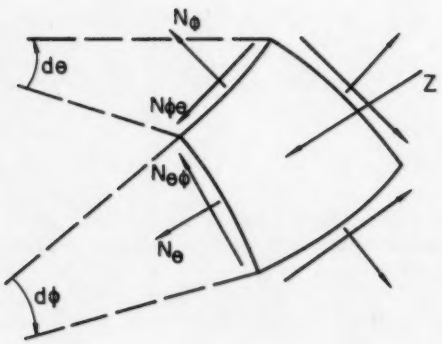

FIG. 4

14 "Vibrations of Ring-Stiffened Cylindrical Shells," Contract No. NR 266-08, Tech. Report No. 13, Columbia Univ., 1955.

roots of Eq. 25a are given by:

$$\mu_{1,2} = \beta_c (1 \pm i); \; \mu_{3,4} = \beta_c (-1 \pm i) \quad \ldots\ldots\ldots\ldots \quad (27)$$

where:

$$\beta_c = \left(\frac{1 - \nu^2}{4 k_c} \right)^{1/4} \quad \ldots\ldots\ldots\ldots\ldots \quad (28)$$

and that the corresponding displacements amplitude ratios are:

$$\frac{U}{W} = \frac{\nu}{\mu} \quad \ldots\ldots\ldots\ldots\ldots\ldots \quad (29a)$$

and

$$\frac{V}{W} = -\frac{2 + \nu}{\mu^2} \quad \ldots\ldots\ldots\ldots\ldots\ldots \quad (29b)$$

The displacements corresponding to the roots $\mu_{1,2}$ decrease rapidly away from the cylinder base, while those corresponding to $\mu_{3,4}$ decrease rapidly away from the cylinder top ($\xi = 0$). If the ratio of cylinder height H to radius a is large and the cylinder is thin, as assumed here, so that:

$$\frac{H}{a} > \sqrt[5]{\frac{h_c}{a}} \quad \ldots\ldots\ldots\ldots\ldots\ldots \quad (30)$$

it can be shown[14] that the bending disturbances at one of the cylinder ends are not felt at the other, so that only the solutions corresponding to the roots $\mu_{3,4}$ need be considered to evaluate bending disturbances in the neighborhood of the cylinder top. By Eqs. 23, 27, and 29, these displacements become:

$$u = \frac{\nu}{2 \beta_c} e^{-\beta_c \xi} \left[-(A_1 + A_2) \cos \beta_c \xi + (A_1 - A_2) \sin \beta_c \xi \right] \cos \theta \ldots \quad (31a)$$

$$v = \frac{2 + \nu}{2 \mu_c^2} e^{-\beta_c \xi} \left[-A_2 \cos \beta_c \xi + A_1 \sin \beta_c \xi \right] \sin \theta \ldots\ldots \quad (31b)$$

$$w = e^{-\beta_c \xi} \left[A_1 \cos \beta_c \xi + A_2 \sin \beta_c \xi \right] \cos \theta \ldots\ldots\ldots \quad (31c)$$

and

$$w' = \beta_c e^{-\beta_c \xi} \left[(A_2 - A_1) \cos \beta_c \xi - (A_1 + A_2) \sin \beta_c \xi \right] \cos \theta \ldots \quad (31d)$$

in which A_1, A_2 are arbitrary constants of integration.
At the cylinder top ($\xi = 0$):

$$u_o = -\frac{\nu}{2 \beta_c} (A_1 + A_2) \cos \theta \quad \ldots\ldots\ldots\ldots \quad (32a)$$

$$v_o = -\frac{2 + \nu}{2 \beta_c^2} A_2 \sin \theta \quad \ldots\ldots\ldots\ldots\ldots \quad (32b)$$

and

$$w_o = A_1 \cos \theta \quad \ldots\ldots\ldots\ldots\ldots\ldots\ldots \quad (32c)$$

$$w'_o = \beta_c (A_2 - A_1) \cos \theta \quad \ldots\ldots\ldots\ldots\ldots \quad (32d)$$

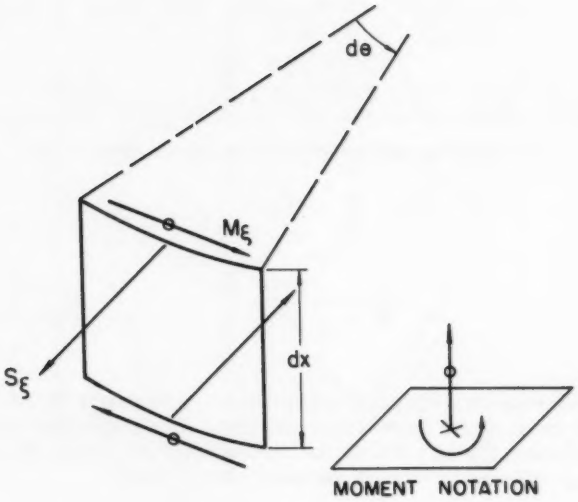

FIG. 5

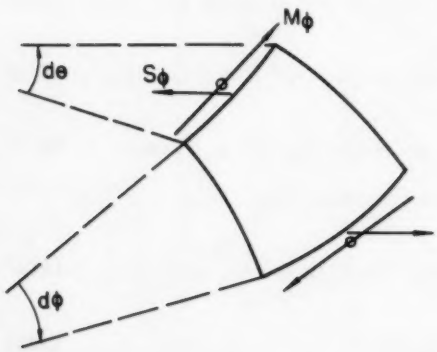

FIG. 6

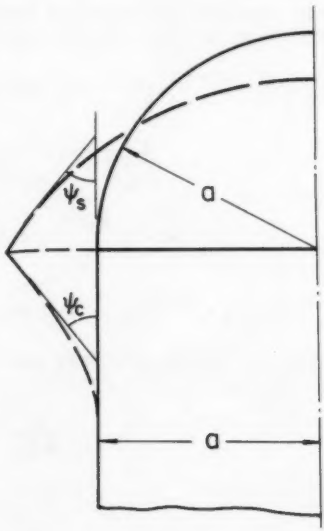

FIG. 7

The transverse equivalent shear

$$S_\xi = Q_\xi + \frac{1}{a} \frac{\partial M_{\xi\theta}}{\partial \theta} \quad \ldots\ldots\ldots\ldots\ldots\ldots \quad (33a)$$

(Q_ξ = shear, $M_{\xi\theta}$ = twisting moment) and bending moment M_ξ per unit of length (Fig. 5) are given in terms of the displacements by[15] (with the notation and sign convention of Fig. 3):

$$S_\xi = - \frac{\overline{E}\, h_c}{a} k_c \left[(2 - \nu)\dot{w}' + w''' + \frac{3 - \nu}{2} \dot{v}' - \frac{1 - \nu}{2} \ddot{u} + u'' \right] \quad \ldots \quad (33b)$$

and

$$M_\xi = - \overline{E}\, h_c\, k_c \left(w'' + \nu \ddot{w} + u' + \nu \dot{v} \right) \quad \ldots\ldots\ldots \quad (33c)$$

Substituting the displacements of Eqs. 31 in Eqs. 33 band c, and neglecting the lower powers of β_c in comparison with its higher powers (since $\beta_c \gg 1$ whenever $k_c \ll 1$), S_ξ and M_ξ become:

$$S_\xi = - \frac{E\, h_c}{2\, a\, \beta_c} e^{-\beta_c \xi} \left[(A_1 + A_2) \cos \beta_c \xi + (A_2 - A_1) \sin \beta_c \xi \right] \cos \theta \ldots \quad (34a)$$

and

$$M_\xi = \frac{E\, h_c}{2\, \beta_c^2} e^{-\beta_c \xi} (A_2 \cos \beta_c \xi - A_1 \sin \beta_c \xi) \cos \theta \ldots\ldots\ldots \quad (34b)$$

and at the cylinder boundary $\xi = 0$ have the values:

$$S_{o\xi} = - \frac{E\, h_c}{2\, a\, \beta_c} (A_1 + A_2) \cos \theta \ldots\ldots\ldots \quad (35a)$$

and

$$M_{o\xi} = \frac{E\, h_c}{2\, \beta_c^2} A_2 \cos \theta \ldots\ldots\ldots\ldots\ldots \quad (35b)$$

Solving Eqs. 35 for the constants A_1, A_2, and substituting in Eqs. 32, the boundary displacements in terms of the boundary tractions become:

$$u_o = \frac{\nu}{E\, h_c} a\, S_{o\xi} \ldots\ldots\ldots\ldots\ldots\ldots \quad (36a)$$

$$v_o = \frac{2 + \nu}{E\, h_c} \overline{M}_{o\xi} \sin \theta \ldots\ldots\ldots\ldots\ldots \quad (36b)$$

$$w_o = - \frac{2\beta_c}{E\, h_c} (a\, S_{o\xi} + \beta_c\, M_{o\xi}) \ldots\ldots\ldots\ldots \quad (36c)$$

and

$$w'_o = \frac{2\, \beta_c^2}{E\, h_c} (a\, S_{o\xi} + 2\, \beta_c\, M_{o\xi}) \ldots\ldots\ldots\ldots \quad (36d)$$

---

15 "Statik und Dynamik der Schalen," by W. Flügge, Springer, Berlin, 1957, p. 147, Eqs. 96(b,f).

Substituting the values of A_1 and A_2 from Eqs. 35 in Eqs. 34 the shears and moments in the cylinder become:

$$S_\xi = \left[\bar{S}_{O\xi}\, e^{-\beta_c \xi} \cos \beta_c \xi - \sin \beta_c \xi - \frac{2\bar{M}_{O\xi}}{a}\, e^{-\beta_c \xi} \sin \beta_c \xi \right] \cos \theta \quad \ldots\ldots\ldots\ldots\ldots\ldots \quad (37a)$$

and

$$M_\xi = \left[\bar{M}_{O\xi}\, e^{-\beta_c \xi} \cos \beta_c \xi + \sin \beta_c \xi + \frac{a}{\beta_c}\, \bar{S}_{O\xi} e^{-\beta_c \xi} \sin \beta_c \xi \right] \cos \theta \quad \ldots\ldots\ldots\ldots\ldots\ldots \quad (37b)$$

Non-Bending Terms of General Solution.—The displacements corresponding to the roots of Eq. 25(b) are of the form:

$$u = \left(U_O + U_1 \xi + U_2 \xi^2 + U_3 \xi^3\right) \cos \theta \ldots\ldots\ldots\ldots \quad (38a)$$

$$v = \left(V_O + V_1 \xi + V_2 \xi^2 + V_3 \xi^3\right) \sin \theta \ldots\ldots\ldots\ldots \quad (38b)$$

$$w = \left(W_O + W_1 \xi + W_2 \xi^2 + W_3 \xi^3\right) \cos \theta \ldots\ldots\ldots\ldots \quad (38c)$$

The ratios U/W and V/W are found by substitution of Eqs. 38 in the original differential equations,[13] and by setting equal to zero the coefficient of each power of ξ. Neglecting k_c in comparison with unity, the non-bending displacements take the form:

$$u = \left[W_1 + 2\, W_2\, \xi + 3\, W_3 \left(\xi^2 + 2(2 + \nu) \right) \right] \cos \theta \ldots\ldots \quad (39a)$$

$$v = \left[W_O + W_1 \xi + W_2 \left(\xi^2 - 2\nu \right) + W_3 \left(\xi^3 - 6\nu\xi \right) \right] \sin \theta \ldots \quad (39b)$$

and

$$w = \left[W_O + W_1 \xi + W_2 \xi^2 + W_3 \xi^3 \right] \cos \theta \ldots\ldots\ldots\ldots \quad (39c)$$

Where the $W_0, \ldots, W_3$ are arbitrary constants. The various terms of Eqs. 39 may be easily identified:

(1) The terms in W_0:

$$u = 0; \quad v = W_O \sin \theta \; ; \quad w = W_O \cos \theta \ldots\ldots\ldots\ldots \quad (40)$$

represent a rigid body translation in the direction $\theta = \pi$.

(2) The terms in W_1:

$$u = W_1 \cos \theta \; ; \quad v = W_1 \xi \sin \theta \; ; \quad w = W_1 \xi \cos \theta \ldots\ldots\ldots \quad (41)$$

represent a rigid body rotation of amplitude W_1/a around the axis $\theta - \pi/2$ at $\xi = 0$.

(3) Substitution of the terms in W_2 in the membrane stress equations, Eqs. 6, shows that

$$N_\xi = \frac{2\, E\, h_c}{a}\, W_2 \cos \theta; \; N_{\xi\theta} = 0 \ldots\ldots\ldots\ldots \quad (42)$$

Thus the terms in W_2 correspond to a state of normal stress, varying sinusoidally with θ and constant with respect to ξ, with boundary tractions:

$$N_{o\xi} = \frac{2\,E\,h_c}{a}\,W_2 \cos\theta;\; N_{o\xi\theta} = 0 \quad \ldots\ldots\ldots\ldots \quad (43)$$

Solving for W_2:

$$W_2 = \frac{a}{2\,E\,h_c}\,\overline{N}_{o\xi} \quad \ldots\ldots\ldots\ldots\ldots\ldots \quad (44)$$

(4) Substitution of the terms in W_3 into Eqs. 6 gives:

$$N_\xi = \frac{6\,E\,h_c}{a}\,\xi\,W_3 \cos\theta;\; N_{\xi\theta} = -\frac{6\,E\,h_c}{a}\,W_3 \sin\theta \quad \ldots\ldots\ldots \quad (45)$$

At the top of the cylinder ($\xi = 0$):

$$N_{o\xi} = 0;\; N_{o\xi\theta} = -\frac{6\,E\,h_c}{a}\,W_3 \sin\theta \quad \ldots\ldots\ldots\ldots \quad (46)$$

$N_{\xi\theta}$ is constant in ξ and $N_{0\xi\theta}$ at the free boundary produces an unbalanced resultant and an unbalanced moment equilibrated by the normal traction N_ξ and the shear traction $N_{\xi\theta}$ at the cylinder base, $\xi = \xi_1$:

$$N_\xi\Big]_{\xi=\xi_1} = \frac{6\,E\,h_c}{a}\,\xi_1\,W_3 \cos\theta \quad \ldots\ldots\ldots\ldots \quad (47a)$$

and

$$N_{\xi\theta}\Big]_{\xi=\xi_1} = -\frac{6\,E\,h_c}{a}\,W_3 \sin\theta \quad \ldots\ldots\ldots\ldots\ldots \quad (47b)$$

Solving Eq. 46 for W_3:

$$W_3 = -\frac{a}{6\,E\,h_c}\,\overline{N}_{o\xi\theta} \quad \ldots\ldots\ldots\ldots\ldots\ldots \quad (48)$$

Thus, from Eq. 39, 44, and 48, the non-bending displacements at the cylinder boundary are expressed in terms of rigid body motions and boundary stresses by:

$$u_o = \left(W_1 - \frac{2+\nu}{E\,h_c}\,a\,\overline{N}_{0\xi\theta}\right) \cos\theta \quad \ldots\ldots\ldots \quad (49a)$$

$$v_o = \left(W_o - \frac{\nu}{E\,h_c}\,a\,\overline{N}_{o\xi}\right) \sin\theta \quad \ldots\ldots\ldots\ldots \quad (49b)$$

$$w_o = W_o \cos\theta \quad \ldots\ldots\ldots\ldots\ldots\ldots \quad (49c)$$

and

$$w_o' = W_1 \cos\theta \quad \ldots\ldots\ldots\ldots\ldots\ldots \quad (49d)$$

GENERAL ANALYSIS OF THE UNLOADED HEMISHPERICAL DOME

Bending Terms of General Solution.—The basic simplifying assumption of Geckeler applied to the present problem implies that the bending terms of the general solution for the hemispherical dome displacements can be approximated

by the bending displacements of the cylinder tangent to the dome at its equator, since bending disturbances are limited to a narrow band at its base.

The hemispherical bending displacements near the dome base are therefore given by Eqs. 31 in which the geometrical characteristics of the dome k_s, β_s are substituted for k_c, β_c and

$$\chi = \frac{\pi}{2} - \phi, \quad (\ldots)' = \frac{\partial}{\partial \phi}(\ldots) \quad \ldots\ldots\ldots\ldots (50)$$

and

$$u = -\frac{\nu}{2\beta_s} e^{-\beta_s \chi}\left[-(A_1 + A_2)\cos\beta_s\chi + (A_1 - A_2)\sin\beta_s\chi\right]\cos\theta \quad \ldots(51a)$$

$$v = \frac{2+\nu}{2\beta_s^2} e^{-\beta_s \chi}\left[-A_2\cos\beta_s\chi + A_1\sin\beta_s\chi\right]\sin\theta \quad \ldots\ldots(51b)$$

$$w = e^{-\beta_s \chi}\left[A_1\cos\beta_s\chi + A_2\sin\beta_s\chi\right]\cos\theta \quad \ldots\ldots\ldots(51c)$$

and

$$w' = -\beta_s e^{-\beta_s \chi}\left[(A_2 - A_1)\cos\beta_s\chi - (A_1 + A_2)\sin\beta_s\chi\right]\cos\theta \quad \ldots\ldots(51d)$$

The constants A_1, A_2 are given by the equations corresponding to Eqs. 35 and the bending displacements at the dome base ($\chi = 0$) become:

$$u_o = -\frac{\nu}{E h_s} a S_{o\phi} \quad \ldots\ldots\ldots\ldots\ldots\ldots(52a)$$

$$v_o = -\frac{2+\nu}{E h_s}\overline{M}_{o\phi}\sin\theta \quad \ldots\ldots\ldots\ldots\ldots\ldots(52b)$$

$$w_o = \frac{2\beta_s}{E h_s}\left(a S_{o\phi} + \beta_s M_{o\phi}\right) \quad \ldots\ldots\ldots\ldots(52c)$$

and

$$w_o' = \frac{2\beta_s^2}{E h_s}\left(a S_{o\phi} + 2\beta_s M_{o\phi}\right) \quad \ldots\ldots\ldots\ldots(52d)$$

Non-Bending Terms of General Solution.—The non-bending terms of the general solution for the hemisphere are only rigid body displacements, representing:

(1) a rigid translation parallel to $\theta = \pi$:

$$u = -C_1\cos\phi\cos\theta \quad \ldots\ldots\ldots\ldots\ldots\ldots(53a)$$

$$v = C_1\sin\theta \quad \ldots\ldots\ldots\ldots\ldots\ldots(53b)$$

$$w = C_1\sin\phi\cos\theta \quad \ldots\ldots\ldots\ldots\ldots\ldots(53c)$$

and

$$w' = C_1\cos\phi\cos\theta \quad \ldots\ldots\ldots\ldots\ldots\ldots(53d)$$

(2) a rigid rotation of amplitude C_2/a around the axis $\theta = \pi/2$:

$$u = -C_2\cos\theta \quad \ldots\ldots\ldots\ldots\ldots\ldots(54a)$$

$$v = C_2\cos\phi\sin\theta \quad \ldots\ldots\ldots\ldots\ldots\ldots(54b)$$

$$w = 0 \quad \ldots\ldots\ldots\ldots\ldots\ldots(54c)$$

and

$$w' = 0 \quad \ldots\ldots\ldots\ldots\ldots\ldots(54d)$$

Thus the non-bending displacements at the dome base at $X = 0$ are given by:

$$u_o = - C_2 \cos \theta \quad \ldots\ldots\ldots\ldots\ldots\ldots (55a)$$

$$v_o = C_1 \sin \theta \quad \ldots\ldots\ldots\ldots\ldots\ldots (55b)$$

$$w_o = C_1 \cos \theta \quad \ldots\ldots\ldots\ldots\ldots\ldots (55c)$$

and

$$w_o' = 0 \quad \ldots\ldots\ldots\ldots\ldots\ldots (55d)$$

CONTINUITY CONDITIONS AT DOME-CYLINDER INTERSECTION

Indicating by ψ_{0c}, ψ_{0s} the rotations of the cylinder generatrix and the meridional tangent to the dome at the cylinder and dome edge, respectively, the compatibility of displacements at the common edge requires that:

$$(u_o)_c = (u_o)_s \; ; \; (v_o)_c = (v_o)_s ; \; (w_o)_c = (w_o)_s \; ; \; (\psi_o)_c = - (\psi_o)_s \ldots . \quad (56)$$

Assuming ψ_c positive for a rotation of the θ - 0 axis towards the ξ - axis, and ψ_s positive for a rotation of the $\theta = 0$ axis towards the $\phi = 0$ axis (Fig. 7):

$$\psi_c = \frac{w'}{a} \quad \ldots\ldots\ldots\ldots\ldots\ldots (57a)$$

and

$$\psi_s = \frac{u + w'}{a} \quad \ldots\ldots\ldots\ldots\ldots\ldots (57b)$$

Substituting in Eqs. 54 the edge displacements of the cylinder given by Eqs. 13, 36, 49, and the edge displacements of the hemisphere given by Eqs. 22, 52, 55, four equations are obtained in the eight boundary tractions at the common edge of cylinder and dome.

However, between these tractions the following relationships subsist:

$$S_{o\xi} = -S_{o\phi} \quad \ldots\ldots\ldots\ldots\ldots\ldots (58a)$$

$$N_{o\xi} = N_{o\phi} \quad \ldots\ldots\ldots\ldots\ldots\ldots (58b)$$

$$M_{o\xi} = M_{o\phi} \quad \ldots\ldots\ldots\ldots\ldots\ldots (58c)$$

and

$$N_{o\xi\theta} = N_{o\phi\theta} = - \frac{2 p a}{a} \sin \theta \quad \ldots\ldots\ldots\ldots\ldots (58d)$$

Since the bending displacement of Eqs. 30 may be shown to produce boundary tractions N_{0b}, $N_{0b\phi}$ and $N_{\phi b\theta}$, $N_{0b\phi\theta}$, Eqs. 58 c and d read:

$$N_{o\phi} + N_{ob\phi} = N_{o\xi} + N_{ob\xi} \quad \ldots\ldots\ldots\ldots\ldots (58e)$$

and

$$N_{o\phi\theta} + N_{ob\phi\theta} = N_{o\xi\phi} + N_{ob\xi\theta} \quad \ldots\ldots\ldots\ldots\ldots (58f)$$

However, the terms depending on the N_b in the expression for $S_{0\phi}$ and $M_{0\phi}$ can be neglected since they are of the order of $1/\beta^3$ as against the remaining terms, which are of the order of one.

Hence, letting:

$$D_1 = W_o - C_1 \quad \ldots\ldots\ldots\ldots\ldots\ldots (59a)$$

and

$$D_2 = W_1 + C_2 \quad \ldots\ldots\ldots\ldots\ldots\ldots (59b)$$

the compatibility equations take the form:

$$\left(\frac{\nu}{E\,h_s} - \frac{\nu}{E\,h_c}\right) a\,\bar{S}_{o\phi} = \left(\frac{2(1+\nu)}{3\,E\,h_s} - \frac{2(2+\nu)}{3\,E\,h_c}\right) p\,a^2 - D_2 \quad \ldots \quad (60a)$$

$$\left(\frac{2+\nu}{E\,h_s} - \frac{2+\nu}{E\,h_c}\right) M_{o\phi} = \left(\frac{1+\nu}{E\,h_s} - \frac{1}{E\,h_c}\right) p\,a^2 - D_1 \quad \ldots\ldots \quad (60b)$$

$$\left(\frac{2\,\beta_s}{E\,h_s} + \frac{2\,\beta_c}{E\,h_c}\right) a\,\bar{S}_{o\phi} + \left(\frac{2\,\beta_s^{\,2}}{E\,h_s} - \frac{2\,\beta_c^{\,2}}{E\,h_c}\right) \bar{M}_{o\phi} = -\frac{\nu}{E\,h_s}\, p\,a^2 - D_1 \quad \ldots (60c)$$

and

$$\left(\frac{2\,\beta_s^{\,2}+\nu}{E\,h_s} - \frac{2\,\beta_c^{\,2}}{E\,h_c}\right) a\,\bar{S}_{o\phi} + \left(\frac{4\,\beta_s^{\,3}}{E\,h_s} + \frac{4\,\beta_c^{\,3}}{E\,h_c}\right) \bar{M}_{o\phi} = -D_2 \quad \ldots\ldots \quad (60d)$$

The constants D_1 and D_2 represent the rigid body translation and rotation of the cylinder with respect to the dome. Eliminating D_1 and D_2, dropping members of the order of unity in comparison with β^2, and letting:

$$\lambda = \frac{\beta_c}{\beta_s} = \left(\frac{h_s}{h_c}\right)^{1/2} \quad \ldots\ldots\ldots\ldots\ldots\ldots \quad (61)$$

the values of $\bar{S}_{o\phi}$ and $\bar{M}_{o\phi}$ become:

$$\bar{S}_{o\phi} = \frac{1-\lambda^2}{\Lambda}\left[1 + \lambda^5 + \frac{\left[1+\nu-(2+\nu)\,\lambda^2\right]\left(1+\lambda^2\right)}{3\,s}\right]\frac{p\,a}{\beta_s} \quad \ldots (62a)$$

$$\bar{M}_{o\phi} = -\frac{1}{\Lambda}\left[\frac{\left(1-\lambda^2\right)\left(1-\lambda^4\right)}{2} + \frac{\left[1+\nu-(2+\nu)\,\lambda^2\right]\left(1+\lambda^3\right)}{3\,\beta_s}\right]\frac{p\,a^2}{\beta_s^{\,2}} \quad \ldots (62b)$$

where:

$$\Lambda = 1 + 2\,\lambda^3\left(1+\lambda+\lambda^2\right) + \lambda^8 \quad \ldots\ldots\ldots \quad (63)$$

When dome and cylinder have the same thickness ($\lambda = 1,\ \Lambda = 8$):

$$\bar{S}_{\bar{o}\bar{\phi}} = 0 \quad \ldots\ldots\ldots\ldots\ldots\ldots \quad (64a)$$

and

$$\bar{M}_{o\phi} = \frac{p\,a^2}{12\,\beta^3} \quad \ldots\ldots\ldots\ldots\ldots\ldots \quad (64b)$$

When the cylinder is infinitely thick, that is, for a dome with a fixed edge ($\lambda = 0,\ \Lambda = 1$):

$$\bar{S}_{o\phi} = \left[1 + \frac{1+\nu}{3\,\beta_s}\right]\frac{p\,a}{\beta_s} \quad \ldots\ldots\ldots\ldots\ldots \quad (65a)$$

and

$$\bar{M}_{o\phi} = -\left[1/2 + \frac{1+\nu}{3\,\beta_s}\right]\frac{p\,a^2}{\beta_s^{\,2}} \quad \ldots\ldots\ldots\ldots\ldots \quad (65b)$$

The shears and moments at any point in the cylinder and shell may be computed by the cylindrical equations, Eqs. 37, in which β_c and ξ or β_s and X respectively, are used with the amplitudes $\overline{S}_{0\phi}$, $\overline{M}_{0\phi}$ of Eqs. 62.

NUMERICAL COMPARISON WITH ASYMPTOTIC SOLUTION

In Example III of Schwerin's paper[8] the boundary shear and moment are computed for a dome built-in at the edge with the following characteristics: p = 100 kg per sq m, a = 10 m, h = 0.25 m, and ν = 0.25.

Table 1 gives the values of the boundary shear and moment evaluated by Schwerin and the corresponding values computed by means of Eqs. 65.

TABLE 1.—BOUNDRY SHEAR AND MOMENT

Boundry shear and moment (1)	Asymptotic solution, in Kg per cm (2)	Approximate solution, in Kg per cm (3)	% of error (4)
$\overline{S}_{o\phi}$	1.23	1.275	3.7
$\overline{M}_{o\phi}$	-76.7	-81.4	6.1

Although the shell considered is comparatively thick (h/a = 1/40) by present day standards of construction, the accuracy of the present solution is satisfactory for engineering purposes. The present solution, moreover, is seen to be on the conservative side.

Since the accuracy of the present solution improves very rapidly with a decreasing thickness ratio, the present method of solution is proved acceptable in all cases of practical significance, since usually h/a is less than 1/100 in modern shell design.

Journal of the
ENGINEERING MECHANICS DIVISION
Proceedings of the American Society of Civil Engineers

BENDING OF PLATES ON A VISCOELASTIC FOUNDATION[a]

By K. S. Pister,[1] M. ASCE and M. L. Williams[2]

SYNOPSIS

In a recent note E. Reissner extended the concept of the classical Winkler-Zimmerman foundation to permit the introduction of a differential shear stiffness parameter in addition to the foundation modulus. The resulting system of differential equations is of sixth order. In this paper the system of equations is modified to incorporate a different interface condition, and the significance of the shear stiffness parameter is examined.

As an example, the solution for a concentrated line load on an infinite plate supported by a Voigt foundation is presented along with response curves of maximum deflection and moment for a step applied force.

INTRODUCTION

The analysis of beams or plates on a deformable foundation rests upon assumptions concerning the behavior of the plate-foundation system. These assumptions involve: (1) description of the foundation, that is, whether a solid continuum or an idealized set of independent elements exists (2) conditions to

Note.—Discussion open until March 1, 1961. To extend the closing date one month, a written request must be filed with the Executive Secretary, ASCE. This paper is part of the copyrighted Journal of the Engineering Mechanics Division, Proceedings of the American Society of Civil Engineers, Vol. 86, No. EM 5, October, 1960.

[a] Presented at the joint ASME-ASCE West Coast Meeting, Stanford University, September, 1959.

[1] Assoc. Prof., Div. of Struct. Engrg. and Struct. Mechanics, Univ. of California, Berkeley, Calif.

[2] Assoc. Prof., Guggenheim Aeronautical Laboratory, California Inst. of Tech., Pasadena, Calif.

be met at the plate-foundation interface (full continuity of displacements or frictionless) and (3) system of equations by which the behavior of the plate is defined, that is, the Poisson-Kirchhoff theory neglecting normal and shearing deformation, the Reissner theory retaining these effects, or consideration of the plate as a solid continuum. In view of the number of possible combinations of these assumptions, many theories of behavior have appeared. No attempt will be made here to present a bibliography but typical treatments may be found in Hetenyi,[3] Burmister,[4] Naghdi and Rowley,[5] and Pickett.[6] A common feature of the work cited so far has been the assumption that both plate and foundation behave as linear elastic bodies. Recent papers by Freudenthal and Lorsch,[7] and Hoskin and Lee[8] have generalized the problem in the sense that a Poisson-Kirchhoff beam or plate resting on a set of independent viscoelastic springs has been treated.

It need hardly be emphasized that in the treatment of the foundation a compromise between the simplicity of the Winkler-Zimmerman set of independent springs and the behavior of the solid continuum must be reached. Recently, E. Reissner[9] generalized the independent spring model by including a differential shear stiffness parameter in addition to the foundation modulus, at the same time retaining mathematical simplicity in the model of the foundation. The plate deflection was governed by the Poisson-Kirchhoff theory and the foundation interface was assumed to experience no displacement in the horizontal plane. In the present paper Reissner's work is modified to obtain continuity of displacement at the interface. This has the feature of emphasizing the role of the ratio of foundation to plate thickness. In addition, the physical significance of the shear stiffness parameter is examined. Inclusion of normal and shear deformation in the plate, following Naghdi and Rowley[4] and Frederick,[10] will be reported at a subsequent time.

Notation.—The letter symbols adopted for use in this paper are defined where they first appear, in the illustrations or in the text, and are arranged alphabetically, for convenience of reference, in the Appendix.

BASIC SYSTEM OF EQUATIONS

Foundation.—Referring to Fig. 1 and following Reissner, the foundation layer is assumed to be capable of transmitting normal stress σ_z and shearing stresses τ_{xz} and τ_{yz}. The remaining stress components, σ_x, σ_y, τ_{xy}, are assumed

---

3 "Beams on Elastic Foundation," by M. Hetenyi, Univ. of Michigan Press, Ann Arbor, Mich., 1946.

4 "The Theory of Stresses and Displacements in Layered Systems and Applications to the Design of Airport Runways," by D. M. Burmister, Proceedings, Highway Reserve Board, Vol. 23, 1943, pp. 126-148.

5 "On the Bending of Axially Symmetric Plates on Elastic Foundations," by P. M. Naghdi and J. C. Rowley, Proceedings, First Midwestern Conf. in Solid Mechanics, Univ. of Illinois, Urbana, Ill., 1953, pp. 119-123.

6 "Deflections, Moments and Reactive Pressures for Concrete Pavements," by G. Pickett, et al., Kansas State College Bulletin No. 65, 1951.

7 "The Infinite Elastic Beam on a Linear Viscolelastic Foundation," by A. M. Freudenthal and H. G. Lorsch, Proceedings, ASCE, Vol. 83, No. EM 1, January, 1957.

8 "Analysis of Flexible Surfaces over Subgrades with Viscoelastic Material Behavior," by B. C. Hoskin and E. H. Lee, Proceedings, ASCE, Vol. 85, No. EM 4, October, 1959.

9 "Deflections of Plates on Viscoelastic Foundation," by E. Reissner, Transactions, ASME, Vol. 80, Part 3, 1958, pp. 144-145.

10 "Thick Rectangular Plates on an Elastic Foundation," by D. Frederick, Transactions, ASCE, Vol. 122, 1957, pp. 1069-1087.

to be negligible. The displacement-stress equations in this region, therefore, take the form

$$w,_z = \sigma_z/E \quad \ldots\ldots\ldots\ldots\ldots\ldots \quad (1a)$$

$$u,_z + w,_x = \tau_{xz}/G \quad \ldots\ldots\ldots\ldots\ldots\ldots \quad (1b)$$

and

$$v,_z + w,_y = \tau_{yz}/G \quad \ldots\ldots\ldots\ldots\ldots\ldots \quad (1c)$$

where partial differentiation of the displacements is indicated in the usual manner. The stress equilibrium equations, in view of the above assumptions, then

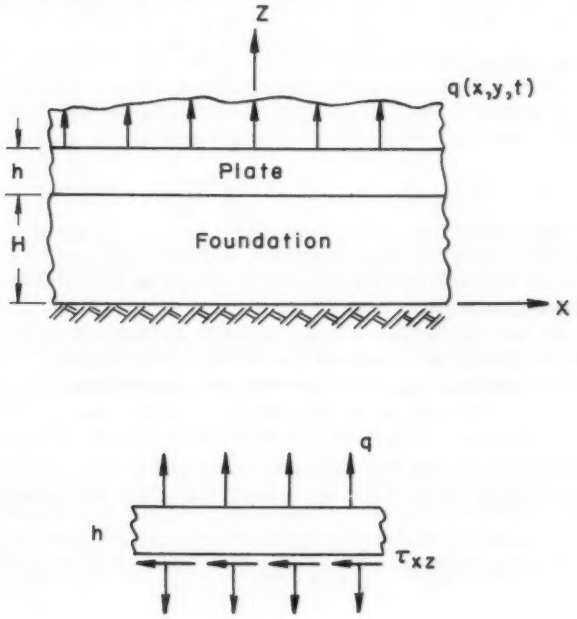

FIG. 1

become, neglecting inertia effects,

$$\tau_{xz,z} = 0 \quad \ldots\ldots\ldots\ldots\ldots\ldots \quad (2a)$$

$$\tau_{yz,z} = 0 \quad \ldots\ldots\ldots\ldots\ldots\ldots \quad (2b)$$

$$\tau_{xz,x} + \tau_{yz,y} + \sigma_{z,z} = 0 \quad \ldots\ldots\ldots\ldots\ldots\ldots \quad (2c)$$

Plate.—The behavior of the plate is assumed to be governed by Poisson-Kirchhoff theory, neglecting the effects of transverse normal stress and shear

deformation. Accordingly, the plate deflection W (x, y, t) satisfies the equation

$$D \nabla^4 W = q - p \quad \ldots\ldots\ldots\ldots\ldots\ldots (3)$$

where q and p are the intensity of external transverse load and foundation interface pressure, respectively.

BOUNDARY AND CONTINUITY CONDITIONS

The usual Kirchhoff plate boundary conditions are assumed to be associated with Eq. 3. For the foundation the following conditions are imposed.

$$\text{At } z = 0: \; u = v = w = 0 \quad \ldots\ldots\ldots\ldots\ldots (4a)$$

$$\text{At } z = H: \; u = +\frac{n}{2} W_{,x} \quad \ldots\ldots\ldots\ldots\ldots (4b)$$

$$v = +\frac{h}{2} W_{,y}$$

$$w = W$$

$$\sigma_z = p \quad \ldots\ldots\ldots\ldots\ldots\ldots (4c)$$

The interface conditions, unlike Reissner's (u = v = 0), assume continuity of displacement between plate and foundation. A final condition imposed upon the foundation is the requirement that the shear stress on the cylindrical boundary of the foundation vanishes.

Choosing the plate deflection W and foundation pressure p as dependent variables, the basic system of equations can be treated as follows:

Eqs. 2 show that τ_{xz}, τ_{yz} are functions of x, y only and that

$$\sigma_z = p + (H - z)\, Q\,(x,y) \quad \ldots\ldots\ldots\ldots\ldots\ldots (5)$$

where the condition $\sigma_z\,(H) = p$ has been used and $Q = \tau_{xz,x} + \tau_{yz,y}$. Integrating Eq. 1, subject to the boundary conditions of Eq. 4a, gives, for the displacements,

$$G\,u = \tau_{xz}\, z - \frac{G}{E}\left[\frac{z^2}{2}\, p_{,x} + \left(\frac{H z^2}{2} - \frac{z^3}{6}\right) Q_{,x}\right] \quad \ldots\ldots (6a)$$

$$G\,v = \tau_{yz}\, z - \frac{G}{E}\left[\frac{z^2}{2}\, p_{,y} + \left(\frac{H z^2}{2} - \frac{z^3}{6}\right) Q_{,y}\right] \quad \ldots\ldots (6b)$$

$$E\,w = p\, z + \left(H z - \frac{z^2}{2}\right) Q \quad \ldots\ldots\ldots\ldots (6c)$$

Inserting the condition of Eq. 4b, w (x, y, H, t) = W (x, y, t) into Eq. 6c gives

$$Q = \frac{2\,p}{H} + \frac{2\,E\,W}{H^2} \quad \ldots\ldots\ldots\ldots\ldots\ldots (7)$$

Making use of Eq. 7 and the continuity conditions of Eq. 4b, Eqs. 6a, and 6b can be solved for the shearing stresses;

$$\tau_{xz} = -\frac{G\,H}{G\,E}\,p,_x + G\left(\frac{2}{3} + \frac{h}{2\,H}\right) W,_x \quad \ldots\ldots\ldots (8a)$$

$$\tau_{yz} = -\frac{G\,H}{G\,E}\,p,_y + G\left(\frac{2}{3} + \frac{h}{2\,H}\right) W,_y \quad \ldots\ldots\ldots (8b)$$

Eliminating the shearing stresses from Eq. 8, combining with Eq. 7 and simplifying leads to

$$W - \frac{G\,H^2}{3\,E}\left(1 + \frac{3\,h}{4\,H}\right)\nabla^2 W = \frac{H}{E}\left(p - \frac{G\,H^2}{12\,E}\,\nabla^2\,p\right) \quad \ldots\ldots (9)$$

Eqs. 3 and 9 constitute the basic system of equations for the dependent variables W, p. In addition to the two boundary conditions involving W, we have the requirement that the shearing stress on the cylindrical boundary of the foundation must vanish. From Eqs. 8a, and 8b this is easily shown to be

$$\tau_n = -\frac{G\,H}{G\,E}\,p,_n + \frac{2}{3}\,G\left(1 + \frac{3\,h}{4\,H}\right) W,_n = 0 \quad \ldots\ldots (10)$$

In Eq. 10 n refers to the outward normal to the foundation boundary. With the exception of the continuity conditions of Eq. 4b and the presence of the term $\left(1 + \frac{3\,h}{4\,H}\right)$ in Eq. 9, the basic system of equations and boundary conditions are those obtained previously by Reissner.[9] When $\frac{h}{H}$ is set equal to zero, Reissner's equations are recovered. However, while he used a single parameter[9] to permit inclusion of viscoelastic behavior of the foundation, the present work will incorporate viscoelastic effects through the well known correspondence principle,[11] connecting elastic and viscoelastic boundary value problems. Briefly, it can be shown for a class of problems that a correspondence exists between the elastic stress and displacement fields and the Laplace transforms (with respect to time) of the viscoelastic stress and displacement fields, provided that the elastic coefficients are replaced by the Laplace transforms of the viscoelastic operators.

PHYSICAL SIGNIFICANCE OF FOUNDATION PARAMETERS

As pointed out by Reissner,[9] the present theory permits description of the foundation using two elastic parameters; the usual axial modulus

$$k = \frac{E}{H} \quad \ldots\ldots\ldots\ldots\ldots\ldots (11)$$

which relates normal pressure to deflection, and a "differential shear stiffness," appearing as the term $\frac{G\,H^2}{3\,E}$ in Eq. 9. Although the physical significance of the

11 "Rheology," by F. R. Eirich, Ed., Vol. I, Academic Press, New York, 1956, Chapter II.

foundation modulus is well known, it is of interest to examine the term $\frac{G H^2}{3 E}$. It will be convenient to introduce the shear stiffness parameter

$$C^2 = \frac{G}{3 E} \quad \ldots\ldots\ldots\ldots\ldots\ldots\ldots\ldots (12)$$

Rewriting Eq. 9 using Eqs. 11 and 12 gives

$$W - C^2 H^2 \left(1 + \frac{3 h}{4 H}\right) \nabla^2 W = \frac{1}{k} \left(p - \frac{C^2 H^2}{4} \nabla^2 p\right) \quad \ldots\ldots\ldots (13)$$

The following problem illustrates the significance of the term C^2. Consider

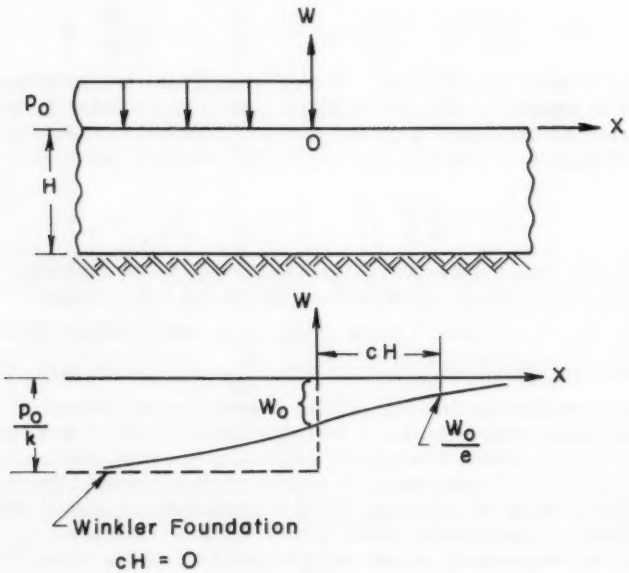

FIG. 2

the foundation layer loaded by a uniform pressure applied directly to the interface $\left(\frac{h}{H} = 0\right)$ such that the pressure is given by

$$p(x) = \begin{cases} -p_o & ; x < 0 \\ 0 & ; x > 0 \end{cases} \quad \ldots\ldots\ldots\ldots (14)$$

Eq. 13 now takes the simpler form

$$\frac{d^2 W}{d x^2} - \frac{1}{C^2 H^2} W = \begin{cases} \dfrac{p_o}{k C^2 H^2} & ; x < 0 \\ 0 & ; x > 0 \end{cases} \quad \ldots\ldots\ldots (15)$$

The solution satisfying the condition of finite deflection at infinity and continuity of slope at x - 0 is

$$W(x) = -\frac{p^o}{2k} \; e^{-x/(C\,H)} \; ; \; x > 0 \quad \ldots\ldots\ldots (16)$$

$$W(x) = -\frac{p_o}{k} \left(1 - \frac{1}{2} \; e^{x/(C\,H)}\right) ; \; x < 0 \quad \ldots\ldots\ldots (17)$$

Eq. 16 is shown in Fig. 2. It can be seen that the parameter C is the dimensionless distance with respect to H in which the foundation deflection diminishes by a factor of e, hence, it is a measure of the differential shear stiffness of the foundation. For the Winkler foundation, C = 0, and the discontinuity shown in the figure results. Accordingly, in the present theory k, C H are the elastic or viscoelastic foundation parameters or a combination of the two.

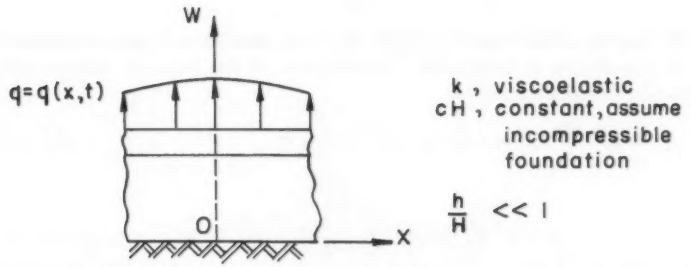

FIG. 3

In applications of the theory to foundation problems it would be customary to base the value of k on results of a plate bearing test, rather than to base the value on its definition k = E/H. A similar test could be performed to obtain a value of C H for the foundation material. In this manner the foundation can be described by two experimentally determined parameters.

ILLUSTRATIVE EXAMPLE

In this section the relatively simple solution of the basic system of Eqs. 3 and 13 will be indicated for an infinite plate supporting a load symmetrically distributed with respect to the y-axis and independent of y as shown in Fig. 3.

The basic system of equations for the elastic case are Eqs. 3 and 13 where W = W (x, y, t), p = p (x, y, t), and q = q (x, y, t). Denote the Laplace transform with respect to time of W (x, y, t) by

$$\overline{W}(x, y, s) = \int_0^\infty W \; (x, y, t) \; e^{-st} \, dt \quad \ldots\ldots\ldots\ldots\ldots (18)$$

and the Fourier cosine transform of W (x, y, t) with respect to x by

$$\overline{W}(\alpha, y, t) = \int_0^\infty W \; (x, y, t) \cos \alpha x \, dx \quad \ldots\ldots\ldots\ldots\ldots (19)$$

The correspondence principle for viscoelasticity states that the same differential equations obtain provided that the dependent variables as well as the viscoelastic operators are replaced by their Laplace transforms with respect to time. Accordingly, for the one-dimensional case under consideration, and for "at rest" initial conditions, the associated Laplace transform equations become

$$D \frac{d^4 \bar{W}(x,s)}{dx^4} = \bar{q}(x,s) - \bar{p}(x,s) \quad \ldots\ldots\ldots\ldots (20)$$

and

$$\bar{W}(x,s) - \bar{C}^2(s) H^2 \left(1 + \frac{3h}{4H}\right) \frac{d^2 \bar{W}(x,s)}{dx^2} = \frac{1}{\bar{k}(s)} \left[\bar{p}(x,s) - \frac{\bar{C}^2(s) H^2}{4} \frac{d^2 \bar{p}(x,s)}{dx^2}\right] \quad \ldots\ldots\ldots\ldots\ldots (21)$$

where it may be noted that the plate has been assumed elastic in behavior and hence no transform is indicated. Application of the Fourier cosine transform to these equations then gives

$$D \alpha^4 \, \bar{\bar{W}}(\alpha, s) = \bar{\bar{q}}(\alpha, s) - \bar{\bar{p}}(\alpha, s) \quad \ldots\ldots\ldots\ldots\ldots (22)$$

and

$$\left[1 + \alpha^2 \bar{C}^2(s) H^2 \left(1 + \frac{3h}{4H}\right)\right] \bar{\bar{W}}(\alpha,s) = \frac{1}{\bar{k}(s)} \left[1 + \frac{\alpha^2 \bar{C}^2(s) H^2}{4}\right] \bar{\bar{p}}(\alpha,s) \quad \ldots\ldots\ldots\ldots (23)$$

Combining these equations, the combined transform of the plate deflection is

$$\bar{\bar{W}}(\alpha,s) = \frac{\bar{\bar{q}}(\alpha,s)}{D \alpha^4 + \bar{k}(s) \left[\dfrac{1 + \alpha^2 \bar{C}^2(s) H^2 \left(1 + \dfrac{3h}{4H}\right)}{1 + \dfrac{\alpha^2 C^2(s) H^2}{4}}\right]} \quad \ldots\ldots\ldots (24a)$$

$$\bar{\bar{W}}(\alpha,s) \equiv \frac{\bar{\bar{q}}(\alpha,s)}{D \alpha^4 + A(\alpha,s) \bar{k}(s)} \quad \ldots\ldots\ldots\ldots (24b)$$

where the definition of $A(\alpha,s)$ is implied.

To be specific, assume a step pressure applied along the y-axis together with a Voigt axial foundation modulus, which is, furthermore, assumed incompressible. Thus, the differential shear stiffness parameter Eq. 12 becomes a constant because if $\nu = 1/2$, $G = E/3$ and hence $C^2 = 1/9$. Therefore,

$$\bar{\bar{q}}(\alpha,s) = \frac{p_o}{s} \quad \ldots\ldots\ldots\ldots\ldots\ldots (25)$$

and the viscoelastic axial modulus is

$$\bar{k}(s) = \eta\left(\frac{1}{\tau} + s\right) \quad \ldots\ldots\ldots\ldots\ldots\ldots (26)$$

where the elastic modulus of the foundation is $m = E/H$, and the retardation time is $\tau = \eta/m$.

With this substitution there results

$$\bar{\bar{W}}(\alpha,s) = \frac{p_o}{s} \frac{1}{D\alpha^4 + \eta\left(s + \tau^{-1}\right) A(\alpha)} \quad \ldots\ldots\ldots\ldots (27)$$

which, after a Laplace inversion, becomes

$$\bar{W}(\alpha,t) = \frac{p_o}{m A(\alpha)} \frac{1 - \exp\left\{-\left(1 + \frac{D\alpha^4}{m A(\alpha)}\right)\frac{t}{\tau}\right\}}{1 + \frac{D\alpha^4}{m A(\alpha)}} \quad \ldots\ldots\ldots\ldots (28)$$

and after the Fourier inversion with the applied concentrated loading along $X = 0$,

$$w(x,t) = \frac{p_o}{\pi} \int_o^\infty \left[\frac{1 - \exp\left\{-\left(1 + \frac{D\alpha^4}{m A(\alpha)}\right)\frac{t}{\tau}\right\}}{m A(\alpha)\left[1 + \frac{D\alpha^4}{m A(\alpha)}\right]}\right] \cos \alpha x \, d\alpha \quad \ldots\ldots\ldots\ldots (29)$$

which is the solution in the physical plane.

It develops that it is more convenient to change the notation slightly in order to exhibit the physical characteristics of the solution more easily. To this end, recall the customary notation where

$$\lambda^4 \equiv m/(4D) = (E/H)/(4D) \quad \ldots\ldots\ldots\ldots\ldots\ldots (30)$$

Then, define

$$z^4 = \frac{D}{m}\alpha^4 = \frac{D}{E/H}\alpha^4 = \frac{1}{12\left[1 - (1/2)^2\right]} \frac{D(\alpha H)^4}{E H^3/12\left[1 - (1/2)^2\right]}$$

$$\equiv \frac{1}{9}\frac{D}{D_f}(\alpha H)^4 \quad \ldots\ldots\ldots\ldots\ldots\ldots (31)$$

where the condition of incompressibility, $\nu = 1/2$, has been used in defining the psuedo-foundation rigidity D_f. Returning now to the definition of $A[\alpha(z)]$, using the fact that $C^2 = 1/9$ and defining

$$\gamma = \frac{1}{\sqrt{6}} \sqrt[4]{\frac{D}{D_f}} \quad \ldots\ldots\ldots\ldots\ldots\ldots (32)$$

one finds

$$A[\alpha(z)] = A(z) = \frac{1 + 2\alpha^2\left(1 - \frac{3h}{4H}\right)z2}{1 + (1/2)\gamma^2 z^2} \quad \ldots\ldots\ldots\ldots (33)$$

whereupon

$$w(x,t/\tau\,;\,\gamma) = \frac{\sqrt{2}\,\lambda\,p_o}{m\,\pi}\int_o^\infty \frac{1 - \exp\left\{-\left[1 + \frac{z^4}{A(z)}\right]\frac{t}{\tau}\right\}}{A(z) + z^4}$$

$$\cos(\sqrt{2}\,\lambda\,x\,z)\,dz \quad \ldots\ldots\ldots\ldots\ldots\ldots (34)$$

Several limit cases may now be distinguished. The first of these pertains to the relative rigidity ratio, γ. If $\gamma \to 0$, one finds $A(z)$ approaches a constant, namely unity. Similarly, when $\gamma \to \infty$, $A(z)$ also approaches a constant, namely $4\left(1 + \frac{3\,h}{4\,H}\right)$, so that the limit deflection at an infinite time under the load may be written down immediately as

$$w(0, \infty; 0) = \frac{p_o\,\lambda}{2\,m} \quad \ldots\ldots\ldots\ldots\ldots\ldots (35)$$

$$w(0, \infty; \infty) = \frac{p_o\,\lambda}{2\,m}\,\frac{1}{\left[4\left(1 + \frac{3\,h}{4\,H}\right)\right]^{3/4}} \quad \ldots\ldots\ldots (36)$$

The velocity of deformation is also of interest and may be computed easily. One finds

$$\dot{w}(x,t/\tau;\,\gamma) = \frac{\partial w}{\partial t} = \frac{\sqrt{2}\,\lambda\,p_o}{m\,\pi\,\tau}\int_o^\infty \frac{1}{A(z)}\exp$$

$$\left\{-\left[1 + \frac{z^4}{A(z)}\right]\frac{t}{\tau}\right\}\cos(\sqrt{2}\,\lambda\,xz)dz \quad \ldots\ldots\ldots\ldots (37)$$

Under the load, the same limit rigidity cases can again be easily found as

$$\dot{w}(0,\,t/\tau;\,0) = \frac{p_o\,\Gamma(1/4)}{4\,\pi\,\tau\,m^{3/4}\,D^{1/4}}\,\frac{e^{-t/\tau}}{(t/\tau)^{1/4}} \quad \ldots\ldots (38)$$

$$\dot{w}(0,t/\tau;\,\infty) = \frac{p_o\,\Gamma(1/4)}{4\,\pi\,\tau\,m^{3/4}\,D^{1/4}}\,\frac{e^{-t/\tau}}{(t/\tau)^{1/4}}\,\frac{1}{\left[4\left(1 + \frac{3\,h}{4\,H}\right)\right]^{3/4}} \quad \ldots\ldots (39)$$

in which it is noted that the initial velocity is infinite, and the velocity for a relatively stiff plate is slower than the opposite situation by the damping factor $4\left(1 + \frac{3\,h}{4\,H}\right)^{-3/4}$.

In a similar fashion, the moment in the plate may be computed as

$$M_x(x,t/\tau;\,\gamma) = -D\,\frac{\partial^2 W}{\partial x^2} = \frac{2\sqrt{2}\,\lambda^3\,p_o\,D}{m\,\pi}\int_o^\infty z^2\,\frac{1 - \exp\left\{-\left[1 + \frac{z^4}{A(z)}\right]\frac{t}{\tau}\right\}}{A(z) + z^4}$$

$$\cos(\sqrt{2}\,\lambda\,x\,z)\,dz \quad \ldots\ldots\ldots\ldots\ldots (40)$$

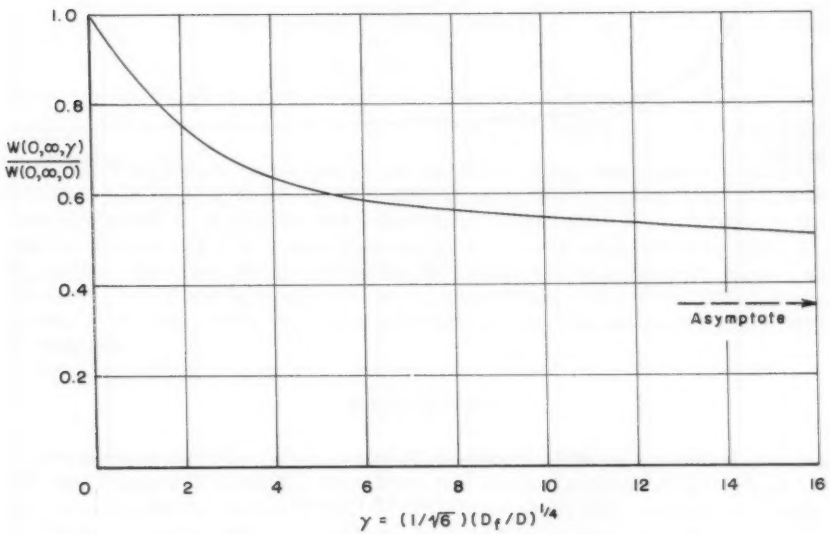

FIG. 4.—VISCOELASTIC DEFLECTION, W = W (X, t/τ; γ)

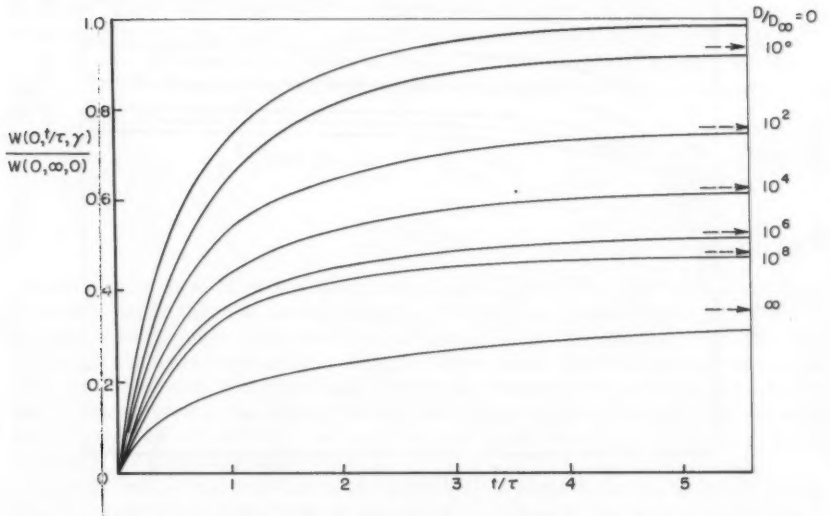

FIG. 5.—TIME DEPENDENCE OF VISCOELASTIC DEFLECTION, W = W (X, t/τ; γ)

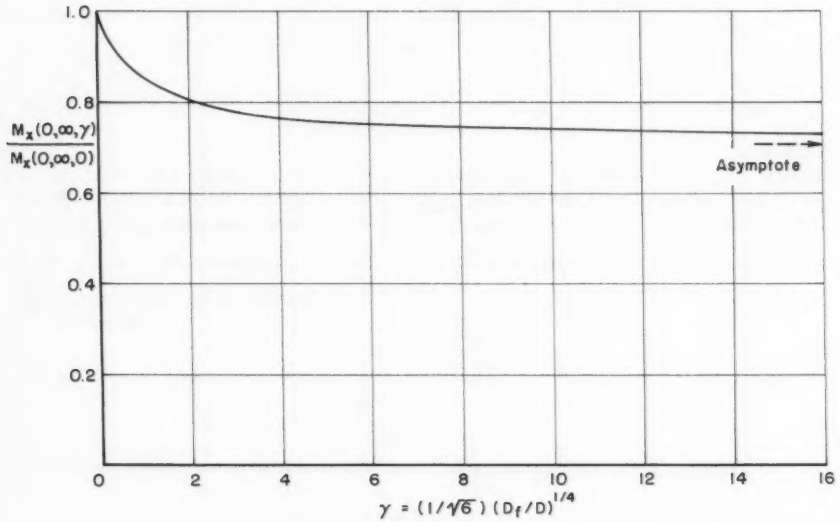

FIG. 6.—VISCOELASTIC MOMENT, $M_X = M_X(X, t/\tau; \gamma)$

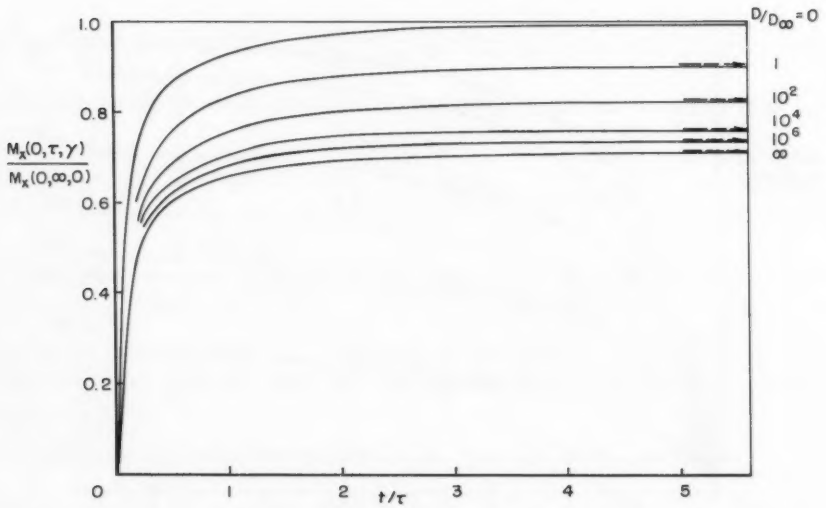

FIG. 7.—TIME DEPENDENCE OF VISCOELASTIC MOMENT, $M_X = M_X(X, t/\tau; \gamma)$

where for long time

$$M_x\,(0,\,\infty;\,0) = \frac{\lambda^3\,p_o\,D}{m} \qquad \ldots\ldots\ldots\ldots\ldots\ldots\ldots (41)$$

$$M_x\,(0,\,\infty;\,\infty) = \frac{\lambda^3\,p_o\,D}{m} \quad \frac{1}{\left[4\left(1 + \frac{3\,h}{4\,H}\right)\right]^{1/4}} \qquad \ldots\ldots\ldots (42)$$

In order to present some idea of the variation of the deflection and moment with time and rigidity ratio, these functions have been computed and plotted in Figs. 4 through 7. It may be noted that these graphs have been plotted for the special case of $h/H = 0$, rather than the more general case given in Figs. 36, 39, and 42. However, by observing the difference between the limit values, as a function of h/H and those where $h/H = 0$, an estimate of the effect of this parameter, which represents the shear bond between the foundation and plate, may be obtained.

CONCLUSION

From a physical standpoint, probably the main deficiency between the theory and the actual behavior of the foundation is a direct result of assuming that the in-plane foundation stresses (σ_x, σ_y, τ_{xy}) are negligible, whether one considers a slip or continuous interface. It is this assumption that leads directly to the linear variation of normal stress σ_z with respect to vertical distance, irrespective of foundation depth. This result appears to be intuitively contradictory with a St. Venant type variation that might otherwise be expected. On the other hand it is encouraging to find that even this set of assumptions predicts an effect depending upon the interface boundary conditions, even though in practical civil engineering applications one is tempted to set $h/H \to 0$.

It is also interesting to observe that a formal elimination between Eqs. 3 and 13 can be obtained through a recurrent substitution of Eq. 13 in Eq. 3 to give

$$\frac{D/D_f}{12\left(1 - \nu_f^2\right)}\,\nabla_H^4\,(W/H) + W/H - \sum_{n=1}^{\infty} 3\left(1 + \frac{h}{H}\right)\left(\frac{C}{4}\right)^n \nabla_H^{2n}\,(W/H)$$

$$= q/E \qquad \ldots\ldots\ldots\ldots\ldots\ldots (43)$$

where lengths have been non-dimensionalized on H in the ∇H^2 operator. While it would appear that the series converges rapidly as a consequence of $C \approx 1/3$, further investigation indicates that a truncation of the series after the first term, giving what amounts to a beam-column term contributed by the foundation, is insufficient for predicting the actual behavior because the non-dimensional derivatives in the higher terms become increasingly large. On the other hand it may be possible to use such an approach combined with particularly simple plate boundary conditions.

In conclusion it is felt that useful engineering results can be obtained by further consideration of the type of viscoelastic interface interaction suggested by Reissner.

APPENDIX. NOTATION

u, v, w	=	rectangular components of displacement vector in foundation;
W	=	vertical displacement of plate middle surface;
$\sigma_x, \ldots; \tau_{xy}, \ldots$	=	rectangular components of stress tensor in foundation;
E, G	=	elastic moduli of foundation;
h, H	=	plate and foundation thicknesses, respectively;
$D = Eh^3/12(1-\nu^2)$	=	plate stiffness;
p, q	=	interface pressure and transverse load on plate;
k	=	axial foundation modulus;
C^2	=	shear stiffness parameter;
$D_f = EH^3/9$	=	pseudo-foundation rigidity; and
$\gamma = (1/\sqrt{6})(D_f/D)^{1/4}$	=	relative stiffness parameter.

Journal of the
ENGINEERING MECHANICS DIVISION
Proceedings of the American Society of Civil Engineers

ELECTRICAL ENERGY ANALOGS OF VIBRATING BEAMS

By Frederick L. Ryder,[1] F. ASCE

SYNOPSIS

For the passive-element electrical analog of a finite increment of a beam vibrating in flexure, improvements over the conventional form of the circuit are found by making explicit use of the energy as an analogous parameter in the beam and in the electrical circuit. For a given beam it is found that these improvements lead to a drastic reduction in the theoretical analog error and also in the number of electrical components required per beam increment. It may therefore generally be expected that for a given allowable overall error the number of required beam increments may be reduced, while the cost of analog components may be reduced both because fewer components are used and also because, in consequence of the smaller number of components, greater imperfections in the components may be tolerated. Alternatively, for a given analog installation, the complexity of problems which may be handled with a given allowable error may be increased.

INTRODUCTION

Analogs for the simulation of the dynamic behavior of beams by means of passive electrical elements are well known.[2,3] It is generally assumed that the beam deflections are small, that the damping is negligible, and that the electrical components (which may consist of capacitances, inductances, and

Note.—Discussion open until March 1, 1961. To extend the closing date one month, a written request must be filed with the Executive Secretary, ASCE. This paper is part of the copyrighted Journal of the Engineering Mechanics Division, Proceedings of the American Society of Civil Engineers, Vol. 86, No. EM 5, October, 1960.

[1] Member, Scientific Research Staff, Republic Aviation Corp., Farmingdale, N. Y.

[2] "Calculation of Normal Modes and Natural Frequencies of Ship Hulls by Means of the Electrical Analog," by E. Kapiloff, David Taylor Model Basin Report 742, July, 1954.

[3] "An Equivalent Circuit for a Vibrating Beam which Includes Shear Motions," by H. M. Trent, The Journal of the Acoustical Soc. of America, May, 1950.

transformers) are ideal. An analog circuit is then found which, in effect, meets the following requirements:

1. The equations of force and moment equilibrium, including inertia effects, in the structure are simulated by Kirchhoff's first law, relating to current summation, in the analog (including the effects of transformer turns ratios on the current relationships).
2. The equations of deflection compatibility, expressed in terms of the forces, moments, and elastic constants, are simulated by the equations governing the compatibility of the time-integrals of voltage, obtained with the aid of Kirchhoff's second law in terms of the currents and impedances (including the effects of transformer turns ratios on the voltage relationships).

Since the equations of equilibrium and of deflection compatibility serve to define the mechanical behavior, and Kirchhoff's two laws serve to define the electrical behavior, the foregoing requirements assure that the various electrical and mechanical parameters are analogous. However, there exists an alternative lesser-known approach in which the simulation of equilibrium relationships is not taken into account explicitly, but results automatically from the following two requirements:

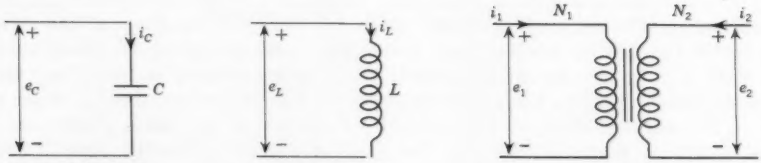

FIG. 1.—ELECTRICAL FUNDAMENTALS

3. The kinetic energy of the mechanical system (written in terms of masses, mass moments of inertia, and velocities) is the same as the capacitive energy of the electrical system (written in terms of capacitances and voltages).
4. The strain energy of the mechanical system (written in terms of deflections and elastic properties) is the same as the inductive energy of the electrical system (written in terms of the time-integrals of voltage and the inductances).

The familiar Lagrange equations of the mechanical system, based on the kinetic and strain energies, are known to define the deflections, or time-integrals of the velocities; hence the identical equations in the electrical system must similarly define the time-integrals of the voltages, so that voltages and velocities are analogous. Further, any force (or moment) is the partial derivative, with respect to its associated velocity component, of the power (or time-rate of energy) in the mechanical system, while current is the partial derivative of power, with respect to its associated voltage difference, in the electrical system, so that currents are analogous to forces and moments. Hence the summations of current must automatically simulate the equations of force and moment equilibrium, although these are not considered explicitly in steps 3 and 4. This will be illustrated subsequently.

For brevity the method of steps 1 and 2 will be termed the equilibrium-compatibility method, while the method of steps 3 and 4 will be called the energy method. The basic purpose of this paper is to show, by applying the two methods to the simple case of a flexurally vibrating beam, that certain advantages may result from the use of the energy method as against the better-known equilibrium-compatibility method.

ELECTRICAL FUNDAMENTALS

In preparation for the analysis of the electrical analogs, it will be well to state certain fundamental relationships pertaining to the ideal capacitance, inductance, and transformer, which are shown subjected to certain currents and voltages in Fig. 1. By basic principles:

$$i_C = C \dot{e}_C \quad \ldots\ldots\ldots\ldots\ldots\ldots \quad (1)$$

where the dot denotes differentiation with respect to time t. The capacitive energy is

$$E_C = \frac{1}{2} C e_C^2 \quad \ldots\ldots\ldots\ldots\ldots\ldots \quad (2)$$

Also,

$$e_L = L \dot{i}_L \quad \ldots\ldots\ldots\ldots\ldots\ldots \quad (3)$$

so that

$$i_L = \frac{\int e_L \, dt}{L} \quad \ldots\ldots\ldots\ldots\ldots\ldots \quad (4)$$

and the inductive energy is

$$E_L = \frac{1}{2} L i_L^2 = \frac{1}{2} \frac{\left[\int e_L \, dt\right]^2}{L} \quad \ldots\ldots\ldots\ldots\ldots\ldots \quad (5)$$

As for the transformer, N_1 and N_2 are the respective numbers of turns, considered positive if positive current produces flux in a prescribed direction in the core. By the law of electro-magnetic induction:

$$\frac{e_1}{N_1} = \frac{e_2}{N_2} \quad \ldots\ldots\ldots\ldots\ldots\ldots \quad (6)$$

Also, the summation of the ampere turns of both windings must be zero, since the net magnetomotive force required to sustain the magnetic flux in the core is zero, so that

$$N_1 i_1 + N_2 i_2 = 0 \quad \ldots\ldots\ldots\ldots\ldots\ldots \quad (7)$$

The total power dissipated in the transformer is therefore

$$e_1 i_1 + e_2 i_2 = 0 \quad \ldots\ldots\ldots\ldots\ldots\ldots \quad (8)$$

FINITE INCREMENT OF BEAM

As is conventional, the beam is divided into a number of incremental lengths. Fig. 2 shows the n^{th} such length, extending from station n to station n + 1. The length of the increment is Δx, and it is assumed that the beam is uniform throughout this length. The mass per unit length is μ, the elastic modulus is E, and the moment of inertia of the cross section about the neutral flexural axis is I. Purely for convenience, it will further be assumed that the two neighboring increments are identical to the one shown.

The accumulated mass from station n - $\frac{1}{2}$ to station n + $\frac{1}{2}$, namely $\mu\ \Delta x$, is assumed concentrated at n, and an identical mass at n + 1. In order to take into account the rotational inertia torque associated with the finite depth of the section, we consider the mass moment of inertia per unit length, namely $\mu\ \rho^2$ (where ρ is the radius of gyration of the cross section), and refer the corresponding value for the whole increment, namely $\mu\ \rho^2\ \Delta x$, to the center of the increment. The external load forces F_n and F_{n+1} are assumed to be applied as indicated. The shear compliance (deflection per unit shear force) for the entire increment is $\Delta x/(K\ A\ G)$, where A is the cross-sectional area, G is the shear modulus, and K A is the fictitious cross-sectional area (always smaller than A) which, if uniformly loaded by shear force, would experience the same vertical shear stress as the actual maximum, which occurs at the neutral axis; this compliance is assumed concentrated at the center of the increment. The bending compliance (angular deflection for unit uniform moment at all points of the increment) is $\Delta x/(E\ I)$, which, together with contributions from the two adjacent increments, is referred as shown to stations n and n + 1.

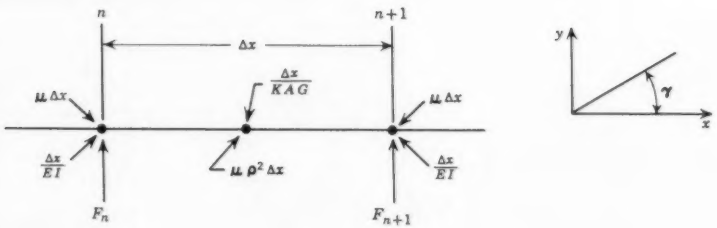

FIG. 2.—INCREMENTAL LENGTH OF BEAM

An electrical analog for this beam increment has already been given[2] and appears in Fig. 3, where all scale factors between corresponding electrical and mechanical parameters are for convenience taken as unity. The upper part of the circuit is devoted, essentially, to the simulation of shear effects, and the lower to moment effects. The capacitances are given the values of corresponding masses and mass moments of inertia, and the inductances correspond to compliances. The voltage at station n is the translational velocity $\dot{y}_n$, and correspondingly for station n + 1. The voltage at station n + $\frac{1}{2}$ is the rotational velocity $\dot{\gamma}_{n+\frac{1}{2}}$, where $\gamma_{n+\frac{1}{2}}$ is the slope of the neutral plane due to bending alone; this must be constant along the whole increment because bending compliance is concentrated at the ends. The supplied currents F_n and F_{n+1} simulate the corresponding load forces.

The currents $V_{n-\frac{1}{2}}$ and $V_{n+\frac{1}{2}}$ simulate the shears immediately to left and right, respectively, of station n, the shear being considered positive when applied in the upward direction by any section to its neighboring section on the right. The currents M_n and M_{n+1} simulate the moments at stations n and n + 1, respectively; moment is considered positive when applied in a counterclockwise direction by any section to its neighbor on the right. The voltage

across one side of the transformer is $\dot{\gamma}_{n+\frac{1}{2}}$, and across the other side $\dot{\gamma}_{n+\frac{1}{2}}$ Δx, so that the magnitude of the turns ratio is Δx, and its polarity can be deduced with the aid of the plus and minus signs on the upper transformer winding.

The validity of the analogy will first be proved by the equilibrium-compatibility method, in a manner which is more suited for the comparison with the energy method than is the proof given in the original paper. Considering shear equilibrium in the beam, we have:

$$V_{n+\frac{1}{2}} = V_{n-\frac{1}{2}} + F_n - \mu \, \Delta x \, \ddot{y}_n \quad \ldots\ldots\ldots\ldots \quad (9)$$

which by Eq. 1 is exactly the equation of current summation at station n in the

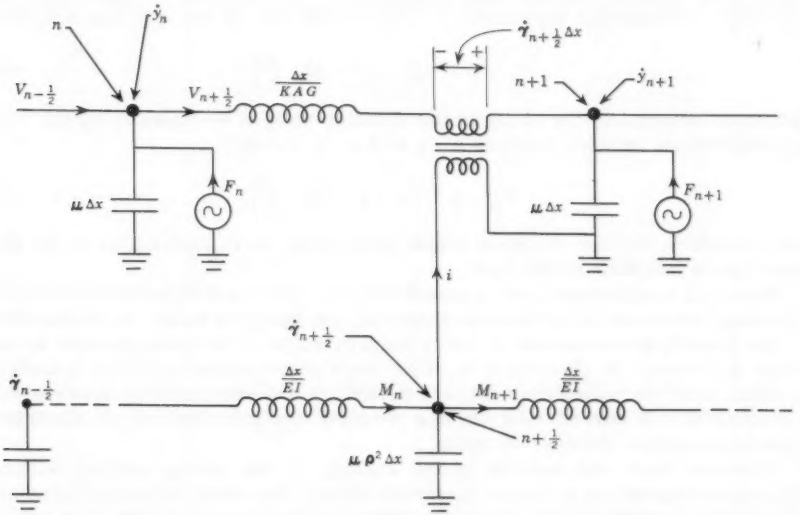

FIG. 3.—ELECTRICAL ANALOG OF BEAM INCREMENT

electrical analog. A corresponding equation holds at station n + 1. Considering moment equilibrium in the beam, we have:

$$M_{n+1} = M_n - V_{n+\frac{1}{2}} \, \Delta x - \mu \, \rho^2 \, \Delta x \, \ddot{\gamma}_{n+\frac{1}{2}} \quad \ldots\ldots\ldots \quad (10)$$

To determine the analogous electrical equation we first evaluate the current i with the aid of Eq. 7, as follows:

$$i \left(1 - V_{n+\frac{1}{2}}\right) \Delta x = 0 \quad \ldots\ldots\ldots\ldots \quad (11a)$$

and

$$i = V_{n+\frac{1}{2}} \, \Delta x \quad \ldots\ldots\ldots\ldots\ldots\ldots \quad (11b)$$

so that Eq. 10 exactly denotes the current summation at station $n + \frac{1}{2}$.

As to the equations of deflection capability, the slope $\gamma_{n+\frac{1}{2}}$ is $1/\Delta x$ times the difference of deflection, due to bending effects alone, between the two ends of the increment; making due allowance for the shear deflection, there results:

$$\gamma_{n+\frac{1}{2}} = \frac{1}{\Delta x}\left[y_{n+1} - y_n + V_{n+\frac{1}{2}}\frac{\Delta x}{K\,A\,G}\right] \quad \ldots\ldots\ldots (12)$$

The corresponding electrical equation, obtained by considering the voltage difference between stations n and n + 1, is:

$$\dot{y}_{n+1} = \dot{y}_n - \frac{\Delta x}{K\,A\,G}\,\dot{V}_{n+\frac{1}{2}} + \dot{\gamma}_{n+\frac{1}{2}}\,\Delta x \quad \ldots\ldots\ldots (13)$$

where use has been made of Eq. 3; this exactly fits the preceding equation (assuming suitable constants of integration). Finally, considering the change of slope between the increment in Fig. 2 and that at the left, one can write

$$\gamma_{n+\frac{1}{2}} - \gamma_{n-\frac{1}{2}} = -\,M_n\,\frac{\Delta x}{E\,I} \quad \ldots\ldots\ldots\ldots\ldots (14)$$

which is effectively the same as the equation yielded by considering the voltage difference between stations $n - \frac{1}{2}$ and $n + \frac{1}{2}$, namely:

$$\dot{\gamma}_{n+\frac{1}{2}} = \dot{\gamma}_{n-\frac{1}{2}} - \dot{M}_n\,\frac{\Delta x}{E\,I} \quad \ldots\ldots\ldots\ldots\ldots (15)$$

and similarly for the change of slope between the increment shown in the figure and its neighbor at the right.

Since all equilibrium and compatibility equations are simulated by corresponding equations in the electrical analog, the latter is valid. Consequently, if the circuit is connected to other such circuits in the same manner as the beam increment is connected to other such increments, and if the boundary conditions of force (and moment) and deflection are simulated by corresponding conditions of current and voltage respectively, then the overall electrical system simulates the overall beam.

Next we prove the validity of the analogy by the energy method, without explicit consideration of forces and moments and their corresponding currents. The kinetic energy of the beam increment, taken for convenience to extend from just to the left of station n to a point just to the left of station n + 1, is

$$E_k = \frac{1}{2}\left[\mu\,\Delta x\,\dot{y}_n^2 + \mu\,\rho^2\,\Delta x\,\dot{\gamma}^2{}_{n+\frac{1}{2}}\right] \quad \ldots\ldots\ldots (16)$$

By Eq. 2, this is exactly simulated in the analog in the form of capacitive energy. To calculate the strain energy in the beam, note that the deflection difference between stations n and n + 1 due to shear alone is

$$y_{n+1} - \gamma_{n+\frac{1}{2}}\,\Delta x - y_n$$

The strain energy is therefore

$$E_S = \frac{1}{2}\left[\frac{\left(\gamma_{n+\frac{1}{2}} - \gamma_{n-\frac{1}{2}}\right)^2}{\Delta x/(E\,I)} + \frac{\left(y_{n+1} - \gamma_{n+\frac{1}{2}}\,\Delta x - y_n\right)^2}{\Delta x/(K\,A\,G)}\right] \quad \ldots\ldots (17)$$

Since the foregoing expression for the deflection difference due to shear alone is exactly the time-integral of the voltage difference across the inductance $\Delta x/(K\,A\,G)$, then by Eq. 5 the strain energy is exactly simulated by inductive energy in the analog. The analogy is therefore valid, with currents

simulating forces and moments because of the analogous power considerations stated in connection with steps 3 and 4. Thus the equilibrium requirements are automatically simulated by current-summation requirements although currents are not necessarily taken into explicit account in devising the analog.

ANALOG IMPROVEMENT BY ENERGY CONSIDERATIONS

An attempt will now be made to improve the analog by altering the capacitances and inductances so that the energy of the electrical analog will more closely approximate the true energy of the actual beam. While similar improvements can be sought by the equilibrium-compatibility method, their investigation by this method seems less obvious and will not be undertaken here.

First considering the kinetic energy, we shall change Eq. 16 so as to take account of the fact that the mass is in actuality uniformly distributed along

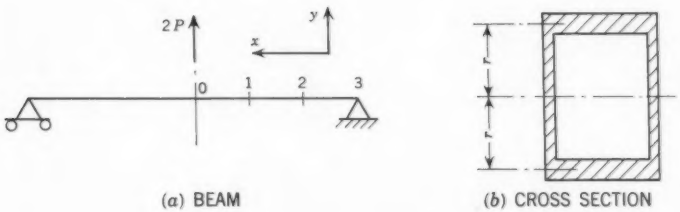

(a) BEAM (b) CROSS SECTION

FIG. 4.—ILLUSTRATIVE EXAMPLE

the beam. In doing so we shall neglect the local deformations caused by shear and bending, so that the beam will be assumed to act as a rigid bar. In that case

$$y = y_n + \gamma_{n+\frac{1}{2}}\, x \quad \ldots\ldots\ldots\ldots\ldots\ldots (18)$$

where x is the distance along the beam, measured from station n. For a differential distance dx the kinetic energy is

$$dE_k = \frac{\mu\, dx}{2}\left[\dot{y}_n + \dot{\gamma}_{n+\frac{1}{2}}\, x\right]^2 + \frac{\mu \rho^2\, dx}{2}\,\dot{\gamma}^2_{n+\frac{1}{2}} \quad \ldots\ldots (19)$$

Since

$$y_{n+1} = y_n + \gamma_{n+1}\,\Delta x \quad \ldots\ldots\ldots\ldots\ldots\ldots (20)$$

then Eq. 19 can be integrated to yield the following value, for the entire beam increment:

$$E_k = \frac{\mu\,\Delta x}{2}\left[\frac{\dot{y}_n^2}{2} + \frac{\dot{y}_{n+1}^2}{2} - \frac{1}{6}\left(\gamma_{n+\frac{1}{2}}\,\Delta x\right)^2\right] + \frac{\mu\rho^2\,\Delta x}{2}\,\dot{\gamma}^2_{n+\frac{1}{2}} \quad \ldots (21)$$

which presumably constitutes a better approximation than Eq. 16.

Next computing the strain energy, we assume that the beam is unloaded except at the end points; this neglects the distributed inertia force and moment. The moment at any point is then

$$M_n - V_{n+\frac{1}{2}}\, x$$

and the differential of the strain energy is, by basic strength of materials,

$$dEs = \frac{dx}{2\,E\,I}\left[M_n - V_{n+\frac{1}{2}}\,x\right]^2 + \frac{dx}{2\,K\,A\,G}\,V^2_{n+\frac{1}{2}} \quad \ldots\ldots\ldots (22)$$

Since

$$M_{n+1} = M_n - V_{n+\frac{1}{2}}\,\Delta x \quad \ldots\ldots\ldots\ldots\ldots (23)$$

then, for the entire beam increment,

$$E_s = \frac{\Delta x}{2\,E\,I}\left[\frac{M_n^2}{2} + \frac{M_{n+1}^2}{2} - \frac{1}{6}\left(V_{n+\frac{1}{2}}\,\Delta x\right)^2\right] + \frac{\Delta x}{2\,K\,A\,G}\,V^2_{n+\frac{1}{2}} \quad \ldots (24)$$

which is strikingly similar to Eq. 21, and is presumably a better approximation than Eq. 17. The term E_s may also be expressed in terms of the deformations, but this is more complicated.

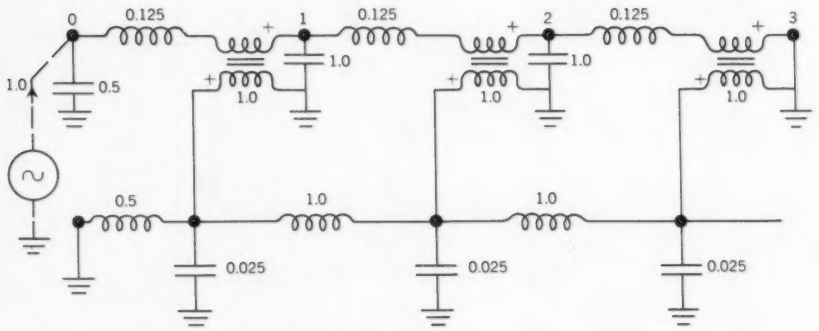

FIG. 5.—CONVENTIONAL ANALOG OF HALF-BEAM

Taking into account that only half of the two capacitances $\mu\,\Delta x$ and the two inductances $\Delta x/(E\,I)$ refer to the n^{th} beam increment itself, it is seen with the aid of Eqs. 2 and 5 that Eqs. 21 and 24 can be satisfied in the analog of Fig. 3 by changing the capacitance in the lower portion and the inductance in the upper portion to the following respective values:

$$\mu\,\rho^2\,\Delta x - \mu\,\frac{(\Delta x)^3}{6} \equiv C_1 \quad \ldots\ldots\ldots\ldots\ldots (25a)$$

and

$$\frac{\Delta x}{K\,A\,G} - \frac{(\Delta x)^3}{6\,E\,I} \equiv L_1 \quad \ldots\ldots\ldots\ldots\ldots (25b)$$

Since only positive capacitance and inductance can be used, the existence of rotary mass moment of inertia (the first term in Eq. 25a) and shear compliance (the first term in Eq. 25b) is actually advantageous in that it serves to improve the accuracy of practical analogs.

ILLUSTRATIVE EXAMPLE

Fig. 4(a) shows a beam hinged at both ends, and having the constant cross section shown in Fig. 4(b). The area of each flange is a, and may be assumed

concentrated at a distance r from the neutral axis. The webs will be considered weightless for simplicity, and are assumed to resist all the shear but none of the moment, the value K A being a.

The problem will be to determine the behavior of the beam after a central transverse force 2 P, which has been built up very slowly, is suddenly removed. Because of symmetry we need consider only the right half of the beam, the left end of which is subject to zero force (after the initial force is removed) and is held to zero slope by an unknown, time-varying moment. The right and experiences zero deflection and zero moment. Fig. 4(a) shows how this half is divided into three equal incremental lengths, and Fig. 5 shows how the conventional analog of Fig. 3 can be arranged with suitable end-conditions to simulate these increments. The following numerical values have been assumed:

$$\Delta x = 1.0 = \sqrt{40}\ r = \sqrt{40}\ \rho \qquad E\,I = 1.0 = 2\,a\,r^2\,E$$

$$\mu = 1.0 \qquad G = 2\,E/5 \qquad P = 1.0$$

The transformer turns ratios are all unity as indicated, with relative winding polarities as shown by the plus signs. As can be judged by inspection of

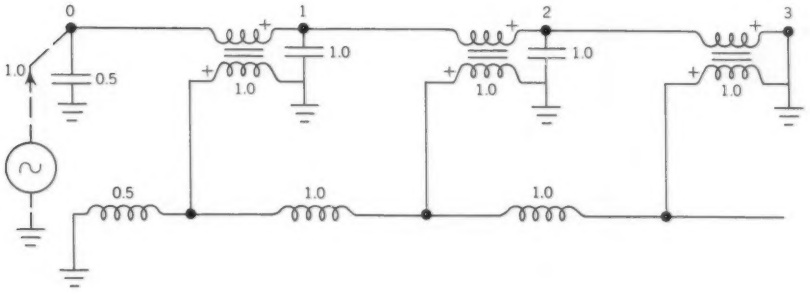

FIG. 6.—IMPROVED ANALOG OF HALF-BEAM

Fig. 5, the effects of direct shear compliance and rotary inertia are small but appreciable.

Fig. 6 shows the improved half-beam analog resulting from the application of Eqs. 25 to Fig. 3. The upper inductances and lower capacitances have been omitted because their values are negative, being theoretically equal to -1/24 and -17/120, respectively.

The accuracy of the analogs of Figs. 5 and 6 has been determined by analytical means, on the assumption of negligible imperfections of the electrical components. Considering first the initial conditions, it is theoretically necessary only to assume that the current generator in Figs. 5 and 6 supplies a steady direct current as shown. In practice, because no transformer is even approximately effective for direct current, it is necessary to maintain appropriate initial currents in the various portions of the analogs by separate auxiliary means, which is however not difficult. On comparing the initial analog behavior with the theoretically exact behavior of the continuous beam, it is

found that all the initial flexural slopes at the half-stations in both analogs have the same error, namely 2.8% of the maximum initial slope of 4.5 (in magnitude) at the right end of the beam. The initial deflection errors Δy, expressed as percentages of the maximum initial deflection y_0, are shown in Fig. 7 by curves 3C and 3I for the conventional and improved analogs, respectively; the increased accuracy of the improved analog is plainly evident. Inspection of the relative size of the inertia-force capacitors (in the upper portion of the circuit) and inertia-moment capacitors (in the lower portion) in Fig. 5 shows that deflections, in general, are far more important than slopes in determining the kinetic energy, although slopes may be important in determining the elastic energy.

In order to get some idea of the effect of an increased number of finite-difference increments, the initial errors have also been worked out for the four-increment analogs corresponding to Figs. 5 and 6. In the improved analog it is found that the lower capacitances are still negative, but the upper inductances now have the positive value 3/128. The resulting initial deflection

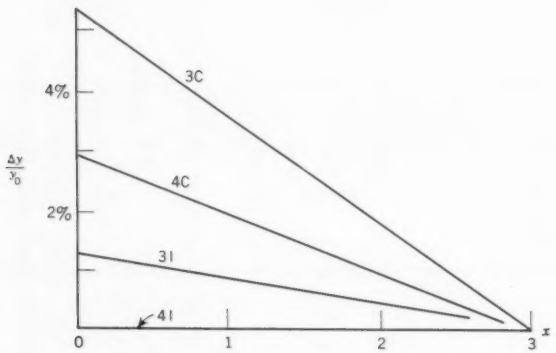

FIG. 7.—INITIAL DEFLECTION ERRORS

errors are shown in Fig. 7 by curves 4C and 4I for the conventional and improved analogs, respectively. The half-station initial slope errors are all 1.6% of the maximum initial slope.

The deflection errors in the dynamic case have been obtained only for the three-increment analogs of Figs. 5 and 6, by comparing the response of these analogs with that of the actual continuous beam. For a time duration not exceeding one full cycle of the fundamental mode of vibration, the latter response can be expressed to within an accuracy of 1/3% of the maximum initial deflection as follows:

$$y = 9.174 \sin \frac{\pi x}{6} \cos 0.2687\, t - 0.143 \sin \frac{3\pi x}{6} \cos 2.1188\, t + 0.026 \sin \frac{5\pi x}{6} \cos 4.9045\, t \quad \ldots\ldots\ldots\ldots (26)$$

where x is measured from the right end of the half-beam. The errors Δy_0, Δy_1, and Δy_2 at stations 0, 1, and 2 of the beam, expressed as percentages of

the maximum deflection in the initial condition, are shown in Fig. 8. The gain in accuracy resulting from the use of the improved analog is seen to be drastic. Further, the improved analog has fewer electrical components than the conventional analog, for the same number of increments.

CONCLUSIONS

It seems reasonable to expect that these same advantages of the improved analog may apply to many other types of beams than the one treated previously, with the following results:

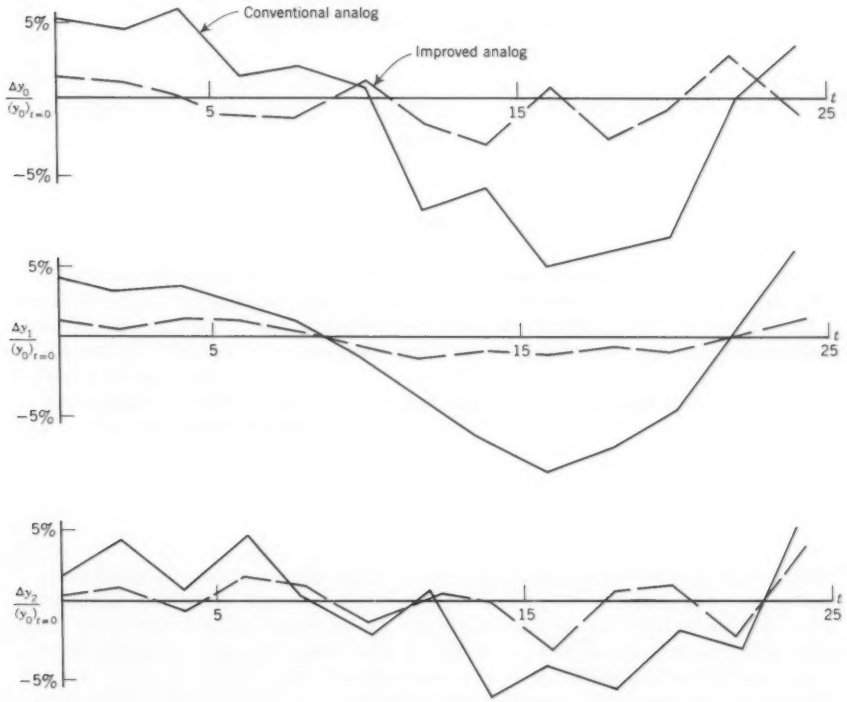

FIG. 8.—RELATIVE DEFLECTION ERRORS AS A FUNCTION OF TIME t

1. For a given allowable overall error, the number of required beam increments may be reduced.
2. The average number of electrical components per beam increment may be reduced.
3. Because the total number of electrical components is reduced as a result of the above two considerations, the sensitivity of the analog to unavoidable imperfections of the electrical components may be reduced, thus further increasing the overall accuracy. An important practical consequence is that

greater imperfections may be allowed in the components, thus greatly reducing their cost since this is usually a sensitive function of the allowable imperfections.

Another way of expressing these advantages is that, for a given analog installation, the complexity of problems which may be handled with a given allowable error is increased.

ACKNOWLEDGMENT

Thanks is given to Melvin Zaid, of Teknik, Inc., Garden City, N. Y., for assistance in clarifying the basic ideas relating to the improved analog.

Journal of the
ENGINEERING MECHANICS DIVISION
Proceedings of the American Society of Civil Engineers

ELASTIC-PLASTIC ANALYSIS OF TRANSVERSELY LOADED PLATES

By John F. Brotchie,[1] M. ASCE

SYNOPSIS

The flexural behavior of thin plates in the post elastic range is discussed. An elastic, purely-plastic relationship between moment and curvature is assumed, and general solutions developed from small deflection theory, for axi-symmetrical yielding over an area, and axi-symmetrical and unsymmetrical yielding along lines.

Applications include the inelastic analysis of metal plates, pavement slabs, and continuous plate structures.

INTRODUCTION

The study of inelastic bending in plates might be considered to have developed along two paths, the classical approach used for metals, and the rather more phenomenalogical basis of the yield line theory for reinforced concrete.

The classical study of plasticity appears to have originated in 1864, when Tresca (1)[2] published a preliminary account of punching and extrusion tests, and deduced that yielding occurred when the maximum shearing stress attained a critical value. Among various other criteria suggested, was that of von Mises (2), derived mathematically, and shown by Hencky (3) to imply that the elastic shear strain energy is the critical factor. Considerable progress has since been made, particularly during the 1950's, in the case of plates, but the criteria of Tresca and von Mises remain as a basis for the theory.

Note.—Discussion open until March 1, 1961. To extend the closing date one month, a written request must be filed with the Executive Secretary, ASCE. This paper is part of the copyrighted Journal of the Engineering Mechanics Division, Proceedings of the American Society of Civil Engineers, Vol. 86, No. EM 5, October, 1960.

[1] Senior Structural Engr., Commonwealth Dept. of Works, Melbourne, Australia.

[2] Numerals in parentheses, thus (1), refer to corresponding items in the Bibliography. See Appendix III.

The study of yield lines or fracture lines in reinforced concrete and similar materials is based on the work of Bach (4), who determined the yield moment for a square slab or plate, and of Ingerslev (5), who extended the theory to rectangular plates. The theory has been subsequently developed by Johansen (6), (7), (8), to the point where it may be simply applied to the determination of ultimate flexural capacity for a wide range of loading and support conditions.

A description (in English) of the yield line theory for reinforced concrete plates is presented in a paper by Hognestad (9), and progress in the classical theory has been summarized by Hodge (10).

The emphasis, in general, has been centered on the development of methods for limit design, where yielding at a boundary or throughout the plate normally reduces the problem to simple statics. A knowledge of behavior in the intermediate stages of yielding is also important however, because deformation, particularly in thin plates, may be the most severe criterion of failure.

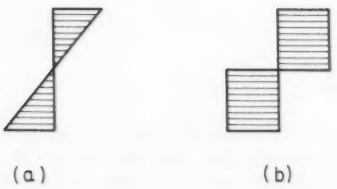

FIG. 1.—ELASTIC (a), AND SIMPLIFIED PLASTIC (b), STRESS BLOCKS

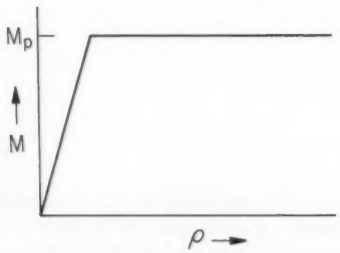

FIG. 2.—MOMENT—CURVATURE RELATIONSHIP

Notation.—The letter symbols adopted for use in this paper are defined where they first appear, in the illustrations or in the text, and are arranged alphabetically, for convenience of reference, in Appendix II.

THEORY

General.—The present paper is limited in scope to small deflections in an ideally elastic-plastic plate with no strain hardening range. The plate is considered initially to be uniformly thin and to be composed of a homogeneous, isotropic material. Other applications of the solutions developed are also noted, and the case of linear strain hardening has been treated separately elsewhere (21).

The distribution of pure bending stress in the elastic range is assumed to be as shown in Fig. 1(a), and in the post elastic range, in Fig. 1(b), and consequently, the relationship between moment and curvature may be approximated as in Fig. 2.

Thus for pure, one-way bending of the plate, the yield moment, M_p in Fig. 2, is given by

$$M_p = M_y = \frac{\sigma_y t^2}{4} \quad \ldots\ldots\ldots\ldots\ldots\ldots (1)$$

in which σ_y is the yield stress in simple tension or compression, and t is the thickness of the plate. The magnitude of the yield moment, when other stresses are present, may be obtained from the yield criteria of Tresca or von Mises, which have been found to be the simplest and most satisfactory for isotropic, ductile metals.

Tresca's yield stress criterion may be written in the form

$$\sigma_1 - \sigma_3 = k_1 \quad (\sigma_1 \geq \sigma_2 \geq \sigma_3) \quad \ldots\ldots\ldots\ldots (2)$$

and von Mises' may be expressed

$$(\sigma_1 - \sigma_2)^2 + (\sigma_2 - \sigma_3)^2 + (\sigma_3 - \sigma_1)^2 = k_2 \quad \ldots\ldots\ldots\ldots (3)$$

in which σ_1, σ_2, and σ_3 are principal stresses. The constants k_1 and k_2 are easily evaluated with $\sigma_2 = \sigma_3 = 0$, in a simple tension test, and are $k_1 = \sigma_y$ and $k_2 = 2\sigma_y^2$.

In deriving criteria for yield moments from these stresses, the orientation of the axes of reference with respect to the directions of principal stress must be considered. It follows also, that the distribution of bending and shear stresses at the critical section must be determined or assumed. Integration over the depth of the plate then gives the relationships required (see Appendix I).

In the particular case of axi-symmetrical bending, using polar coordinates, if radial shear is assumed, for simplicity, to be carried only by a central core, the Tresca criterion for plastic radial moment is

$$k\,M_r = M_y \quad \ldots\ldots\ldots\ldots\ldots\ldots (4a)$$

for bending in the first quadrant, that is for moments of the same sign, or

$$k\,M_r = M_\phi - M_y \quad \ldots\ldots\ldots\ldots\ldots\ldots (4b)$$

where bending is in the second quadrant,[2] and moments are of opposite sign. For convention used see Fig. 3. Yield moments in the third and fourth quadrants are obtained by substituting $-M_y$ for M_y in Eqs. 4 through 10. The von Mises criterion in each quadrant is

$$k^2 M_r^2 - k\,M_r\,M_\phi + M_\phi^2 = M_y^2 \quad \ldots\ldots\ldots\ldots (5)$$

In these equations, M_r and M_ϕ are radial and tangential moments respectively, and

$$k = 1 \Big/ \left[1 - \left(\frac{Q_r}{Q_y}\right)^2\right] \quad \ldots\ldots\ldots\ldots\ldots\ldots (6)$$

in which Q_r is the radial shear, and Q_y is the capacity of the plate in pure shear, as determined from the appropriate yield criterion.

If, for comparison, the shear stress were small and were arbitrarily assumed to be distributed uniformly through the depth of the plate, the Tresca criterion for radial yield would be given, approximately, by

$$M_r = \left[1 - \frac{1}{2}\left(\frac{Q_r}{Q_y}\right)^2\right] M_y \quad \ldots\ldots\ldots\ldots\ldots\ldots (7a)$$

or

$$M_r = M_\phi - \left[1 + \frac{1}{2}\left(\frac{Q_r}{Q_y}\right)^2 \frac{M_y}{M_\phi - M_y}\right] M_y \quad \ldots\ldots\ldots\ldots \quad (7b)$$

Introducing the further assumption that the stress blocks for moment are rectangular, the von Mises criterion becomes

$$M_r^2 - M_r M_\phi + M_\phi^2 = \left[1 - \left(\frac{Q_r}{Q_y}\right)^2 \left(1 - \frac{2}{3}\frac{M_\phi}{M_r}\right)\right] M_y^2 \quad \ldots\ldots\ldots \quad (8)$$

In particular cases of axi-symmetrical bending, a distribution of shear and bending stresses may be determined from the equations for equilibrium of an element and the Tresca yield criterion, by extending the method of solution described by Drucker (11) for a rectangular beam. For the limiting cases considered in Appendix I, the resultant radial yield moment is given by

$$M_r = \left[1 - \frac{1}{3}\left(\frac{Q_r}{Q_y}\right)^2\right] M_y \quad \ldots\ldots\ldots\ldots\ldots\ldots \quad (9a)$$

where bending is in the first quadrant, and

$$M_r = M_\phi - \left[1 + \frac{1}{3}\left(\frac{Q_r}{Q_y}\right)^2 \frac{M_y}{M_\phi - M_y}\right] M_y \quad \ldots\ldots\ldots\ldots \quad (9b)$$

for bending in the second quadrant. The assumption is made in each case, that loading in the region of the critical section is zero, or of uniform intensity, and that the powers $\left(\frac{Q_r}{Q_y}\right)^4$, and higher, are sufficiently small to be neglected. Eqs. 9 have approximate application to symmetrical bending, in general, provided these conditions are reasonably satisfied, as discussed in Appendix I. Eqs. 9 apply to yielding at an internal, or external, circular boundary, and in the limit where the radius of the critical section approaches infinity, to one-way bending in the plate.

The stress distributions determined in each case lay between the two extremes previously assumed and produce a greater moment of resistance than either.

Generally, shear effects will be insignificant. The slight moment reduction due to shear tends to be offset by a higher yield stress in bending than is obtained in simple tension, apparently due to non-uniform strain and a smaller volume of yield involved. Furthermore, at points of maximum shear the moment curve is generally steepest and the above factors are accentuated. The moment criteria of Tresca and von Mises reduce respectively to

$$M_r = M_y \quad \ldots\ldots\ldots\ldots\ldots\ldots \quad (10a)$$

or

$$M_r = M_\phi - M_y \quad \ldots\ldots\ldots\ldots\ldots\ldots \quad (10b)$$

and

$$M_r^2 - M_r M_\phi + M_\phi^2 = M_y^2 \quad \ldots\ldots\ldots\ldots \quad (11)$$

These relationships are shown diagrammatically in Fig. 3.

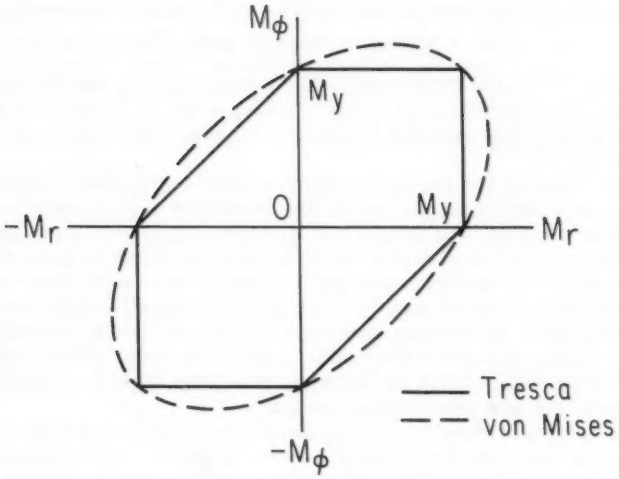

FIG. 3.—YIELD MOMENT CRITERIA

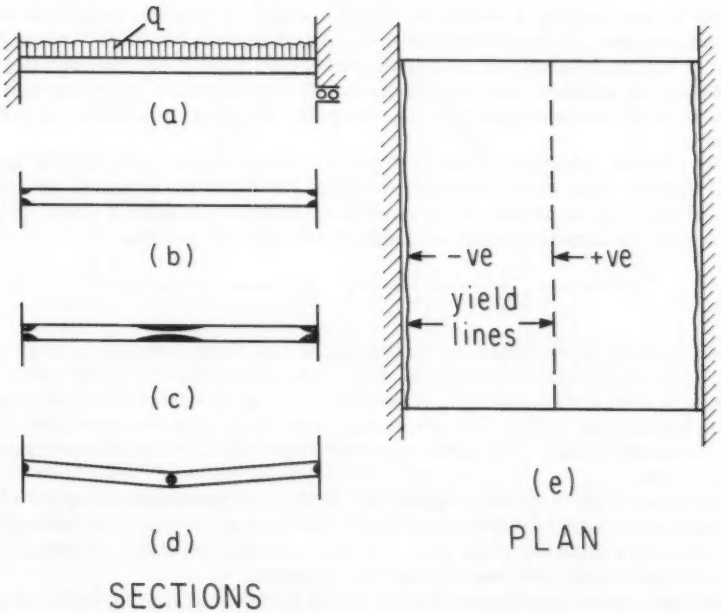

FIG. 4.—YIELDING IN CLAMPED, ONE-WAY PLATE

For the general case of unsymmetrical bending, with polar coordinates, the yield criterion of von Mises is the simpler, and may be expressed as

$$M_r^2 - M_r M_\phi + M_\phi^2 + 3 M_{r\phi}^2 = M_y^2 \quad \ldots\ldots\ldots (12)$$

where $M_{r\phi}$ is the twisting moment. The above criteria may be expressed in rectangular coordinates (u, v) by substituting u and v, in which u and v are directions of principal moment, in the case of Eqs. 4 through 11, for r and ϕ in Eqs. 4 through 12.

Yielding.—Where the requirements of statics or the geometry of the plate prescribe that moments should vary in the directions of yield, yielding will tend to be confined to lines, and the plate will remain elastic except at these lines. Where no such requirement exists, yielding may extend over an area of the plate.

In the case of first quadrant bending, yielding over an area may occur either in one direction of principal moment only, in which case the plate behaves elastically in the other, or yielding may occur in each direction, causing the plate to act essentially as a membrane under additional loads. When bending is in the second quadrant, yielding occurs simultaneously in each direction of principal moment, but in a predictable manner.

A simple example in which yielding is confined to lines is a uniformly loaded one-way plate, clamped at each end as shown in Fig. 4. In the elastic range of stresses, maximum moment occurs at the supports, with maximum stress in the extreme fibers; it is here that yielding commences. Under increasing load, the yielding extends to the middle surface of the plate, and the plastic moment M_p (Fig. 2) is reached. Further load produces rotation at the ends without increase in restraining moment, so that, in effect, a "plastic hinge" is formed at each support. Under additional loads, the plate behaves as if it were pinned at each end, the moment at the center increasing until it too reaches M_p, and a third hinge is formed. An arbitrarily small load increase produces unlimited rotation about these hinges causing the plate to fold and collapse as a mechanism.

The zones of yield are shown in Fig. 4(c). Since the width of yield is greater at the midspan than at the supports, because the different slopes of the bending moment diagram at these points results in different lengths of plate, in which the (actual) maximum elastic moment M_e is exceeded where

$$M_e = \frac{\sigma_y t^2}{6} = \frac{2}{3} M_y \quad \ldots\ldots\ldots\ldots\ldots (13)$$

Viewed in plan, these zones, or hinges, appear as bands over the surface of the plate. For the purpose of analysis, each band is considered to be reduced, in width, to a line, and is termed a yield line. This is consistent with the approximation introduced in Fig. 2, in which the plate is considered to remain elastic up to the moment M_p. The errors produced by this assumption are normally insignificant.

The lines at the edge of the plate (Fig. 4(e)) are produced by negative moments and are termed negative yield lines. The line at the center is correspondingly termed a positive yield line. Further distinction might be made on the basis of whether or not shear forces are present.

The three lines together form a yield line pattern. Yield line patterns might themselves be classified by the degree to which they contribute to failure by collapse of the plate, and on this basis, a pattern might be divided into one of three groups.

The first group consists of patterns that form a complete failure mechanism, allowing collapse by folding of the plate as in the previous example.

The second group of patterns requires some contributing cause such as tension, compression, or shear failure to produce collapse. A uniformly loaded square plate, simply supported on all sides and producing the yield line pattern shown in Fig. 5, is typical of this group. Here a purely flexural failure is impossible and tensile yielding across the diagonals or buckling along the edges is necessary to produce collapse.

The third group consists of yield patterns that are active only during a certain stage of deformation in the plate and do not contribute directly to collapse. The line of distinction between groups two and three is not always particularly

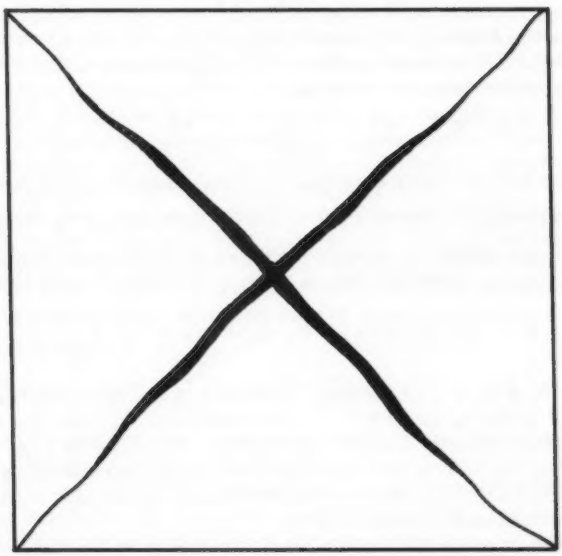

FIG. 5.—YIELD LINES, UNIFORMLY LOADED, SIMPLY SUPPORTED, SQUARE PLATE (NEGLECTING CORNER EFFECT).

sharp. An example of the third group is the yield pattern that forms around a cylindrical support in a continuous plate (Fig. 9(a-c)).

Patterns of the first and second groups are normally capable of analysis by simple statics, whereas patterns of the third group generally are not; these will be considered in particular.

Thus, for bending in the inelastic range, yielding may be confined to lines or may extend over areas of the plate. If the moment curvature relationship is assumed to be approximated by Fig. 2, the lines may be considered of zero width. For the same reason, the yield areas may be considered to have definite boundaries.

Method of Analysis.—For the purpose of analysis, the plate may be divided into elastic and inelastic zones or areas, and each zone may be considered separately.

The analysis of a plate on a liquid type elastic foundation will be considered initially, as a general case. The solution for an edge supported plate may then be obtained from this as the limiting case where the density or reaction modulus of the supporting liquid approaches zero. In certain cases, such as continuous plates, it is convenient to consider the reaction modulus to have a small but finite value in order to reduce the interaction of loads and reactions, and so simplify the analysis (19), (20).

Considering, firstly, the elastic portions of the plate, the differential equation for deflection, w, is given by

$$\nabla^4 w = (q - \gamma w)/D \quad \ldots\ldots\ldots\ldots\ldots \quad (14a)$$

in which q is the intensity of lateral load, γ is the density or reaction modulus of the foundation, D is the flexural rigidity of the plate, and ∇^2 is the Laplace operator, the polar form of which is

$$\nabla^2 \equiv \frac{\partial^2}{\partial r^2} + \frac{1}{r}\frac{\partial}{\partial r} + \frac{1}{r^2}\frac{\partial^2}{\partial \phi^2} \quad \ldots\ldots\ldots\ldots\ldots \quad (14b)$$

where r and ϕ are the polar coordinates. (The case of a point load on the plate was first considered by Hertz (12) in 1884.) Introducing $\frac{1}{s^4}$ for $\frac{\gamma}{D}$, and x for $\frac{r}{s}$, in which s is the radius of relative stiffness of the floating plate, the solution of the homogeneous equation (that is, with q = 0) may be expressed as

$$w = \sum_{n=0,1}^{\infty} Re\left[A_n J_n(x\sqrt{i}) + B_n H_n^{(1)}(x\sqrt{i})\right] \begin{Bmatrix}\cos n\phi \\ \sin n\phi\end{Bmatrix} \quad \ldots\ldots \quad (15)$$

where $J_n(\ )$ and $H_n(\ )$ are Bessel functions of the first and third kinds respectively, of order n, and $i \equiv \sqrt{-1}$. The constants A_n, and B_n, are complex and are evaluated from the boundary conditions. The functions $J_0(\ )^{(1)}$, $J_i(\ )$, $H_0^{(1)}(\ )$, and $H_i^{(1)}(\ )$, or their mathematical equivalents, are tabulated elsewhere (16), (17), (18), and functions of higher order may be obtained from these using recurrence formulae (18).

Where there is more than one internal boundary in the plate, it is convenient to consider the two functions of x in the solution separately and superimpose the results. Thus, the plate may be considered to be initially infinite and the conditions at the positions of the boundaries satisfied by superposition.

The external problem of deflection produced in the surrounding plate by a deformation at or within an internal boundary, whether due to loading, temperature variation, or yielding, is given by the series

$$w = \sum_{n=0,1}^{\infty} Re\left[B_n H_n^{(1)}(x\sqrt{i})\right] \begin{Bmatrix}\cos n\phi \\ \sin n\phi\end{Bmatrix} \quad \ldots\ldots\ldots \quad (16)$$

In a particular case, the solution may usually be expressed in terms of the cosine series only, by choosing a suitable origin for ϕ.

Likewise, the internal problem of deflection within an external boundary produced by forces or by yielding at or outside the edge is given by the series

$$w = \sum_{n=0,1}^{\infty} Re\left[A_n J_n(x\sqrt{i})\right] \begin{Bmatrix}\cos n\phi \\ \sin n\phi\end{Bmatrix} \quad \ldots\ldots\ldots \quad (17)$$

Thus, Eq. 16 is used to describe the conditions at each internal boundary in the infinite plate and Eq. 17 to satisfy the conditions at the external boundary. The constants in each equation are evaluated with all loads and boundary effects superimposed.

Where the boundaries remain elastic, the conditions for a clamped boundary are that w and $\frac{\partial w}{\partial n}$ are zero, in which n is the normal to the edge Similarly, for a simply supported edge, $w = 0$ and $M_n = 0$; and at a free edge, $M_n = 0$ and $V_n = 0$. ($V_u \equiv Q_u - \partial M_{uv}/\partial_v$, the effective shear at the edge.) In the case of an integral elastic support the conditions of continuity must be fulfilled, and in the case of a non-integral elastic support the displacements must be compatible.

Where a yield line occurs at a clamped boundary, the boundary conditions are $w = 0$ as before, and $M_n = M_p$, where M_p is the appropriate plastic moment. The subscript n, in this case, is the direction of yield, which does not necessarily remain normal to the (original) line as load increases. Where a straight yield line develops within the plate, and not at a boundary (of a support, load, or change in plate thickness), it may be treated as a boundary in itself and the conditions $M_n = M_p$ and $Q_n = 0$ satisfied, except at an intersection of more than two lines, or at points where the line meets a boundary in the plate. Deflections, in each case, are assumed to be continuous at the line.

An incomplete line may be considered as an internal boundary and be described by the series of Eq. 16. Alternatively, the moment condition $M_n = M_p$ might be considered to be satisfied by a row of coupled point loads, or concentrated moments, acting along each edge of the line, in the normal direction n. The deflection produced by a balanced pair of these concentrated moments is given by

$$w = C\,R\,e\left[\left(\cos^2\phi\,\frac{\partial^2}{\partial x^2} - \sin^2\phi\,\frac{\partial}{x\,\partial x}\right)H_o^{(1)}\,(x\sqrt{i})\right] \ldots\ldots (18)$$

where C is a real constant, and ϕ is measured from the direction n. Integration along the line of yield gives the solution required.

If a yield line at a boundary is incomplete, the appropriate elastic and yield conditions are applied at the respective sections involved. The extent of yield, in the general case, is necessarily determined by trial.

Hence, where yielding is confined to a line it may be treated as a boundary condition. Expressions for moments and shears in terms of deflections, in the elastic zones of the plate, are available elsewhere (15), (20).

Where bending is axi-symmetrical, and yielding extends over an area, expressions for deflection may be obtained by modifying the procedures used for a purely elastic zone. The maximum shearing stress criterion will be adopted in this case, and for yielding in the first quadrant three different conditions are possible; for tangential yielding only,

$$M_\phi = M_y > M_r \quad (\sigma_\phi > \sigma_r > \sigma_z) \ldots\ldots\ldots\ldots (19a)$$

and plastic strain is confined to the ϕz plane, where z is the direction normal to the plate. The direction of the symbol > in Eq. 19a refers to moments in the first quadrant of Fig. 3, and stresses in the lower half of the plate. For radial yielding only,

$$M_r = M_y > M_\phi \quad (\sigma_r > \sigma_\phi > \sigma_z) \ldots\ldots\ldots\ldots (19b)$$

Here plasticity is confined to the rz plane and the only case of practical importance is that in which the yield area is reduced in width to a line. For the condition

$$M_r = M_\phi = M_y \qquad (\sigma_r = \sigma_\phi > \sigma_z) \quad \ldots\ldots\ldots\ldots \quad (19c)$$

yielding may occur in all three directions of principal stress, and the plate behaves essentially as a membrane under additional loads. Hence, the bending in the first quadrant, only the case of tangential yielding (Eq. 19a) need be considered further. For bending in the second quadrant, the yield criterion is

$$M_\phi = M_y + M_r \qquad (\sigma_\phi > \sigma_z > \sigma_r) \quad \ldots\ldots\ldots\ldots \quad (20)$$

and plasticity is restricted to the $r\phi$ plane.

The differential equations for deflection in each case are derived in Appendix I, and it is of interest to compare them with the corresponding equation for an elastic zone. For symmetrical bending in the elastic range, the differential equation for deflection, from Eq. 14a, is

$$w'''' + \frac{2}{r}\, w''' - \frac{1}{r^3}\, w'' + \frac{1}{r^3}\, w' = (q - \gamma\, w)/D \quad \ldots\ldots\ldots \quad (21)$$

For first quadrant bending and tangential yielding only, the corresponding equation, from Appendix I, is

$$w'''' + \frac{2}{r}\, w''' = (q - \gamma\, w)/D_1 \quad \ldots\ldots\ldots\ldots \quad (22)$$

For yielding in the second quadrant, the deflection, w, is conveniently divided into two components; that is

$$w = w_e + w_p \quad \ldots\ldots\ldots\ldots\ldots\ldots \quad (23)$$

in which w_e is produced by the elastic component of radial strain and w_p by the plastic component, resulting in the equations

$$w_e'''' + \frac{1}{r}\, w_e''' = (q - \gamma\, w)/D_2 \quad \ldots\ldots\ldots\ldots \quad (24a)$$

and

$$w_p'' + \frac{1}{r}\, w_p' = 0 \quad \ldots\ldots\ldots\ldots\ldots\ldots \quad (24b)$$

Primes in the preceding equations denote differentiation with respect to r, and D_1 and D_2 are defined as

$$D_1 = \frac{E\, t^3}{12} \quad \ldots\ldots\ldots\ldots\ldots\ldots \quad (25a)$$

and

$$D_2 = \frac{E\, t^3}{12(1 - \mu)} \quad \ldots\ldots\ldots\ldots\ldots\ldots \quad (25b)$$

in which μ represents Poisson's ratio. Introducing the variable $x = r/s$ where $s = \left[\frac{D}{\gamma}\right]^{\frac{1}{4}}$, $\left[\frac{D_1}{\gamma}\right]^{\frac{1}{4}}$, or $\left[\frac{D_2}{\gamma}\right]^{\frac{1}{4}}$ in the different zones of the plate, and setting $q = 0$, Eqs. 21, 22, and 24 reduce, respectively, to

$$w'''' + \frac{2}{x}\, w''' - \frac{1}{x^2}\, w'' + \frac{1}{x^3}\, w' + w = 0 \quad \ldots\ldots\ldots \quad (26)$$

$$w'''' + \frac{2}{x} w''' + w = 0 \quad \ldots\ldots\ldots\ldots\ldots (27)$$

$$w_e'''' + \frac{1}{x} w_e''' + w = 0 \quad \ldots\ldots\ldots\ldots\ldots (28a)$$

$$w_p'' + \frac{1}{x} w_p' = 0 \quad \ldots\ldots\ldots\ldots\ldots (28b)$$

where primes in this case, and from here on, denote differentiation with respect to x. Hence, x has slightly different values in each zone, where Poisson's ratio $\mu \neq 0$.

For an edge supported plate (where $\gamma = 0$) the preceding equations further reduce to

$$w'''' + \frac{2}{x} w''' - \frac{1}{x^2} w'' + \frac{1}{x^3} w' = 0 \quad \ldots\ldots\ldots\ldots (29)$$

$$w'''' + \frac{2}{x} w''' = 0 \quad \ldots\ldots\ldots\ldots\ldots (30)$$

$$w'''' + \frac{1}{x} w_e''' = 0 \quad \ldots\ldots\ldots\ldots\ldots (31a)$$

$$w_p'' + \frac{1}{x} w_p' = 0 \quad \ldots\ldots\ldots\ldots\ldots (31b)$$

where x, in this case, is introduced only for dimensional consistency with Eqs. 26 through 28 and may be replaced by r. The solution of Eq. 26 (from Eq. 15) is

$$w = Re\left[A\, J_o (x\sqrt{i}) + B\, H_o^{(1)} (x\sqrt{i}) \right] \quad \ldots\ldots\ldots\ldots (32)$$

From Eq. 27, the deflection w is

$$w = C_1 R_1 + C_2 R_2 + C_3 R_3 + C_4 R_4 \equiv C_j R_j \quad \ldots\ldots\ldots (33)$$

where R_j are four independent series solutions and C_j are real constants.

$$R_1 = 1 + \sum_{n=4,8,12..}^{\infty} [-1]^{n/4} \frac{x^n}{n(n-1)^2 (n-2).(n-4)\ (n-5)^2\ (n-6)\ldots 4.3^2.2.} \quad \ldots (34a)$$

$$R_2 = x + \sum_{n=5,9,13..}^{\infty} [-1]^{(n-1)/4} \frac{x^n}{n(n-1)^2\ (n-2)\ \ldots\ldots\ldots\ldots 5.4^2.3.} \quad \ldots (34b)$$

$$R_3 = x^2 + \sum_{n=6,10,14..}^{\infty} [-1]^{(n-2)/4} \frac{x^n}{n(n-1)^2\ (n-2)\ \ldots\ldots\ldots\ldots 6.5^2.4.} \quad \ldots (34c)$$

$$R_4 = R_2 \log_e x + \sum_{n=5,9}^{\infty} \left[[-1]^{(n-5)/4} \frac{x^n}{n(n-1)^2 (n-2)\ \ldots\ldots 5.4^2.3.} \right.$$

$$\left. \sum_{r=5,9}^{n} \frac{2(2r^2 - 4r + 1)}{r(r-1)(r-2)} \right] \quad \ldots\ldots\ldots\ldots (34d)$$

Values of R_j and their diravatives (R'_j, R''_j and R'''_j) in the range $0 \leq x \leq 5$ are given in Table 1 and elsewhere (21) (for values of x in the range 0(0.1)10).

TABLE 1

x	R_1	R_1'	R_1''	R_1'''
0	1.000000	0	0	0
0.1	0.999999	-0.555556×10^{-4}	-0.166667×10^{-2}	-0.333333×10^{-1}
0.2	0.999978	-0.444444×10^{-3}	-0.666665×10^{-2}	-0.666660×10^{-1}
0.3	0.999888	-0.149999×10^{-2}	-0.149998×10^{-1}	-0.999952×10^{-1}
0.4	0.999644	-0.355548×10^{-2}	-0.266653×10^{-1}	-0.133313
0.5	0.999132	-0.694408×10^{-2}	-0.416615×10^{-1}	-0.166605
0.6	0.998200	-0.119987×10^{-1}	-0.599846×10^{-1}	-0.199846
0.7	0.996666	-0.190517×10^{-1}	-0.816278×10^{-1}	-0.233000
0.8	0.994312	-0.284345×10^{-1}	-0.106580	-0.266017
0.9	0.990890	-0.404774×10^{-1}	-0.134824	-0.298829
1.0	0.986117	-0.555083×10^{-1}	-0.166336	-0.331350
2.0	0.779288	-0.438408	-0.645558	-0.603449
3.0	-0.864722×10^{-1}	-1.397546	-1.262089	-0.528380
4.0	-2.175345	-2.801888	-1.367942	0.559498
5.0	-5.471925	-3.488111	0.487812	3.518006

x	R_2	R_2'	R_2''	R_2'''
0	0	1.000000	0	0
0.1	0.100000	0.999998	-0.833333×10^{-4}	-0.250000×10^{-2}
0.2	0.199999	0.999967	-0.666666×10^{-3}	-0.999997×10^{-2}
0.3	0.299990	0.999831	-0.224998×10^{-2}	-0.224996×10^{-1}
0.4	0.399957	0.999467	-0.533321×10^{-2}	-0.399979×10^{-1}
0.5	0.499870	0.998698	-0.104161×10^{-1}	-0.624919×10^{-1}
0.6	0.599676	0.997300	-0.179979×10^{-1}	-0.899757×10^{-1}
0.7	0.699300	0.994998	-0.285772×10^{-1}	-0.122439
0.8	0.798635	0.991468	-0.426511×10^{-1}	-0.159863
0.9	0.897540	0.986335	-0.607144×10^{-1}	-0.202223
1.0	0.995834	0.979176	-0.832589×10^{-1}	-0.249479
2.0	1.867195	0.669045	-0.657159	-0.966755
3.0	2.007760	-0.626825	-2.088661	-1.875383
4.0	0.878164×10^{-3}	-3.734699	-4.146898	-1.956127
5.0	-6.063151	-8.545081	-4.979717	1.066036

x	R_3	R_3'	R_3''	R_3'''
0	0	0	2.000000	0
0.1	0.100000×10^{-1}	0.200000	1.999995	-0.200000×10^{-3}
0.2	0.399999×10^{-1}	0.399997	1.999920	-0.160000×10^{-2}
0.3	0.899988×10^{-1}	0.599976	1.999595	-0.539996×10^{-2}
0.4	0.159993	0.799898	1.998720	-0.127997×10^{-1}
0.5	0.249974	0.999688	1.996875	-0.249986×10^{-1}
0.6	0.359922	1.199222	1.993520	-0.431948×10^{-1}
0.7	0.489804	1.398319	1.987996	-0.685848×10^{-1}
0.8	0.639563	1.596724	1.979524	-0.102361
0.9	0.809114	1.794096	1.967205	-0.145711
1.0	0.998334	1.990003	1.950023	-0.199815
2.0	3.893597	3.681316	1.205919	-1.576337
3.0	7.800144	3.620423	-0.899000	-4.998497
4.0	9.440605	-1.574239	-9.310481	-9.848338
5.0	1.415191	-0.163799×10^{2}	-0.206052×10^{2}	-0.114823×10^{2}

x	R_4	R_4'	R_4''	R_4'''
0	0	$-\infty$	∞	$-\infty$
0.1	-0.230258	-1.302579	0.100002×10^{2}	-0.999936×10^{2}
0.2	-0.321884	-0.609357	5.001462	-0.249814×10^{2}
0.3	-0.361169	-0.203629	3.337355	-0.110784×10^{2}
0.4	-0.366433	0.846424×10^{-1}	2.507998	-6.203353
0.5	-0.346349	0.308840	2.013296	-3.941068
0.6	-0.305995	0.492803	1.686358	-2.709344
0.7	-0.248699	0.649277	1.455430	-1.966591
0.8	-0.176800	0.785869	1.284386	-1.486986
0.9	-0.920235×10^{-1}	0.907464	1.152899	-1.162957
1.0	0.430397×10^{-2}	1.017348	1.048514	-0.938103
2.0	1.431206	1.738134	0.421016	-0.708572
3.0	3.220881	1.631206	-0.858161	-2.040522
4.0	3.999928	-0.582715	-3.918171	-4.100659
5.0	0.707198	-6.801707	-8.660231	-4.862110

Primes in each case denote differentiation with respect to x.

For yielding in the second quadrant, Eq. 28b gives

$$w_p = C_5 \log_e x + C_6 \quad \ldots\ldots\ldots\ldots \quad (35a)$$

and substituting for w_p in Eq. 28a gives

$$w_e = C_1 S_1 + C_2 S_2 + C_3 S_3 + C_4 S_4 + C_5 S_5 - C_6 \equiv C_j S_j - C_6 \quad \ldots(35b)$$

in which S_1 through S_4 are four independent solutions to the homogeneous equation (in w_e), and $(C_5 S_5 - C_6)$ is the particular integral. Hence,

$$S_1 = 1 + \sum_{n=4,8,12}^{\infty} [-1]^{n/4} \frac{x^n}{n(n-1)\,(n-2)^2.(n-4)\,(n-5)\,(n-6)^2.\ldots..4.3.2^2.} \quad \ldots \quad (36a)$$

$$S_2 = x + \sum_{n=5,9,13}^{\infty} [-1]^{(n-1)/4} \frac{x^n}{n(n-1)\,(n-2).^2 \ldots\ldots\ldots\ldots 5.4.3^2.} \quad \ldots \quad (36b)$$

$$S_3 = x^2 + \sum_{n=6,10,14}^{\infty} [-1]^{(n-2)/4} \frac{x^n}{n(n-1)\,(n-2.^2 \ldots\ldots\ldots\ldots 6.5.4^2.} \quad \ldots \quad (36c)$$

$$S_4 = S_3 \log_e x + \sum_{n=6,10}^{\infty} \left[[-1]^{(n-6)/4} \frac{x^n}{n(n-1)\,(n-2).^2\ldots..6.5.4^2.} \sum_{r=6,10}^{n} \frac{4r^2 - 7r + 2}{r(r-1)(r-2)} \right] \quad \ldots\ldots\ldots\ldots \quad (36d)$$

$$S_5 = \sum_{n=4,8}^{\infty} [-1]^{n/4} \left[\frac{x^n \log_e x}{n(n-1)(n-2)^2\ldots4.3.2^2} - \frac{x^n}{n(n-1)(n-2)^2..4.3.2^2} \sum_{r=4,8}^{n} \frac{4r^3 - 15r^2 + 16r - 4}{r(r-1)\,(r-2)} \right] \quad \ldots\ldots\ldots\ldots \quad (36e)$$

For the particular case of an edge supported plate, the solution of Eq. 29, for bending in the elastic range, is

$$w = C_1 + C_2 x^2 + C_3 \log_e x + C_4 x^2 \log_e x. \quad \ldots\ldots\ldots\ldots \quad (37)$$

Likewise, for tangential yield and first quadrant bending, the deflection from Eq. 30 is

$$w = C_1 + C_2 x + C_3 x^2 + C_4 x \log_e x \quad \ldots\ldots\ldots\ldots \quad (38)$$

and, for yielding in the second quadrant, from Eq. 31,

$$w_e = C_1 + C_2 x + C_3 x^2 + C_4 x^2 \log_e x \quad \ldots\ldots\ldots\ldots \quad (39a)$$

$$w_p = C_5 \log_e x + C_6 \quad \ldots\ldots\ldots\ldots \quad (39b)$$

Eqs. 37 to 39a might alternatively have been obtained from the condition that, in the limit $\gamma \to 0$, $x(= r/s)$ also approaches zero, and that only the first term

in each series solution for the plate on a liquid support is significant. An example would be, in Eq. 33 as $\gamma \to 0$,

$$R_1 \to 1,\ R_2 \to x,\ R_3 \to x^2,\ \text{and}\ R_4 \to x \log_e x,$$

so that the solution for w in Eq. 33 approaches the solution for w in Eq. 38.

Cases of nearly symmetrical yielding may be approximated by the symmetrical case, but less symmetrical yielding is not so easily analyzed. Fortunately, where bending is unsymmetrical, yielding tends to a greater extent to be confined to (single) lines, so that a wide range of problems may still be readily handled.

For symmetrical bending in the elastic range, moments and shears may be expressed as derivatives of deflection. As example,

$$M_r = -D \left[\frac{d^2w}{dr^2} + \mu \frac{1}{r} \frac{dw}{dr} \right] \quad \ldots\ldots\ldots\ldots (40)$$

$$M_\phi = -D \left[\frac{1}{r} \frac{dw}{dr} + \mu \frac{d^2w}{dr^2} \right] \quad \ldots\ldots\ldots\ldots (41)$$

and

$$Q_r = -D \frac{d}{dr} \nabla^2 w \quad \ldots\ldots\ldots\ldots (42)$$

In the case of first quadrant bending and tangential yield, the corresponding relationships are, from Appendix I,

$$M_r = -D_1 \frac{d^2w}{dr^2} + \nu M_y \quad \ldots\ldots\ldots\ldots (43)$$

$$Q_r = -D_1 \left[\frac{d^3w}{dr^3} + \frac{1}{r} \frac{d^2w}{dr^2} \right] - \frac{1}{r} (1 - \nu) M_y \quad \ldots\ldots\ldots\ldots (44)$$

and the value of M_ϕ from Eq. 19a holds.

For yielding in the second quadrant

$$M_r = -D_2 \frac{d^2w_e}{dr^2} + \frac{\nu}{1 - \nu} M_y \quad \ldots\ldots\ldots\ldots (45)$$

$$Q_r = -D_2 \frac{d^3w_e}{dr^3} - \frac{1}{r} M_y \quad \ldots\ldots\ldots\ldots (46)$$

and the value of M_ϕ given in Eq. 20 holds.

Hence, for the case of a plate on an elastic foundation and symmetrical bending in the elastic range, setting

$$w = \frac{s^2}{D} \mathrm{Re}\,[Z] \quad \ldots\ldots\ldots\ldots (47)$$

in which

$$Z \equiv A J_o (x\sqrt{i}) + B H_o^{(1)} (x\sqrt{i}) \quad \ldots\ldots\ldots\ldots (48)$$

gives

$$M_r = -\mathrm{Re}\left[Z'' + \mu \frac{1}{x} Z' \right] \quad \ldots\ldots\ldots\ldots (49)$$

$$M_\phi = -\mathrm{Re}\left[\frac{1}{x} Z' + \mu Z'' \right] \quad \ldots\ldots\ldots\ldots (50)$$

and

$$Q_r = \frac{1}{s} \, Re\,[i \;\; Z'] \quad \ldots\ldots\ldots\ldots\ldots (51)$$

where primes again denote differentiation with respect to x.

For first quadrant bending and tangential yield, setting

$$w = \frac{s^2}{D_1} \left[C_j \, R_j\right] \;, \; j = 1,2,3,4 \ldots\ldots\ldots\ldots (52)$$

gives

$$M_r = - \, C_j \, R_j'' \; + \; \mu \, M_y \quad \ldots\ldots\ldots\ldots\ldots (53)$$

and

$$Q_r = - \frac{1}{s} \left[C_j \left(R_j''' + \frac{1}{x} \, R_j''\right) + \frac{1}{x} (1 - \mu) \, M_y\right] \ldots\ldots\ldots (54)$$

and for yielding in the second quadrant,

$$w = \frac{s^2}{D_2} \left[C_j \, S_j \; + C_5 \log_e x\right] j = 1,2,..5 \ldots\ldots\ldots\ldots (55)$$

$$M_r = - \, C_j \, S_j'' + \frac{\mu}{1 - \mu} \, M_y \quad \ldots\ldots\ldots\ldots\ldots (56)$$

and

$$Q_r = - \frac{1}{s} \left[C_j \, S_j''' + \frac{1}{x} \, M_y\right] \quad \ldots\ldots\ldots\ldots\ldots (57)$$

For the case of an edge supported plate under symmetrical bending in the elastic range, setting

$$w = \frac{s^2}{D} \left[C_1 + C_2 \, x^2 + C_3 \log_e x + C_4 \, x^2 \log_e x\right] \quad \ldots\ldots\ldots (58)$$

gives

$$M_r = - \left[2(1+\mu) \, C_2 - (1 - \mu) \, C_3 \frac{1}{x^2} + C_4 \left[2 \log_e x + 3 + \mu(2 \log_e x + 1)\right]\right] \ldots (59)$$

$$M_\phi = - \left[2(1+\mu) \, C_2 + (1 - \mu) \, C_3 \frac{1}{x^2} + C_4 \left[2 \log_e x + 1 + \mu(2 \log_e x + 3)\right]\right] \ldots (60)$$

and

$$Q_r = - \frac{1}{s} \, C_4 \left(\frac{4}{x}\right) \quad \ldots\ldots\ldots\ldots\ldots (61)$$

In the case of tangential yield and first quadrant bending, setting

$$w = \frac{s^2}{D_1} \left[C_1 + C_2 x + C_3 x^2 + C_4 \, x \log_e x\right] \ldots\ldots\ldots (62)$$

gives

$$M_r = - \, 2 \, C_3 - \frac{C_4}{x} + \mu \, M_y \quad \ldots\ldots\ldots\ldots\ldots (63)$$

and

$$Q_r = - \frac{1}{s} \left[\frac{2 \, C_3}{x} + \frac{1}{x} (1 - \mu) \, M_y\right] \ldots\ldots\ldots\ldots (64)$$

and in the second quadrant,

$$w = \frac{s^2}{D_2} \left[C_1 + C_2 x + C_3 x^2 + C_4 x^2 \log_e x + C_5 \log_e x \right] \quad \ldots\ldots (65)$$

$$M_r = - 2 C_3 - C_4 (2 \log_e x + 3) + \frac{\mu}{1 - \mu} M_y \quad \ldots\ldots\ldots (66)$$

and

$$Q_r = - \frac{1}{s} \left[C_4 \frac{2}{x} + \frac{1}{x} M_y \right] \quad \ldots\ldots\ldots\ldots (67)$$

The constants in each case may be evaluated from the boundary conditions.

APPLICATIONS

Plate on Elastic Foundation with Concentrically Loaded Circular Insert.— Consider the case of a large or infinite plate on a liquid type elastic foundation, with a rigid circular insert, concentrically loaded (Fig. 6).

In the elastic range of stresses, the deflection is given by Eq. 48; the constants may be evaluated from the conditions of zero deflection and slope at infinity, zero slope at the edge of the insert, and from the shear at this point. Hence, from Eq. 49, the maximum moment occurs at the edge of the insert, in the radial direction, and it is here that yielding commences. Yielding about the edge of the insert allows rotation of the plate, and a yield line is formed. Further rotation, with load increase, allows tangential moment to build up until it too reaches the yield moment.

Under increased load, yielding occurs in the tangential direction at or near the edge of the insert and spreads concentrically outwards. At any particular load, the edge of yield may be determined and the constants evaluated, as follows. Since bending in the region of the insert is in the first quadrant, deflection within the yielded zone is given by Eq. 52, and radial moments and shears by Eqs. 53 and 54, respectively. The conditions, at the edge of the insert, are $M_r = M_y$ from Eq. 10 and $Q_r = - \frac{P}{2 \pi r_b}$, in which r_b is the radius of the insert, and, at the outer edge of the yielded zone, $M_\phi = M_y$, and continuity in the plate. In the surrounding elastic portion of the plate, the constants are evaluated from these conditions at the edge of the yielded zone, and the condition that slope and deflection approach zero for large values of r. For the particular case of $r_b = 0.4$ s and $\mu = 0$, the moments at various stages of yield are as shown in Fig. 6.

Where the plate is thick and yielding is considered to be confined to a line, the effect of shear deformation in the surrounding plate may be included using a refined theory. From the work of Frederick (13), the deflection in the infinite elastic plate is

$$w = \frac{s^2}{D} \, Re \left[B H_0^{(1)} \left(x e^{i\alpha/2} \right) \right] \quad \ldots\ldots\ldots\ldots (68)$$

where

$$\alpha = \arccos \left[- \frac{2 - \mu}{20(1 - \mu)} \frac{t^2}{s^2} \right] \quad \ldots\ldots\ldots\ldots (69)$$

and the complex constant B may be evaluated in this case by introducing the plastic moment condition $M_r = M_p$, in which M_p is given by Eq. 9, and from the

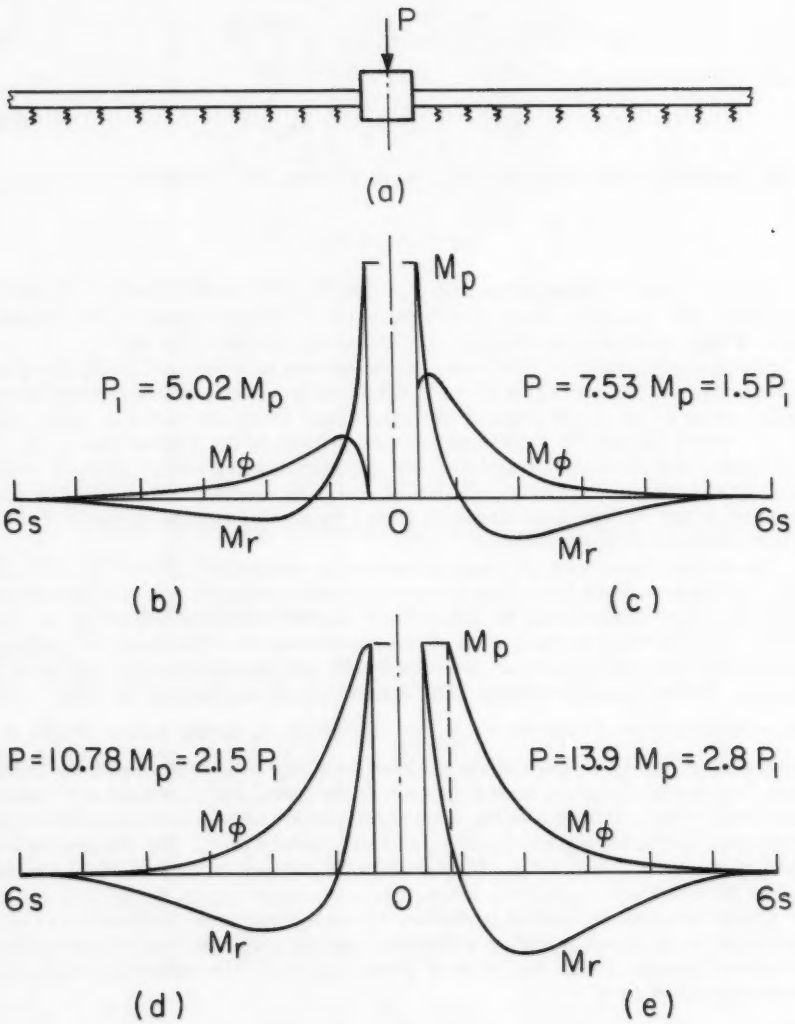

FIG. 6.—MOMENTS AROUND A LOADED INSERT IN A PLATE ON AN ELASTIC FOUNDATION. (V = 0)

magnitude of the shear at the insert edge. General expressions for elastic moments and shear are given by Frederick (13).

Simply Supported Circular Plate with Concentric Ring Load.—The case of a circular plate, simply supported at the edge and with a ring load concentric about the center (Fig. 7), will now be considered. This case is treated by Hodge (10) in a slightly different manner.

In the elastic range the moments are greatest within the loaded area where a state of pure bending exists; that is $M_r = M_\phi = M_0$ (constant). Under increasing load, M_0 increases to M_p, so that the moment everywhere within the loaded circle is at the yield moment, and pure, two dimensional yielding may occur. Rotation of the plate at the edge of the loaded area, under increasing load, produces an increase in tangential moments in the surrounding plate, and tangential yielding extends gradually outwards to the edge of the plate.

The bending is again in the first quadrant, so that, for yielding within the loaded area, $M_r = M_\phi = M_y$, and for tangential yielding in the surrounding plate,

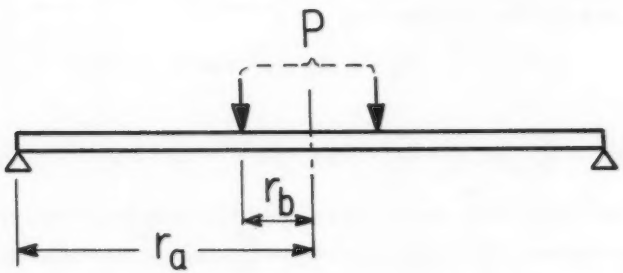

FIG. 7.—SIMPLY SUPPORTED, CIRCULAR PLATE WITH RING LOAD P.

$M_\phi = M_y$. Deflection and radial moment are given by Eqs. 62 and 63. In the case where the tangential moment just reaches M_y at the exterior edge, the constants C_1 through C_4 are determined from the conditions $M_r = M_y$ and $Q_r = -\frac{P}{2\pi r}$ at the edge of the load, and $w = 0$ and $M_\phi = M_y = -D_1 \frac{1}{r}\frac{dw}{dr}$ at the external edge. The load, P, is given by the additional condition $M_r = 0$ at this edge. Hence,

$$C_1 = \frac{a^2}{2}\left[\frac{P}{2\pi} + (1+\mu)\,M_y\right] - \frac{P\,a\,b}{2\pi} \quad \ldots\ldots\ldots\ldots \quad (70a)$$

$$C_2 = -a\left[\frac{P}{2\pi} + \mu\,M_y\right] + \frac{P\,b}{2\pi}\left[\log_e a + 1\right] \quad \ldots\ldots\ldots \quad (70b)$$

$$C_3 = \frac{P}{4\pi} - \frac{1}{2}(1-\mu)\,M_y \quad \ldots\ldots\ldots\ldots\ldots\ldots \quad (70c)$$

and

$$C_4 = -\frac{P\,b}{2\pi} \quad \ldots\ldots\ldots\ldots\ldots\ldots \quad (70d)$$

in which $r_a (\equiv a\ s)$ is the radius of the plate and $r_b (\equiv b\ s)$, the radius of the loaded circle. The magnitude of the load to produce this condition is

$$P = \frac{2\pi M_y}{\left(1 - \frac{r_b}{r_a}\right)} \quad \ldots\ldots\ldots\ldots\ldots\ldots \quad (71)$$

Uniformly Loaded Circular Plate.—A uniformly loaded plate may be treated similarly. This case is already treated by Tekinalp (14), but is included to show the general applicability of the present approach. The particular deflection due to the uniform load is given by integration (of Eq. 105 in Appendix I) as $w = \frac{q\ r^4}{72\ D_1}$ for first quadrant bending, and this when added to the homogeneous solution, Eq. 62 gives the total deflection in the plate. The same result may be obtained by considering the edge supported plate as the limiting case of a plate on an elastic foundation. The load, q, may then be considered to extend to infinity producing no moments or shears, only a uniform deflection, $w = \frac{q\ s^4}{D_1}$, and for this limiting case,

$$R_1 \to 1 - \frac{x^4}{72},\quad R_2 \to x,\quad R_3 \to x^2, \text{ and } R_4 \to x \log x$$

giving

$$w = \frac{q\ s^4}{D_1} + \frac{s^2}{D_1}\left[C_1\left(1 - \frac{x^4}{72}\right) + C_2\ x + C_3\ x^2 + C_4\ x \log x\right] \quad \ldots\ldots\ldots \quad (72)$$

The first two terms of the series must necessarily be included here since there is another constant term in the equation and $\frac{x^4}{72}$ may not be negligible in comparison with their sum. Hence, for a uniformly loaded plate, simply supported, and with tangential yield just extending to the edge, as before,

$$\lim_{s \to \infty} w = \frac{q}{72\ D_1}\left[3(3 + 2\nu)\ r_a{}^4 - 4(1 + 3\nu)\ r_a{}^3 r - 6(1 - \nu)\ r_a{}^2 r^2 + r^4\right] \quad \ldots \quad (73)$$

and

$$q = 6\ M_y / r_a{}^2 \quad \ldots\ldots\ldots\ldots\ldots\ldots \quad (74)$$

Continuous Plate, Intermittent Supports.—Slightly more complex, but still readily handled during certain stages of yield, is the case of a continuous plate with intermittent cylindrical supports (such as Fig. 8), each providing an axisymmetrical reaction to the plate.

Consider an internal panel of the plate, under a steadily increasing, uniform load. The example will be simplified by considering a material for which the plastic moment, M_p, is constant in each quadrant.

The plate may be readily analyzed in the elastic range by introducing a small but finite liquid reaction and using superposition techniques, as described elsewhere (19), (20). In this way, the plate may be considered as initially infinite in extent and supported only by the liquid. Each load and reaction may then be separately applied. The uniform load alone produces no moments or shears in the floating plate, only a uniform deflection. Superimposing the effects of each support reaction effectively eliminates the liquid reaction, leaving only an arbitrarily small residual reaction due to the actual, net deflections in

the plate. Hence the sum of the moments produced by each reaction acting separately is, in effect, the actual moment in the plate. Shear and deflection may be treated similarly.

Let the supports be arranged in a square grid of spacing, L, and let each have an effective radius, r_b, of 0.05 L. If the supports are assumed to completely restrain the plate so that the slope at the edge is zero, moments in the elastic range are as shown in Fig. 8(b).

Bending in the region of a support is essentially axi-symmetrical about its center. Maximum elastic moment occurs at the edge of the support, in the radial direction, and it is here that yielding commences. Thus, a yield line is

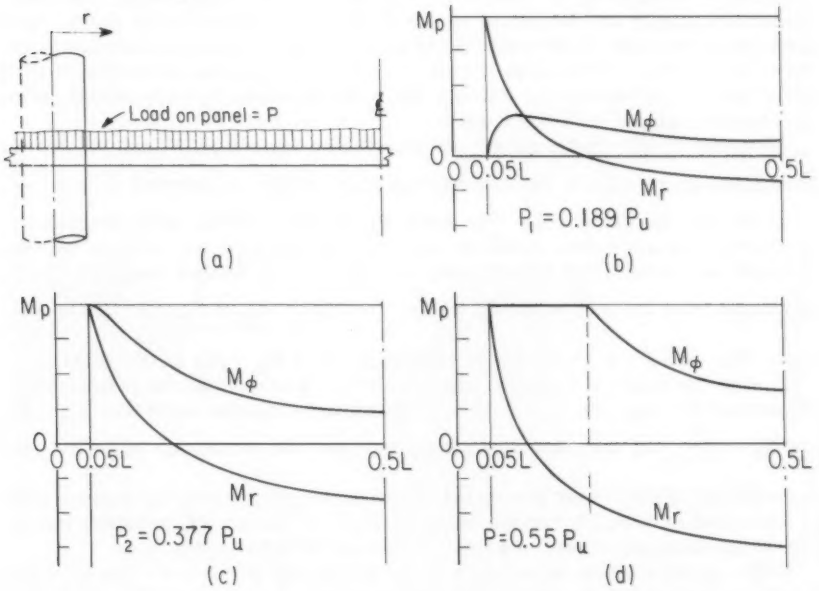

FIG. 8.—CONTINUOUS PLATE, UNIFORMLY-LOADED SQUARE, INTERNAL PANEL. MOMENTS AT CENTER-LINE OF SUPPORTS. (V = 0)

formed around the edge of the support (Fig. 9(a)). Rotation about this line, under increasing load, allows the tangential moment at the edge to gradually increase from zero (for μ = 0, Fig. 8(b)) to M_p (Fig. 8(c)). Further load produces tangential yielding which commences at or near the edge of the support and spreads concentrically, or nearly concentrically, outwards in the surrounding plate (Figs. 8(d) and 9(b)).

Bending is nearly symmetrical only in the region of the supports. As yielding spreads outside this area it tends to extend farthest along the lines of maximum curvature, which, on the assumption that the shear is uniformly distributed around the support, are along the panel edges (Fig. 9(c)). Hence, the zone of yielding tends to narrow to a line, eventually reaching midspan.

Meanwhile, positive yielding commences midway between the supports, where positive moment is a maximum, and spreads with increasing load, to form a

line along the panel center. Thus, a yield pattern of the third kind is completed (Fig. 9(c)).

The plate will be assumed at this stage to develop a preference (to an arbitrarily small degree), to yield in one direction of span. Since, in practice, no plate behaves ideally, an actual plate will possess such a preference, and at this stage of yielding, its effect will tend to become significant. A purely flexural failure cannot occur, however, for although the positive yield line is straight and thus capable of unlimited rotation, the negative line curves around the face of the supports where radial shear resistance prevents collapse.

Limited yielding about these lines in the preferred direction, causes further bending in the region of the support to be less symmetrical. This produces a significant variation in the distribution of shear force at the edge, and a consequent change in the directions of yield. Thus, a straight yield line tends to form along the edge of the supports (Fig. 9(d)), and completion of this line results in a pattern of the first group. Further load causes unlimited yielding along this line and along the positive line at the panel center, allowing the plate to fold and collapse as a mechanism.

Moments in the elastic range are determined from Eqs. 49 and 50, for the conditions, at the edge of the support, that radial slope is zero and $Q_r = \frac{P}{2\pi r_b}$, in which P is the panel load. The load, P_1, at which radial yield commences, is given by the additional condition that $M_r = M_p$ at the edge. If P_2 is the load at which tangential yield commences, moments in the loading range $P_1 < P < P_2$ are found from the conditions $Q_r = \frac{P}{2\pi r_b}$ and $M_r = M_p$ at the edge of the support. The load P_2 is given by the conditions $M_r = M_p = M_\phi$ at this edge.

During the range of symmetrical, or nearly symmetrical, tangential yielding around the supports, moments are determined from the conditions $M_r = M_p$ and $Q_r = \frac{P}{2\pi r_b}$ at the edge of the supports, and the conditions $M_\phi = M_p$, and of continuity, at the outer perimeter of yield. Bending within the yielded zone is described by Eqs. 52 through 54, or by Eqs. 62 through 64, provided the effect of the distributed load is separately included in the latter case.

Under greater loads, moments are not so readily predicted. The load P_3, at which a pattern of the third group is completed, and the load P_4, at which a pattern of the first group is formed, and consequent collapse occurs, are each given by statics. Hence, moments in the elastic range, up to load P_1, are as shown in Fig. 8(b). Moments at the load P_2, at which tangential yield commences, are given in Fig. 8(c), and moments at a load greater than P_2, possibly near the limit of reasonably symmetrical yielding, are shown in Fig. 8(d).

From the procedure outlined, with $\mu = 0$,

$$P_1 = \frac{-2\pi M_p}{\left[\log_e \frac{r_b}{L} + k\right]} = 3.73\, M_p = 0.189\, P_u$$

$$P_2 = \frac{-4\pi M_p}{\left[\log_e \frac{r_b}{L} + k\right]} = 7.46\, M_p = 0.377\, P_u$$

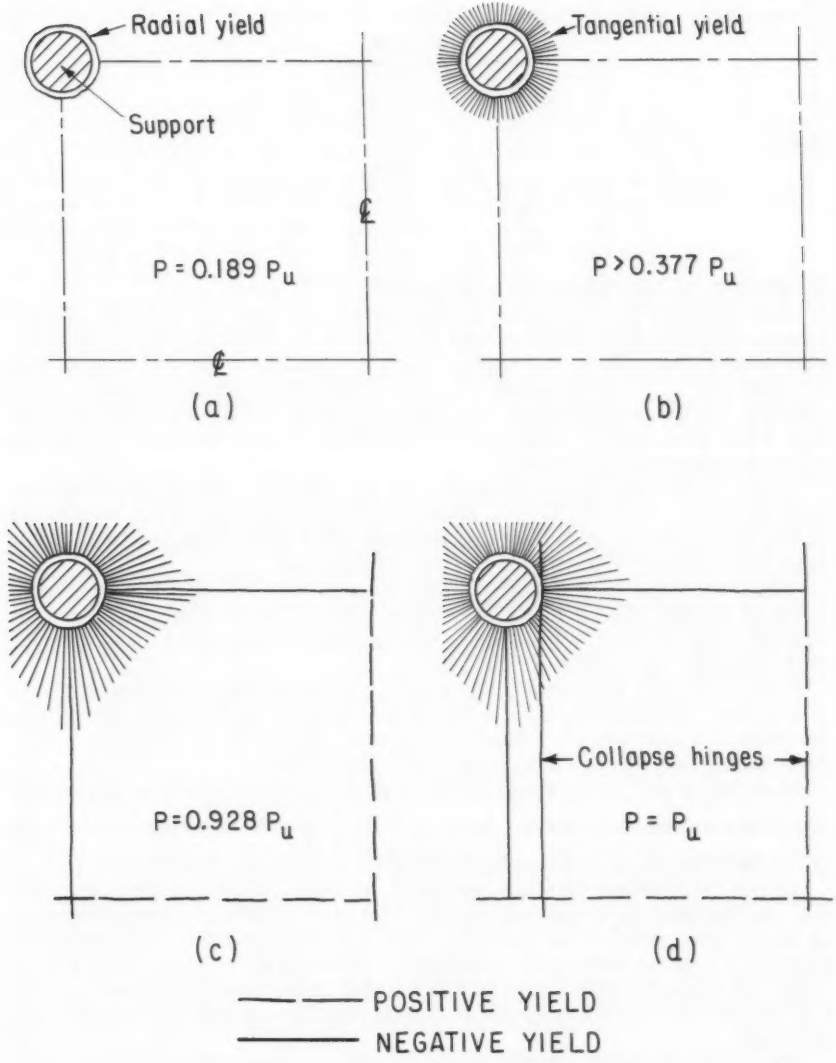

FIG. 9.—DEVELOPMENT OF YIELD IN A SQUARE, INTERNAL PANEL OF A CONTINUOUS PLATE WITH CYLINDRICAL SUPPORTS (QUARTER PANEL SHOWN—YIELD AREA NOT TO SCALE)

in which k = 1.310 for a square panel, and, from statics,

$$\frac{P_3 = 16\ M_p}{\left[1 - \frac{8\ r_b}{\pi\ L}\right]} = 18.33\ M_p = 0.928\ P_u$$

and

$$\frac{P_4 = 16\ M_p}{\left[1 - \frac{2\ r_b}{L}\right]^2} = 19.75\ M_p = P_u$$

in which P_u is the ultimate flexural capacity of the panel.

Whereas load P_3 is based on the assumption of a uniform shear distribution around the edge of the support, load P_4 requires the shear to be (largely) concentrated at the point on the edge to which the straight yield line is tangential (in Fig. 9(d)). If, in an actual plate, a preferred direction of span were to develop significantly at a load less than P_3, shear variations would occur at this lower load, and the completion of the pattern corresponding to the load P_3 would be retarded or prevented.

Loads P_1 through P_4 are computed for the condition that M_p is constant in each quadrant. For the Tresca yield criterion, P_1 and P_2 would remain the same, but P_3 and P_4 would each be reduced, since part of the yielding, in this case, is produced by bending in the second quadrant.

The same procedure of analysis may be used for thick plates in the elastic range of stress (20). It might be extended also to the inelastic range, for the condition that yielding is confined to an axi-symmetrical line around the edge of the support, as in the first example.

Plate on Elastic Foundation, Effect of Local Thickening.—Consider the plate of the first example, that is, a large or infinite plate on an elastic foundation, but with a circular area of (uniformly) greater thickness, or a flexible insert, surrounding and concentric with the loaded rigid insert.

Moments in the elastic range are determined from the equations presented. The necessary conditions are, shear $Q_r = -\frac{P}{2\ \pi\ r_b}$ and zero slope, at the edge of the rigid insert, and continuity at the outer edge of the flexible insert.

Due to the different plastic moments of the plate and the flexible insert, radial yielding may first commence at the internal boundary of either, depending on the relative proportions involved. Under increasing load, yield lines will eventually form at both these boundaries. Rotation about these lines allows tangential moments to increase, and at greater loads, zones of tangential yield are also produced, commencing at the radial yield lines and spreading outwards as before.

The position at which yielding first commences is determined from the elastic moment diagram. Under further loads, the condition $M_r = M_p$ is substituted for the elastic restraint condition at this edge, and the load at which radial yielding commences at the other internal boundary may then be similarly determined. Under additional loads, the plastic moment condition is used at each edge, and moments are again determined from the previous equations. Similarly, the loads at which tangential yielding commences may be calculated and the plate analyzed during tangential yield.

The above procedure has application also to the corresponding problem in a continuous plate with intermittent supports, as will be readily appreciated.

ANALYSIS

Thus, yielding may be confined to lines or may occur over an area of the plate. Yielding over an area may be in one direction or in two. Yield lines, it is shown, may be straight or curved, and a curve might be considered the general form. Lines producing collapse, however, must be necessarily straight, at least under finite rotations.

Yielding patterns have been nominally classified into three groups. The formation of any of these groups may be nominated as a design criterion using factored loads, although since they contribute in different degrees to eventual collapse, it would be reasonable to use different load factors for each.

Yield line patterns of the first group produce the ultimate flexural capacity and collapse of the plate as a mechanism. Yield patterns of the second group generally also represent the ultimate flexural capacity of the plate, but collapse in this case is resisted by the additional capacity produced by in-plane or shear forces.

Yield patterns of the third group do not normally represent ultimate flexural capacity and do not properly fit into the yield line theory as such. The examples considered herein were generally of this group, and the case of symmetrical bending, in particular, may be readily handled by the solutions presented.

In the case of symmetrical bending about an insert, the condition that yielding is confined to a line might be used as a design criterion, with suitably factored loads. In this case the plate may be analyzed by conventional elastic methods except that at the insert edge the plastic boundary condition $M_r = M_\phi = M_p$ is substituted for the elastic condition of zero slope. Moments and deflections in the surrounding plate are the same as in a continuous, purely elastic plate with a rigid insert merely bearing on it, so that utilization of this degree of plasticity is by no means unjustified. If symmetrical tangential yield is permitted, the solutions in this region are as simple as in the elastic case.

Although in the preceding theory a homogeneous, isotropic material is assumed, use is made of the assumption only in the calculation of the moment ordinate M_p; many of the solutions presented may be applied to other cases, including yielding in (isotropically) reinforced concrete plates, or slabs. In the range of reinforcement ratios practicable for slabs, and for flat slab construction in particular, the relationship between moment and curvature is approximated fairly well by the idealized curve (4), (5), (6), (7), (8), (9), of Fig. 2. The moment ordinate, M_p, represents, in effect, the point at which yielding commences in the reinforcement, which may be estimated with reasonable accuracy, and may be considered to be independent of the other stresses in the plate. Hence, the equations presented for first quadrant bending in a metal plate may be used in each quadrant of the slab.

The fact that deflections may be determined in the inelastic range is a big advantage. This is generally not possible with limit methods of design, and is of considerable importance for thin plates, in which deflection may be the most severe design criterion.

The advantage of utilizing the plastic properties of materials in plate design may be substantial, particularly when loads or reactions are concentrated over small areas.

In the case of metal plates, yielding through the depth of the plate increases the moment capacity per unit width, while yielding along a line or over an area eliminates moment concentrations producing a more favorable distribution of stress in the other two dimensions. Thus, considerable material savings are possible.

In the case of reinforced concrete plates, yielding gives only a slight increase in moment capacity per unit width, but plastic redistribution of moments in plan again provides significant savings. Instability does not enter the problem as it does in the case of steel frames, and the effect of local imperfections in the plate is generally relatively small. The advantage over established, permissable stress methods of design is not always so great, because in many cases allowance for plasticity has already been made either from experience or tests.

Inelastic analysis in these cases at least allows design practice to be reexamined, providing a justification for many of the reductions and simplifications introduced, and allowing their extension outside the limits of previous experience, and to new fields and materials of design. Connected closely to economy is the question of safety factors. Permissable stress methods of design generally result in inconsistent factors of safety for different elements of a structure. Using inelastic methods, the behavior in the post elastic range can be accurately determined with the following effect: the same over-all probability of failure may be retained, as in conventional design, allowing savings in materials and costs. The same material quantities might also be used, but proportioned to provide both a larger margin for safety and better performance under service loads.

CONCLUSION

Solutions are presented for small deflections due to axi-symmetrical, and unsymmetrical, yielding along lines in a plate and axi-symmetrical yielding over an area.

The equations were developed for thin plates of an isotropic, homogeneous, ductile material obeying the Tresca criterion for yield. Many of the results obtained are applicable also to isotropically reinforced concrete plates, since a similar moment curvature relationship may be assumed for each.

The solutions for axi-symmetrical yielding are relatively simple, and are suitable for use in design. They may be extended also to cases of nearly symmetrical bending, including yielding around cylindrical supports in a continuous plate structure.

APPENDIX I

Interaction of Moment and Shear.—The distribution of shear and bending stresses at a line of yield may be determined from the yield stress criterion and the equations of equilibrium of an element. For axi-symmetrical bending,

the equilibrium equations, in conventional notation, are

$$\frac{\partial(r\,\sigma_r)}{\partial r} - \sigma_\phi + r\,\frac{\partial \tau_{rz}}{\partial z} = 0 \quad \ldots\ldots\ldots\ldots\ldots (75)$$

$$\frac{\partial(r\,\tau_{rz})}{\partial r} + r\,\frac{\partial \sigma z}{\partial z} = 0 \quad \ldots\ldots\ldots\ldots\ldots (76)$$

The origin of coordinates is at the middle surface of the plate. If σ_z in Eq. 76 is considered identically equal to zero, the term $r\,\tau_{rz}$ is constant with respect to r, and hence the term $r\,\frac{\partial \tau_{rz}}{\partial z}$ in Eq. 75 is similarly constant.

Consider initially the specific case $\sigma_r = \sigma_\phi$ for values of r in the region of the yield line. Here, Eq. 75 reduces to

$$\frac{\partial \sigma_r}{\partial r} + \frac{\partial \tau_{rz}}{\partial z} = 0 \quad \ldots\ldots\ldots\ldots\ldots (77)$$

and for $\sigma_z = 0$, integration with respect to r gives

$$\sigma_r = -\frac{\partial \tau_{rz}}{\partial z}\, r \log_e \frac{r}{r_c} \quad \ldots\ldots\ldots\ldots\ldots (78)$$

in which r_c is the radius of contraflexure, or of a moment free edge. The area between this circle and the critical section is considered to be unloaded, or approximately so, as a consequence of the condition $\sigma_z = 0$.

From the Tresca criterion for yield in the first quadrant,

$$\sigma_r{}^2 + 4\,\tau_{rz}{}^2 = \sigma_y{}^2 \quad \ldots\ldots\ldots\ldots\ldots (79)$$

Substituting for σ_r from Eq. 78, and solving the differential equation so obtained gives, for positive z (in the lower half of the plate),

$$\tau_{rz} = \frac{1}{2} \sin\left[\frac{2}{r_b \log_e \frac{r_c}{r_b}}\,(z - t/2)\right] \sigma_y \quad \ldots\ldots\ldots (80a)$$

and hence,

$$\sigma_r = \cos\left[\frac{2}{r_b \log_e \frac{r_c}{r_b}}\,(z - t/2)\right] \sigma_y \quad \ldots\ldots\ldots\ldots (80b)$$

in which r_b is the radius of the critical section. Eqs. 80 are applicable in the range $\left|\frac{t}{r_b \log_e \frac{r_c}{r_b}}\right| \le \frac{\pi}{2}$, which appears to include all practical cases.

Integration of these expressions gives

$$Q_r = \int_{-t/2}^{t/2} \tau_{rz}\, dz = \frac{r_b \log_e \frac{r_c}{r_b}}{t} \left[1 - \cos \frac{t}{r_b \log_e \frac{r_c}{r_b}}\right] Q_y \quad \ldots\ldots (81a)$$

and

$$M_r = \int_{-t/2}^{t/2} z\,\sigma_r\,dz = 2\left(\frac{r_b \log_e \frac{r_c}{r_b}}{t}\right)^2 \left[1 - \cos \frac{t}{r_b \log_e \frac{r_c}{r_b}}\right] M_y \quad \ldots\ldots \quad (81b)$$

in the range $\frac{Q_r}{Q_y} \leq \frac{2}{\pi}$. Expanding each in series form and substituting Q_r into the expression for M_r gives the general relationship

$$M_r = \left[1 - \frac{1}{3}\left(\frac{Q_r}{Q_y}\right)^2 - \frac{8}{45}\left(\frac{Q_r}{Q_y}\right)^4 - \text{- - - -}\right] M_y \quad \ldots\ldots \quad (82)$$

which equals Eq. 9a in the range $\left(\frac{Q_r}{Q_y}\right)^4 \ll 1$. Similarly for $\frac{Q_r}{Q_y} \geq \frac{2}{\pi}$, $\tau_{rz} = \frac{\sigma_y}{2}$ over a central core, and varies as a quarter sine wave on each side of this, leading to

$$M_r = \frac{4}{\pi - 2}\left[1 - \frac{Q_r}{Q_y}\right]\frac{Q_r}{Q_y} \quad M_y \quad \ldots\ldots\ldots\ldots \quad (83)$$

although this is outside the range of $\frac{Q_r}{Q_y}$ that might be expected in a plate.

The case of axi-symmetrical, first quadrant bending, for any distribution of σ_ϕ with respect to r, and with a loading of uniform intensity, q, between the radii r_b and r_c, is now considered.

If the normal stress σ_z is approximated, for simplicity, by

$$\sigma_z = -\frac{q}{2}\left[1 - \frac{2z}{t}\right]^2 \quad \text{(for z positive)} \quad \ldots\ldots\ldots\ldots \quad (84)$$

substitution into Eq. 76 and integration with respect to r gives

$$r\,\tau_{rz} = -\frac{r^2}{2}\,q\left[\frac{2}{t} - \frac{4z}{t^2}\right] + f(z) \quad \ldots\ldots\ldots\ldots \quad (85)$$

Utilizing this result when integrating Eq. 75 with respect to r, gives

$$\sigma_r = \frac{1}{r}\int_{r_c}^{r} \sigma_\phi\,dr - (r - r_c)\,\frac{\partial \tau_{rz}}{\partial z} - \frac{2}{3}\,\frac{(r - r_c)}{r}\left(r_c^2 + r_c r - 2r^2\right)\frac{q}{t^2} \quad \ldots \quad (86)$$

In the range $\left(\frac{\tau_{rz}}{\sigma_y}\right)^4 \ll 1$, the Tresca yield criterion may be expressed as

$$\sigma_r = \sigma_y - \frac{2\,\tau_{rz}^2}{\sigma_y} \quad \ldots\ldots\ldots\ldots\ldots\ldots \quad (87)$$

Eliminating σ_r from Eqs. 86 and 87, introducing the simplifying approxima-

tion that σ_ϕ is constant with respect to z (which is true in the limiting case $\sigma_\phi = \sigma_y$), and solving for τ_{rz} gives

$$\tau_{rz} = \sqrt{\frac{b}{a}} \tanh \left[\sqrt{a\,b}\ (z - t/2)\right] \quad \ldots\ldots\ldots\ldots \quad (88a)$$

and hence

$$\sigma_r = \sigma_y - \frac{2}{\sigma_y} \frac{b}{a} \tanh^2 \left[\sqrt{a\,b}\ (z - t/2)\right] \quad \ldots\ldots\ldots \quad (88b)$$

where

$$a \equiv \frac{2}{\sigma_y \left(r_c - r_b\right)} \quad \ldots\ldots\ldots\ldots\ldots \quad (89a)$$

and

$$b \equiv \frac{\sigma_y}{r_c - r_b} - \frac{1}{r_b \left(r_c - r_b\right)} \int_{r_c}^{r_b} \sigma_\phi \, dr - \frac{2}{3\, r_b} \left(r_c^2 + r_c\, r_b - 2\, r_b^2\right) \frac{q}{t^2} \quad \ldots\ldots\ldots (89b)$$

$$b \equiv \frac{r_c}{r_b} \frac{\sigma_y}{\left(r_c - r_b\right)} - \frac{2}{3\, r_b} \left(r_c^2 + r_c\, r_b - 2\, r_b^2\right) \frac{q}{t^2} \quad \ldots\ldots\ldots (89c)$$

for the limiting case $\sigma_\phi = \sigma_y$, in the range of r considered. For σ_ϕ proportional to z, and σ_z a cubic function of z, the resultant differential equation for τ_{rz} is a special case of Riccati's equation for which a solution is again available, but in a slightly less convenient form. Integrating Eq. 1, gives

$$Q_r = \frac{2}{a} \log_e \cosh \left[\sqrt{a\,b} \left(\frac{t}{2}\right)\right] \quad \ldots\ldots\ldots\ldots \quad (90a)$$

and

$$M_r = M_y - \frac{4\,b}{\sigma_y\, a} \left[\frac{t^2}{a} - \frac{1}{a\,b} \log_e \cosh \left[\sqrt{a\,b} \left(\frac{t}{2}\right)\right]\right] \quad \ldots\ldots\ldots\ldots \quad (90b)$$

Expanding each of Eqs. 90 in series form, substituting one into the other, and truncating the series obtained, gives Eq. 9a in the range $\left(\frac{Q_r}{Q_y}\right)^4 \ll 1$, as before,

Using the same procedure for second quadrant bending, for which the yield criterion may be written

$$\sigma_r = \sigma_\phi - \sigma_y - \frac{2\,\tau_{rz}^2}{\sigma_\phi - \sigma_y} \quad \ldots\ldots\ldots\ldots\ldots \quad (91)$$

where $\left(\frac{\tau_{rz}}{\sigma_\phi - \sigma_y}\right)^4 \ll 1$, and again assuming a rectangular stress block for σ_ϕ gives

$$\tau_{rz} = \sqrt{\frac{b}{a}} \tanh \left[\sqrt{a\,b} \left(z - \frac{t}{2}\right)\right] \quad \ldots\ldots\ldots\ldots \quad (92a)$$

and

$$\sigma_r = \sigma_\phi - \sigma_y - \frac{2}{\left(\sigma_\phi - \sigma_y\right)} \frac{b}{a} \tanh^2 \left[\sqrt{a\,b} \left(z - \frac{t}{2}\right)\right] \quad \ldots\ldots \quad (92b)$$

where

$$a \equiv \frac{2}{(\sigma_\phi - \sigma_y)(r_c - r_b)} \quad \ldots\ldots\ldots\ldots \quad (93a)$$

and

$$b \equiv \frac{\sigma_\phi - \sigma_y}{r_c - r_b} - \frac{1}{r_b(r_c - r_b)} \int_{r_c}^{r_b} \sigma_\phi \, dr - \frac{2}{3 r_b} \left(r_c^2 + r_c r_b - 2 r_b^2\right) \frac{q}{t^2} \ldots \quad (93b)$$

and as a final result, the value of M_r given in Eq. 9b is obtained in the range $\left(\frac{Q_r}{Q_y}\right)^4 \ll 1$.

Eqs. 9 apply to yielding at internal and external circular boundaries and, in the limit $r_b \to \infty$, to one way bending in a plate. Eqs. 82 and 83 may be derived directly, for the latter case, from the results of Drucker (11), for a beam.

The Eqs. 82, 83 and 9, being based on states of stress that satisfy both equilibrium and a yield criterion, are lower bounds or approximations to the lower bounds for the cases considered. They may also be shown to be close to the upper bounds, however, and hence, may be considered as approximations to the actual interaction curves.

The independence of Eqs. 9 of the magnitudes of the constants a and b, that is of r_b, r_c, t, σ_ϕ (radially), σ_y and q, tends to suggest that they may have wider application. The stress distributions derived, in fact, are in the neighborhood of a stationary point on the interaction curve (for significant values of $\frac{Q_r}{Q_y}$ in the range considered), and the effect of any distribution of shear stress over the depth of the plate, from a linear (triangular) variation, to one approaching a half sine wave, is approximated by Eqs. 9. Hence, where approximations for $\sigma\phi$ and σ_z are introduced, the effect on moment is unlikely to be significant.

For shear distributions outside the previous range, the coefficient of $\left(\frac{Q_r}{Q_y}\right)^2$ increases to unity, in the limit where shear is carried only by a central core, or to one-half if shear is uniformly distributed over the depth of the section. All practical cases would appear to lie between the linear distribution and the uniform one so that the coefficient of $\left(\frac{Q_r}{Q_y}\right)^2$ would be between $\frac{1}{3}$ and $\frac{1}{2}$. Over a substantial portion of this range, the value $\frac{1}{3}$ is directly applicable, and provided $\left(\frac{Q_r}{Q_y}\right)^4 \ll 1$, Eqs. 9 might be considered to have reasonably general application.

Deflection.—In the case of axi-symmetrical yielding over an area, the differential equations for deflection are determined from the requirements of equilibrium and from the relationship in the radial direction between stress and elastic strain.

For a plate on an elastic foundation, moments, shear, and the intensity of external loading are related by the equilibrium equations

$$\frac{d}{dr}\left(r\,M_r\right) - M_\phi - r\,Q_r = 0 \quad \ldots\ldots\ldots\ldots\ldots \quad (94)$$

$$\frac{d}{dr}\left(r\,Q_r\right) - r(q - \gamma\,w) = 0 \quad \ldots\ldots\ldots\ldots\ldots \quad (95)$$

which may be obtained by integration (with respect to z), of Eqs. 75 and 76 respectively. Eliminating Q_r from Eqs. 94 and 95 results in the useful relationship,

$$\frac{1}{r}\,\frac{d^2}{dr^2}\left(r\,M_r\right) - \frac{1}{r}\,\frac{dM_\phi}{dr} + q - \gamma\,w = 0 \quad \ldots\ldots\ldots\ldots \quad (96)$$

For bending in the first quadrant and tangential yielding over an area of M_ϕ equal to Eq. 19a and substituting M_y for M_ϕ in Eq. 96 gives

$$\frac{1}{r}\,\frac{d^2}{dr^2}\left(r\,M_r\right) + q - \gamma\,w = 0 \quad \ldots\ldots\ldots\ldots\ldots \quad (97)$$

The relationship between radial moment and deflection is given by Eq. 43 in which $D_1 = E\,t3/12$, and primes denote differentiation with respect to r. In relating moments to displacements, no previous history of plastic strain is assumed. The term μ represents the elastic value of Poisson's ratio, and yielding is restricted to the ϕz plane. Substituting for M_r in Eq. 97, results in Eq. 22. Similarly, for yielding in the radial direction only, Eq. 19b results and

$$M_\phi = -\,D_1\,\frac{1}{r}\,w' + \mu\,M_y \quad \ldots\ldots\ldots\ldots\ldots \quad (98)$$

and substituting for M_r and M_ϕ in Eq. 96 gives

$$-\,\frac{1}{r^2}\,w'' + \frac{1}{r^3}\,w' = (q - \gamma\,w)/D_1 \quad \ldots\ldots\ldots\ldots \quad (99)$$

For the case of first quadrant bending and yielding in each direction, Eq. 19c results substituting for M_r and M_ϕ in Eq. 96 leaves

$$q - \gamma\,w = 0 \quad \ldots\ldots\ldots\ldots\ldots\ldots \quad (100)$$

For yielding in the second quadrant, we utilize Eq. 20 and substituting for M_ϕ in Eq. 96 gives

$$\frac{d^2M_r}{dr^2} + \frac{1}{r}\,\frac{dM_r}{dr} + q - \gamma\,w = 0 \quad \ldots\ldots\ldots\ldots \quad (101)$$

Yielding occurs in the $r\phi$ plane and the bending strain ϵ may be divided into two components, an elastic component ϵ_e and a plastic component ϵ_p. The corresponding deflections, produced by these strain components are denoted by w_e and w_p respectively. Radial moment is related only to the elastic component, that is,

$$M_r = -D_1\,w_e'' + \mu\,M_\phi \quad \ldots\ldots\ldots\ldots\ldots \quad (102)$$

which results in Eq. 45 in which $D_2 = E\,t^3/\left[12(1 - \mu)\right]$. Substituting for M_r in Eq. 101 gives Eq. 24a. Because yielding is restricted to the $r\phi$ plane and oc-

curs at constant volume,

$$\epsilon_{pr} = - \epsilon_{p\phi} \quad \ldots\ldots\ldots\ldots\ldots\ldots \quad (103)$$

which requires that Eq. 24b hold true.

Eq. 45 assumes ϵ_{er} and ϵ_{pr} proportional to z, which satisfies the linear relationship of moment and curvature shown in Fig. 2. Alternatively, if only total strain is assumed proportional to z, if the Tresca criterion for yield stress throughout the depth of the section is satisfied, and if w_e'' is defined as the curvature corresponding to the elastic component of radial strain in the extreme fibers, that is

$$w_e'' = - \left(\frac{\epsilon_{er}}{z} \right)_z = \frac{t}{2} \quad \ldots\ldots\ldots\ldots\ldots\ldots \quad (104)$$

Radial moment and curvature are found to be related by

$$M_r = - D_2 w_e'' + \frac{5\mu - 1}{6(1 - \mu)} M_y \quad \ldots\ldots\ldots\ldots \quad (105)$$

which, for large strains may give better results than Eq. 45. Deflections are given by Eqs. 24, as before.

For an edge supported plate, $\gamma = 0$, and Eqs. 22 and 23a reduce respectively to

$$w'''' + \frac{2}{r} w''' = q/D_1 \quad \ldots\ldots\ldots\ldots \quad (106)$$

$$w_e'''' + \frac{1}{r} w_e''' = q/D_2 \quad \ldots\ldots\ldots\ldots \quad (107)$$

Expressions for shear are obtained in each case by substituting for M_r and M_ϕ in Eq. 94.

APPENDIX II.—NOTATION

- M = moment per unit width of plate
- Q = shear force per unit width of plate
- V = effective shear per unit width $\left(V_u \equiv Q_u - \frac{\partial M_{uv}}{\partial v} \right)$
- w = deflection
- σ = direct stress
- τ = shear stress
- r, ϕ, z = cylindrical coordinates
- u, v, z = rectangular coordinates
- 1, 2, 3 = directions of principal stress
- e, y, p = subscripts denoting elastic behavior, yield in simple tension, and yield due to combined stress, respectively

E, μ = elastic constants

t = plate thickness

D = flexural rigidity $\left(D = \frac{E\,t^3}{12(1-\mu^2)};\ D_1 = \frac{E\,t^3}{12};\ D_2 = \frac{E\,t^3}{12(1-\mu)}\right)$

γ = reaction modulus of elastic foundation

$s = \left[\frac{D}{\gamma}\right]^{\frac{1}{4}}$

$x = \frac{r}{s}$

APPENDIX III.—BIBLIOGRAPHY

---

1. Tresca, H., "Comptes Rendus Acad. Sci.," Paris, 59, 1864, p. 754.
2. von Mises, R., "Mechanik der festen Korper in plastisch deformablen Zustand," Gottinger Nachrichten Math. Phys. Klasse, 1913, pp. 582-592.
3. Hencky, H., Zeits. ang. Math. Mech. 4, 1924, p. 323.
4. Bach, C., Elasticitat und Festigkeit, 3rd Edition, Julius Springer, Berlin, 1898, pp. 552-564.
5. Ingerslev, Aa., "The Strength of Rectangular Slabs," Journal of the Institution of Structural Engs., London, Vol. 1, No. 1, January, 1923, pp. 3-14.
6. Johansen, K. W., Brudlinieteorier, Jol. Gjellerups Forlag, Copenhagen, August, 1943, p. 189.
7. Johansen, K. W., "The Ultimate Strength of Reinforced Concrete Slabs," Final Report, Third Congress, Internatl. Assn. for Bridge and Structural Engr., Liege, September, 1948, pp. 565-570.
8. Johansen, K. W., "Pladeformler," 2. Udgave, Polyteknisk Forening, Copenhagen, 1949, p. 172.
9. Hognestad, E., "Yield-Line Theory for the Ultimate Flexural Strength of Reinforced Concrete Slabs," ACI Journal, Vol. 24, No. 7, March, 1953.
10. Hodge, P. G., "Plastic Analysis of Structures," McGraw-Hill Publishing Co., Inc., New York, 1959, pp. 249-268.
11. Drucker, D. C., "The Effect of Shear on the Plastic Bending of Beams," Trans. ASME, Vol. 78, 1956, J. App. Mech., pp. 509-514.
12. Hertz, H., "Uber das Gleichgewickt schwimmender elastischer Platten," Wiedermann's Annalen der Physik und Chemie, Vol. 22, 1884, pp. 449-455.
13. Frederick, D., "On Some Problems in Bending of Thick Circular Plates on an Elastic Foundation," Trans. ASME, Vol. 78, 1956, J. App. Mech., pp. 195-200.

14. Tekinalp, B., "Elastic, Plastic Bending of a Simply Supported Circular Plate Under a Uniformly Distributed Load," DAM Rept. C 11-6, Brown Univ., Providence, 1955.

15. Timoshenko, S., "Theory of Plates and Shells," McGraw-Hill Publishing Co., Inc., New York, 1940, pp. 257-287.

16. Jahnke, E., and Emde, F., "Tables of Functions," Dover Publications, New York, 1943.

17. Lowell, H. H., "Tables of the Bessel-Kelvin Functions, Ber, Bei, Ker, Kei, and Their Derivatives for the Argument Range 0.(0.01)107.50," NASA Tech. Report R-32, National Aeronautics and Space Administration, Washington, 1959.

18. Dwight, H. F., "Tables of Integrals and Other Mathematical Data," The MacMillan Co., New York, Revised Edition, 1947.

19. Brotchie, J. F., "General Method for Analysis of Flat Slabs and Plates," Journal ACI, July, 1957, pp. 31-50.

20. Brotchie, J. F., "General Elastic Analysis of Flat Slabs and Plates," Journal ACI, August, 1959, pp. 127-152, and Discussion by Frederick, D., scheduled for the March, 1960 issue.

21. Brotchie, J. J., Penzien, J., and Popov, E. P., "Analysis of Plates of Linear Strain Hardening Material," Institute of Engrg. Research Tech. Report, University of California Press, scheduled for publication in March, 1960.

Journal of the
ENGINEERING MECHANICS DIVISION
Proceedings of the American Society of Civil Engineers

DYNAMIC RESPONSE OF BEAMS TRAVERSED BY TWO-AXLE LOADS

By Robert K. Wen,[1] A. M. ASCE

SYNOPSIS

An analysis of the response of beams traversed by two-axle loads is made based on the assumption that the dynamic deflection is proportional to the static deflection due to the weights of the beam and loads. Numerical results show quasi resonance effects due to successive applications of loads and to wavy beam surfaces.

INTRODUCTION

Problem Considered.—This paper deals with the elastic deflections and bending moments in simply supported beams under the passage of two-axle loads. The system considered is shown in Fig. 1. It consists of a simply supported beam spanned between two rigid supports and approaches, and a two-axle load moving from left to right at a constant speed.

The surface of the beam, and that of the approaches, may be uneven. The beam, however, is assumed to have a uniform mass distribution and constant flexural rigidity. In other words, the surface unevenness of the beam is assumed to be small as compated to its depth, so that its effect on the distribution of mass and flexural rigidity is negligible. Under the usual assumption that the elastic deflection is due entirely to bending, the deflection of any point in a cross-section of the beam is equal to the deflection of the neutral axis.

Note.—Discussion open until March 1, 1961. Separate discussions should be submitted for the individual papers in this symposium. To extend the closing date one month, a written request must be filed with the Executive Secretary, ASCE. This paper is part of the copyrighted Journal of the Engineering Mechanics Division, Proceedings of the American Society of Civil Engineers, Vol. 86, No. EM 5, October, 1960.

[1] Asst. Prof., Dept. of Civ. Engrg., Michigan State Univ., East Lansing, Michigan.

In Fig. 1, the depth of the beam is not shown; the line designated as "neutral axis of beam" completely defines the elastic deflection curve.

The load unit is shown to be composed of a "sprung mass" connected to two "unsprung masses" through two linearly elastic springs. A sprung mass is simply a mass that is suspended on a spring; an unsprung mass is not.

The usual method of dynamic analysis of elastic structures, by expressing the deflection configuration of the structure as an infinite series involving its normal modes of vibration, is ineffective for this problem if the mass of the moving load is to be taken into account. This is due to the fact that this method requires the normal modes to be functions of the space coordinate only, whereas with the moving mass on the beam, the normal modes of the structures are obviously dependent on the position of the mass and, hence, on time as well as on the space or length coordinate.

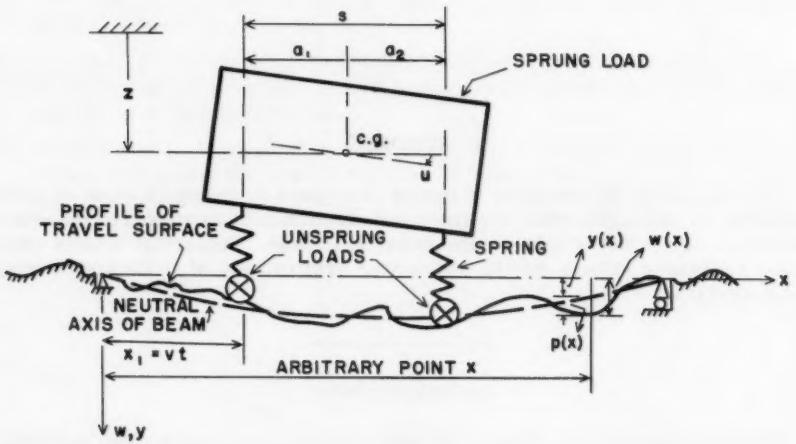

FIG. 1.—BEAM-LOAD SYSTEM.

In order to arrive at a workable method of analysis, it has been found necessary by investigators of this problem of moving loads on beams, to make some major simplifying assumptions. The simplifications or assumptions fall into two categories.

Under the first category, the system itself is modified so that an exact analysis is obtainable. The system of a massless beam and a single unsprung mass was first considered by R. Willis,[2,3] who derived the differential equation for the system, a linear differential equation with variable coefficients. An exact solution of the equation was reported by Stokes.[4] The system of a simply sup-

[2] "Report of the Commissioners appointed to inquire into the Application of Iron to Railway Structures," Appendix by R. Willis, H. M. Stationery Office, London, 1849.

[3] "Vibration Problems in Engineering," by S. Timoshenko and D. H. Young, 3d Ed., Van Nostrand Co., New York, 1955, p. 359.

[4] "Discussions of a Differential Equation Relating to the Breaking of Railway Bridges," by G. G. Stokes, Transactions, Cambridge Phil. Soc., 1869.

ported beam with uniformly distributed mass subjected to a moving force (a load devoid of mass), a system with (an infinite number of degrees) of freedom, was analyzed by Timoshenko.[5] In this case, the method of analysis using normal modes mentioned previously does work. Although an infinite number of differential equations are involved, each equation can be solved exactly, because it is linear and contains only one dependent variable. The complete solution is, of course, in the form of an infinite series.

The second category of simplifications includes those which prescribe the beam a given shape at any given time during the passage of the load; this, in effect, reduces the number of degrees of freedom of the structure to one. Inglis[6] solved the problem of moving mass by making use of the assumption that the deflection shape of the beam at any time is that of the first natural mode of the unloaded beam, that is, a half sinusoidal wave. In studying the effects of a moving sprung mass on beams, Hillerborg[7] made the approximation that the (dynamic) deflection curve of the beam at any time is proportional to its instantaneous static deflection curve due to the moving load (the deflection curve if the load on the beam at that instant were applied statically). The case of a moving load consisting of an unsprung mass supporting a sprung mass has been considered by Tung et al.[8], and by Biggs et al.[9], who had respectively used Hillerborg's and Inglis' assumptions in regard to the shape of the dynamic deflection curve.

All of the work cited dealt with the case of a single-axle load. In the case of multiple-axle loads, if the moving loads are massless, the principle of superposition applies. That is, the total effect of several massless moving loads on the beam is equal to the sum of the separate effect of each load. This superposition, however, does not apply if the loads possess mass. Hence, the solution of a problem involving multiple moving masses cannot be obtained by combining solutions of problems each involving only a single mass. However, making the same assumption regarding the mode of vibration of the beam as Inglis did, Looney,[10] using a numerical procedure, has obtained solutions of the problem involving multiple unsprung masses. Hillerborg[7] has also indicated that the problem of multiple loads could be handled by use of his theory.

General Description of Present Analysis.—A fundamental assumption made in the present analysis is that the dynamic deflection curve of the neutral axis of the beam is of the same shape (not necessarily in actual values) as that which would result if the weights of the moving loads on the beam at that instant and the weight of the beam itself were statically applied to the beam.

It is an improvement of Hillerborg's assumption. Consider the case of a two-axle load with an axle spacing greater than the span length. During the interval after the departure of the front axle, but before the entry of the rear axle, there is no load on the beam. According to Hillerborg's assumption, the

---

5 "Vibration Problems in Engineering," by S. Timoshenko and D. H. Young, 3d. Ed., Van Nostrand Co., New York, 1955, p. 351.

6 "A Mathematical Treatise on Vibrations in Railway Bridges," by C. E. Inglis, Cambridge Univ. Press, London, 1934.

7 "Dynamic Influences of Smoothly Running Loads on Simply Supported Girders," by A. Hillerborg, Inst. of Structural Engrg. and Bridge Building of the Royal Inst. of Tech., Stockholm, 1951.

8 "Highway Bridge Impact Problems," by T. P. Tung, L. E. Goodman, T. Y. Chen, and N. M. Newmark, Bulletin 124, Highway Research Bd., 1956.

9 "Vibration of Simple-Span Highway Bridges," by J. M. Biggs, H. S. Suer, and J. M. Louw, Transactions, ASCE, Vol. 124, 1959, p. 291.

10 "Impact on Railway Bridges," by C. T. Looney, Univ. of Illinois Bulletin Series No. 352, 1944.

structure would be motionless. But this does not seem logical. This difficulty, of course, does not exist under the present assumption owing to the inclusion of the weight of the beam itself in the determination of the basic shape of the structure in motion.

Another feature of the analysis reported herein lies in the considerations of a more general type of moving loads, that is, loads involving rotary inertia, and possible unevenness of the surface of the approaches and the beam.

In the following sections of the paper, the differential equations that govern the behavior of the beam-load system are first derived. This is followed by a listing of the dimensionless parameters of the system. After an explanation of the computations of the dynamic responses, some numerical results are presented. Among them are those pertaining to the effects of axle spacing and surface unevenness. It is shown that a synchronization of the applications of axle loads with the fundamental frequency of vibration of the beam could augment the dynamic response in the structure. Resonance phenomena due to sinusoidal unevenness on the beam surface are also noted in an example.

Notation.—The letter symbols adopted for use in this paper are defined where they first appear in the text. Symbols used more than once are arranged alphabetically for convenience of reference, in Appendix II.

DERIVATION OF DIFFERENTIAL EQUATIONS

The general precedure of deriving the differential equations consists of first writing out the energy expressions for the system and then substituting them into the noted Lagrange's equation in dynamics.

In the following derivations, it is assumed that the moving loads are in contact with the beam at all times. The usual beam theory is used, and the effect of rotary inertia on the motion of the beam is neglected.

Profile of Travel Surface.—For a given point on the surface of the beam or the approach, the term "profile of travel surface" is defined to be the vertical distance measured from a horizontal line through the end supports of the beam to the surface of the beam or the approach. Denoting this quantity by the symbol w and referring to Fig. 1,

$$w(x,t) = p(x) + y(x,t) \quad \ldots\ldots\ldots\ldots\ldots \quad (1)$$

in which the symbols $w(x,t)$ denote the fact that w depends on both the length coordinate x, and the time coordinate t; $p(x)$, which may be called the "initial profile function," represents the initial profile of travel surface when the beam is in its unloaded position (not even loaded by its own weight); and $y(x,t)$, is the deflection curve of the neutral axis measured with reference to the unloaded position of the beam. All three quantities in Eq. 1 are considered positive in the downward direction. It should be noted that for any given problem, whereas y is an unknown function to be determined from the analysis, the function p should be prescribed.

Dynamic Deflection Curve.—By virtue of the previously mentioned assumption regarding the dynamic deflection shape of the neutral axis, Eq. 2 may be written.

$$y(x,t) = \bar{f}(t)\, Y(x,t) \quad \ldots\ldots\ldots\ldots\ldots \quad (2)$$

in which $\bar{f}(t)$ represents a coefficient of proportionality which may vary with time, but not with distance; $Y(x,t)$ denotes the deflection curve of the neutral

axis if the weights of the beam and the moving loads were statically applied to the beam. The function Y depends on time t (as well as on distance x), because the positions of the loads depend on t. Letting the time t = 0 correspond to the instant of the entry of the rear axle to the beam, and x_1 and x_2 denote the distance from the left support to the rear and front axle, respectively, one sees that $x_1 = v\,t$, and $x_2 = v\,t + s$, where v denotes the horizontal velocity of the loads and s the axle spacing. Since both v and s are constants, for a given t, the function Y may be computed by statics. In other words, it is a known function of time.

The function Y can be written as a polynomial (this is done in Appendix I), or, it can be expressed as a trigonometric series[11] as follows:

$$Y = \frac{2}{E\,I}\left(\frac{L}{\pi}\right)^4\left[\left(\sum_{n=1}^{\infty}\sum_{j=1}^{2}\epsilon_j\frac{W_j}{n^4\,L}\sin\frac{n\pi x_j}{L}\right)+\left(\sum_{n=1,3,5,\ldots}\frac{2\,m_6\,g}{\pi\,n^5}\right)\right]\sin\frac{n\pi x}{L} \quad . . \quad (3)$$

in which E I denotes the flexural rigidity of the beam, L the span length, m_b the mass of the beam per unit length, and g the gravitational acceleration. The subscript, j, refers to the rear, or front axle according as it is equal to 1 or 2. W_j denotes the weight of the jth axle; the symbol ϵ_j, defined as: $\epsilon_j = 1$ for $0 \leq x_j \leq L$, $\epsilon_j = 0$ otherwise, is introduced to ensure that any axle load outside the beam span will not be included in computing the deflection of the beam. The summation in the second bracket extends over odd values of n only, because the static deflection of the beam, due to its own weight, is symmetrical about its mid-point.

In order to avoid writing lengthy expressions in later developments, Eq. 3 may be written in the following form:

$$Y = \frac{\Psi(x,t)}{K_1} = \frac{1}{K_1}\sum_{n=1}^{\infty}\eta_n\,(t)\,\sin\frac{n\pi x}{L} \quad . . . . . \quad (4)$$

in which K_1 is some arbitrarily chosen constant and

$$\Psi\,(x,t) = \sum_{n=1}^{\infty}\eta_n\sin\frac{n\pi x}{L} \quad . . . . . \quad (5)$$

and, for odd values of n,

$$\eta_n\,(t) = \frac{1}{K_2}\left[\left(\sum_{j=1}^{2}\epsilon_j\frac{W_j}{n^4}\sin\frac{n\pi x_j}{L}\right)+\frac{2\,m_b\,g\,L}{\pi\,n^5}\right] \quad . . . . . \quad (6)$$

in which K_2 is some constant depending on the choice of K_1. For even values of n, the second term inside the brackets in Eq. 6 should be dropped.

Now Eq. 2 may be written as

$$y\,(x,t) = \bar{f}\,(t)\,\Psi\,(x,t) \quad . . . . . \quad (7)$$

---

11 "Advanced Mathematics for Engineers," by H. W. Reddick and F. H. Miller, John Wiley and Sons Co., New York, 3d Ed., 1955, p. 214.

in which f(t), obviously representing $K_I \bar{f}$, will be considered the dependent variable that specifies the dynamic deflection curve since Ψ is a known function.

Potential Energy.—The initial energy level of this system is defined by the following conditions: (a) The beam is not strained (not even by its own weight as yet); (b) the weight of the beam and that of the unsprung loads are at a horizontal line having the same elevation as that of the unstrained beam; (c) the springs of the loads are undeformed (not even by the sprung weight as yet); and (d) the sprung weight is situated at the upper ends of the undeformed springs.

Following the foregoing definition, the strain energy of the beam is given by the expression:

$$\frac{E\,I}{2} \int_0^L \left(y_{xx}\right)^2 dx \quad \ldots\ldots\ldots\ldots\ldots \quad (8)$$

in which each subscript x denotes a differentiation with respect to x.

For a linearly elastic spring its strain energy is equal to 1/2 ($k\,d^2$), where k denotes the spring constant and d the deformation. For the spring in the j th axle the deformation is equal to

$$d_j = Z + (-1)^j a_j\, u + (Z_s)_j - w_j \quad \ldots\ldots\ldots\ldots \quad (9)$$

in which the symbols used are illustrated in Fig. 1. The letter z denotes the vertical displacement of the centroid of the sprung mass (positive if downward); u denotes the rotation of the sprung mass about its centroidal axis (positive if clockwise); a_j is the horizontal distance from the centroid of the sprung mass to the j th axle; $(z_s)j$ stands for the compression in the spring when supporting the sprung weight statically; and w_j denotes w evaluated at x_j.

The expression for the strain energy of both springs is then equal to

$$\sum_j \frac{1}{2} k_j\, d_j^2 \quad \ldots\ldots\ldots\ldots\ldots\ldots \quad (10)$$

in which k_j denotes the spring constant of the j th axle, and the symbol $\sum_j$ stands for $\sum_{j=1}^{2}$.

The potential energy of the weight of the beam is given by the expression

$$-\int_0^L m_b\, g\, y\, dx \quad \ldots\ldots\ldots\ldots\ldots \quad (11)$$

The potential energy of the weights of the loads is given by the expression

$$-\frac{1}{2}\overline{M}\, g\, \Delta_v - \overline{M}\, g\, z - \sum_j m_j\, g\, w_j \quad \ldots\ldots\ldots\ldots \quad (12)$$

in which $\overline{M}$ denotes the total sprung mass, Δ_v the deflection of the centroid of $\overline{M}$ when the sprung weight is statically applied to the springs, and m_j denotes the unsprung mass of the j th axle.

Adding Eqs. 8, 10, 11 and 12, and noting the following identities:

$$\sum_j k_j\, (z_s)_j = \overline{M}\, g \quad \ldots\ldots\ldots\ldots\ldots \quad (13a)$$

$$\sum_j k_j (z_s)_j^2 = \overline{M}\ g\ \Delta_v \quad \ldots\ldots\ldots\ldots \quad (13b)$$

and

$$\sum_j k_j (z_s)_j (-1)^j a_j = 0 \quad \ldots\ldots\ldots\ldots \quad (13c)$$

the following expression is obtained for the total potential energy of the system:

$$V = \frac{E\,I}{2} \int_0^L (y_{xx})^2 dx - \sum_j \left[k_j (z_s)_j w_j - \frac{1}{2} k_j \left(z + (-1)^j a_j u - w_j \right)^2 + m_j g w_j \right] - \int_o^L m_b g y\, dx \quad \ldots (14)$$

Kinetic Energy.—The Kinetic energy of the system is given by the expression

$$T = \frac{m_b}{2} \int_o^L y_t^2\, dx + \frac{1}{2} \overline{M} z_t^2 + \frac{1}{2} J u_t^2 + \sum_j \frac{1}{2} m_j w_{j,t}^2 \quad \ldots\ldots \quad (15)$$

in which the subscript t denotes a differentiation with respect to time t, and J represents the polar moment of inertia of the sprung mass about its centroid. The first term of the right-hand side of this equation represents the kinetic energy of the beam; the second and the third terms represent the kinetic energy of the sprung mass due to the vertical and angular motion, respectively; and the fourth term represents the kinetic energy of the unsprung masses.

Differential Equations.—The differential equations for the beam-load system are obtained by substituting Eqs. (14) and (15) into Lagrange's equation:

$$\frac{d}{dt} \left(\frac{\partial T}{\partial q_t} \right) - \frac{\partial T}{\partial q} + \frac{\partial V}{\partial q} = 0 \quad \ldots\ldots\ldots\ldots \quad (16)$$

in which q denotes a dependent variable of the system. Setting q successively equal to f, z, and u, the following equations that govern the response of the system are obtained:

$$m_b \frac{L}{2} \sum_{n=1}^{\infty} \eta_n^2 f_{tt} + m_b L f_t \sum_{n=1}^{\infty} \eta_n \eta_{n,t} + m_b \frac{L}{2} f \sum_{n=1}^{\infty} \eta_n \eta_{n,tt}$$

$$- m_b g \sum_{n=1,3,5,\ldots,} \eta_n \frac{2L}{n\pi} + \sum_j m_j w_{j,tt} \psi_j + EI \left(\frac{\pi}{L} \right)^4 \frac{L}{2} f \sum_{n=1}^{\infty} n^4 \eta_n^2$$

$$- \sum_j \psi_j \left[k_j (z_s)_j + k_j \left(z + (-1)^j a_j u - w_j \right) + m_j g \right] = 0 \quad \ldots\ldots \quad (17)$$

$$\overline{M} z_{tt} + \sum_j k_j \left(z + (-1)^j a_j u - w_j \right) = 0 \quad \ldots\ldots\ldots\ldots \quad (18)$$

and

$$J u_{tt} + \sum_j (-1)^j a_j k_j \left[z + (-1)^j a_j u - w_j \right] = 0 \quad \ldots\ldots \quad (19)$$

In Eq. 17 the symbol ψ_j denotes ψ evaluated at x_j. By virtue of Eq. 5, this quantity may be represented by the series $\sum_{n=1}^{\infty} \eta_n \sin \frac{n\pi x_j}{L}$. In this equation, the "fastest" converging series is $\sum_{n=1}^{\infty} \eta_n{}^2$, for which the terms due to the weights of the beam and the loads decrease in magnitude as fast as n^{-10} and n^{-8}, respectively. The "slowest" converging series is $\sum_{n=1}^{\infty} n^4 \eta_n{}^2$, for which the aforementioned terms decrease in magnitude at the rate of n^{-6} and n^{-4}, respectively. Since this series and those series involving η_n in Eq. 17 converge rapidly, to facilitate numerical computations, it seems reasonable to keep only the first term of each of these series. Consequently, Eq. 17 is reduced to the following form:

$$m_b \frac{L}{2}\eta f_{tt} + m_b L \eta_t f_t + \left(m_b \frac{L}{2}\eta_{tt} + EI\left(\frac{\pi}{L}\right)^4 \frac{L}{2}\eta\right) f - m_b g \frac{2L}{\pi}$$

$$+ \sum_j \epsilon_j \sin \frac{\pi x_j}{L} \left[m_j \left(w_{j,tt} - g\right) - M_j g - k_j \left(z + (-1)^j a_j u - w_j\right)\right] = 0 \quad \ldots (20)$$

in which $M_j = k_j (z_s)_j / g$ is called the "sprung mass of the j th axle" and $\eta = \eta_1$.

It may be noted that Eqs. 18, 19 and 20 constitute a system of three linear differential equations with coefficients that are functions of time. These equations may be integrated numerically.

Dimensionless Parameters and Variables.—To obtain the dimensionless parameters and variables of the system the preceding differential equations could be transformed into dimensionless form. This may be accomplished by first dividing Eqs. 18 and 20 by the quantity $m_b g L$, and Eq. 19 by the quantity $2g/s(v T_b/L)^2 \sum_j M_j a_j{}^2$, in which T_b, denoting the fundamental natural period of the beam, is equal to $(2L^2/\pi)\sqrt{m_b/EI}$. Next, let the following dimensionless quantities be introduced:

Parameters of System.—

$$\alpha = \frac{v T_b}{2L} = \frac{1 \text{ fundamental natural period of beam}}{2 \text{ time for an axle to cross beam}} \quad \ldots\ldots (21a)$$

$$\frac{s}{2L} = \frac{1 \text{ axle spacing}}{2 \text{ length of beam}} \quad \ldots\ldots (21b)$$

$$\Gamma_j = \frac{M_j}{m_b L} = \frac{\text{sprung mass of j th axle}}{\text{total mass of beam}} \quad \ldots\ldots (21c)$$

$$\gamma_j = \frac{m_j}{m_b L} = \frac{\text{unsprung mass of j th axle}}{\text{total mass of beam}} \quad \ldots\ldots (21d)$$

$$\lambda = \frac{1}{4} \frac{J}{\sum_j M_j a_j{}^2} = \frac{1}{4} \frac{\text{polar moment of inertia about centroid}}{\text{sum of moments of } M_j \text{ about centroid}} \quad \ldots\ldots (21e)$$

$$\sigma_j = \left(\frac{\omega_j}{\omega_b}\right)^2 = \left(\frac{\text{"frequency" of j th axle}}{\text{frequency of beam}}\right)^2 \quad \ldots\ldots (21f)$$

in which $\omega_j^2 = k_j/M_j$, and $\omega_b = 2\pi/T_b$; $\bar{p} = (\omega_b^2/32\ g)\rho = \frac{1}{16}\frac{\text{initial surface profile;}}{\Delta_b}$

$\Delta_b = \frac{2\ g}{\omega_b 2} \cong \frac{m_b\ g\ L^4}{48.7\ E\ I} \cong$ mid-span deflection due to a force equal to weight of beam applied at mid-span; and $\bar{p}_j = \bar{p}$ evaluated at x_j.

Dependent Variables of System.—

$$\phi = \frac{\eta_f}{\Delta_b} = \frac{\text{first harmonic component of beam deflection}}{\Delta_b} \quad \ldots\ldots \quad (22a)$$

$$\zeta = \frac{z}{\Delta_b} = \frac{\text{vertical displacement of sprung mass}}{\Delta_b} \quad \ldots\ldots\ldots \quad (22b)$$

and

$$\theta = \frac{u\ s}{\Delta_b} = \frac{\text{rotation of sprung mass x axle spacing}}{\Delta_b} \quad \ldots\ldots\ldots \quad (22c)$$

Independent Variables of System.—

$$\tau = \pi\frac{vt}{L} = \pi\frac{\text{distance of rear axle from left support}}{\text{span length}} \quad \ldots\ldots\ldots \quad (23a)$$

$$\xi = \pi\frac{x}{L} = \pi\frac{\text{distance from left support}}{\text{span length}} \quad \ldots\ldots\ldots\ldots\ldots \quad (23b)$$

With the foregoing definitions of dimensionless quantities, it can be verified by direct substitution that the differential equations may be written in the following form:

$$\phi_{\tau\tau} = \frac{1}{A1}\left(A_2\,\zeta + A_3\,\theta + A_4 - A_5\,\phi_\tau - A_6\,\phi - A_7\right) \ldots\ldots \quad (24)$$

$$\zeta_{\tau\tau} = B_1\,\phi - B_2\,\zeta + B_3\,\theta + B_4 \quad \ldots\ldots\ldots \quad (25)$$

and

$$\theta_{\tau\tau} = C_1\,\phi + C_2\,\zeta - C_3\,\theta + C_4 \quad \ldots\ldots\ldots \quad (26)$$

in which each subscript τ represents a differentiation with respect to τ, and the letters A, B, and C (with subscripts) represent known functions of the dimensionless parameters and the independent variable τ. These functions are given in Appendix I.

COMPUTATIONS OF DYNAMIC RESPONSES

In the derivation of the differential equations, the quantity y, the deflection of the neutral axis, is measured from its original position when the beam is not even loaded by its own weight. However, in the case of such practical engineering problems as the dynamic behavior of highway bridges under moving vehicles, (for which the present beam-load model was devised), the weight of the beam (representing the bridge) must be considered as already applied to the structure at the start of the problem. It is this case that is considered in the following sections.

Before describing the computations of response, it may be pointed out that for the prior-mentioned case the initial value of y, for the integration of the differential equations, should be set equal to the static deflection due to the weight of the beam. Furthermore, if the beam is cambered in order to have a horizontal surface under the action of its weight, the initial profile function p(x) must be set equal to the negative of the static deflection due to the dead weight.

It may be noted also that the expressions of responses given subsequently do not include the static effects due to the weight of the beam itself.

Dynamic Deflections.—Denoting by y_d the dynamic deflection due to the applications of the axle loads, it is seen that

$$y_d = y - Y_b \quad \ldots\ldots\ldots\ldots\ldots \quad (27)$$

in which Y_b represents the static deflection due to the weight of the beam.

Dynamic Bending Moments.—The dynamic bending moments are computed by treating the dynamic reactions between the axles and the beam surface and the inertia forces of the beam as forces statically applied to the structure.

Denoting by P_j the dynamic reaction between the j th axle and the beam surface,

$$P_j = \left[(M_j + m_j)g\right] + \left[k_j\left(z + (-1)^j a_j u - w_j\right)\right] - m_j w_{j,tt} \ldots\ldots \quad (28)$$

The first term in brackets represents the weight of the axle; the second term represents the dynamic force in the spring; and the third term the inertia force due to the unsprung mass.

The dynamic bending moment at section x due to the j th axle is given by the equations:

$$(M_d)_x^j = \epsilon_j (P_j/L)(L - x_j)x, \; (x_j \geq x) \ldots\ldots\ldots \quad (29a)$$

and

$$(M_d)_x^j = \epsilon_j (P_j/L)(L - x)x_j, (x_j < x) \ldots\ldots\ldots \quad (29b)$$

The dynamic shear at any section x due to the inertia forces of the beam is given by the expression:

$$(Q_d)_x^b = -\int_o^L \frac{L - x}{L} m_b y_{tt}\, dx + \int_o^x m_b y_{tt}\, dx \ldots\ldots \quad (30)$$

The first integral in Eq. 30 represents the reaction at the left support; the second integral represents the total load to the left of section x. It has been noted previously that $y = f\sum_{n=1}^{\infty} \eta_n \sin \frac{n\pi x}{L}$, and the series in Eq. 30 converges rapidly. Since the inertia forces do not constitute the primary part of the loading when the total maximum dynamic bending moment is considered, it seems reasonable to use only the first term of the series expansion. On subsitution of $y = f\eta \sin \frac{\pi x}{L}$ into Eq. 30, Eq. 31 is obtained.

$$(Q_d)_x^b = -m_b (f\eta)_{tt} \frac{L}{\pi} \cos \frac{\pi x}{L} \ldots\ldots\ldots\ldots \quad (31)$$

The bending moment due to the inertia forces of the beam is then given by the equation:

$$(M_d)_x^b = \int_o^x (Q_d)_x^b\, dx = -m_b \left(\frac{L}{\pi}\right)^2 (f\eta)_{tt} \sin \frac{\pi x}{L} \ldots\ldots \quad (32)$$

The total dynamic bending moment at section x, $(M_d)x$, is then equal to the

sum of Eqs. 29 and 32, that is,

$$(M_d)_x = \left[\sum_j (M_d)_x^j\right] + (M_d)_x^b \quad \ldots\ldots\ldots\ldots (33)$$

NUMERICAL SOLUTIONS

As mentioned previously the governing differential equations, Eqs. 18, 19, and 20 or Eqs. 24, 25 and 26, may be integrated numerically. The method of numerical integration used for the solutions presented herein is due to Newmark.[12]

The numerical problems considered here pertain to the case mentioned previously; that is, as an initial condition of the system, the weight of the beam has already been applied to it. Furthermore, the response of the beam is considered for the time interval between the entry of the front axle to the span and the departure of the rear axle from the span. Unless otherwise stated, the results are obtained for the following conditions at the instant the front axle enters the beam: (a) The sprung part of the load has no vertical or angular motion; (b) the beam is at rest; and (c) the beam surface profile is perfectly smooth and horizontal.

In the following, the dynamic response are presented as values of the ratio of the dynamic response to certain reference static response. In each case, the reference static response used may be computed from theories of determinate structures.

The solutions were obtained with a computer program[13] prepared for use on the ILLIAC, the digital computer of the University of Illinois.

History Curves.—A history curve is a graph of the response of the beam as a function of time. Fig. 2 shows a history curve of the bending moment at the mid-span. This is due to a two-axle load in terms of the maximum static bending moment at the same section of the beam, due to the same load. The horizontal axis in this figure denotes the dimensionless quantity $v\,t/L$, which represents the distance over which the rear axle has traveled on the beam as a fraction of the span length. The numerical values of the parameters of the problem solved are given as follows: $\alpha = 0.15500$; $s/(2L) = 0.30110$; $\Gamma_1 = 0.12600$; $\Gamma_2 = 0.11820$; $\gamma_1 = 0.01498$; $\gamma_2 = 0.02282$; $\sigma_1 = 0.30400$; $\sigma_2 = 0.27000$; and $\lambda = 0.25000$.

These numerical values correspond approximately to a 45-foot highway bridge and a 20 ton two-axle vehicle with an axle spacing of 30 feet traveling at a speed of about 51 miles per hour.

Also plotted in Fig. 2 is a curve representing the static response, that is, the response when the speed of the moving load approaches zero. It may be noted that, approximately speaking, the dynamic curve "oscillates" about the static curve. The maximum dynamic moment, occurring at $v\,t/L = 0.55$ is about 15% larger than the maximum static moment.

For the same problem as that considered in Fig. 2, the dynamic and static history curves for mid-span deflection (in terms of maximum static mid-

---

12 "A Method of Computation for Structural Dynamics," by N. M. Newmark, Journal of Engineering Mechanics Division, ASCE, Vol. 85, No. EM 3, July, 1959.

13 "Dynamic Behavior of Simple Span Highway Bridges Traversed by Two-axle Vehicles," R. K. Wen, thesis presented to the Univ. of Illinois, at Urbana, in 1957, in partial fulfilment of the requirements for the degree of Doctor of Philosophy.

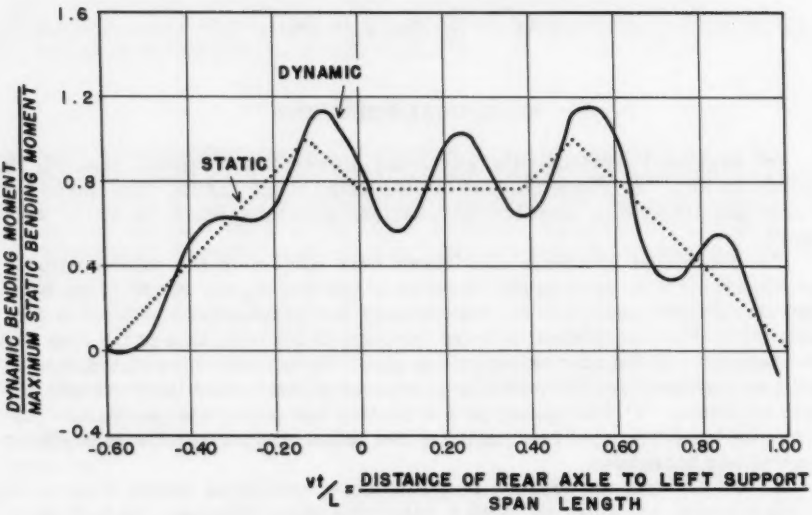

FIG. 2.—HISTORY CURVES FOR MID-SPAN BENDING MOMENTS.

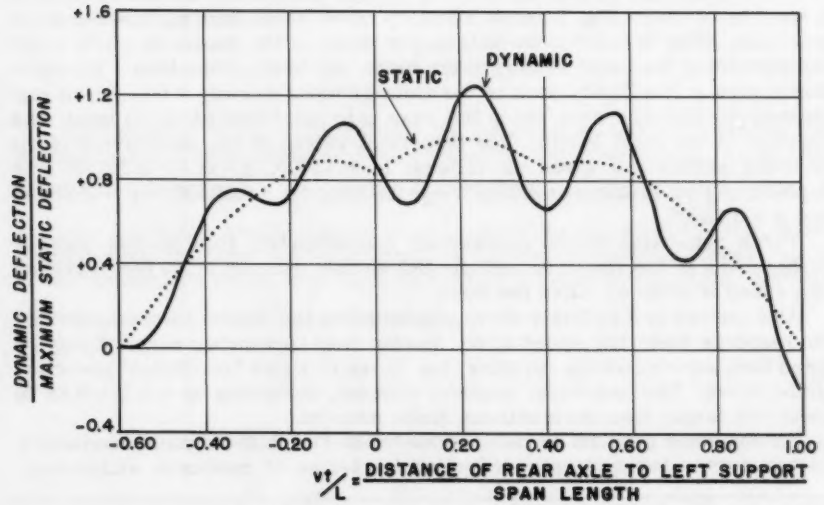

FIG. 3.—HISTORY CURVES FOR MID-SPAN DEFLECTIONS.

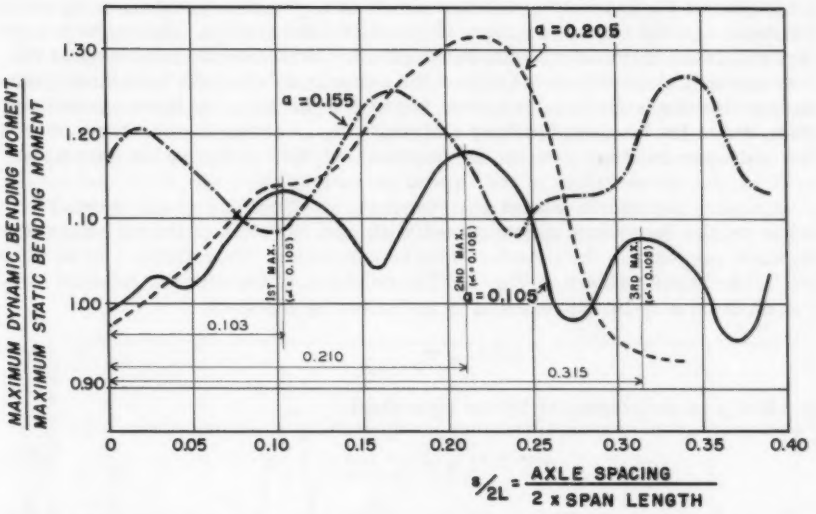

FIG. 4.—MAXIMUM RESPONSE AS FUNCTION OF AXLE SPACING PARAMETER.

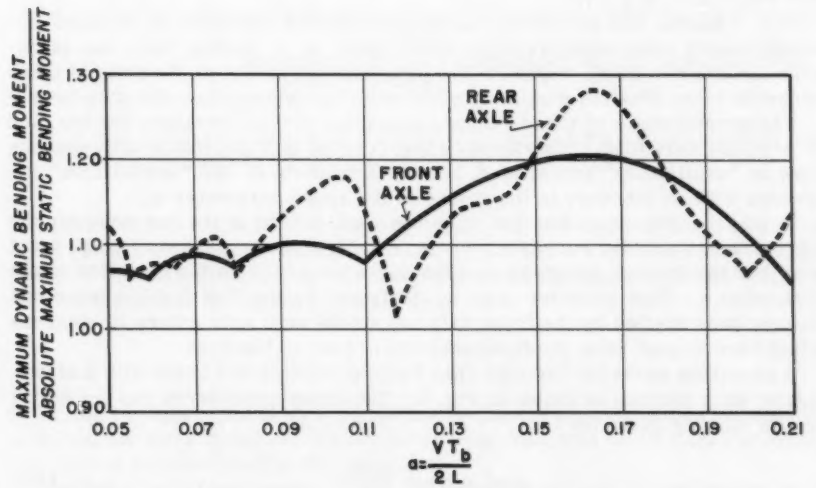

FIG. 5.—MAXIMUM RESPONSE AS FUNCTION OF SPEED PARAMETER.

span deflection) are shown in Fig. 3. In this case, the maximum dynamic deflection is seen to be about 25% larger than the maximum static deflection.

Spectrum Curves.—A "spectrum curve" is a plot of the maximum dynamic response against some parameter of the beam-load system. Hence, each point of a spectrum curve represents the maximum ordinate taken from some history curve. Unless otherwise stated, the numerical values of the various parameters for the solutions presented below are the same as those previously, given under the heading, "History Curves." Fig. 4 shows the spectrum curves for mid-span bending moment as functions of the "axle spacing parameter" $s/(2\,L)$, for three values of the "speed parameter" α.

It seems logical to expect that when the applications of the moving axle loads on the beam are synchronized with the vibration of the structure, the dynamic response in the structure may be augmented. This appears to be born out by the results shown in Fig. 4. The condition of the afore-mentioned synchronization may be represented by the following equation:

$$s/v = n\,T_b \quad \ldots\ldots\ldots\ldots\ldots\ldots \quad (34)$$

in which n is an integer, or by the equivalent,

$$\frac{s}{2\,L} = n\left(\frac{v\,T_b}{2\,L}\right) = n\,\alpha \quad \ldots\ldots\ldots\ldots\ldots \quad (35)$$

It can be seen from Fig. 4, that for a given curve the peak responses occur at values of $s/(2\,L)$, that are very close to multiples of the value of α, to which the curve corresponds. For example, take the curve for $\alpha = 0.105$. The first, second, and third peaks occur respectively at values of $s/(2\,L)$ equal to 0.103, 0.210, and 0.315.

Fig. 5 shows two spectrum curves for bending moments at sections instantaneously underneath the axles as functions of α. In this case, the maximum dynamic bending moments are presented as values of the ratio of these moments to the absolute maximum static bending moment due to the axle loads.

The general shape of these curves are similar to those obtained for the case of a single axle load.[7] They indicate that the values of the maximum response have an "oscillatory" appearance, but the amplitude of the "oscillations" increases with an increase in the values of the speed parameter α.

It may be observed that not only the peak values of the response for the section underneath the rear axle are appreciably larger than those for the front axle, but the former response is also more sensitive to the variation of the parameter α. This behavior may be explained by the fact that the beam has already been excited by the front axle before the rear axle enters it, whereas it had been at rest when the front axle first came on the span.

A spectrum curve for the mid-span bending moment of a beam with a sinusoidally wavy surface is shown in Fig. 6. The beam considered has an initial profile function given by

$$p(x) = b \sin \frac{m\,\pi x}{L} \quad \ldots\ldots\ldots\ldots\ldots \quad (36)$$

in which b and m denote, respectively, the amplitude and the number of half sine waves representing the surface of the beam. For the problem considered

in Fig. 6, the value of m, represented by the horizontal axis, is varied, while b is held at a constant value of $0.0032\ g/\omega_b^2$. The values of the other parameters for this problem are: $\alpha = 0.10000$; $s/2\ L = 0.10000$; $\Gamma_1 = \Gamma_2 = 0.07184$; $\gamma_1 = \gamma_2 = 0.01112$; $\sigma_1 = \sigma_2 = 0.82180$; and $\lambda = 0.25000$.

It may be noted that the graph in Fig. 6 has the characteristic appearance of a "resonance diagram" for some oscillating system. It shows that there are two "critical" values of m: m = 8.5, and m = 12.5, at which the responses attain a relative maximum. It is of interest to note that these values may be predicted approximately by a simple consideration of possible "resonance" behavior due to the wavy surface.

Picturing the crossing of the load over the wavy surface of the beam as a stationary load resting on a horizontally moving surface, and neglecting the

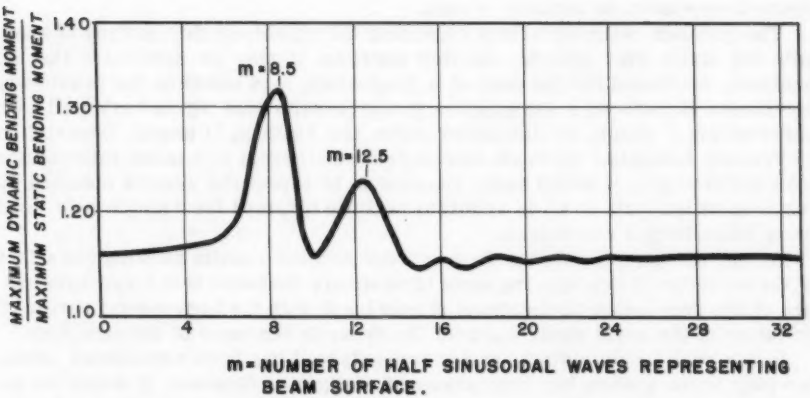

FIG. 6.—MAXIMUM RESPONSE AS FUNCTION OF NUMBER OF HALF SINUSOIDAL WAVES REPRESENTING BEAM SURFACE.

flexibility of the beam, the load may be thought of as being subjected to a periodic disturbance with a period equal to $(2\ L)/(m\ v)$. Setting this quantity equal to the natural period of vibration of the moving load a "critical" value of m is obtained for the problem considered.

$$m = \frac{\omega_1 L}{v}\left(\frac{1}{\pi}\right) = \frac{\sqrt{\sigma_1}}{\alpha} = 9.1$$

It can be shown that if $\sigma_1 = \sigma_2$, which is the case for the system being considered, the two natural periods of the moving load, that of vertical oscillation and that of angular oscillation, are equal.

Setting $(2\ L)/(m\ v)$ equal to the fundamental natural period of the beam, another "critical" value of m equal is obtained as follows:

$$m = \frac{\omega_b L}{v}\left(\frac{1}{\pi}\right) = \frac{1}{\alpha} = 10.0$$

The preceding values of 9.1 and 10.0 are rather close to the "critical" values of 8.5 and 12.5 as indicated in Fig. 6.

For large values of m (greater than about 16), the response becomes, for all practical purposes, the same as that for m = 0, that is, for a smooth beam surface.

CONCLUSION

A method of analysis is presented for the dynamic response of a simply supported beam subjected to a moving two-axle load. The analysis is based on the assumption that the shape of the dynamic deflection curve of the beam is similar to that of the static deflection curve under the weights of the beam and the moving loads. It may be noted that this assumption would lead to an exact solution of the problem if the speed of the moving loads approaches zero, and the beam-load system is initially at rest.

The question naturally arises regarding the validity of this method of analysis for finite load speeds. On this question, it may be mentioned that an analysis, developed for the case of a single axle load based on the previously mentioned Hillerborg's assumption, yields results that agree very well with experiments.[7] Since, as discussed under the heading, "General Description of Present Analysis," the basic assumption used herein is a more rational one than Hillerborg's, it would seem reasonable to expect the results obtained by the present analysis to be as accurate as those obtained for a single axle load using Hillerborg's assumption.

Among the few numerical solutions presented, the results showing the effect of the variation of axle spacing seem to vindicate the belief that a synchronization of the successive applications of axle loads with the fundamental period of vibration of the beam would augment the dynamic response of the structure.

In this paper, only a single unit of two-axle load has been considered. Also, damping in the system has been assumed negligible. However, it would not be difficult to consider in the analysis multiple units of two-axle loads and damping effects. In fact, the differential equations governing the motion of such a system have been derived elsewhere.[12]

ACKNOWLEDGMENTS

This paper is based on part of a thesis, by the author, submitted to the Grad. College of the Univ. of Illinois, in partial fulfillment of the requirements for the degree of Doctor of Philosophy in Engrg. The thesis was wrtiten under the supervision of Professor A. S. Veletsos.

The investigation was sponsored by the Illinois Division of Highways and the U.S. Bureau of Public Roads. The statements made in this paper, however, do not necessarily represent the views of these organizations.

APPENDIX I. COEFFICIENTS OF DIMENSIONLESS DIFFERENTIAL EQUATIONS (Eqs. 24, 25 and 26)

$$A_1 = 1 + \frac{2}{\eta} \sum_j \gamma_j \psi_j \sin \xi_j;$$

$$A_2 = \frac{2}{\alpha^2} \sum_j \epsilon_j \Gamma_j \sigma_j \sin \xi_j;$$

$$A_3 = \frac{2}{\alpha^2} \sum_j \epsilon_j (-1)^j \sigma_j \frac{\Gamma_1 \Gamma_2}{\Gamma_1 + \Gamma_2} \sin \xi_j;$$

$$A_4 = \frac{1}{\alpha^2} \left[\frac{2}{\pi} + \sum_j \epsilon_j \left(\Gamma_j + \gamma_j \right) \sin \xi_j \right];$$

$$A_5 = \frac{4}{\eta} \sum_j \epsilon_j \gamma_j \sin \xi_j \left(\psi_{j,\tau} - \frac{\eta_\tau}{\eta} \psi_j \right);$$

$$A_6 = \frac{1}{\alpha^2} + \frac{2}{\eta \alpha^2} \left(\sum_j \epsilon_j \sigma_j \Gamma_j \psi_j \sin \xi \right)_j + \sum_j \epsilon_j \sin \xi_j \left(\gamma_j \psi_j \frac{4\eta_\tau^2 - 2\eta\, \eta_{\tau\tau}}{\eta^3} - \gamma_j \psi_{j,\tau} \frac{4\eta_\tau}{\eta^2} + \gamma_j \psi_{j,\tau\tau} \frac{2}{\eta} \right);$$

$$A_7 = \frac{1}{\alpha^2} \sum_j \epsilon_j 32 \sin \xi_j \left(\sigma_j \Gamma_j \bar{p}_j + \alpha^2 \gamma_j \frac{d^2 \bar{p}_j}{d \xi^2} \right);$$

$$B_1 = \frac{1}{\alpha^2} \frac{1}{\sum_j \Gamma_j} \left(\sum_j \sigma_j \Gamma_j \psi_j \right) \frac{1}{\eta};$$

$$B_2 = \left(\frac{1}{\alpha^2 \sum_j \Gamma_j} \right) \sum_j \sigma_j \Gamma_j;$$

$$B_3 = \frac{\Gamma_1 \Gamma_2}{\alpha^2 \left(\sum_j \Gamma_j \right)^2} \sum_j (-1)^{j+1} \sigma_j;$$

$$B_4 = \left(\frac{16}{\alpha^2 \sum_j \Gamma_j} \right) \sum_j \sigma_j \Gamma_j \bar{p}_j;$$

$$C_1 = \frac{1}{\alpha^2 4\, \lambda \eta} \sum_j (-1)^j \sigma_j \psi_j;$$

$$C_2 = \frac{1}{4 \alpha^2 \lambda} \sum_j (-1)^{j+1} \sigma_j;$$

$$C_3 = \frac{1}{4 \alpha^2 \lambda \sum_j \Gamma_j} \sum_j \sigma_{\bar{j}}; \quad (\bar{j} = 1 \text{ if } j = 2;\ \bar{j} = 2 \text{ if } j = 1)$$

$$C_4 = \frac{4}{\alpha^2 \lambda} \sum_j (-1)^j \sigma_j \bar{p}_j$$

. . . . . (37)

The functions Ψ_j (in polynomial form), η, and their derivatives that appear in the preceding expressions are derived as follows:

as first defined in Eq. 4 $\Psi = K_1 Y$. Considering

$$Y = Y_b + \sum_j Y_j \quad \ldots\ldots\ldots\ldots\ldots \quad (38)$$

in which Y_b and Y_j denote the static deflections due to the weight of the beam and the j th axle, respectively, Eq. 39 may then be written

$$\Psi = K_1 Y_b + \sum_j K_1 Y_j$$

or

$$\Psi = \Psi_b + \sum_j \Psi_j \quad \ldots\ldots\ldots\ldots\ldots \quad (39)$$

in which $\Psi_b = K_1 Y_b$ and $\Psi_j = K_1 Y_j$.

Choosing $K_1 = \dfrac{E I}{16 m_b g} \left(\dfrac{\pi}{L}\right)^4$, the following function is obtained:

$$\Psi_b = \frac{E I}{16 m_b g}\left(\frac{\pi}{L}\right)^4 \frac{m_b g x}{24 E I}\left(L^3 - 2 L x^2 + x^3\right)$$

$$= \frac{\pi^4}{24} \bar{\xi}\left[\frac{1}{8} - \bar{\xi}^2 + \bar{\xi}^3\right] \quad \ldots\ldots\ldots\ldots\ldots \quad (40)$$

in which $\bar{\xi}$ is equal to $x/(2 L)$.

The function Ψ_j can be derived in a similar manner. Hence, one can readily verify that the function Ψ and its derivatives, evaluated at ξ_j, are given by the following expressions:

$$\Psi_j = \frac{\pi^4}{24} \bar{\xi}_j\left(\frac{1}{8} - \bar{\xi}_j^2 + \xi_j^3\right)$$

$$+ \sum_{k=1}^{2} \epsilon_k \left\{\frac{\pi^4}{6}\left(\gamma_k + \Gamma_k \bar{\xi}_j\left(\frac{1}{2} - \bar{\xi}_k\right)\left[\frac{1}{4} - \left(\frac{1}{2} - \bar{\xi}_k\right)^2 - \bar{\xi}_j^2\right]\right\} \quad \ldots (41)$$

$$\Psi_{j,\tau} = \frac{\pi^3}{48}\left(\frac{1}{8} - 3 \xi_j^2 + 4 \bar{\xi}_j^3\right)$$

$$+ \sum_{k=1}^{2} \epsilon_k \left\{\frac{2}{3}\pi^3\left(\gamma_k + \Gamma_k\right)\left[\frac{1}{2} - \frac{1}{2}\left(\bar{\xi}_k + \bar{\xi}_j\right)\right]\left(\bar{\xi}_k + \bar{\xi}_j\right)\left[\frac{1}{4} - \frac{1}{2}\left(\bar{\xi}_k + \bar{\xi}_j\right)\right]\right\} \ldots (42)$$

and

$$\Psi_{j,\tau\tau} = \frac{\pi^2}{8}\ \bar{\xi}_j\left(\bar{\xi}_j - \frac{1}{2}\right)$$

$$+\sum_{k=1}^{2} \epsilon_k \left[\frac{\pi^3}{3}(\Gamma_k + \gamma_k)\right]\left\{\frac{1}{8} - \frac{3}{2}\left(\bar{\xi}_k + \bar{\xi}_j\right)\left[\frac{1}{2} - \frac{1}{2}\left(\bar{\xi}_k + \bar{\xi}_j\right)\right]\right\} \quad \ldots\ldots\ (43)$$

in which the subscript k, representing an axle, is a "dummy" index used in summation; $\bar{\xi}_j$ and ξ_k represent $x_j/(2L)$ and $x_k/(2L)$, respectively.

Eq. 41 holds true only when $\bar{\xi}_j \leq \bar{\xi}_k$. For the case in which $\bar{\xi}_j > \bar{\xi}_k$, the symbols $\bar{\xi}_j$ and $\bar{\xi}_k$ should be interchanged. It may be noted that Eqs. 42 and 43 are symmetrical in $\bar{\xi}_j$ and $\bar{\xi}_k$.

The η - function is give by Eq 6. In order to be consistent with the previous choice of the value of K_1, the value of K_2 in Eq. 6 should be set equal to $1/8\ (m_b\ g\ L)$. This yields the expression

$$\eta_n = \frac{1}{4\pi} + \frac{1}{8}\sum_j \epsilon_j(\Gamma_j + \gamma_j)\sin\xi_j \quad \ldots\ldots\ (44)$$

The first and second derivatives of are, respectively,

$$\eta_\tau = \frac{1}{8}\sum_j \epsilon_j\left(\Gamma_j + \gamma_j\right)\cos\xi_j \quad \ldots\ldots\ (45)$$

and,

$$\eta_{\tau\tau} = -\frac{1}{8}\sum_j \epsilon_j\left(\Gamma_j + \gamma_j\right)\sin\xi_j \quad \ldots\ldots\ (46)$$

APPENDIX II. NOTATION

The following symbols were adopted for use in the paper and for the guidance of discussers.

- a_j = horizontal distance between j th axle and centroid of $\overline{M}$;
- E I = flexural rigidity of beam;
- f = a function of time defined in Eq. 7;
- g = gravitational acceleration;
- J = polar moment of inertia of $\overline{M}$ about centroidal axis;
- j = axle index; j = 1 and j = 2 refer respectively to the rear and front axle;
- k_j = spring constant of j th axle;
- L = span length of beam;
- $\overline{M}$ = total sprung mass;

M_j = $(z_s)_j/g$;

m_b = mass of beam per unit length

m_j = unsprung mass of j th axle;

n = an integer;

p = a function of x definirg the initial profile of travel surface;

$\bar{p}$ = $p\left(\frac{\omega_b^2}{32\,g}\right)$;

s = spacing between axles;

T = kinetic energy;

T_b = $\frac{2\,L^2}{\pi}\sqrt{\frac{m_b}{E\,I}}$ = fundamental period of beam;

t = time coordinate;

u = angular displacement of centroid of $\overline{M}$;

V = potential energy;

v = horizontal velocity of load;

w = p + y = profile of travel surface;

w_j = w evaluated at x_j;

x = length coordinate, see Fig. 1;

x_j = distance from left support to j th axle;

Y = static deflection of beam;

Y_b = static deflection of beam due to its own weight;

y = deflection of neutral axis of beam;

z = vertical displacement of centroid of $\overline{M}$;

$(z_s)_j$ = static deformation of spring in j th axle;

α = defined in Eq. 21;

Γ_j = defined in Eq. 21;

γ_j = defined in Eq. 21;

ϵ_j = 1 if $0 \leq x_j \leq L$; $_j$ = 0 otherwise

η = $\eta_{n=1}$;

η_n = defined by Eq. (6);

λ = defined in Eq. 21;

ξ = defined in Eq. 23;

σ_j = defined in Eq. 21;

τ = defined in Eq. 23;

Ψ = a function defined in Eq. 4;

Ψ_j = evaluated at x_j, also see Appendix I.

$\omega_b = \frac{2\pi}{T_b}$; and

$\omega_j = \sqrt{k_j / M_j}$.

Journal of the
ENGINEERING MECHANICS DIVISION
Proceedings of the American Society of Civil Engineers

BEARING CAPACITY OF FLOATING ICE SHEETS

By G. G. Meyerhof,[1] F. ASCE

SYNOPSIS

The collapse of floating ice sheets under load is estimated on the basis of a rigid-plastic plate on an elastic foundation for various loading and boundary conditions. The results are compared with field observations in the operation of ice roads and floating airfields and some small-scale loading tests.

INTRODUCTION

A large floating ice sheet under load can be represented by a plate on an elastic foundation of which the reaction pressure at every point is directly proportional to the deflection of the plate at that point. This approach using a theory of elastic plates in the problem of the bearing capacity of ice sheets was first made by Hertz some 75 yr ago (1884) and has been used ever since. Investigations have shown that the estimated strains and deflections under short-time loads, much less than the ultimate, agree well with observations. However, as the failure load is approached, or under long-time loading conditions, the theory of elasticity becomes less applicable. It is believed that a better

Note.—Discussion open until March 1, 1961. To extend the closing date one month, a written request must be filed with the Executive Secretary, ASCE. This paper is part of the copyrighted Journal of the Engineering Mechanics Division, Proceedings of the American Society of Civil Engineers, Vol. 86, No. EM 5, October, 1960.

[1] Head, Dept. of Civ. Engrg., Nova Scotia Tech. College, Halifax, Nova Scotia, Canada.

estimate of the ultimate load can be obtained from a limit analysis of plates on the basis of plastic theory.

CENTRAL LOAD ON LARGE ICE SHEETS (INFINITE PLATES)

Circular Load.—When a central concentrated load, much less than the ultimate, is applied over a small circular area on a large floating ice sheet of uniform thickness, the stresses and deflection of the sheet can be computed as for a thin, elastic, and infinite plate on a discontinuous-elastic foundation (Fig. 1(a)). The maximum positive radial and circumferential bending moments per unit length, M_r and M_t respectively, are equal under the center of the load, and the corresponding principal tensile stresses at the bottom of the plate are (1), (2), (3).[2]

$$s_r = s_t = 1.1\,(1 + u)\,(\log L/a + 0.26)\,P/h^2 \quad \ldots\ldots\ldots \quad (1)$$

in which L is the characteristic length or radius of relative stiffness, and

$$s_r = \left[\frac{E\,h^3}{12(1 - \mu^2)k}\right]^{1/4} \quad \ldots\ldots\ldots\ldots \quad (2)$$

E is the modulus of elasticity of the plate, P is the applied load, a is the contact radius of the load (for $a \geqslant 0.5\,h$), h is the plate thickness, k is the foundation modulus and μ is Poisson's ratio of the plate. The maximum negative radial bending moment occurs at a distance of about $r = 1.9\,L$ from the load and is, approximately, $M_r = -0.02\,P$. The maximum deflection is

$$w_o = P/8\,k\,L^2 \quad \ldots\ldots\ldots\ldots\ldots\ldots \quad (3)$$

and the radius of the deflection dish, below the original level surface, is about $r = 3.9\,L$.

As the load on the ice sheet increases the bending stresses below the load become equal to the flexural strength of the ice and the sheet begins to yield leading to radial tension cracks at the bottom (Fig. 1(b)). The yield load can be estimated from Eqs. 1 and 2 and is shown in Fig. 2a for various ratios of a/L and using Poisson's ratio of 1/3 for ice (4). The yield load is expressed in terms of the maximum elastic or yield bending moment per unit length, $M_y = f_b\,h^2/6$, where f_b is the flexural strength of the material. In the limit of a point load (a=0) the theoretical yield load is zero. Since the maximum negative radial bending moment is small compared with the moment under the load, large elastic ice sheets may be classified as infinite when they have a radius $R \geqslant 3\,L$. Further, a concentrated load would have to be more than 3 L from the edge of large sheets to satisfy these equations and to develop the estimated yield load.

With increasing load the radial cracks in the ice sheet increase in length and number until the bending stresses along a circumferential section of the sheet become equal to the flexural strength of the ice and a circumferential tension crack is formed on top (Fig. 1(b)). The ultimate bearing capacity or collapse load of the sheet is then reached. In order to determine the theoretical collapse load it is assumed that the ice sheet is a thin, rigid, ideally-plastic, and infinite plate, which can, without cracking, resist a full plastic or

[2] Numerals in parenthesis, thus (1), refer to corresponding items in the Bibliography. See Appendix II.

limit bending moment per unit length, $M_o = f_o h^2/4$, in which f_o is the yield strength of the material in tension. At collapse radial yield hinge lines extend from a plastic section below the load to a circumferential yield-hinge-circle of radius b (Fig. 1(b)).

The load carrying capacities of simply supported and fixed ideally-plastic circular plates under central concentrated and uniformly distributed loads have been discussed by several authors (5),(6),(7). The method of analysis can be extended to plates on a discontinuous-elastic foundation by neglecting, as previously, membrane action and shearing deformation. Full details are given in Appendix I, for a concentrated load on an infinite plate of which the material obeys the Tresca yield condition (shearing strength equal to one-half of yield strength in tension) and the associated flow rule. The theoretical

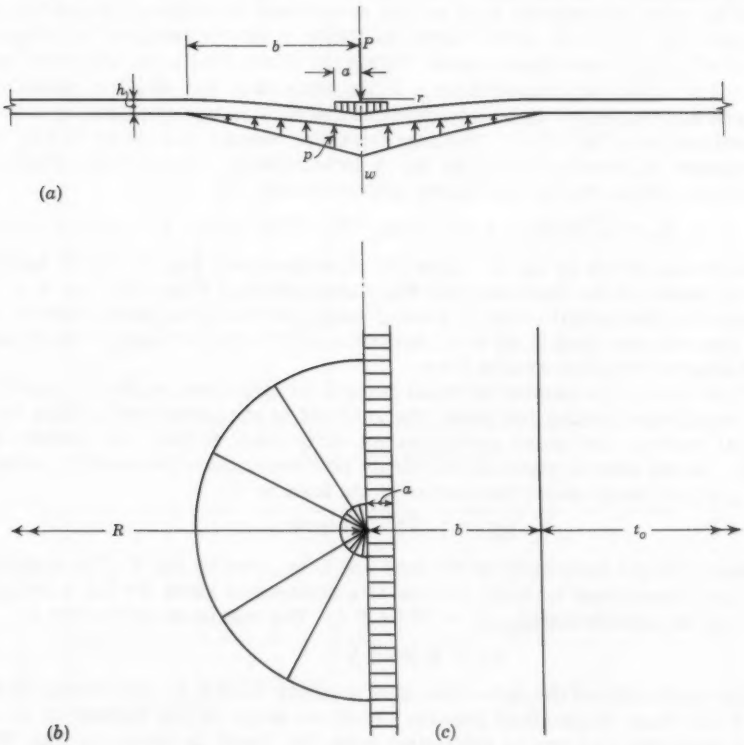

FIG. 1.—INFINITE PLATE UNDER LOAD

collapse load is shown in Fig. 3(a) for various ratios of a/b. While local bearing capacity under the load governs the minimum contact radius a, as shown later, the collapse value for a point load is found to be independent of the size and boundary conditions of the plate and the reaction pressure below the plate. The collapse load is

$$P_o = 2\pi M_o \text{ (for } a = 0) \quad \ldots\ldots\ldots\ldots\ldots\ldots \quad (4)$$

and, within the practical range of the contact radius,

$$P_O = 3.3\,\pi\,(1 + 6\,a/b)\,M_O \text{ (for } 0.02 < a/b < 0.2) \ldots\ldots\ldots (5)$$

The radial deflection of the plate is in the form of an inverted cone near the load and passes into a logarithmic shape at greater distance.

The radius b in the present analysis can only be expressed in terms of the characteristic plate parameter L by making a complete elastic-plastic analysis. When a concentrated load exceeds the yield load, the plate material near the load passes from the elastic to the plastic state and the central deflection increases more rapidly than the load. Since overall equilibrium of the applied load and the total reaction pressure below the plate is maintained, the radius of the deflection dish at collapse is less than the value of 3.9 L of an elastic plate. Similarly, the position of the maximum negative radial bending moment tends to move towards the load so that at collapse the critical circumferential section with the yield hinge circle is likely to have a radius of less than the 1.9 L obtained in the elastic state. Within the above limits, an effective radius of b = 3.9 L may be suggested for a large plate (and for smaller plates considered subsequently) as an approximate and safe value in estimating the collapse load from Fig. 3(a). The corresponding results are shown in Fig. 4(a) for various ratios of a/L. While Eq. 4 is unaffected, the collapse load from Eq. 5 can, therefore, be expressed, approximately, by

$$P_O = 3.3\,\pi\,(1 + 3\,a/2\,L)\,M_O \text{ (for } 0.05 < a/L < 1) \ldots\ldots\ldots (6)$$

in which L is given by Eq. 2. Since the yield moment, M_y, of ice is approximately equal to the limit moment M_O, comparison of Figs. 2(a) and 4(a) indicates the theoretical collapse load of large, floating ice sheets under a central concentrated load is, at least, approximately twice the load at which yielding begins or the first cracks form.

Strip Load.—If a number of equal central concentrated loads are applied in line on a large floating ice sheet, the analysis is simplified by ignoring longitudinal bending and using an equivalent strip load, P, per unit length (Fig. 1(a)). In the elastic state the maximum positive transverse bending moment, M_r, per unit length under the center of the load is (8)

$$M_r = (\sqrt{2}\,L - a)\,P/4 \ldots\ldots\ldots\ldots\ldots (7)$$

in which a is the half-width of the load and L is given by Eq. 2. The maximum negative transverse moment occurs at a distance of about 4 = 2.2 L from the load and is, approximately, $M_r = -0.07\,P\,L$. The maximum deflection is

$$w_O = P/2\,\sqrt{2}\,k\,L \ldots\ldots\ldots\ldots\ldots\ldots (8)$$

and the half-width of the deflection dish is about r = 3.3 L. The yield load at which the first longitudinal tension crack develops at the bottom of the ice sheet below the load can be estimated from Eq. 7 and is shown in Fig. 2(b). A strip load has to be more than 3 L from the edge of large sheets to satisfy the above equations and develop the estimated yield load.

As the load is increased, the longitudinal crack in the ice sheet increases until a longitudinal crack on each side of the load is formed on top of the sheet, and the collapse load is reached. At collapse, longitudinal yield hinge lines run along the center-line of the load and on each side of the load at a distance b from the axis (Fig. 1(c)). A solution of the collapse load has been obtained in Appendix I and is shown in Fig. 3(b) for various ratios of a/b. While the

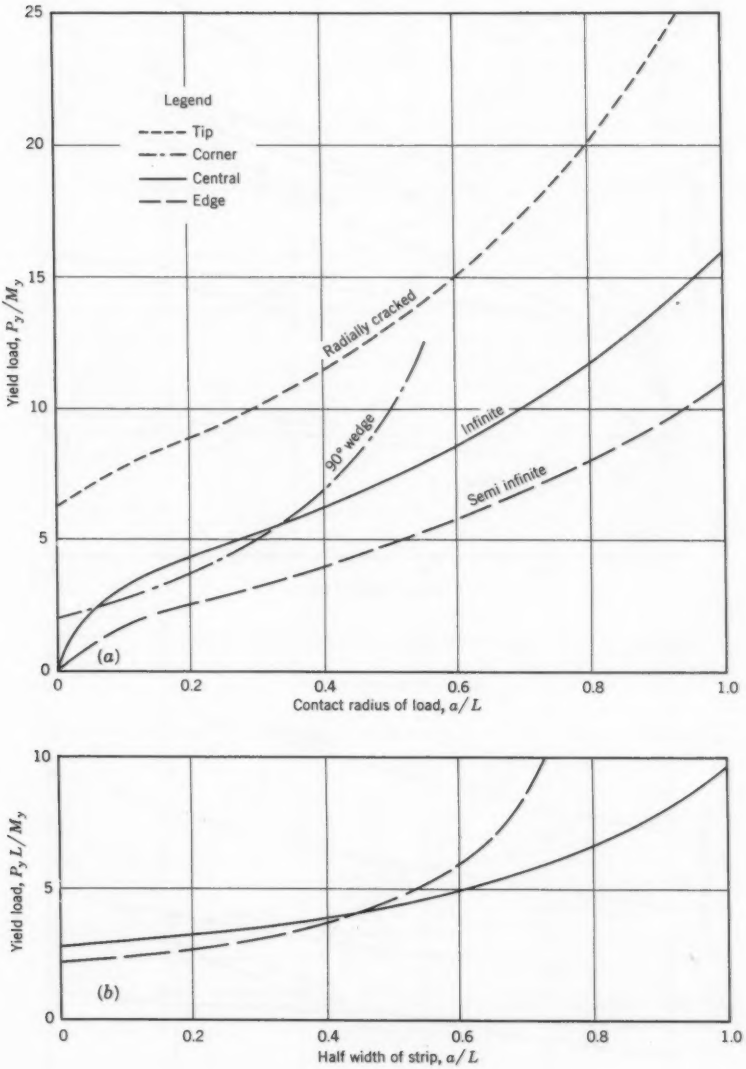

FIG. 2.—THEORETICAL YIELD LOAD OF PLATES

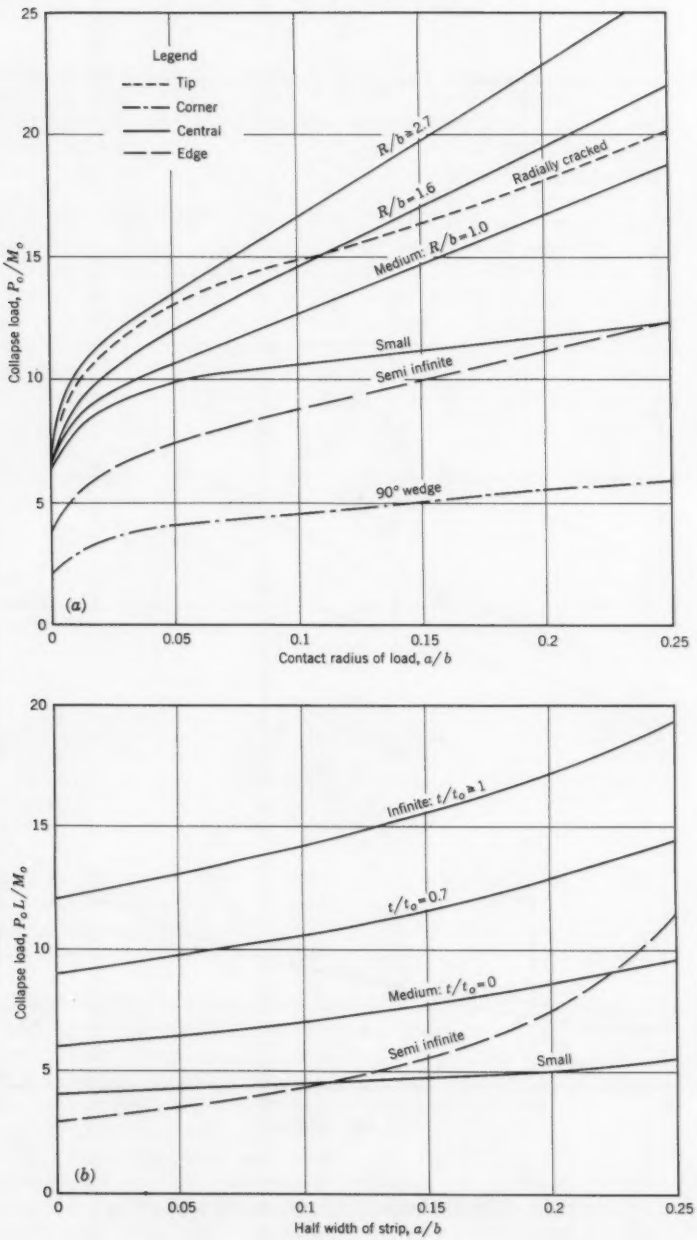

FIG. 3.—THEORETICAL COLLAPSE LOAD OF PLATES

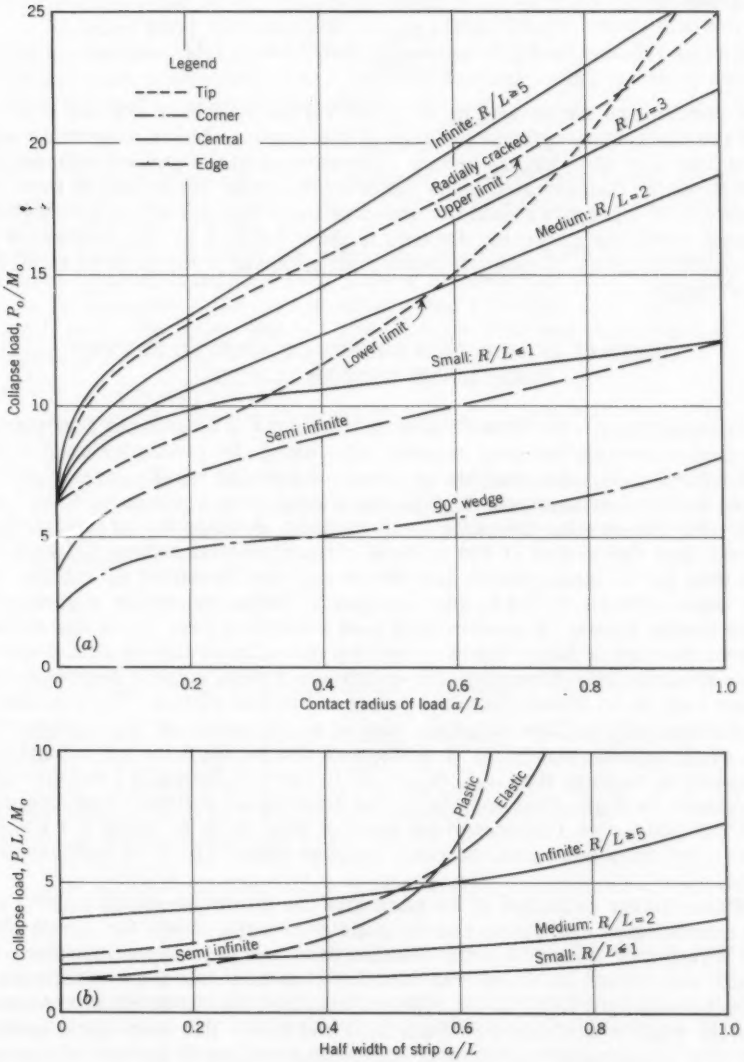

FIG. 4.—THEORETICAL COLLAPSE LOAD OF PLATES

distance b is likely to be between the limits of 2.2 L and 3.3 L mentioned previously, using the latter safe value the collapse load per unit length is, approximately,

$$P_o = \frac{3.6\ M_o}{L - a/2} \text{ (for } 0 < a/L < 1) \quad \ldots\ldots\ldots\ldots \quad (9)$$

The results are shown in Fig. 4(b) for various ratios of a/L and it is found that the theoretical collapse load is of the same order of magnitude as the yield load (for $M_y = M_o$, as before . Comparison of the present collapse loads with those for concentrated loads indicates that point loads spaced more than about b/2 or 2 L apart should be treated as individual loads, while for a greater contact width the governing distance is about 3 L to 4 L. The transverse deflection of the plate at collapse under a strip load is in the form of an inverted right wedge.

CENTRAL LOAD ON ICE SHEETS OF LIMITED EXTENT (SMALL AND MEDIUM PLATES)

Circular Load.—The size of floating ice sheets is sometimes less than that required to develop the limit moment, M_o, along the circumferential section at r = b (Fig. 1). An analysis of simply supported ideally-plastic circular plates with overhang shows (6) that plates must have a minimum total radius of R = 2.7 b to develop the radial limit moment. Because it was indicated previously that the radius of the critical circumferential section is likely to be less than 1.9 L, large plastic ice sheets may be classified as infinite when they have a radius $R \geqslant 5$ L, which is nearly twice the radius suggested for large elastic sheets. A concentrated load would thus have to be more than 5 L from the edge of large sheets to develop the collapse load of Eqs. 4 and 6.

As the plate size decreases, the maximum stress under a central concentrated load on an elastic plate decreases below that given by Eq. 1 so that the theoretical yield or first cracking load of an ice sheet is then greater than that of an infinite plate (2). A solution of this problem for the collapse load of a plate of medium size ($2 < R/L < 5$) is given in Appendix I and the results are shown in Figs. 3(a) and 4(a). The theoretical collapse load decreases with the plate size (expressed as ratio of R/b or R/L, using b = 1.9 L as above), but for a point load the same collapse value (Eq. 4) is obtained in all cases.

With a further reduction of the plate size the maximum stress under a central concentrated load on an elastic plate decreases, while for small plates with a radius of about $R \leqslant L$ the reaction pressure is practically uniform (2). On the assumption of a uniform reaction pressure below a centrally loaded plate of small size ($R \leqslant L$) the collapse load has been determined in Appendix I and the results are shown in Figs. 3(a) and 4(a). The theoretical collapse load of a small plate varies with the contact radius of the central load in a similar way to that of a medium plate, but it is generally smaller, except for a point load when Eq. 4 applies. The collapse load for a larger contact radius and b = 3.9 L as for larger plates is, approximately,

$$P_o = \frac{3\pi\ M_o}{1 - a/4L} \text{ (for } 0.1 < a/L < 1) \quad \ldots\ldots\ldots\ldots (10)$$

Strip Load.—In order to develop the limit moment, M_o, along the longitudinal section at r = b under a strip load, the cantilever overhang of the plate beyond that section must have a minimum length of t_o, so that a large plate must have a minimum total half-width $R = b + t_o$ (Fig. 1(c)). Since the critical longitudinal section is likely to be at a distance of b less than 2.2 L, as previously indicated, a safe estimate of the minimum half-width is, after substituting the value of t_o given in Appendix I,

$$R = 2.2\ L + \sqrt{2\ M_o/q\ h} \quad \ldots\ldots\ldots\ldots\ldots \quad (11)$$

in which q is the unit weight of the material. A strip load would have to be more than the distance given by Eq. 11, from the edge of large sheets to develop the collapse load of Eq. 9.

For a smaller plate width, the yield load increases while the collapse load decreases. The collapse load of a plate of medium size ($0 < t < t_o$ has been derived in Appendix I and the results are shown in Figs. 3(b) and 4(b) using b = 3.3 L as for the larger plates. The collapse load per unit length is, approximately,

$$P_o = \frac{1.8\ M_o \left[1 + (t/t_o)^2\right]}{L - a/2} \text{(for } 0 < a/L < 1 \text{ and } 0 < t < t_o) \quad \ldots\ldots (12)$$

For small plates with $R \leqslant L$, as before, the deflection is approximately uniform. The corresponding collapse load has been derived in Appendix I and is shown in Figs. 3(b) and 4(b) for b = 3.3 L. The collapse load per unit length is, approximately,

$$P_o = \frac{1.2\ M_o}{L - a/3} \text{ (for } 0 < a/L < 1) \quad \ldots\ldots\ldots\ldots\ldots (13)$$

EDGE LOAD ON LARGE ICE SHEETS (SEMI-INFINITE PLATES)

Circular Load.—When a large floating ice sheet is cracked, the bearing capacity is reduced and it is assumed that a crack cannot transmit bending moments or shearing forces. For a concentrated load applied over a small circular area tangent to the edge of an elastic semi-infinite plate, the maximum tensile stress at the edge under the load is (3)

$$s_r = \frac{(1+u)P}{(3+u)h^2}\left[8.8 \log \frac{L}{a} + 0.09 - 1.75\,u + 1.13\,(1+2\,u)\,\frac{a}{L}\right] \ldots (14)$$

The maximum negative radial bending moment occurs at the edge at a distance of about 2 L from the load and is, approximately, $M_r = -0.075$ P. The corresponding maximum moment at right angles to the edge occurs at a distance of about 1.4 L from the load and is, approximately, $M_r = -0.04$ P. Both moments are found on about the same deflection contour of the plate, as shown by model tests on elastic plates (4). The maximum deflection is

$$w_o = (1 - 0.89\ a/L)\ P/2.1\ k\ L^2 \quad \ldots\ldots\ldots\ldots (15)$$

and the radius of the deflection dish is about r = 3.9 L along the edge and r = 2.9 L at right angles to the edge. The yield load from Eq. 14 is shown in Fig. 2(a) and is about two-thirds of that of a center-loaded large plate. As the distance of the load from the free edge of the sheet increases, the yield load increases and approaches that of a central load when this distance is about 3 L.

As the concentrated edge load increases, radial cracks develop at the bottom of the sheet in the central zone and spread outwards until a circumferential crack is formed on top of the sheet extending to the free edge thereby leading to collapse (Fig. 5(a)). The state of plastic equilibrium and the deflection shape in the central sector are similar to those of an infinite plate with radial yield hinge lines and a circumferential yield hinge arc. Within the two outer zones, however, the radial and circumferential bending moments are less than the limit moment, which obtains only along the circumferential section along yield lines continuous with the yield hinge arc of the central sector. An approximate analysis of this problem is given in Appendix I and indicates that at collapse the outer zones are roughly triangular with an angle of 45° along the edge, and that the central sector has a center angle of 90° (Fig. 5(a)). The results shown in Figs. 3(a) and 4(a) for a semi-circular contact area of the load can be applied to a circular area by using an equivalent contact radius of $\sqrt{2}a$. The theoretical collapse load of an edge-loaded plate is thus about one-half of that of a center-loaded large plate.

With increasing distance of the load from the free edge of the sheet the collapse load increases and approaches that of a central load when this distance is about 5 L. An approximate solution of this problem is given in Appendix I by extending the analysis of an edge-loaded plate, which indicates that at collapse the central sector lies between two outer quadrilateral zones extending to the free edge (Fig. 5(b)). Using a safe value of b = 3.9 L as for a central load (the radius b increases from about 2.9 L for an edge load to about 3.9 L for a central load), the collapse load is, for $0 < e/L < 5$, approximately,

$$P_O = (2 + \pi/2)(1 + e/4L)M_O \quad \text{(for } a = 0) \quad \ldots\ldots\ldots \quad (16)$$

and

$$P_O = \left[0.82\pi(1+3a/2L) + \frac{4}{(1-a/3L)(1-e/16L)}\right](1+e/4L)M_O$$

$$\text{(for } 0.2 < a/L < 1) \quad \ldots\ldots\ldots\ldots \quad (17)$$

where e is the distance of the load from the free edge. The results of Eqs. 16 and 17 show that at the upper limit of e = 5 L the theoretical collapse load is about one-third greater than the value for a central load from Eqs. 4 and 6. This difference is due to the approximate (upper bound) nature of the analysis.

Strip Load.—If a strip load of width 2 a is adjacent to the edge of an elastic semi-infinite plate, the maximum negative transverse bending moment occurs at a distance of about 1.1 L from the load and is (8)

$$M_r = -0.32\,(\sqrt{2}\,L - 3a/2)\,P \quad \ldots\ldots\ldots\ldots (18)$$

The maximum deflection is

$$w_O = \sqrt{2}\,P/k\,L \quad \ldots\ldots\ldots\ldots\ldots\ldots (19)$$

and the width of the deflection dish is about r = 2.2 L. The yield load derived from Eq. 18 is shown in Fig. 2(b) and is roughly the same as for a center-loaded large plate.

At collapse of an edge-loaded plate when the deflected shape is a plane, a longitudinal yield hinge line develops at a distance b from the load. The collapse load has been derived in Appendix I and is shown in Figs. 3(b) and 4(b) using a safe value of b = 2.2 L, as indicated above. The collapse load per unit

length is, approximately,

$$P_o = \frac{4M_o/3}{L - 4a/3} \quad (\text{for } 0 < a/L < 3/4) \quad \ldots\ldots\ldots (20)$$

These estimates may be compared with the solution using elastic theory (Eq. 18) when

$$P_o = \frac{3.1\ M_o}{\sqrt{2}\,L - 3a/2} \quad (\text{for } 0 < a/L < 1) \quad \ldots\ldots\ldots\ldots (21)$$

The collapse load, according to Eq. 21 is likely to approximate the result of an elastic-plastic analysis and exceeds that estimated from Eq. 20. The difference decreases rapidly with increasing contact width and is reversed for greater widths (Fig. 4(b)). Hence, the theoretical collapse load of an edge-loaded sheet is generally above one-half that of a center-loaded large sheet. Comparing the present collapse loads with those for concentrated edge-loads, it is found that the latter should be treated as individual loads if they are spaced more than about b or 2 L apart.

With increasing distance e of the strip load from the free edge of the sheet the collapse load increases and approaches that of a central load at e = R (Eq. 11). A solution of this problem is given in Appendix I and, using a safe value of b = 3.3 L as for a central load, the collapse load per unit length is, approximately,

$$P_o = \frac{(1 + e/2\ L)M_o}{L - a(1 - e/8\ L)} \quad (\text{for } 0 < a/L < 1 \text{ and } 0 < e/L < 5). \ldots (22)$$

which approaches the value for a central load (Eq. 9) at the upper limit of e = 5 L, as mentioned before.

CORNER AND TIP LOADS ON LARGE ICE SHEETS (WEDGES AND SECTORIAL PLATES)

When a load is applied at the corner or tip of a wedge formed by a large floating ice sheet that is cracked along several radial sections, the stresses and deflection in the elastic state and the collapse load in the plastic state can be determined as for an edge-loaded sheet. For a concentrated load applied over a small circular area at the corner of a large elastic plate (90° wedge of infinite extent) the maximum tensile stress is (3),

$$s_r = \frac{3P}{h^2}\left[1 - \left(\frac{a\sqrt{2}}{L}\right)^{0.6}\right] \quad \ldots\ldots\ldots\ldots\ldots (23)$$

This stress occurs at the top of the plate at a distance from the corner of

$$r = 2.38\sqrt{a\ L} \quad \ldots\ldots\ldots\ldots\ldots\ldots (24)$$

measured along the bisector of the angle. The maximum deflection is

$$w_o = (1.1 - 0.88\ a\sqrt{2/L})\ P/k\ L^2 \quad \ldots\ldots\ldots (25)$$

and the radius of the deflection dish is about r = 3.6 L along the edge and about r = 2.7 L along the bisection (4). The yield load from Eq. 23 is shown in Fig. 2(a) and is, roughly, the same as for the center of a large sheet.

A complete analysis for a concentrated load at the tip of an infinite elastic wedge or sectorial plate with an apex angle of less than 90° does not appear to be available (9). However, an approximate solution can be obtained by extending the analysis leading to Eq. 23, which was based on the assumption that the corner-loaded plate acts like a beam of variable width without transverse bending. This assumption is closely supported by the results of model tests on tip-loaded elastic plates with a 90° angle. It is in complete agreement with tests on sectorial plates with an apex angle of 60° or less, when the deflection contours remained straight and the radius of the deflection dish along the bisector was about $r = 2.7\ L$ (4). If the original circular contact area of radius a of the concentrated load adjacent to the corner of a 90° sectorial plate is replaced by a quarter-circle of equal area with the center at the corner of the plate (or by a similar equivalent triangle), the center of gravity of either latter area is at a distance of about 1.2 a from the corner, compared with $\sqrt{2}a$ for the original contact area. Assuming that a concentrated load at the tip of a wedge with an apex angle of $\theta < 90°$ is uniformly distributed over a contact sector of the same radius 2 a as before, then the center of gravity of the contact sector for a small θ is at a distance of 4 a/3 from the corner, which is close to that of the original circular contact area of a plate with $\theta = 90°$. Accordingly, the magnitude and position of the maximum stress and the deflection of a tip-loaded elastic wedge or sectorial plate can be obtained with little, if any, loss of accuracy by modifying Eqs. 23 to 25 for the apex angle ($\theta < 90°$) and the distance g from the tip to the center of gravity of the concentrated load, applied over a contact sector of radius a or similar triangle (Fig. 6).

Thus, the maximum tensile stress at the top of an infinite elastic wedge plate with $\theta \leq 90°$ is (using Eq. 23),

$$s_r = \frac{3\,P}{h^2 \tan \theta/2} \left[1 - (g/L)^{0.6}\right] \quad \ldots\ldots\ldots (26)$$

This stress occurs at a distance from the tip of $r = 2\sqrt{g\,L}$, measured along the bisector (using Eq. 24). The distance g varies from 0.60 a for $\theta = 90°$ to the upper limit of 2 a/3 for a very small θ ($< 10°$, say) or narrow wedge for which the maximum stress, from Eq. (26), is

$$s_r = \frac{6\,P}{h^2\,\theta} \left[1 - (2\,a/3\,L)^{0.6}\right] \quad \ldots\ldots\ldots (27)$$

at a distance $r = 1.63\sqrt{a\,L}$ from the tip. Further, the maximum deflection is (using Eq. 25),

$$w_o = (1.1 - 0.88\,g/L)\,P/k\,L^2 \quad \ldots\ldots\ldots\ldots (28)$$

or, for a narrow wedge,

$$w_o = (1.1 - 0.59\,a/L)\,P/k\,L^2 \quad \ldots\ldots\ldots\ldots (29)$$

For a concentrated load applied over a small sector of radius a at the corner of a plate the yield load, from Eq. 26 for $\theta = 90°$ is somewhat less than that given by Eq. 23 because of the smaller contact radius. The theoretical yield load of a large floating ice sheet cracked radially into numerous long narrow wedges and supporting a common concentrated load at their tips can be estimated from Eq. 27 for $\theta = 2\pi$ and is shown in Fig. 2(a). This yield load is roughly twice that of a large uncracked sheet. The great difference of the theo-

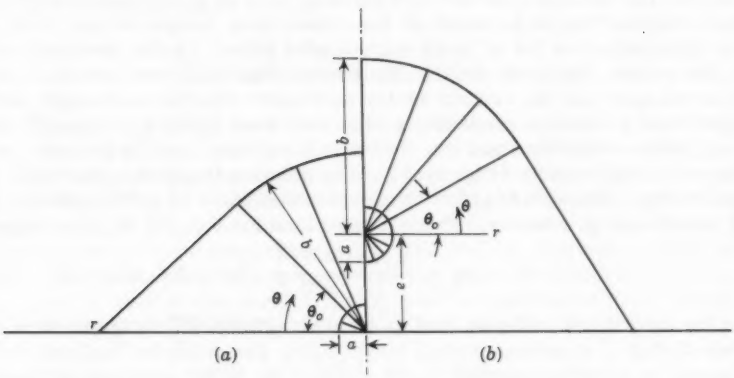

FIG. 5.—SEMI-INFINITE PLATE UNDER LOAD

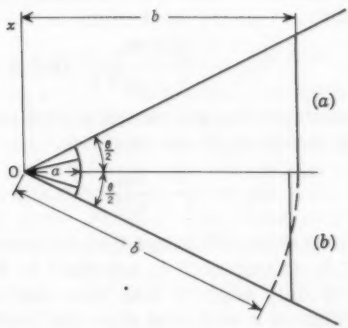

FIG. 6.—WEDGE PLATE UNDER LOAD

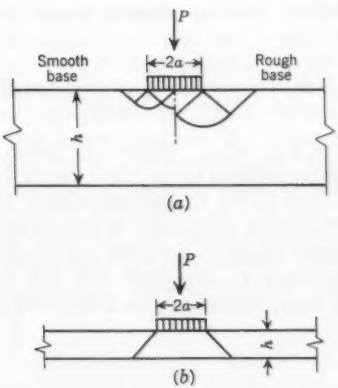

FIG. 7.—LOCAL BEARING CAPACITY FAILURE

retical yield loads may be explained by the influence of the local circumferential bending moment near the concentrated load on an uncracked sheet.

The collapse load of a corner or tip-loaded long wedge or sectorial plate can be determined as for a large edge-loaded plate. As the apex angle of the plate decreases, the outer triangular zones (Fig. 5(a)) are assumed to remain unchanged but the central sector decreases with the apex angle, and the collapse load decreases accordingly. For the lower limit of a large 90° wedge the central zone vanishes and the theoretical collapse load is the same as for a beam of variable width (Fig. 6(a)). The solution is given in Appendix I and shown in Figs. 3(a) and 4(a) for a corner-loaded plate ($\theta = 90°$), using b = 2.7 L as mentioned previously. The collapse load for $\theta \leq 90°$ is, approximately

$$P_o = \frac{4\ M_o \tan \theta/2}{1 - a/2\ L} \quad (\text{for } 0.2 < a/L < 1) \quad \ldots(30)$$

While the theoretical collapse load of a corner-loaded 90° wedge is about one-quarter of that of a center-loaded large plate, the collapse load for $\theta < 90°$ decreases in direct proportion to the width of the wedge as would be expected from the bending strength.

The theoretical collapse load of tip-loaded sectorial plates (Fig. 6(b)) is directly proportional to the angle θ, as shown in Appendix I and, using b = 2.7 L as before, approximately,

$$P_o = \frac{2\ \theta\ M_o}{1 - a/2\ L} \quad (\text{for } 0.2 < a/L < 1) \quad \ldots(31)$$

If a large floating ice sheet is cracked radially into numerous long wedges, the total collapse load at the tip is, from Eq. 31 for $\theta = 2\pi$,

$$P_o = \frac{4\ \pi\ M_o}{1 - a/2\ L} (\text{for } 0.2 < a/L < 1) \quad \ldots(32)$$

These results are shown in Figs. 3(a) and 4(a) together with an approximate relationship for $a/L < 0.2$, as indicated in Appendix I. It is of interest to note that this collapse load is only slightly less than that of a large uncracked sheet. The deflected shape of a wedge or sectorial plate with $\theta \leq 90°$ at collapse is generally in the form of a plane surface.

The result for a large radially-cracked sheet (Eq. 32) represents an upper limit of the collapse load and may be compared with the solution (Eq. 27) of the same problem using elastic theory, when a lower limit of the collapsed load is obtained as

$$P_o = \frac{2\ \pi\ M_o}{1-(2\ a/3\ L)^{0.6}} \quad (\text{for } 0 < a/L < 1) \quad \ldots(33)$$

These results are shown in Fig. 4(a). While the latter collapse load for a point load is the same as using plastic theory, for small contact areas the collapse load using elastic theory is up to approximately 30% smaller than the corresponding value from the limit analysis. Similar results are obtained for edge-loaded and corner-loaded radially-cracked sheets, since the corresponding collapse loads are respectively, one-half and one-quarter, of the loads given by Eqs. 32 and 33. It may, therefore, be concluded that the actual col-

lapse load of large radially-cracked sheets could be approximately 10% or 20% smaller than indicated by plastic theory.

LOCAL BEARING CAPACITY UNDER LOAD

In the preceding analysis concentrated loads were assumed to be distributed over a small area to limit local shearing stresses and ensure the full limit moment. The local ultimate bearing capacity under the load is governed either by surface penetration resistance to local shearing failure or by punching resistance to local circumferential tension failure, whichever is smaller (Fig. 7). Surface bearing or penetration resistance can be estimated from plastic theory. The corresponding ultimate load, P_u, which is distributed over a circular area of radius a on a rigid ideally-plastic material of great lateral extent and great thickness h (Fig. 7(a) is (10)

$$P_u = 2.85 \pi a^2 f_o \text{ to } 3.07 \pi a^2 f_o \quad \ldots\ldots\ldots (34)$$

in which f_o is the yield strength of the material in tension. The lower limit of Eq. 34 applies to a perfectly smooth contact surface and the upper limit to a rough surface. Hence, to avoid penetration failure the minimum contact radius for a concentrated load P is, approximately,

$$a = 0.33 \sqrt{P/f_o} \quad (\text{for } a/h < 0.2) \ldots\ldots\ldots (35)$$

If the contact radius is greater than about one-fifth of the thickness of the bearing material or sheet, the surface penetration resistance decreases with smaller ratios of h/a until the lower limit of punching resistance is obtained at about a = h. Punching resistance can be estimated from the vertical component of the total tensile strength of the sheet on a conical circumferential section inclined at 45° to the vertical and having an average radius of a + h/2 (Fig. 7b). Hence, the corresponding ultimate load is

$$P_u = (2a + h)\pi h f_o \quad \ldots\ldots\ldots\ldots (36)$$

or, the minimum contact radius in order for a load P to avoid punching failure is

$$a = P/2 \pi h f_o - h/2 \quad (\text{for } a \geqslant h) \quad \ldots\ldots\ldots (37)$$

However, because this minimum contact radius the tensile and shearing strength of the ice sheet has been reached under the load, the corresponding local limit moment is zero. With distance from the load the shearing stresses decreases rapidly and the limit moment increases accordingly. Analysis has shown that for a concentrated load with a radius a = h the collapse load is about 10% less than that determined on the assumption of negligible shearing stresses, while for a = 2 h the difference is very small. The contact radius of the load should, therefore, at least be equal to the thickness of the ice sheet. Since both the theoretical collapse load and the local bearing capacity are about directly proportional to the center angle of large sectorial sheets, the minimum contact radius deduced, applies also approximately to semi-infinite sheets, wedges, and sectorial sheets. Similar analyses of the local bearing

capacity under a strip load show that the minimum half-width of the strip should also be equal to the thickness of the ice sheet.

APPLICATION OF ANALYSIS AND COMPARISON WITH OBERVATIONS

In order to apply the present analysis to an estimate of the bearing capacity of floating ice sheets and compare this with the results of observations, it is necessary to know the yield strength of ice in tension and the moment-rotation capacity of ice in bending. The most important physical characteristics affecting the strength of ice are its structure, density, and salinity (11). Ice is an anisotropic material having needle-like crystals with a vertical axis in floating sheets when the horizontal strength is about 25% less than in the vertical direction. Stratification and a greater air porosity reduce the strength roughly in direct proportion to the resulting change in density. Similarly, a greater salt content and higher temperature reduce the strength. Thus, sea-water ice with about 3% of salt has approximately one-half of the strength of river or lake (fresh-water) ice at the same temperature, and, at approximately 10°F, the strength of both types is about twice that at their melting points. The strength also decreases considerably with slower rates of loading and a larger size of specimens. While the static strength with a few minutes to failure is less than the dynamic strength, the creep strength deduced from laboratory tests and the movement of (fresh-water) glaciers was found to be less than one-quarter of the static strength and amounted to a yield strength in tension of about 15 psi to 45 psi (12). Moreover, the strength of about 6-in.-thick specimens is only about two-thirds of that of 2-in.-thick specimens (11), and even smaller strengths are likely to be given by very large specimens. This is shown by cantilever bending tests on lake ice (13) and sea ice (14) in the field, when the flexural strength of 4 ft to 6 ft deep beams was only one-third to one-half of that obtained on small beams of 2 in. to 3 in. depth.

At very slow rates and long duration of stressing the strain capacity of ice is large, as shown by creep tests and observations on the flow of glaciers (12). It may, therefore, be assumed that in this case the moment-rotation capacity of ice in bending is adequate to enable the limit moment M_0 (using the plastic section modulus and creep strength) to be mobilized at the critical sections. Hence, the collapse load of floating ice sheets under long-time loading can probably be estimated as proposed for ideally-plastic plates. However, at normal rates of loading (a few minutes to failure), ice is fairly brittle and its moment-rotation capacity after yielding is limited. In the absence of experimental knowledge of this limit it may be assumed that the most highly stressed or first critical section of an ice sheet begins to crack in tension when the yield moment, M_Y (using the elastic section modulus and flexural strength) has been reached at this section. On further loading of the sheet the moment capacity at this section is reduced, and the bending moment is transferred to the second critical section until the latter is subjected to the yield moment and begins to crack. Again, the bending moment is transferred to the third critical section until the yield moment is reached here, resulting in cracking and complete collapse under the ultimate load. When there is only one critical section, as for a concentrated load at the tip of a wedge-shaped sheet with an apex angle of 90° or less and for a strip load near the edge of a large sheet, it follows that the collapse load can be estimated as proposed for ideally-plastic plates using the yield moment. For sheets with larger angles

and in particular for infinite ice sheets, however, the ultimate collapse load will be less than for ideally-plastic plates because the limited moment-rotation capacity leads to premature cracking under the yield moment at the first critical section (under the load). On further loading these cracks rapidly spread to the second critical (radial) sections and subsequently a tensile crack at the third critical (circumferential) section causes complete collapse under a concentrated load, while tensile cracks at the second critical (longitudinal) sections produce collapse under a strip load.

Because the first critical section is of small lateral extent (of an order of magnitude as the ice thickness), the corresponding yield moment will not govern the collapse load under short-time concentrated loading. A safe lower estimate of the collapse load under this condition can, therefore, be obtained by taking that load at which the second critical (radial or longitudinal) sections are subjected to the yield moment. Any third critical (circumferential) section is then still under an elastic radial bending moment, which is small compared with the yield moment and could well be neglected. By assuming that the ice sheet is cracked at the latter section (with radius or half-width R = b = 2 L, approximately), the solutions for plates of medium size in conjunction with the yield moment can be used to estimate the collapse load under short-time concentrated or strip loads on large ice sheets. Alternatively, a safe estimate of the collapse load of large ice sheets under short-time concentrated loads can be made as previously indicated for wedges. Thereby, it is assumed that the first and second critical sections are cracked and unable to resist any bending moment, but the yield moment obtains at the third critical section. It is of interest to note that both methods give, sensibly, the same collapse load within the practical range of the contact radius of concentrated loads ($0 < a/L < 0.5$) (Fig. 4(a)). Moreover, this theoretical collapse load is about directly proportional to the apex or wedge angle of the sheet.

It may sometimes be desirable to have simple conservative formulas for estimating the collapse load of floating ice sheets under various short-time loading conditions in practice. From the previous considerations the following expression may be suggested for a concentrated load:

$$P_o = (1 + 2\,a/L)\;\theta\;M_u \quad (\text{for } a \geq h) \quad \ldots\ldots\ldots\ldots \quad (38)$$

in which a is the contact radius of the load, h is the thickness of the sheet, θ is the apex angle of the sheet, L is the stiffness radius of the sheet (Eq. 2), and M_u is the moment of resistance of the section per unit length. Because the ratio a/L is usually small and can frequently be neglected and $M_u = f_b\,h^2/6$, in which f_b is the flexural strength of ice on the basis of an elastic section modulus, Eq. 38 simplifies to the following design equations:

$$\text{Central load} - P_o = f_b\,h^2 \quad \ldots\ldots\ldots\ldots\ldots \quad (39a)$$

$$\text{Edge load} - P_o = f_b\,h^2/2 \quad \ldots\ldots\ldots\ldots\ldots \quad (39b)$$

$$\text{Corner load} - P_o = f_b\,h^2/4 \quad \ldots\ldots\ldots\ldots\ldots \quad (39c)$$

From the same considerations, the collapse load per unit length of a strip load is given by the following design equations:

$$\text{Central load} - P_o = f_b\,h^2/2\,L \quad \ldots\ldots\ldots\ldots \quad (40a)$$

$$\text{Edge load} - P_o = f_b\,h^2/3\,L \quad \ldots\ldots\ldots\ldots \quad (40b)$$

in which L is given by Eq. 2. In these design equations P_o may be taken as the total collapse load of an individual unit (such as a vehicle or aircraft) because

the usual wheel spacing within a unit has no significant effect on the collapse load in practice. For a row or line of such units (load train), however, the total collapse load is given either by the sum of the collapse loads of the individual units or by the collapse load of an equivalent strip load, whichever is smaller.

While it is known that a number of full-scale loading tests to failure have been carried out on floating ice sheets (15), results of such tests together with the corresponding properties of the ice have not yet (1960) been published. Meanwhile a comparison of the present method of analysis with field observations is only possible within the ultimate and working range of loads on various thicknesses of floating ice sheets for which the factor of safety can be deduced on the basis of an average probable strength of the ice.

Surveys have been made of the collapse loads and the normal and maximum working loads on floating fresh-water ice sheets used as roads, bridges, and landings of pulp and paper companies in eastern Canada (16),(17), and the results are shown in Fig. 8. It is found that the observed collapse loads vary mainly from about $P_o = 100\ h^2$ lb to $500\ h^2$ lb, while the customary safe loads of traffic with speeds limited to about 10 or 15 mph vary from about $P = 70\ h^2$ lb to $250\ h^2$ lb, where h is the thickness of ice in inches. The theoretical collapse load for central concentrated loads on large ice sheets can be estimated from Eq. 39, so that the flexural strength of the ice deduced from the observed collapse loads would vary from about $f_b = 100$ psi to 500 psi. These strengths are within the range of flexural test results on large and small thicknesses, respectively, of fresh-water ice (11). Moreover, the average factor of safety deduced from the working loads and these flexural strengths is thus about 2, which appears reasonable for slowly moving loads when the fatigue strength of ice would govern. On the other hand, an elastic analysis using these flexural strengths (Eq. 1 with a = h) gives yield or first cracking loads of about $P_y = 50\ h^2$ lb to $250\ h^2$ lb. These estimated yield loads are equal to the working loads used in practice, therefore, the corresponding factor of safety is unity. Hence, some local cracking on the bottom of large ice sheets under slowly moving loads does not appear to be detrimental, as such cracks would heal in time. It is of interest to note that for very slowly applied loads of long duration and using a creep strength $f_o = 15$ psi to 45 psi for ice, as mentioned previously, the theoretical creep collapse load from Eq. 4 varies from about $P_c = 25\ h^2$ lb to $70\ h^2$ lb. This estimate indicates that long-time storage loads or parked vehicles should be restricted to about one-third of safe slowly moving loads, since a factor of safety of unity could undoubtedly be used in such extreme cases using the creep strength. On the other hand, vehicles moving at about 20 mph or more on ice over deep water and more slowly on ice over shallow water may set up resonance deflections and collapse of ice sheets, which have been considered elsewhere (18).

A further comparison of theoretical collapse loads with maximum (emergency) and normal working loads on the basis of average flexural strengths is possible from recommended minimum ice thicknesses for landing aircraft on floating airfields (19). This information is shown in Fig. 8 for single slowly moving or briefly parked aircraft on freshwater ice far from the edge of the sheets and in the absence of resonance and other deteriorating conditions at two extremes of ice temperature (14°F and 31°F). Using again Eq. 39 for the theoretical collapse load, it is found that the emergency loads correspond to a flexural stress of about 100 psi to 200 psi or assuming a factor of safety of 1.5, the deduced flexural strength of the ice would vary from about

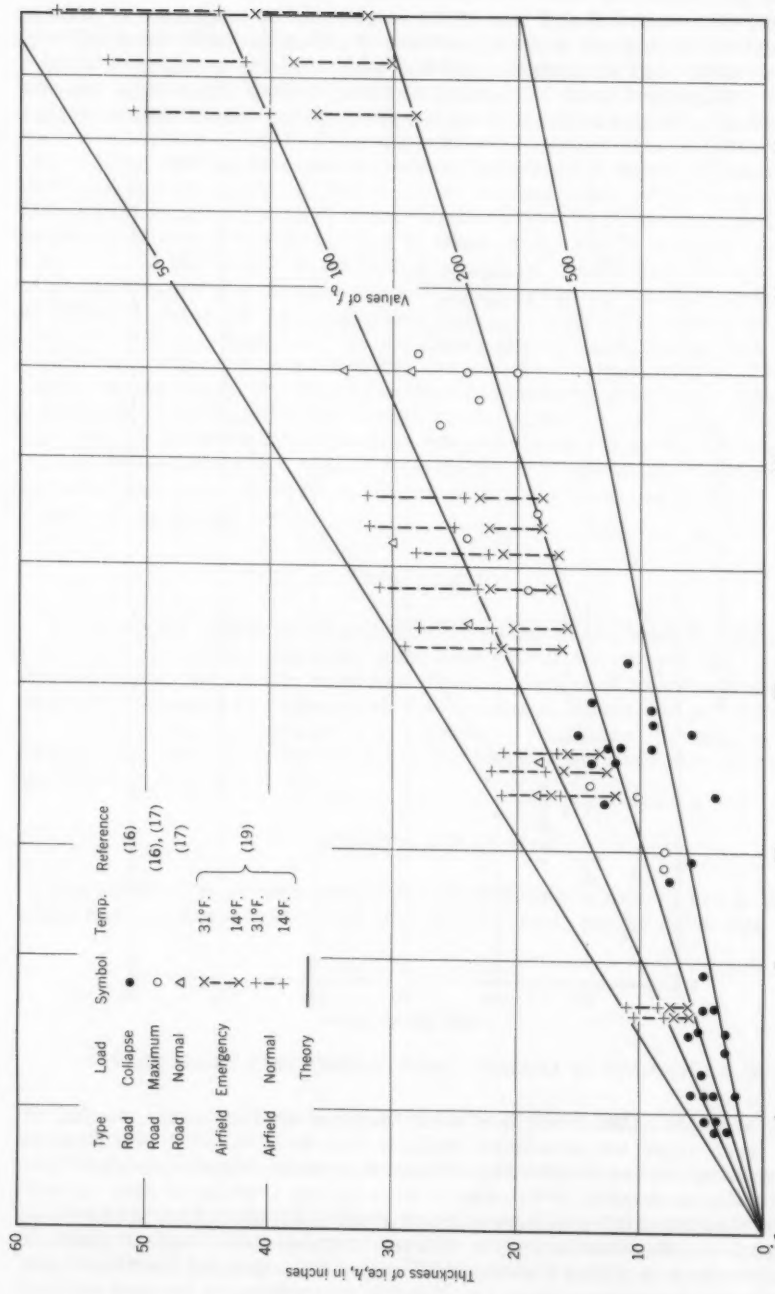

FIG. 8.—OBSERVED COLLAPSE AND WORKING LOADS ON FRESH-WATER ICE SHEETS

f_b = 150 psi to 300 psi. This strength is within the range of flexural test results on fresh-water ice and it is of the same order of magnitude as deduced previously from pulp and paper operations. Further, the theoretical factor of safety deduced from the normal loads and these flexural strengths is about 3 against collapse and about 1.5 against cracking, both of which seem reasonable. From a similar analysis of the minimum thicknesses recommended for

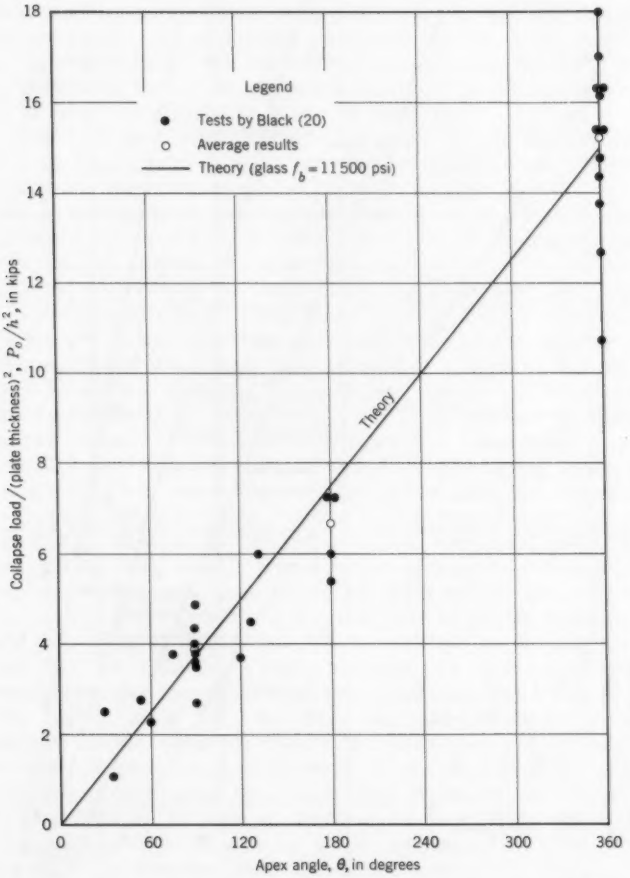

FIG. 9.—RESULTS OF LOADING TESTS ON SECTORIAL GLASS PLATES

floating airfields on sea ice a flexural strength of approximately one-half of that of fresh-water ice is deduced, which is also in agreement with flexural test results on sea ice mentioned earlier and gives the same theoretical factors of safety as deduced previously.

In the absence of full-scale loading test results of edge and corner loads on floating ice sheets, laboratory tests with concentrated loads on glass plates of various shapes on a rubber foundation (20) support the present theoretical relationship that the collapse loads are directly proportional to the apex angle of

sectorial plates and that the collapse load of corner-loaded plates is about one-quarter and of edge-loaded plates is about one-half of that of corresponding center-loaded plates (Fig. 9). Moreover, the lines of constant deflection of edge-loaded and corner-loaded (90° wedge) elastic plates (4) agreed closely with the estimated shape at collapse and indicated a central sector between two roughly triangular outer zones with an edge angle of about 45°. Collapse occurred by rupture along similarly shaped yield-hinge sections. A further analysis of these loading tests can be made on the basis of subsequent flexure tests on the glass used (conducted by the author on small beams cut from an original plate kindly supplied by the National Research Council of Canada), which gave an average flexural strength of f_b = 11500 psi with a coefficient of variation of about 40%. In the plate loading tests the ratio of the effective contact radius of the load (measured at mid-surface of the plate) to the characteristic length or stiffness radius of the plate was about $a/L = 0.03$. Thus, the theoretical collapse load of a (medium) center-loaded plate (Fig. 4(a)) is about P_o/h^2 = 15000 psi, which compares well with the observed average value of 15240 psi. Similar agreement is found between the estimated and observed average collapse loads of edge-loaded and corner-loaded plates as well as for tip-loaded sectorial plates with a smaller apex angle, as shown in Fig. 9. The scatter of the individual loading test results from the average values can be explained by the relatively large variation in the strength of the glass, as indicated by the results of the flexure tests.

CONCLUSIONS

If floating ice sheets are represented by plates on an elastic foundation, the yield or first cracking loads and maximum deflections can readily be determined from elastic theory. A method has been developed to estimate the corresponding ultimate or collapse loads from plastic theory and solutions have been obtained for various loading and boundary conditions. Simplified design formulas for use in practice are supported by the results of field observations and some small-scale tests.

ACKNOWLEDGMENTS

The author is indebted to D. C. Drucker of Brown University and L. W. Gold of the National Research Council of Canada for their helpful comments.

APPENDIX I

CENTRAL LOAD ON INFINITE PLATE

Circular Load.—A concentrated load P is distributed uniformly over a small circular area of radius a on the surface of a thin, rigid, ideally-plastic, and infinite plate of uniform thickness h; the plate can resist a full plastic or limit moment, M_o, per unit length and rests on a discontinuous-elastic foundation (Fig. 1). The minimum value of the contact radius a is governed by the local

shearing stresses and bearing capacity under the load, which have been considered previously. If membrane action and shearing deformation of the plate are neglected, the collapse load, P_O, of the plate can be determined as follows.

Let r and θ be cylindrical coordinates, M_r and M_t be the radial and circumferential bending moments, respectively, per unit length and Q be the vertical shearing force per length of arc with the directions as shown in Fig. 10. Then for the present case of rotational symmetry, the equations of equilibrium are (5):

$$d(rQ)/dr = - rp \quad \ldots\ldots\ldots\ldots\ldots\ldots \quad (41)$$

and

$$d(rM_r)/dr = M_t + rQ \quad \ldots\ldots\ldots\ldots\ldots\ldots \quad (42)$$

in which p is the pressure on element of plate with downward forces and moments producing tension on the bottom of the plate being taken as positive (Fig. 10).

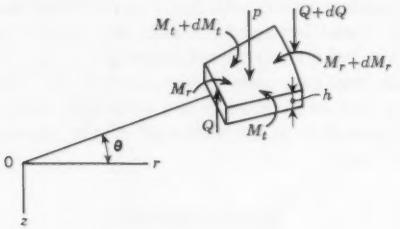

FIG. 10.—ELEMENT OF PLATE UNDER LOAD

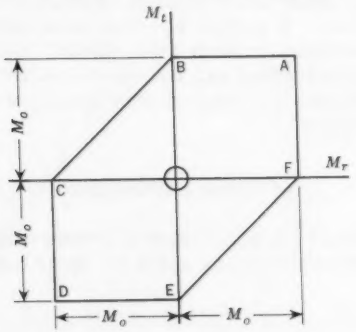

FIG. 11.—TRESCA YIELD CONDITION

Using the Tresca yield condition for the plate material (Fig. 11), it can be shown (5) that the radial bending moment M_r varies from M_O at the center of the load P(r = 0) to - M_O at the circumferential yield hinge circle (r - b) and that with $M_r = 0$ at an intermediate radius r = c, say, the following relations hold in the plastic regimes:

$$\left.\begin{array}{ll}
\text{at } r = 0; & M_r = M_t = M_o \quad \text{(Tresca regime A)},\\
\text{at } 0 < r < c; \quad 0 < M_r < M_o & \text{and } M_t = M_o \quad \text{(Tresca regime AB)},\\
\text{at } r = c; \quad M_r = 0 & \text{and } M_t = M_o \quad \text{(Tresca regime B)},\\
\text{at } c < r < b; \quad 0 > M_r > -M_o & \text{and } M_t = M_r + M_o \quad \text{(Tresca regime BC)},\\
\text{at } r - b; \quad M_r = -M_o & \text{and } M_t = 0 \quad \text{(Tresca regime C)}.
\end{array}\right\} \ldots (43)$$

Moreover, the rate of the deflection w of the plate has to satisfy the flow rule associated with the yield condition, and in the present case the principal rates of curvature are given by the relationships

$$d^2w/dr^2 = 0 \quad \text{or} \quad w = C_1 + C_2\, r \quad (\text{for } 0 < r < c) \ldots\ldots\ldots (44a)$$

$$d^2w/dr^2 = -dw/r\, dr \quad \text{or} \quad w = C_3 + C_4 \ln r \quad (\text{for } c < r < b) \ldots . (44b)$$

in which C_1, C_2, C_3 and C_4 are constant of integration in accordance with the following boundary and equilibrium conditions.

The boundary conditions are satisfied by the function (5)

$$w/w_o = 1 - r/[c(1 + \ln b/c)] \quad (\text{for } 0 < r < c) \ldots\ldots\ldots (45a)$$

and

$$w/w_o = (\ln b/r)/(1 + \ln b/c) \quad (\text{for } c < r < b) \ldots\ldots\ldots (45b)$$

in which w_o is the deflection under load (at r = 0).

The radial deflection is thus in the form of an inverted obtuse right cone for $0 < r < c$ with the apex at the load. The conical shape merges at r = c into a logarithmic shape which obtains for $c < r < b$.

The overall equilibrium condition requires that the load P is balanced by the total reaction pressure on the bottom of the plate, which is given by k times the volume of the deflection dish, where k = foundation modulus. Because this reaction pressure is

$$p = -k\, w \ldots\ldots\ldots\ldots\ldots\ldots (46)$$

the applied load is

$$P = 2\pi k \int_o^b w\, r\, dr \ldots\ldots\ldots\ldots\ldots\ldots (47)$$

Putting Eq. 45 into 47 the integrating gives

$$P = \frac{\pi k w_o (b^2 - c^2/3)}{2(1 + \ln b/c)} \ldots\ldots\ldots\ldots\ldots\ldots (48)$$

Hence, Eq. 46 becomes, after substituting Eqs. 45 and 48,

$$p = \frac{-2P(1 + \ln b/c - r/c)}{\pi(b^2 - c^2/3)} \quad (\text{for } 0 < r < c) \ldots\ldots\ldots\ldots (49a)$$

and

$$p = \frac{-2P(\ln b/r)}{\pi(b^2 - c^2/3)} \quad (\text{for } c < r < b) \ldots\ldots\ldots\ldots\ldots (49b)$$

Substituting Eq. 49 into 41 and integrating with the boundary conditions of r Q = 0 at r = 0 and r = b, and the continuity condition of r Q at r = c furnishes

$$r\,Q = \frac{Pr^2(1 + \ln b/c - 2r/3c)}{\pi(b^2 - c^2/3)} - \frac{Pr^2}{2\pi a^2} \text{ (for } 0 < r < a) \quad \ldots\ldots\ldots \quad (50a)$$

$$r\,Q = \frac{Pr^2(1 + \ln b/c - 2r/3c)}{\pi(b^2 - c^2/3)} - P/2\pi \text{ (for } a < r < c) \quad \ldots\ldots\ldots \quad (50b)$$

and

$$r\,Q = \frac{P\,r^2(1 + 2\ln b/r) - b^2}{2\pi(b^2 - c^2/3)} \text{ (for } c < r < b) \quad \ldots\ldots\ldots \quad (50c)$$

if $c > a$, as will be shown later for the small ratios of a/b used.

Substituting Eq. 50 into Eq. 42 and integrating with the boundary conditions (Eq. 43) and continuity requirement of M_r at $r = a$ yields

$$M_r = M_o + \frac{P\,r^2(1 + \ln b/c - r/2\,c)}{3\,\pi(b^2 - c^2/3)} - \frac{P\,r^2}{6\,\pi\,a^2} \text{ (for } 0 < r < a) \quad \ldots\ldots \quad (51a)$$

$$M_r = M_o + \frac{P\,r^2(1 + \ln b/c - r/2\,c)}{3\,\pi(b^2 - c^2/3)} - \frac{P(1 - 2\,a/3\,r)}{2\pi} \text{ (for } a < r < c) \ldots \quad (51b)$$

and

$$M_r = M_o \ln r/c + \frac{P}{2\,\pi(b^2 - c^2/3)}$$

$$\left[r^2(1 + \ln b/r) - c^2(1 + \ln b/c) - b^2 \ln r/c\right] \text{ (for } c < r < b) \ldots\ldots \quad (51c)$$

Putting $M_r = -M_o$ at $r = b$ into Eq. 51c gives

$$M_o(1 + \ln b/c) = \frac{P}{2\,\pi(b^2 - c^2/3)}\left[b^2(1 - \ln b/c) - c^2(1 + \ln b/c)\right] = 0 \ldots \quad (52)$$

which is the transcendental equation for c/b. When the latter value is substituted into Eq. 51b, and using the boundary condition of $M_r = 0$ at $r = c$, a solution is obtained for the collapse load for various ratios of a/b. It is found that the assumption of $c > a$ holds for $a/b \leq 0.2$, but the above equations can readily be modified for $c < a$, when $a/b > 0.2$. These results, which satisfy both static and kinematic requirements, are shown in Fig. 3.

In the limit of a point load when $a = 0$, Eq. 52 shows that $c = 0$ and the collapse load is

$$P_o = 2\,\pi\,M_o \quad \ldots\ldots\ldots\ldots\ldots\ldots \quad (53)$$

The corresponding deflection shape of the plate outside the loaded zone itself is logarithmic throughout the plastic area. The latter is small because the deflection under the load is large at collapse while the overall equilibrium condition (Eq. 48) holds. This conclusion is borne out by the observation that the present collapse load is identical with the result obtained for simply supported or fixed circular plates under point loads (5), so that the present support by an upward reaction pressure on the bottom of the plate has not increased the collapse load. It may, therefore, safely be assumed that Eq. 53 is independent of the size and boundary conditions of the plate and that for a plate material

obeying the Mises yield condition (corresponding to an ellipse circumscribed to the hexagon in Fig. 11) and the associated flow rule the present collapse load would be

$$P_o = 2.31 \pi M_o \quad \ldots\ldots\ldots\ldots\ldots\ldots \quad (54)$$

in accordance with the result for a point load on a fixed circular plate (7).

As the radius of the contact area of the load increases, the collapse load rapidly increases (Fig. 3). Within the practical range of the contact radius, the collapse load is very closely given by

$$P_o = 3.3 \pi (1 + 6\, a/b)\, M_o \quad (\text{for } 0.02 < a/b < 0.2) \quad \ldots\ldots\ldots \quad (55)$$

For greater contact areas the collapse load increases more rapidly and approaches infinity for a/b = 0.8, approximately, when the rate at which the load does work on the deforming plate approaches zero.

Strip Load.—A load P per unit length is uniformly distributed over a narrow strip of width 2 a and great length resting on the surface of an infinite ideally-plastic plate, as before. An elemental strip of unit width along a transverse section of the plate can then be considered as a beam of unit width, uniform depth, and great length on a discontinuous-elastic foundation (Fig. 1).

The deflection w of the beam satisfying the flow rule is given by Eq. 44a or, using the boundary conditions,

$$w/w_o = 1 - r/b \quad (\text{for } 0 < r < b) \quad \ldots\ldots\ldots\ldots\ldots \quad (56)$$

in which b is the distance from load axis to longitudinal yield hinge line and w_o refers to the deflection under load (at r = 0). The reaction pressure on the bottom of the beam is given by Eq. 46.

The overall equilibrium condition requires that

$$P = k\, w_o\, b \quad \ldots\ldots\ldots\ldots\ldots\ldots\ldots\ldots \quad (57)$$

so that Eq. 46 becomes, after substituting Eq. 56 and 57,

$$p = -P(1 - r/b)/b + P/2\,a \quad (\text{for } 0 < r < a) \quad \ldots\ldots\ldots \quad (58a)$$

and

$$p = -P(1 - r/b)/b \quad (\text{for } a < r < b) \quad \ldots\ldots\ldots\ldots \quad (58b)$$

The transverse bending moment is

$$M_r = -\int_o^r p\, dr \quad \ldots\ldots\ldots\ldots\ldots\ldots\ldots \quad (59)$$

or, after substituting Eq. 58 and integrating with the boundary condition of $M_r = M_o$ at r = 0 and the continuity condition of M_r at r = a,

$$M_r = M_o + \frac{P\, r^2}{2}\left[(1 - r/3b)/b - 1/2\,a\right] \quad (\text{for } 0 < r < a) \quad \ldots\ldots \quad (60a)$$

and

$$M_r = M_o + \frac{P}{2}\left[r^2(1 - r/3\,b)/b - r + a/2\right] \quad (\text{for } a < r < b) \quad \ldots\ldots \quad (60b)$$

Putting $M_r = -M_o$ at r = b into Eq. 60b, gives the collapse load per unit length

$$P_o = \frac{12\, M_o}{b - 3\,a/2} \quad (\text{for } 0 < a/b < 2/3) \quad \ldots\ldots\ldots\ldots \quad (61)$$

This result, which satisfies both static and kinematic requirements, is shown in Fig. 3.

CENTRAL LOAD ON MEDIUM AND SMALL PLATES

Circular Load.—When the size of the plate is less than that required to develop the radial limit moment $M_r = -M_o$ at $r = b$, the collapse load will be less than that of an infinite plate, except in the case of a point load as mentioned before. The analysis previously given can readily be extended to obtain a solution for a central concentrated load on a circular plate of medium size (deflecting in a similar way to an infinite plate) by putting the moment $M_r = -M_b > -M_o$ at $r = b$ or the equivalent relationship (6) of

$$M_b = M_o \ln R/b \quad (\text{for } b < R < 2.72\,b) \quad \ldots\ldots\ldots\ldots \quad (62)$$

into Eq. 51c in which R is the total radius of plate (Fig. 1). In this way a transcendental equation is again obtained for c/b which can be substituted into Eq. 51b to obtain a solution of the collapse load for various ratios of a/b if $c > a$ (which holds for a/b 0.2 if $M_b/M_o = 1$, increasing to $a/b \leq 0.5$ if $M_b/M_o = 0$).

The results, which satisfy static and kinematic requirements, are shown in Fig. 3 for M_b/M_o or $\ln R/b$ of 0.5 and 0. It is found that the collapse load increases roughly in direct proportion to the magnitude of M_b above the lower limit for $M_b = 0$ and that for a point load the same value (Eq. 53) is obtained in all cases.

For small circular plates when the deflection may be taken as uniform, the reaction pressure below the plate under a central concentrated load is given by

$$p = -P/\pi b^2 \quad \ldots\ldots\ldots\ldots\ldots\ldots \quad (63)$$

in which b is the radius of the plate. Substituting Eq. 63 into Eq. 41 and integrating with the boundary condition of $rQ = 0$ at $r = b$ yields

$$rQ = \frac{Pr^2}{2\pi}\,(1/b^2 - 1/a^2) \quad (\text{for } 0 < r < a) \quad \ldots\ldots\ldots \quad (64a)$$

and

$$rQ = \frac{P}{2\pi}\,(r^2/b^2 - 1) \quad (\text{for } a < r < b) \quad \ldots\ldots\ldots\ldots \quad (64b)$$

Substituting Eq. 64 into Eq. 42 and integrating with the boundary conditions and the continuity requirement of M_r at $r = a$ furnishes

$$M_r = M_o + \frac{P\,r^2}{6\,\pi}\,(1/b^2 - 1/a^2) \quad (\text{for } 0 < r < a) \quad \ldots\ldots\ldots \quad (65a)$$

and

$$M_r = M_o + \frac{P}{6\,\pi}\,(r^2/b^2 + 2\,a/r - 3) \quad (\text{for } a < r < b) \quad \ldots\ldots\ldots \quad (65b)$$

Putting $M_r = 0$ at $r = b$ into Eq. 65b gives the collapse load

$$P_o = \frac{3\,\pi\,M_o}{1 - a/b} \quad (\text{for } 0.05 < a/b < a) \quad \ldots\ldots\ldots\ldots\ldots \quad (66)$$

For a small contact radius of the load (about $a/b < 0.05$) Eq. 66 satisfies static but no long kinematic requirements. The deformation of the plate will then not be uniform under the load but be similar to that of a medium plate, so

that the corresponding collapse load is approached with the lower limit of Eq. 53 for a point load. The corresponding results are shown in Fig. 3 and indicate that for greater contact areas the collapse load increases rapidly and approaches infinity for a/b - 1, as would be expected theoretically for a uniformly loaded plate.

Strip Load.—Under a strip load resting on a large plate the limit moment of $M_r = -M_o$ can be developed at the section of r = b only, if the cantilever overhang of the plate beyond r = b has a length of t_o such that

$$M_o = q\,h\,t_o^2/2 \quad \ldots\ldots\ldots\ldots\ldots\ldots \quad (67)$$

in which q is the unit weight of the plate. The half-width of the plate is then $R = b + t_o$ (Fig. 1).

For a central strip load on a medium-sized rectangular plate (deflecting in a similar way to an infinite plate) with an overhang of length $t < t_o$, the moment at r = b is

$$M_b = q\,h\,t^2/2 \quad \ldots\ldots\ldots\ldots\ldots\ldots \quad (68)$$

$$M_b = (t/t_o)^2 M_o \quad \ldots\ldots\ldots\ldots\ldots\ldots \quad (69)$$

by substituting Eq. 67. Equating Eq. 69 to the last Eq. of 60 at r = b, furnishes the collapse load per unit length

$$P_o = \frac{6\left[1 + (t/t_o)^2\right]M_o}{b - 3a/2} \quad (\text{for } 0 < a/b < 2/3 \text{ and } 0 < t < t_o) \quad \ldots\ldots\ldots \quad (70)$$

For a central strip load on small plates when the deflection may be taken as uniform, the reaction pressure under the plate is uniform and is

$$p = -\frac{P}{2}(1/b - 1/a) \quad (\text{for } 0 < r < a) \quad \ldots\ldots\ldots\ldots \quad (71a)$$

and

$$p = -P/2b \quad (\text{for } a < r < b) \quad \ldots\ldots\ldots\ldots\ldots\ldots \quad (71b)$$

in which b is the half-width of plate. Substituting Eq. 71 into Eq. 59 and integrating with the boundary and continuity conditions, yields

$$M_r = M_o + \frac{P\,r^2}{4}(1/b - 1/a) \quad (\text{for } 0 < r < a) \quad \ldots\ldots\ldots\ldots \quad (72a)$$

and

$$M_r = M_o + \frac{P}{4}\left(r^2/b - 2\,r + a\right) \quad (\text{for } a < r < b) \quad \ldots\ldots\ldots\ldots \quad (72b)$$

Putting $M_r = 0$ at r = b into Eq. 72b, gives the collapse load per unit length

$$P_o = \frac{4\,M_o}{b - a} \quad (\text{for } 0 < a < b) \quad \ldots\ldots\ldots\ldots\ldots\ldots \quad (73)$$

The various solutions given satisfy both static and kinematic requirements and are shown in Fig. 3.

EDGE AND CORNER LOADS ON SEMI-INFINITE PLATES, WEDGES, AND SECTORIAL PLATES

Circular Load.—Let a concentrated load P be distributed uniformly over a small semi-circle of radius a at the edge of a semi-infinite ideally-plastic

plate as before, and r and θ be cylindrical coordinates measured from the load and edge of the plate with the bending moments M_r and M_t and the shearing force Q as before (Fig. 5). Then at the collapse load the equilibrium equations are the same as Eq. 41 and Eq. 42 but the boundary conditions of Eq. 43 are modified to the extent that the bending moments and shearing forces are zero along the free edge ($\theta = 0$). Since the problem is symmetrical about $\theta = 90°$ only one-half of the plate about the axis of symmetry will be considered subsequently.

Thus, setting $M_t = 0$ along the free edge gives a conical deflection shape at the edge ($\theta = 0$) according to the Tresca flow rule (see above). As the angle θ increases, M_t increases until $M_t = M_o$ (Tresca regime AB for $0 < r < c$) and $M_t = M_r + M_o$ (Tresca regime BC for $c < r < b$) at $\theta = \theta_o$, say, as well as for larger angles. Accordingly, for $\theta > \theta_o$ the combined conical and logarithmic deflection shape similar to that of an infinite plate obtains, which approaches the purely logarithmic deflection shape along the axis of symmetry ($\theta = 90°$) according to the flow rule because then $M_r < 0$ (Tresca regime BC) for $0 < r < b$ (Fig. 11).

A complete solution of the aforementioned problem has not been possible, but an approximate analysis can be made by using the flow field shown in Fig. 5. This assumes that the stress and deformation conditions in the central sector ($\theta_o < \theta < 90°$) are identical to those of a similarly loaded infinite plate, while in the outer triangular zones ($0 < \theta < \theta_o$) the deflection and the moment M_t vary monotonically with r and θ as has been indicated. For the whole central sector an approximate solution can, therefore, be obtained from the previous equations for an infinite plate by using an angle of $\pi - 2\theta_o$ in place of 2π for the overall equilibrium of the concentrated load in Eqs. 47 and 48. The collapse load of the central sector from Eqs. 53 and 54 is then found to be directly proportional to the center angle of this sector.

In the outer triangular zones ($0 < \theta < \theta_o$) the requirement of zero resultant bending moment along the free edge can be expressed by

$$\int_o^b M_{ro}\, r \sin^2\theta \, dr + \int_o^b M_{to}\, r \cos^2\theta \, dr = 0 \quad \ldots\ldots\ldots \quad (74)$$

where M_{ro} and M_{to} are the terminal bending moments along these zones. Considering in particular the critical circumferential section at r equals b, the radial bending moment M_{ro} equals $- M_o$. Further along any radial section of the central sector ($\theta_o < \theta < 90°$) it was found from integrating Eq. 51 and using Eq. 43, that the circumferential bending moment M_t equals M_o, very nearly. Hence, in particular $M_{to} \cong M_o$, along the junction between the central and outer zones ($\theta = \theta_o$), where the radial and circumferential yield hinge lines meet at a right angle (Fig. 5). Accordingly, from Eq. 74, $\theta_o = 45°$, which indicates that the outer zones deform as wedge-shaped plates with a width of b at r = b, where b is the radius of circumferential yield hinge arc of central sector.

The wedges are subjected to a twisting moment since they remain straight along the free edge while their deformation along the junction with the central sector follows the deflected shape of the radius of this sector. Since the twisting moment reduces the collapse load of the outer zones below the value for bending alone, an upper limit of the collapse load will, in the first instance, be obtained by ignoring twisting. A solution of this problem is then identical with that of an ideally-plastic infinite wedge or sectorial plate without transverse

bending and with a concentrated load at the tip, the load being distributed over a small sector (or triangle) with its apex at the tip and having a radius (or height) of a (Fig. 6). The collapse load of such a plate can be determined as follows.

Consider an infinite wedge of variable half-width x at a distance r, measured along bisector from tip, so that

$$x = r \tan (\theta/2) \quad \ldots\ldots\ldots\ldots\ldots\ldots \quad (75)$$

in which θ is the apex angle (Fig. 6). The deflection w of the wedge satisfying the flow rule is then

$$w/w_o = 1 - r/b \text{ (for } 0 < r < b) \quad \ldots\ldots\ldots\ldots \quad (76)$$

in which w_o refers to the deflection under the tip ($r = 0$) and b is the distance of yield hing line from tip.

Since the reaction pressure on the bottom of the wedge is given by Eq. 46, the overall equilibrium condition requires that

$$P = 2k \int_o^b w\, x\, dr \quad \ldots\ldots\ldots\ldots\ldots\ldots \quad (77)$$

or, after substituting Eqs. 75 and 76 into Eq. 77 and integrating,

$$P = \frac{k\, w_o\, b \tan (\theta/2)}{3} \quad \ldots\ldots\ldots\ldots\ldots\ldots \quad (78)$$

Hence, Eq. 46 becomes, after substituting Eqs. 76 and 77,

$$p = \frac{-3P(1 - r/b)}{b \tan (\theta/2)} + \frac{P}{a^2 \tan (\theta/2)} \quad (\text{for } 0 < r < a) \ldots\ldots\ldots \quad (79a)$$

and

$$p = \frac{-3P(1 - r/b)}{b \tan (\theta/2)} \quad (\text{for } a < r < b) \quad \ldots\ldots\ldots \quad (79b)$$

The bending moment per unit width of the wedge is

$$M_r = - \int_o \int^r p\, dr \quad \ldots\ldots\ldots\ldots\ldots\ldots \quad (80)$$

or, after substituting Eq. 79 and integrating with the boundary condition of $M_r = 0$ at $r = 0$ and the continuity condition of M_r at $r = a$,

$$M_r = \frac{P r^2}{2 \tan (\theta/2)} \left[\frac{1}{b^2} \left(1 - \frac{r}{2b} \right) - \frac{1}{3a^2} \right] \quad (\text{for } 0 < r < a) \ldots\ldots \quad (81a)$$

and

$$M_r = \frac{P}{2 \tan (\theta/2)} \left[\frac{r^2}{b^2} \left(1 - \frac{r}{2b} \right) + \frac{2a}{3r} - 1 \right] \quad (\text{for } a < r < b) \ldots\ldots \quad (81b)$$

Putting $M_r = - M_o$ at $r = b$ into Eq. 81b gives the collapse load

$$P_o = \frac{4 M_o \tan (\theta/2)}{1 - 4a/3b} \quad (\text{for } 0.05 < a/b < 3/4) \ldots\ldots\ldots \quad (82)$$

for a wedge ($0 < \theta \leq 90°$). Setting $\theta = \tan\theta$ in Eq. 82 gives the collapse load

$$P_o = \frac{2\,\theta\,M_o}{1 - 4\,a/3\,b} \quad (\text{for } 0.05 < a/b < 3/4) \quad \ldots\ldots\ldots (83)$$

for a sectorial plate ($0 < \theta \leq 90°$). These results satisfy both static and kinematic requirements.

It is of interest to note that similar computations using Eq. 45 for the deflected shape of the wedge have shown that the collapse load of the wedge is still closely given by Eq. 82, which, therefore, appears to be sensibly unaffected by the deflected shape. On the other hand, trial computations of the plastic state within the contact sector (or triangle), where the bending moment is positive under the load and conditions are similar to those of an infinite plate, have shown that the collapse load, estimated from Eqs. 82 and 83 is excessive for small contact areas with about $a/b < 0.05$. In that case the collapse load decreases rapidly with smaller ratios of a/b to one-half of the above loads at $a = 0$. A similar decrease applies also to a plane wedge as a point load is approached, because the reaction pressure on the bottom of the plate below the load is then negligible, as shown above infinite plates. The results are shown in Fig. 3 for a wedge with $\theta = 90°$.

Using the above results, the total collapse load for a point load at the edge of a semi-infinite plate is obtained by combining the collapse load of the central sector with a center angle of 90° ($P_o = \pi\,M_o/2$ from Eq. 53) with the collapse load of both outer zones with a combined wedge angle of 90° ($P_o = 2\,M_o$, that is one-half of Eq. 82). Hence, the total collapse load of the semi-infinite plate under a point load is

$$P_o = (2 + \pi/2)M_o \quad \ldots\ldots\ldots\ldots\ldots (84)$$

Similarly, for a concentrated load the collapse load of wide wedge or sectorial plates ($90° < \theta < 360°$) is, from Eqs. 55 and 82,

$$P_o = \left[1.65\,(\theta - \pi/2)(1 + 6\,a/b) + \frac{4}{1 - 4\,a/3\,b}\right] M_o \quad (\text{for } 0.05 < a/b < 0.2) \ldots (85)$$

from which the collapse load of an edge-loaded plate is obtained for $\theta = 180°$ with the results shown in Fig. 3.

Comparing the results of Eqs. 84 and 85 for different ratios of a/b with the corresponding values for an infinite plate (Eqs. 53 and 55), the collapse load of a semi-infinite plate is found to be about one-half of that of an infinite plate. An allowance for twisting moments would reduce this ratio somewhat. On the other hand, Eq. 83 shows that, on the assumption of zero transverse bending, the collapse load of a sectorial plate increases in direct proportion to the apex angle of the plate, so that the collapse load of an edge-loaded semi-infinite plate would then be one-half of that of an infinite plate.

Strip Load.—If a strip load of width 2 a is applied adjacent to the free edge of a semi-infinite plate, the deflection is given by Eq. 56 and the reaction pressure under the plate is similar to that under one-half of an infinite plate. The maximum transverse bending moment occurs at $r = b$ and is, for the cantilever of span b, given by

$$M_b = P\,(b - a) - 2\,P\,(b/3) \quad \ldots\ldots\ldots\ldots (86)$$

and setting $M_b = M_o$, the collapse load per unit length is

$$P_o = \frac{3\,M_o}{b - 3\,a} \quad (\text{for } 0 < a/b < 1/3) \quad \ldots\ldots\ldots\ldots (87)$$

This result, which satisfies both static and kinematic requirements, is shown in Fig. 3.

LOAD AT SHORT DISTANCE FROM EDGE OF SEMI-INFINITE PLATE

Circular Load.—Let a concentrated load P be uniformly distributed over a small circular area of radius a at a centroidal distance of $e < b$ from the free edge of an ideally-plastic semi-infinite plate, as before (Fig. 5). An approximate solution of this problem can be obtained as for an edge-loaded semi-infinite plate, but assuming that at collapse the stress and deformation conditions in the central sector are identical to that of a similarly loaded infinite plate, while the moments and deformation in the outer zones vary monotonically from the junction with the central sector ($\theta = \theta_o$) to the free edge. The corresponding flow field is shown in Fig. 5 for one-half of the plate about the axis of symmetry, as considered subsequently.

Measuring θ from an axis parallel to the free edge and passing through the load, the collapse load of the central sector ($\theta_o < \theta < 90°$) can then be determined from Eqs. 53 and 54 in direct proportion to the center angle ($\pi - 2\theta_o$) as before. In the outer quadrilateral zones ($0 < \theta < \theta_o$) the requirement of zero resultant bending moment along the free edge is, approximately, satisfied by the following expression containing the terminal bending moments along the yield sections of the outer zones (with right angles at junction with central sector and at free edge on axis of symmetry which is a yield-hinge line, as shown in Fig. 5), that is

$$M_o\, b \cos^2\theta - M_o \sin\theta\,(e + b \sin\theta) = 0 \quad \ldots\ldots\ldots \quad (88)$$

or,

$$e/b = \cos\theta \cot\theta - \sin\theta \quad \ldots\ldots\ldots\ldots\ldots \quad (89)$$

in which b is the radius of circumferential yield hinge arc of central sector.

Ignoring twisting moments in the outer zones and applying to them the principle of virtual work, an upper limit of the collapse load is obtained in the first instance. In this way it can be shown that the collapse load of each outer zone is, approximately, given by

$$P_o = \left[\tan\theta + \left(\frac{2.5 + \cos^2\theta}{2\cos\theta}\right)\frac{e}{b}\right]\frac{b\,M_o}{(1 - 4\,a/3\,b)(b - \Sigma\,A\,x^2/\Sigma\,A\,x)} \quad \ldots \quad (90)$$

in which $\Sigma\,A\,x^2$ refers to the moment of inertia of outer zone about outermost yield hinge line ($r = b$), ΣAx = first moment of outer zone about outermost yield hinge line, and the ratio of these terms represents the effect of the reaction pressure below the plate.

The total collapse load of the semi-infinite plate is obtained by combining the collapse load of the central sector (using Eqs. 53 or 55) with the collapse load of each outer zone (Eq. 90). Hence, for a point load ($a = 0$ and negligible reaction pressure below plate, as for an infinite plate) the total collapse load is found to be

$$P_o = (2 + \pi/2)(1 + 0.95e/b)M_o \quad (\text{for } 0 < e/b < 4/3) \quad \ldots\ldots\ldots \quad (91)$$

while for a concentrated load the total collapse load is

$$P_o = \left[0.82\,\pi(1 + 6\,a/b) + \frac{4}{(1 - 4\,a/3b)(1 - e/4\,b)}\right] (1 + 0.95\,e/b)M_o$$

(for $0.05 < a/b < 0.2$ and $0 < e/b < 4/3$). . . . . (92)

very nearly. An allowance for twisting moments would reduce these values somewhat, as would a statically admissable lower bound solution in the outer quadrilateral zones.

Strip Load.—If a strip load of width 2 a is applied at a centroidal distance of $a < e < b + t_o$ from the free edge of a semi-infinite plate, equations analogous to Eqs. 86 and 87 hold until the transverse bending moment under the load (at r = e) becomes equal to the limit moment, M_o. The upper limit of the collapse load is given by an equation analogous to Eq. 70 when the reaction pressure below the plate between the sections at r = 0 and r = e becomes triangular. In this way it can be shown that the collapse load per unit length for $0 < a/b < 1/3$ is

$$P_o = \frac{3\,M_o}{b - 3\,e} \quad (\text{for } a \le e < b/3) \ldots\ldots\ldots\ldots \quad (93a)$$

$$P_o = \frac{M_o}{e^2/(b+e) - a/4}, \text{ approximately, (for } 0.4 < e/b < 0.6) \ldots \quad (93b)$$

and

$$P_o = \frac{\left[9 + 3(e-b)^2/t_o^2\right]M_o}{b - 3\,a/2} \quad (\text{for } b < e \le b + t_o) \ldots\ldots\ldots \quad (93c)$$

in which t_o is given by Eq. 67.

Eqs. 87 and 93 can be approximated by a safe linear relationship of the collapse load per unit length

$$P_o = \frac{3(1 + 2\,e/b)M_o}{b - 3\,a(1 - e/2\,b)} \quad (\text{for } 0 < a/b < 1/3 \text{ and } 0 < e < b + t_o) \ldots \quad (94)$$

APPENDIX II.—BIBLIOGRAPHY

1. "Über das Gleichgewicht schwimmender elastischer Platten," by H. Hertz, Wiedemann's Annalen der Physik und Chemie, Leipzig, Germany, Vol. 22, 1884, p. 449.

2. "Kreisplatten auf elastischer Unterlage," by F. Schleicher, J. Springer, Berlin, Germany, 1926.

3. "Stresses in Concrete Pavements Computed by Theoretical Analysis," by H. M. Westergaard, Public Roads, Vol. 7, 1926, p. 25; and

   "New Formulas for Stresses in Concrete Pavements of Airfields," by H. M. Westergaard, Transactions, ASCE, Vol. 113, 1948, p. 425.

4. "Deflections of Plates on Elastic Foundation," by L. W. Gold, L. D. Black, F. Trofimenkof, and D. Matz, Transactions, Engrg. Inst., Canada, Vol. 2, 1958, p. 123.

5. "The Load Carrying Capacities of Circular Plates," by H. G. Hopkins and W. Prager, Journal of the Mechanics and Physics of Solids, Vol. 2, 1953, p. 1.

6. "Combined Concentrated and Distributed Load on Ideally-Plastic Circular Plates," by D. C. Drucker and H. G. Hopkins, Proceedings, Second U. S. Natl. Congress of Applied Mechanics, 1954, p. 517.

7. "Load-Carrying Capacities for Circular Plates of Perfectly-Plastic Material with Arbitrary Yield Condition," by H. G. Hopkins and A. J. Wang, Journal of the Mechanics and Physics of Solids, Vol. 3, 1954, p. 117.

8. "Beams on Elastic Foundation," by M. Hetenyi, Univ. of Michigan Press, Ann Arbor, Mich., 1946.

9. "The Theory of a Narrow Infinite Wedge on an Elastic Foundation," by D. E. Nevel, Transactions, Engrg. Inst., Canada, Vol. 2, 1958, p. 132.

10. "The Ultimate Bearing Capacity of Foundations," by G. G. Meyerhof, Geotechnique, Vol. 2, 1951, p. 301.

11. "Ultimate Strength of Ice," by T. R. Butkovich, Snow, Ice and Permafrost Res. Est., Corps of Engrs., U. S. Army, Research Paper No. 11, 1954; and

"Recommended Standards for Small-Scale Ice Strength Tests," by T. R. Butkovich, Transactions, Engrg. Inst., Canada, Vol. 2, 1958, p. 112.

12. "The Mechanics of Glacier Flow," by J. F. Nye, Journal of Glaciology, Vol. 2, 1952, p. 82.

13. "Preliminary Measurements of the Strength of Melting Lake Ice," by D. F. Barnes, Transactions, Engrg. Inst., Canada, Vol. 2, 1958, p. 108.

14. "Strength Studies of Sea Ice," by T. R. Butkovich, Snow, Ice and Permafrost Res. Est., Corps of Engrs., U. S. Army, Research Report No. 20, 1956.

15. "Aircraft Operations on Floating Ice Sheets," by S. R. Stearns, Proceedings, ASCE, Vol. 83, No. AT 1, 1957.

16. "Recent Studies on Ice-Their Application to Logging Operations in Eastern Canada," by C. R. Siversides. Discussion by L. W. Gold, Publications, Woodlands Section, Pulp and Paper Assn., No. 1845, B-1, 1959.

17. "The Preparation of Ice Landings by Pulp and Paper Companies in Eastern Canada," by L. B. Rose and C. R. Silversides, Transactions, Engrg. Inst., Canada, Vol. 2, 1958, p. 101.

18. "Moving Loads on Floating Ice Sheets," by J. T. Wilson, Univ. of Michigan Research Inst., Final Report, 1958.

19. "Airfields on Floating Ice Sheets," by A. Assur, Snow, Ice and Permafrost Res. Est., Corps of Engrs., U. S. Army, Report No. 36, 1956.

20. "Relative Strengths of Plates on Elastic Foundation," by L. D. Black, Transactions, Engrg. Inst., Canada, Vol. 2, 1958, p. 129.

Journal of the
ENGINEERING MECHANICS DIVISION
Proceedings of the American Society of Civil Engineers

MEMBRANE STRESSES IN HYPERBOLOID SHELLS OF REVOLUTION

By Placido Cicala[1]

SYNOPSIS

The computation of membrane stresses and of the corresponding deformations for a hyperboloid shell of revolution under the most general loading is reduced to the evaluation of simple integrals. For the determination of wind effects, diagrams capable of simplifying computations are presented and an approximate formula is suggested.

INTRODUCTION

Reinforced concrete shells having as middle surface a rotation hyperboloid are currently used in the construction of cooling towers. Wind action constitutes the severest loading for such structures. If the distribution of wind pressure along any parallel circle is assumed to be proportional to the cosine of the angle that the radial direction makes with the meridian plane containing the wind direction, the computation of the stresses can be performed according to well known methods.[2] However, it is recognized[3] that the wind pressure is distributed quite differently from the mentioned law and that much higher

Note.—Discussion open until March 1, 1961. To extend the closing date one month, a written request must be filed with the Executive Secretary, ASCE. This paper is part of the copyrighted Journal of the Engineering Mechanics Division, Proceedings of the American Society of Civil Engineers, Vol. 86, No. EM 5, October, 1960.

1 Professor of Applied Elasticity, Polytechnic of Torino, Italy.

2 "Theory of Plates and Shells," by S. Timoshenko, McGraw-Hill Book Co., Inc., New York and London, 1940.

3 "Sulla teoria elastica della parete sottile di rivoluzione e l'applicazione agli involucri iperboloidici," by P. Cicala, Pubblicazioni del Corso di Costruzioni in Cemento Armato, Politecnico di Milano (in publication).

stresses arise than computed from the cosine distribution giving the same resultant thrust. A more exact computation is therefore in order. The peculiar geometrical properties of the rotation hyperboloid furnish important simplifications in the stress analysis of the shells having this middle surface. This was pointed out by Flügge[4] who indicated a homogeneous solution; that is, a stress system produced by a special edge loading. Here the problem is dealt with in general terms. The solution for membrane stresses and corresponding deformation under any arbitrary loading is obtained. These results can be arrived at using the theory of characteristics for the resultant equation. This is a second order partial differential equation of the hyperbolic type. However, an elementary deduction has been preferred as leading, more immediately, to the final results.

THEORY

Analysis of Stress.—The equilibrium equations of the membrane stresses for a surface of revolution are written[2] as follows:

$$\frac{\partial}{\partial \phi}(r N_\phi) + r_1 \frac{\partial}{\partial \theta} N_{\theta\phi} - r N_\theta \cos \phi + r r_1 Y = 0 \quad \ldots\ldots (1)$$

$$\frac{\partial}{\partial \phi}(r N_{\phi\theta}) + r_1 \frac{\partial}{\partial \theta} N_\theta + r_1 N_{\theta\phi} \cos \phi + r r_1 X = 0 \quad \ldots\ldots (2)$$

and

$$r N_\phi + r_1 N_\theta \sin \phi + r r_1 Z = 0 \quad \ldots\ldots\ldots\ldots (3)$$

in which N_ϕ and $N_{\phi\theta}$ are the normal and tangential forces per unit arch of the parallel circle; N_θ and $N_{\theta\phi}$ are the normal and tangential forces per unit arch of the meridian; X, Y, and Z are the components of the external force per unit surface on the tangent to the parallel, the tangent to the meridian and the normal to the surface, respectively; r is the radius of the parallel; r_1 the radius of curvature of the meridian; θ is the angle defining the position of the meridian plane; and ϕ is the angle made by the normal to the surface and the axis of rotation. Along this axis the coordinate z is measured. For the elemental arch of the meridian the equivalent expressions hold

$$r_1 d\phi = \frac{dr}{\cos \phi} = \frac{dz}{\sin \phi} \quad \ldots\ldots\ldots\ldots\ldots\ldots (4)$$

Using L to denote a constant length, we introduce the notation

$$N_\phi = \frac{H_1}{r \sin \phi} \qquad N_{\phi\theta} = N_{\theta\phi} = \frac{L H_2}{r^2} \quad \ldots\ldots\ldots\ldots (5)$$

Consequently, Eq. 3 yields

$$N_\theta = -\frac{r Z}{\sin \phi} - \frac{H_1}{r \sin^2 \phi} \quad \ldots\ldots\ldots\ldots\ldots\ldots (6)$$

---

[4] "Statik und Dynamik der Schalen," by W. Flügge, Springer, Berlin, 1957.

Substituting Eqs. 5 and 6 into Eqs. 1 and 2 and taking account of Eq. 4 leads to the equations defining the unknown functions H_1, H_2:

$$\frac{1}{r\, r \sin\phi}\frac{\partial H_1}{\partial \phi} + \frac{L}{r}\frac{\partial H_2}{\partial \theta} = -Y - Z\cot\phi \quad \ldots\ldots\ldots\ldots (7a)$$

$$\frac{L \sin\phi}{r\, r}\frac{\partial H_2}{\partial \phi} - \frac{1}{r\, r \sin\phi}\frac{\partial H_1}{\partial \theta} = \frac{\partial Z}{\partial \theta} - X \sin\phi \quad \ldots\ldots\ldots (7b)$$

In the present case, in which the meridian m (Fig. 1) is a hyperbola, the coordinates r, z may be expressed in the parametric form

$$r = R \sec\omega \qquad z = a \tan\omega \quad \ldots\ldots\ldots\ldots (8)$$

with

$$a = R \cot\alpha \quad \ldots\ldots\ldots\ldots\ldots\ldots (9)$$

Here R is the throat radius of the hyperboloid, α is the angle made by the asymptote s of the hyperbola with the axis of rotation. The parameter $\omega°$ ranges

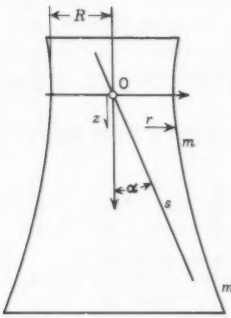

FIG. 1.—NOTATION

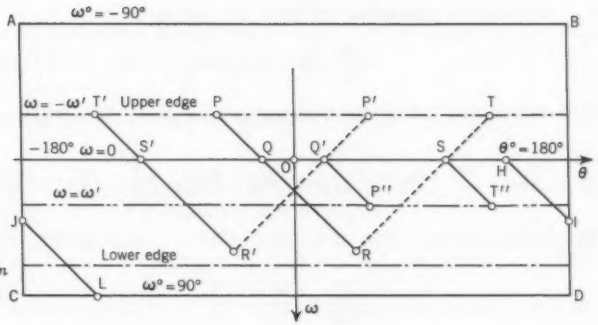

FIG. 2.—MAPPING OF THE HYPERBOLOID SURFACE ON A θ, ω PLANE

from −90° to +90° while the point running the hyperbola goes from $z = -\infty$ to $+\infty$. Correspondingly $\phi°$ varies from $90° + \alpha°$ to $90° - \alpha°$. Eq. 8 by means of Eq. 4, yields

$$\cot\phi = \tan\alpha \sin\omega \quad \ldots\ldots\ldots\ldots\ldots (10)$$

$$\frac{a}{r_1} = -\tan\alpha \sin^3\phi \cos^3\omega \quad \ldots\ldots\ldots\ldots (11)$$

If f is a generic function, according to Eq. 10 we get

$$\frac{\partial f}{\partial \omega} = \frac{\partial f}{\partial \phi}\frac{d\phi}{d\omega} = -\tan\alpha \sin^2\phi \cos\omega \frac{\partial f}{\partial \phi} \quad \ldots\ldots\ldots\ldots (12)$$

By using Eqs. 10 to 12, if $L = R^2/a$, Eqs. 7 are reduced to the form:

$$\frac{\partial H_1}{\partial \omega} + \frac{\partial H_2}{\partial \theta} = F_1 \qquad \frac{\partial H_2}{\partial \omega} + \frac{\partial H_1}{\partial \theta} = F_2 \quad \ldots\ldots\ldots \quad (13)$$

in which

$$F_1 = -\frac{a\,R}{\cos^3 \omega}\,(Y + Z \cot \phi)$$

$$F_2 = \frac{a^2}{\sin^2 \phi \cos^4 \omega}\left(\frac{\partial Z}{\partial \theta} - X \sin \phi\right) \quad \ldots\ldots\ldots\ldots \quad (14)$$

The surface of the hyperboloid may be mapped into the rectangle ABCD in the plane of coordinates θ, ω (Fig. 2). To every point of the hyperboloid there is a corresponding point within this rectangle. Parallel circles and meridian lines are transformed into horizontal and vertical lines, respectively. Generators are transformed into straight lines making angles of 45° with the contour sides. Along one such line as PR, having the slope $d\omega/d\theta = 1$ we have

$$\frac{df}{d\omega} = \frac{\partial f}{\partial \omega} + \frac{\partial f}{\partial \theta} \quad \ldots\ldots\ldots\ldots\ldots\ldots \quad (15)$$

Therefore, summing up Eqs. 13 yields

$$\frac{d}{d\omega}\left(H_1 + H_2\right) = F_1 + F_2 \quad \ldots\ldots\ldots\ldots\ldots \quad (16)$$

the derivative being taken along such a line. Integrating from P to R yields

$$\left(H_1 + H_2\right)_R - \left(H_1 + H_2\right)_P = \int_P^R \left(F_1 + F_2\right) d\omega \quad \ldots\ldots\ldots \quad (17)$$

Similarly, along a line of slope $d\omega/d\theta = -1$ such as TR, the derivative is

$$\frac{df}{d\omega} = \frac{\partial f}{\partial \omega} - \frac{\partial f}{\partial \theta} \quad \ldots\ldots\ldots\ldots\ldots\ldots \quad (18)$$

Therefore, subtracting Eqs. 13 and integrating along TR gives

$$\left(H_1 - H_2\right)_R - \left(H_1 - H_2\right)_T = \int_T^R \left(F_1 - F_2\right) d\omega \quad \ldots\ldots\ldots \quad (19)$$

If P and T are points of a free edge, then there is $H_1 = H_2 = 0$. Thus the stress resultants at R are written

$$2\,H_1 = \int_P^R \left(F_1 + F_2\right) d\omega + \int_T^R \left(F_1 - F_2\right) d\omega \quad \ldots\ldots\ldots \quad (20)$$

$$2\,H_2 = \int_P^R \left(F_1 + F_2\right) d\omega - \int_T^R \left(F_1 - F_2\right) d\omega \quad \ldots\ldots\ldots \quad (21)$$

If the load distribution is symmetrical with respect to the plane $\theta = 0$, that is, if

$$F_1(\omega, \theta) = F_1(\omega, -\theta) \; ; \; F_2(\omega, \theta) = -F_2(\omega, -\theta) \quad (22)$$

then, for any couple of integration paths such as TR, T'R'

$$\int_T^R (F_1 + F_2)d\omega = \int_{T'}^{R'} (F_1 - F_2)d\omega \quad (23)$$

Further simplifications arise if the load distribution is also symmetrical with respect to the throat plane $\omega = 0$. That is, if

$$F_1(\omega, \theta) = -F_1(-\omega, \theta), \; F_2(\omega, \theta) = F_2(-\omega, \theta) \quad (24)$$

Then the relationship (See Fig. 2)

$$\int_{T'}^{S'} (F_1 + F_2)d\omega = \int_T^S (F_1 - F_2)d\omega = -\int_S^{T''} (F_1 + F_2)d\omega \quad (25)$$

is obtained. In conclusion, in the case of double symmetry, the integrals in Eqs. 20 and 21 need not be computed on both systems of lines $d\omega/d\theta = 1$ and $d\omega/d\theta = -1$. It suffices to integrate along one system, on one side of the line $\omega = 0$. In other words, it suffices to compute the function

$$J(\omega, \theta) = \int_0^{\omega} (F_1 + F_2)d\bar{\omega} \quad (26)$$

in which the arguments of the integrand function are $\bar{\omega}$, $\theta + \bar{\omega} - \omega$. Hence, if $\omega = -\omega'$ is a free edge, the stress resultants are expressed by

$$2H_1(\omega, \theta) = J(\omega, \theta) + J(\omega, -\theta) - J(\omega', \omega' + \omega - \theta) - J(\omega', \omega' + \omega + \theta) \quad (27)$$

$$2H_2(\omega, \theta) - J(\omega, \theta) - J(\omega, -\theta) + J(\omega', \omega' + \omega - \theta) - J(\omega', \omega' + \omega + \theta) \quad (28)$$

If an integration path, such as HI (Fig. 2), intersects the contour $\theta° = 90°$, it is to be prosecuted as indicated by line JL.

If the hyperboloid is subjected to normal pressures $p = Z$, with $X = Y = 0$, and if p does not depend on ω, then, by Eqs. 14, replacing $\partial p/\partial\theta$ by $dp/d\omega$ in accordance with Eq. 15, Eq. 26 may be written as

$$J = a^2 \int_0^{\omega} \frac{dp/d\bar{\omega}}{\cos^4 \bar{\omega} \sin^2 \phi} - p \frac{\tan^2 \alpha \sin \bar{\omega}}{\cos^3 \bar{\omega}} d\bar{\omega} \quad (29)$$

Introducing the reference pressure p_0, Eq. 29 is transformed by product integration in the form

$$J = p_0 a^2 (J_2 \sin^2 \alpha - J_1)/\cos^2 \alpha \quad (30)$$

in which

$$J_1 = 4\int_0^{\omega} \frac{p \sin \bar{\omega}}{p_o \cos^5 \bar{\omega}}\, d\bar{\omega} - \frac{p/p_o}{\cos^2 \bar{\omega}}\Bigg|_0^{\omega} \quad \ldots\ldots\ldots\ldots (31)$$

$$J_2 = \int_0^{\omega} \frac{p \sin \bar{\omega}}{p_o \cos^3 \bar{\omega}}\, d\bar{\omega} - \frac{p/p_o}{\cos^2 \bar{\omega}}\Bigg|_0^{\omega} \quad \ldots\ldots\ldots\ldots (32)$$

Here p is the pressure corresponding to the argument $\theta + \bar{\omega} - \omega$. The sign $f\Big|_0^{\omega}$ stands for $f(\omega) - f(0)$.

If the pressure distribution is represented by

$$p = p_o \cos m\,\theta \quad \ldots\ldots\ldots\ldots\ldots\ldots (33)$$

in which m is a positive integer, the stress resultants are given by

$$H_1 = H_1^* \cos m\,\theta \qquad H_2 = H_2^* \sin m\,\theta \quad \ldots\ldots\ldots (34)$$

in which H_1^*, H_2^* are functions of m, a, ω' and ω. For m = 2, H_1^* may be written as

$$\frac{1}{p_o} H_1^* = K \tan^2 \alpha + \frac{\sec^2 \alpha}{1.5} \frac{(z+h)^2}{a^2 + z^2} \left(3a^2 - 2hz + z^2\right) \ldots\ldots (35)$$

with $h = a \tan \omega'$.

These relationships, as well as the explicit expression for K, a function of ω' and ω, may be deduced from Eqs. 27, 28, 30, 31, and 32, or, more directly, from the aforementioned note.[3]

Analysis of Deformation.—The deformation of the membrane shell of revolution is expressed by the relationships[4]

$$\epsilon_\phi = \frac{1}{Et}\left(N_\phi - \mu N_\theta\right) = \frac{\partial v}{r_1 \partial \phi} + \frac{w}{r_1} \quad \ldots\ldots\ldots\ldots\ldots (36)$$

$$\epsilon_\theta = \frac{1}{Et}\left(N_\theta - \mu N_\phi\right) = \frac{\partial u}{r\,\partial \theta} + \frac{v}{r}\cos\phi + \frac{w}{r}\sin\phi \quad \ldots\ldots\ldots (37)$$

and

$$\gamma_{\theta\phi} = \frac{2(1+\mu)}{Et} N_{\theta\phi} = \frac{\partial u}{r_1 \partial \phi} - \frac{u}{r}\cos\phi + \frac{\partial v}{r\,\partial \theta} \quad \ldots\ldots\ldots\ldots (38)$$

in which ϵ_θ, ϵ_ϕ, and $\gamma_{\theta\phi}$ are the strain components of the middle surface (circumferential, meridional and shear strain, respectively); E is the Young's modulus, μ the Poisson's ratio; v, u, w are the components of displacement tangent to the meridian, tangent to the parallel circle and normal to the surface, respectively; and t is the thickness of the shell.

Introducing the notation

$$u = H_2' r \qquad v = H_1' L \sin\phi \quad \ldots\ldots\ldots\ldots (39)$$

and eliminating w from the Eqs. 36 and 37 yields

$$\frac{\partial H_2'}{\partial \theta} - \frac{L}{r}\sin^2\phi \frac{\partial H_1'}{\partial \phi} = \epsilon_\theta - \frac{r_1}{r}\epsilon_\phi \sin\phi \quad \ldots\ldots\ldots (40)$$

$$\frac{r}{r}\frac{\partial H_2'}{\partial \phi} + \frac{L \sin \phi}{r}\frac{\partial H_1'}{\partial \theta} = \gamma_{\theta\phi} \quad \ldots\ldots\ldots\ldots (41)$$

In the particular case of the hyperboloid shell, the same transformations, leading to Eqs. 13, yield the analogous equations

$$\frac{\partial H_1'}{\partial \omega} + \frac{\partial H_2'}{\partial \theta} = F_1' \qquad \frac{\partial H_2'}{\partial \omega} + \frac{\partial H_1'}{\partial \theta} = F_2' \quad \ldots\ldots\ldots (42)$$

in which

$$F_1' = \epsilon_\theta + \frac{\cot^2 \alpha}{\cos^2 \omega \sin^2 \phi}\epsilon_\phi$$

$$F_2' = \frac{\cot \alpha}{\cos \omega \sin \phi}\gamma_{\theta\phi} \quad \ldots\ldots\ldots\ldots\ldots (43)$$

Hence the unknown functions H_1', H_2' can be computed by the same procedure as suggested for H_1 and H_2, from Eqs. 13.

Boundary Conditions.—The situation for arbitrary end-conditions on the two parallel edge circles has been dealt with in the mentioned note[3] where states of strain represented by sinus functions of θ have been considered. In the general case the solution is obtained by combining the following:

1) a particular solution of Eq. 13 for stresses and of Eqs. 42 for displacements taking account of the applied loads;
2) two homogeneous membrane solutions, that is two independent solutions obtained from Eq. 13 with $F_1 = F_2 = 0$.
3) two homogeneous inextensional solutions, that is, two solutions obtained from Eqs. 42 with $F_1' = F_2' = 0$.
4) four solutions for edge effects.

The solutions of type[4] are well known in the case of axial symmetry.[2] They can be determined[3] in the general case for a shell of revolution by using a power expansion of a thickness parameter.

The combination of the above solutions may be prescribed to satisfy four conditions along each edge. With upper edge free, the three components of the stress resultants and the bending moment are to be equated to zero. Along the lower edge, the shell forming the cooling tower is supported by truss members. The constraint condition thus afforded may be assumed to nullify the components u, v of displacement as well as the transverse shear and the bending moment. In this situation, if solution[1] is computed by prescribing that $H_1 = H_2 = 0$ along the upper edge $\omega = -\omega'$ and that $H_1' = H_2' = 0$ along the other edge $\omega = \omega''$, then no correction is needed, as previously shown[3] for any component in a Fourier expansion of the strain configuration. In other words, the contributions of the stress systems 2, 3, and 4 become negligible, within the usual approximation limits.

CALCULATION OF WIND EFFECTS

The existing information concerning the distribution of wind pressure on bodies of revolution is not yet complete. Consequently, McKelvey and Brooke[5]

5 "The Industrial Cooling Tower," by K. McKevey and M. Brooke, Elsevier, Amsterdam, 1959.

used the data, as given by French regulations[6] for long cylinders, to compute wind effects on conical cooling towers. If these same data are assumed to be valid for the hyperboloid, the results plotted on Figs. 3, 4, and 5 are obtained. The abscissa θ is the angle made by the meridian plane with the direction of wind velocity, $\theta = 0$ being the upstream meridian. The reference pressure p_o is the dynamic pressure (half air density times square velocity). The data referred to indicates that in the downstream sector (that is, $\theta° < -90°$ or $> 90°$) the pressure is constant and equals $-0.52\ p_o$. Therefore, the computation is carried conveniently for pressure values increased by $0.52\ p_o$, the effects of the additive constant being separately accounted for. The line a of Fig. 3 represents the adopted pressure distribution. The values marked near the curve, with a spacing of 5° or 10°, are taken from the aforementioned regulations or interpolated. They were used to compute J_1 and J_2 according to Eqs. 31 and 32. The integrations are performed by the Simpson formula, over intervals of 5°.

For a constant pressure, Eq. 31 yields $J_1 = 0$. Therefore, the values of J_1 are not modified by the constant added to p. They are plotted against θ in Fig. 3 for $\omega° = 10°, 20°, \ldots, 60°$. Each curve is to be read according to the scale marked at its end. The curves should enclose zero area, except for slight imprecision due to the integration process.

For a constant pressure $p = 2\,k\,p_o$ Eqs. 32 yields

$$J_2 = -\,k \tan^2 \omega \quad \ldots\ldots\ldots\ldots\ldots\ldots \quad (44)$$

Hence, because of the constant added to p, the curves of Fig. 4 represent the values of $\overline{J}_2 = J_2 - 0.26 \tan^2 \omega$, to be read according to the scales marked at the end of each curve. The mean ordinate should equal $-0.125 \tan^2 \omega$ since $0.25\ p_o$ is the mean ordinate of curve a in Fig. 3.

Out of the interval $-90° < \theta° < 90° + \omega°$ the values for J_1 and J_2 are zero. Both series of curves, in Figs. 3 and 4, show more or less abrupt changes in slope for $\theta° = -90° + \omega°$ and for $\theta° = 90°$, in addition to their end-points.

By using the charts of Figs. 3 and 4 for double interpolation, the stresses at any point of a hyperboloid shell can be computed for any set of data, provided the value $\omega° = 60°$ is not exceeded. This is usually the case in design practice of cooling towers. The geometry of the surface is assigned by fixing two out of the quantities a, R and α, related by Eq. 9. The correspondence between z and ω is established by means of Eq. 8 and the value ω' corresponding to the free edge is computed. For a given point of the shell $\omega = \omega_1, \theta = \theta_1$ the values for J_1 and $J_2 = \overline{J}_2 + 0.26 \tan^2 \omega$ are determined from the charts of Figs. 3 and 4 for the arguments $\omega = \omega_1, \theta = \theta_1$ and $\theta = -\theta_1; \omega = \omega', \theta = \omega_1 + \omega' - \theta_1$ and $\theta = \omega_1 + \omega' + \theta_1$. Then the corresponding J values are computed from Eq. 30 and replaced in Eqs. 27 and 28 to obtain H_1 and H_2 at the point considered. Finally, the unit forces are computed from Eqs. 5 and 6. Dividing by the shell thickness furnishes the stresses.

It is to be remarked that the angle α enters explicitly in Eq. 30. This makes the indicated charts valid for any value of α.

These diagrams have been deduced under the assumption that p depends only on θ. A generalization is readily feasible. If the pressure distribution is represented by a law such as $C(z)p(\theta)$ in which C is a coefficient having a stepped diagram when plotted versus z, then the value of J may be expressed by the

---

[6] "Règles Neige et Vent," Ministère de la Reconstruction et de l'Urbanisme, Paris, 1947.

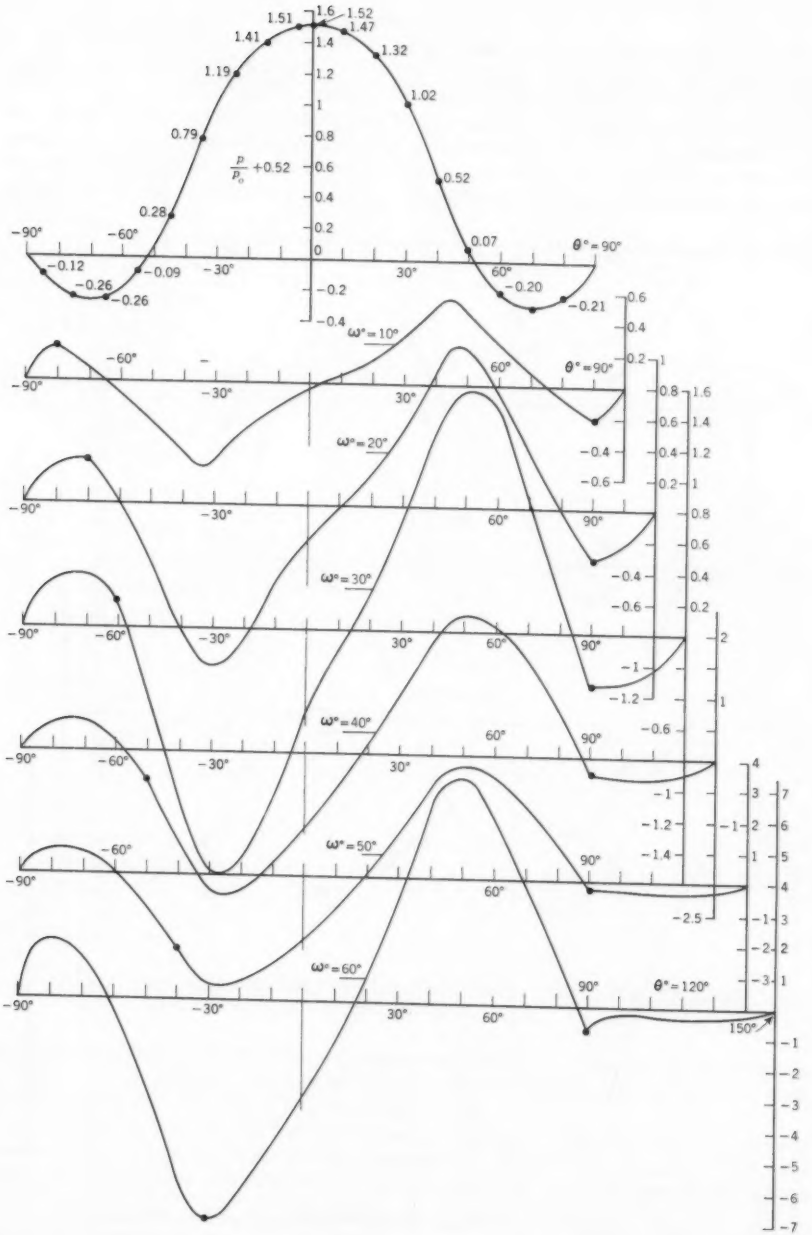

FIG. 3.—J_1 VERSUS $\theta°$

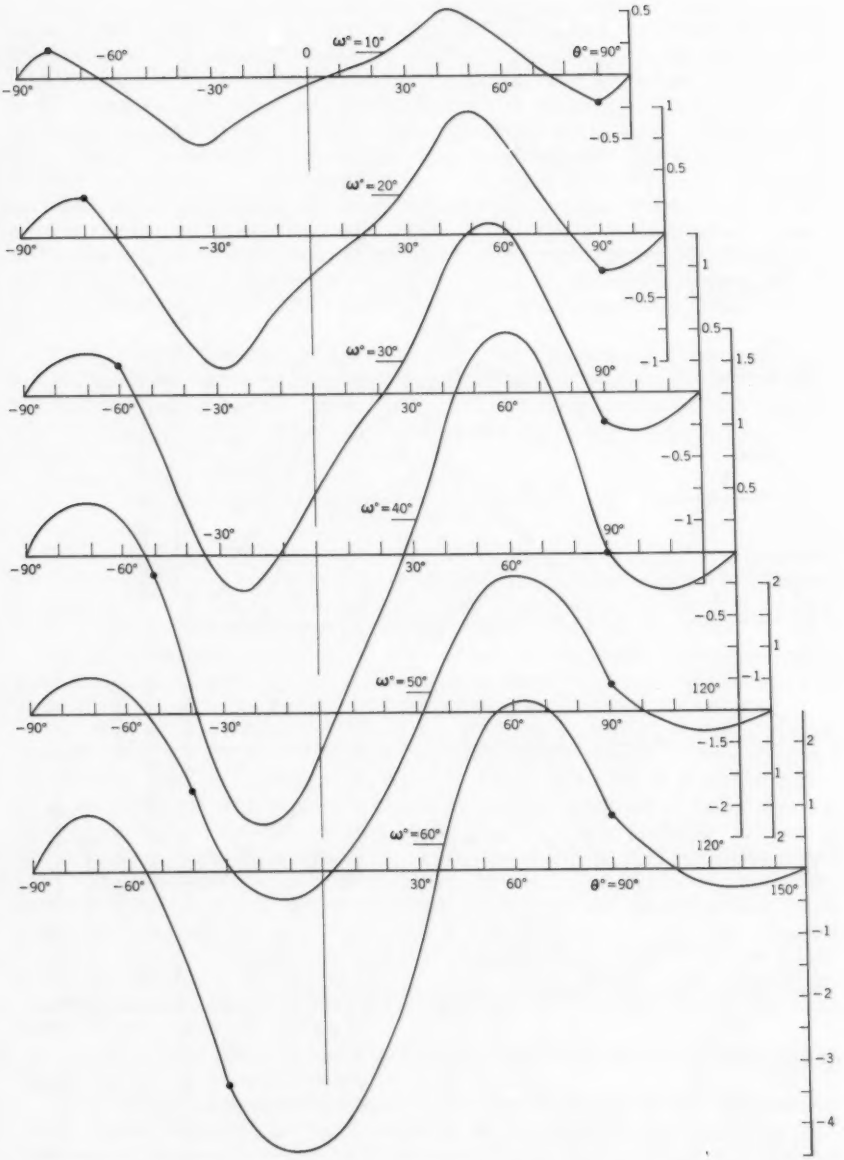

FIG. 4.—J_2 VERSUS θ°

summation $\Sigma C_i \Delta_i J$ in which $\Delta_i J$ is the difference of the values taken by J at the ends of the generic interval where $C = C_i$.

A particular example representative of usual cooling tower design has been considered. The values fixed are $(a/R) = 2.4$, $\omega' = 22°$, $\omega'' = 56°$. The correlated shape of the shell is represented in Fig. 1. The line a of Fig. 5 shows the values of H_1 computed along the lower edge of the shell according to the graphs of Figs. 3 and 4. The dotted line b indicates the values obtained from the same data when taking into account only the first harmonic in the Fourier expansion of the pressure diagram. It appears that the computation is very

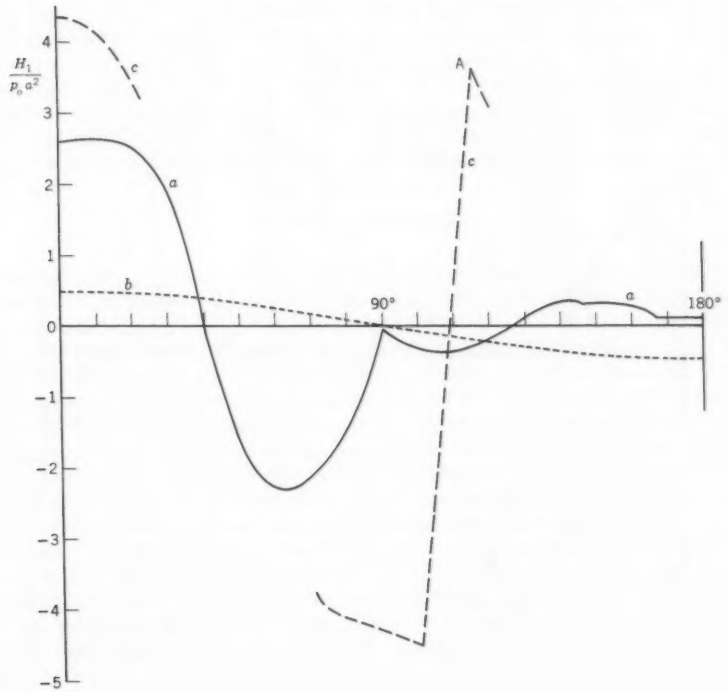

FIG. 5.—NORMAL STRESS DIAGRAMS AT LOWER EDGE FOR VARIOUS WIND PRESSURE DISTRIBUTIONS.

unconservative if it is carried by assuming the wind pressure to be proportional to $\cos\theta$. Though this is the component from which the resultant wind thrust originates, its effect is a secondary one.

The same structure, in the previous example, has been considered as subjected to the pressure distribution represented by line a in Fig. 6. This diagram is taken from the data obtained by Golubović[7] in wind tunnel measure-

[7] "Etude aérodynamique d'une tour réfrigérante en forme d'hyperboloide de révolution," by G. Golubović, Int. Ass. for Bridge and Struct. Eng. XVII Vol., 1957, p. 90, Fig. 3.

ments on a hyperboloid model having a relatively smooth surface. In this case, a strong depression exists in the neighborhood of the meridian plane perpendicular to the wind direction. On the contrary, measurements on models having a rough surface effected by Golubović and others[5,7] indicate diagrams akin to the one to which line a in Fig. 3 refers. The computations were carried on the basis of the dotted line of Fig. 6, that follows the original graph closely but corresponds to a simple diagram for $dp/d\theta$, as shown by line b of Fig. 6. On this basis, the integrations were performed analytically. The values for H,

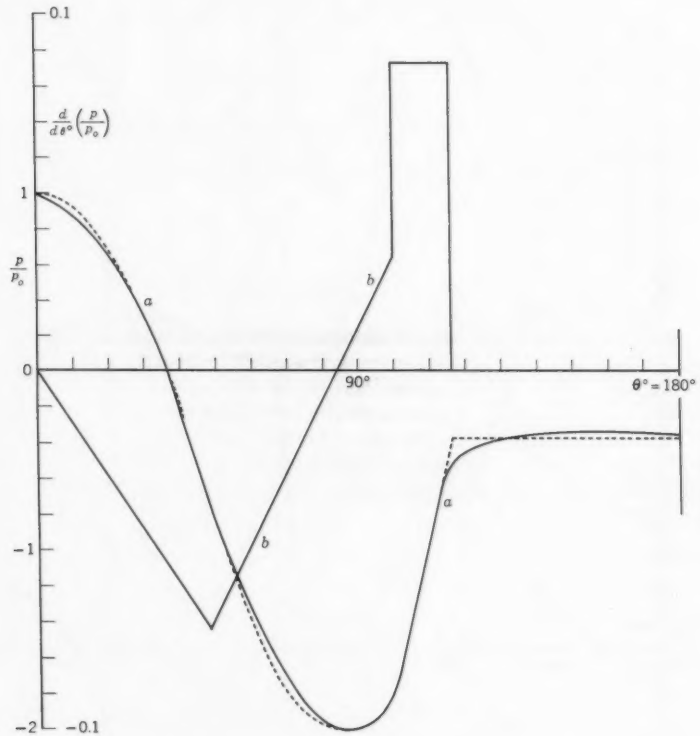

FIG. 6.—PRESSURE DISTRIBUTION ON A HYPERBOLOID MODEL HAVING A SMOOTH SURFACE

along the lower edge of the structure were computed. The most significative branches of the diagram obtained are represented by line c of Fig. 5. Of course, the pointed peaks, such as the sharp corner at C, are actually rounded off by the effect of the flexural stiffness of the shell; but the maxima existing in the neighborhood of the (positive or negative) maxima of the pressure diagram are not likely to be reduced greatly by the said effect. Therefore, comparison of line c with line a shows that the stresses attained are considerably higher in the second case considered.

The numerical investigation showed that the maximal values of stresses are mainly due to the component proportional to cos 2θ in the Fourier expansion of the pressure diagram. This fact suggests the use of Eq. 35 for an approximate evaluation of these maxima. According to actual design trends for cooling towers, terms containing $\sin^2 \alpha$ can be neglected. Thus the modified equation

$$|H_1|_{max} = \frac{\Delta p}{3} \frac{(z+h)^2}{a^2+z^2} \left(3a^2 - 2hz + z^2\right) \quad \ldots\ldots\ldots \quad (45)$$

is suggested. This formula furnishes the absolute value of the maximal positive and negative direct stresses. The unit Δp is the interval of values within which the pressure ranges. The remaining symbols are explained by Fig. 1.

Application of Eq. 45 in the cases considered shows excellent agreement with the results of the rather lengthy exact computations. In the case of pressure diagram a of Fig. 3, for which $\Delta p = 1.8\ p_o$, Eq. 44 indicates the range of values for H_1 denoted by Δ_a on Fig. 5, in agreement with line a. For the pressure diagram of Fig. 6, giving $\Delta p = 3\ p_o$ the range of values for H_1 furnished by Eq. 45 is denoted by Δ_c on Fig. 5 and compares satisfactorily with line c.

CONCLUSIONS

The particular geometrical properties of the rotation hyperboloid allow the computation of the membrane solution to be reduced to simple integrations for any distribution of loads. Further simplifications arise in the case of normal pressures distributed according to laws that depend only on θ. The charts presented greatly reduce the computational labor. They are based on a standard diagram of pressure and allow one to take into account the influence of all the geometrical parameters of the shell. Moreover, an approximate formula of immediate use is suggested for the evaluation of maximal direct stresses.

Concerning the quantitative results of the present investigation on the effects of wind action, it is to be remarked that the consideration of the actual distribution of pressure leads to much higher stresses than the simplified analysis based on a distribution proportional to cos θ. Furthermore, considerable differences are detected in the maximal stresses corresponding to the pressure diagrams obtained on aerodynamic models having a smooth surface or a rough one. A paradoxical result is reached on this point. The wind action on the smooth shell gives a smaller resultant thrust but higher stresses than in the case of a rough surface.

These facts stress the need for more complete aerodynamic information. For instance, precise quantitative indication on the influence of surface roughness should be offered to the stress analyst. As long as the information is lacking the calculation cannot be carried out with sufficient reliability. The diagrams presented here are intended for demonstrative purposes, however, they clearly show the practical importance of the problems dealt with.

Journal of the
ENGINEERING MECHANICS DIVISION
Proceedings of the American Society of Civil Engineers

DISCUSSION

Note.—This paper is a part of the copyrighted Journal of the Engineering Mechanics Division, Proceedings of the American Society of Civil Engineers, Vol. 86, EM 5, October, 1960.

BEHAVIOR OF STRUCTURES DURING EARTHQUAKES[a]

Closure by George W. Housner

GEORGE W. HOUSNER.[1]—In his discussion, Mr. Berg presents an interesting and novel comparison between earthquake spectra-ratios and the ideal cases of a single-impulse and a constant-energy input. The spread of these response computations can be attributed to differences in earthquake records, and also to the manner in which response spectra are computed. In the case of the constant energy input with effect of damping being as $\sqrt{1/\nu}$, the ensemble average is computed at the end of a specified time that is sufficiently long to permit the process to be treated as stationary. In the case of an earthquake, the response spectrum is computed at the time that gives the maximum value. Because of this, it is found that the average earthquake spectra indicate that stationarity has not been reached for the longer periods and smaller damping.

Mr. Berg's finding, that for elasto-plastic systems on the average the energy input does not exceed the maximum input for an equivalent, elastic, undamped structure, is very interesting and helps to explain the observed behavior of structures during earthquakes. He is, of course, correct in stating that the maximum energy input should not be computed from a low point on the undamped spectrum curve.

In his discussion, Mr. Derrick makes numerous statements of a rather general nature whose complete rebuttal would be beyond the scope of a closing discussion. The following comments are offered in response to the stated and implied points of difference set forth by him.

The El Centro, 1940 ground motion is the strongest so far recorded. It is certainly not the strongest possible ground motion. That ground motion has been estimated by the writer[2] to be perhaps twice as intense (63% g) without making any special allowance for type of soil. Of course, in the special cases of structures located directly on top of a slipping fault, or some unusual geological conditions, there is no telling what motions might be involved.

The El Centro accelerometer was not located on sedimentary rock but was located on very deep, sandy alluvium, and for this reason seismologists attribute an amplifying effect to the site. For example, Gutenberg[3] compared seismograms obtained on the rock outcropping at the Pasadena Seismological Laboratory with those obtained at Long Beach and at El Centro. According to him, the amplification factor at Long Beach was 2.5 and at El Centro was 8, or in other words, for earthquakes of the same magnitude and at the same distance,

---

[a] October, 1959, by George W. Housner.

[1] Asst. Prof., Applied Mech., Calif. Inst. of Tech., Pasadena, Calif.

[2] "Intensity of Ground Motion During Strong Earthquakes," by G. W. Housner, Second Tech. ONR Report, Earthquake Research Lab., Calif. Inst. of Tech., August, 1952.

[3] "Effects of Ground Shaking in Earthquakes," by B. Gutenberg, Trans. Amer. Geophysical Union, Vol. 37, No. 6, December, 1956.

the ground acceleration at El Centro would be in the ratio of 8 to 2.5, or 3.2 times as great as at Long Beach. This was not, however, observed to be the case during strong ground motion. The 1933 Long Beach earthquake had a magnitude of 6.25 and the El Centro, 1940 shock had a magnitude of 7.0, so that, according to Gutenberg's findings, the maximum acceleration at El Centro should have been some five or six times greater than at Long Beach. However, neither instrumental recordings nor damage observations indicated that the ground motion at El Centro was appreciably more intense than in the Long Beach-Compton area. The records obtained during the Long Beach earthquake and those obtained during the El Centro shock are consistent with each other if it is assumed that there was no significant effect of ground.[2]

It should be noted that Gutenberg's measurements were of extremely weak ground motions that were far below the threshold of human sensibility. His findings are not directly applicable to strong ground motions. For example, in addition to the El Centro-Long Beach discrepancy noted above, the accelerograms obtained during the San Francisco earthquake of March 22, 1957 do not agree with his findings. These accelerations were recorded at five different locations that were on filled ground, on alluvium of various depths and on rock. The deepest and softest ground did not amplify the motion over that recorded on rock.[4,5] While it is true that the local geology can affect the earthquake ground motion, it appears that it is not a simple relationship that depends only upon the depth and softness of alluvium. More strong earthquake recordings on different types of soils are required before the effect of ground can be elucidated.

The average spectra were obtained from accelerograms located on different types of ground, however, despite this, the individual spectra were all similar in their general shapes and did not indicate any significant influence of ground. The spectra for El Centro 1934 differed as much from the spectra for El Centro 1940 as did those of Taft, 1952, which accelerograms were recorded on sedimentary rock several hundred miles distant from El Centro.

The average spectra, when multiplied by the prescribed factors, do not reproduce the actual spectra. The factors that were given in the paper, scale the average spectra so that the spectrum intensity corresponds to that of the average of the two components of the actual spectra. Presumably, the point that Mr. Derrick is making is that the ordinates of the actual spectrum curves have some statistical distribution about the average and if the range of this distribution could be determined, it would be better than the average. There is, however, no reason to suppose that this would give significantly different results. Specifically, Mr. Derrick points out that one of the spectrum curves for the El Centro 1940 shock is higher than average in the low period region. This can probably be attributed, at least partly, to the fact that the accelerometer was within 10 miles of the surface trace of the fault and hence the high frequency components of the ground motion were only lightly attenuated. It would probably be correct to say that for points so close to a fault the average spectrum curves should be boosted in the low period end. On the other hand, for

---

4 "Analysis of Strong-Motion Accelerometer Data from the San Francisco Earthquake of March 22, 1957," by D. E. Hudson and G. W. Housner, Bull. Seismo. Soc. Amer., Vol. 48, No. 3, July, 1958.

5 "Response Spectrum Analysis of the March 22, 1957 San Francisco Earthquake," by D. E. Hudson and G. W. Housner, The San Francisco Earthquakes of March, 1957, Special Report 57, Calif. Div. of Mines, 1959.

points at greater distances from the fault the average spectrum curves should, perhaps, be depressed in the short period end. If the average spectrum curves are used for design it should, of course, be kept in mind that the spectra of future earthquakes will have statistical fluctuations about the average.

Mr. Derrick states that, "the assumption that the distribution of mass does not influence the amount of work performed by an earthquake is open to question." The writer believes that the statements regarding this matter that were made in the paper are correct so that Mr. Derrick's question presumably arises from a misinterpretation of the statistical implications of those statements. Mr. Derrick states that, "there is no positive evidence on which to base either an analytical or an empirical solution involving plastic action or damping in modern type multistory buildings." If by this statement he means that we are not able to reduce the problem to simple design rules and that further research is required, he would certainly find everyone in agreement with him. There is, of course, a great deal of positive evidence available on plastic behavior of steel frames, on random excitations and on non-linear vibrations. Mr. Derrick makes the statement, "that the conservative designer has no alternative but limitation of distortions to linear or almost linear levels; many designers are already doing this." In comment on this, the writer would say that no multi-story building has been designed to remain elastic when subjected to the strongest possible ground motion, as, for example, the most intense motion produced by an earthquake of 8.6 magnitude. If the linear design is based on less intense ground motion, as that at El Centro, 1940, then in the event of the 8.6 magnitude shock the structure will go beyond the elastic limit. It is, in the writer's opinion, very important that designers recognize this fact.

Mr. Blume has commented on the reliability of the average spectrum curves. As this is a point that may be misunderstood, a short explanation will be given here. All of the many ground acceleration spectra so far computed are consistent among each other, except two that will be discussed later. The four ground motions that were recorded near the epicenters of relatively large earthquakes all have spectrum curves of the same general shapes even though the El Centro records were obtained on very deep, sandy alluvium, whereas the Taft records were obtained on sedimentary rock and the Olympia, Washington records were obtained on terrain of quite different geology. Ground motions recorded at greater distances from the epicenters of large earthquakes and at smaller distances from the epicenters of small earthquakes have spectra that are consistent with these, along the lines set forth in the paper. The only spectra that are not consistent with these are two cases where relatively strong ground motion was recorded on extremely soft, water-filled ground. These are the Seattle, Washington, 1949, and the Southern Pacific Building, San Francisco, 1957 records that are referenced in the paper. It may be noted, however, that in both of these cases there was no evidence that the local geology had an amplifying effect on the ground motion. It may be stated that, other than such exceptional cases, the average spectra of future earthquakes can be expected to have essentially the same shapes as the average spectra of past earthquakes. Although geological conditions may be expected to have an influence on the ground motion, it is quite certain that large influences can be expected only if the geology is markedly different from the geology of those sites where most of our past earthquakes have been recorded. The precise shapes of individual spectra, will, of course, be subject to statistical fluctuations. The spectrum intensities will depend upon the magnitude of the earthquake and the distance from the epicenter, as well as being affected by such things as type and extent

of faulting. It must be kept in mind that earthquake ground motions are statistical phenomena. There will never be another earthquake just like the El Centro, 1940 shock. The only precise statement that can be made about future earthquakes is that their average spectra can be expected to be like those of past shocks, and the statistical deviations about the average can also be expected to be similar.

Mr. Blume appears to have misunderstood the significance of the statements made in the paper regarding energy input and energy dissipation of over-stressed structures. The exact analysis of non-linear vibrations of multi-degree-of-freedom actual structures has not yet progressed to the point where its results can be applied in design, and, therefore, design based on inelastic behavior must perforce make use of a more crude and approximate analysis. The crux of any such method is the way of estimating the energy input that must be absorbed. In his 1956 paper[6] the writer proposed the method set forth in the present paper (Eqs. 20 and 21) which Mr. Blume also adopted in his paper. It is, of course, not obvious that this is a satisfactory method of computing the energy input, for the input might actually depend upon the energy absorption of the system. Recently the writer's colleague, T. K. Caughey, completed a mathematical proof that for a random (white noise) excitation of a single-degree-of-freedom structure with viscous damping, the proposed method (Eq. 21) is indeed correct as regards average values of energy input for different amounts of damping. This fact, together with Mr. Berg's findings on inelastic action with earthquake excitations, makes it quite certain that the proposed method is reasonable to use so long as the increments of inelastic energy dissipation are small compared to the total vibrational energy. The ability of the structure to absorb energy, Mr. Blume's so-called reserve energy, is of course a necessary piece of information in the application of the method. For simple structures this quantity can be computed, but for complex structures it is not yet known how to evaluate it, for the various locations where yielding, and so on, will develop depend strongly upon the precise properties of the structure as well as on the prior history of yielding.

In his Fig. 1 and Table 1 Mr. Blume compares the spectrum for the average of the two components with his curves that represent single components. In Table 1 of his paper, the writer has presented the spectrum intensities of all the individual components of the various earthquakes so that the reader can see how these differ from the averages. Since this point seems to be easily misunderstood, it should be emphasized that the average spectra presented in the paper are the statistical (ensemble) averages and they should not be confused with the statistical fluctuations of the samples about the average. Neither should the average spectra be confused with various proposed design spectra curves.

A statement is perhaps in order as to the accuracy of the spectrum curves and spectrum intensities that were presented in the paper. Any method of spectrum computation is, of course, subject to inaccuracies in recording, reading and plotting, transcribing data, and so on. These errors will show up in the final results, so that in earthquake spectra computations there is no possibility of obtaining 100% accuracy. In this case, the best check on the accuracy of a set of computations is to make a comparison with a completely independent set

---

[6] "Limit Design of Structures to Resist Earthquakes," by G. W. Housner, Proceedings, 1956 World Conference on Earthquake Engrg., Earthquake Engrg. Research Inst., 1956.

of calculations. Such a completely independent computation of spectra has been made by Mr. G. V. Berg on the digital computer at the University of Michigan, Ann Arbor, Mich., and satisfactory agreement was found between his results and those of the writer. The differences were such as might be expected from independent handling of the raw data. The writer would also like to take this opportunity to clarify the statements regarding the accuracy of the spectra that were made by Mr. Blume.[7] His paragraph that begins, "Another interesting finding was that for stiffness system C the 1940 and 1934 El Centro earthquakes produced the same absolute maximum base shear for the low damping values. . . ," states that there was poor agreement between the spectra and the computed response of multi-story buildings, particularly for low damping. Independent computations now show that the discrepancy can be attributed to errors in the dynamic analyses presented in Mr. Blume's paper, and it is not the result of inaccuracies in the spectrum curves.

Mr. Blume and Mr. Derrick make statements and recommendations concerning methods and values to be used in the design of structures. With some of these the writer would agree, and with some he would disagree. However, since the design of structures is beyond the scope of the paper, and since a rigorous treatment of design would require more space than is available in a closing discussion, these questions will not be treated here.

The writer agrees with Mr. Cohen and Mr. Weissman that the maximum anticipated earthquake is not the same as the maximum experienced earthquake and it was not intended that the paper should imply that it is proper to assume them to be the same.

In any engineering discussion of C. F. Richter's "Seismic Regionalization Maps" his method of constructing them should be pointed out. His maps are combinations of seismic zone maps (showing where earthquakes occur) and geological maps (showing the type of soil). He makes the assumption that, other things being equal, the intensity of ground shaking will be proportional to the depth and softness of alluvium. He makes no claim that his maps have an accuracy suitable for engineering purposes and, in fact, measurements of strong earthquake ground motions show that his method of constructing the maps is not accurate in detail. Further strong-motion earthquake measurements are required in order to assess the true accuracy and the engineering value of these maps. As Mr. Cohen and Mr. Weissman state, engineering "risk zoning" is still some time off. These discussors also present an interesting description of the nuclear explosion ground shock problem and point out that, in essence, it is the same as the earthquake problem. It appears to the writer that any differences between the two problems are probably such that the nuclear problem is more difficult than the earthquake problem. For example, in the nuclear problem coupling between ground and structure is often important, whereas in the earthquake problem (in the United States) this appears to be important only in exceptional cases. Similarly the influence of local geology appears to be much more pronounced in the case of the nuclear problem.

In closing this discussion, the writer would like to thank Messrs. Berg, Derrick, Blume, Cohen and Weissman for their discussions. He would also like to emphasize that his paper was intended to give a succinct (and necessarily incomplete) account of the essential facts known about the behavior of structures during earthquakes. The paper was not intended to present recommendations

---

[7] "Structural Dynamics in Earthquake Resistant Design," by John A. Blume, Proceedings, ASCE, Vol. 84, No. ST 4, July, 1958.

on the actual design of structures. Discussions of design and building code regulations are always heavily surcharged with personal opinions on such things as the magnitude of earthquake to design against, the allowable stresses to be used, the appropriate factors of safety, the permissible degree of simplification and approximation, the empirical curves to be used, and so forth. In this regard, the following two statements are, perhaps, in order. First, it is not possible to make a dynamic analysis that will describe exactly the future behavior of a proposed (but not yet existing) structure during a future earthquake. Second, simple design rules such as are incorporated in building codes can be expected to be satisfactory only for simple, ordinary types of structures, and cannot be expected to give good results when applied to structures that are unusual in some respect.

The following corrections should be made to the working of the author's original paper. The last sentence in Section 3 should be changed to read, "For such cases it has been proposed to use the square root of the sum of the squares of the maxima." The last sentence on page 126 should read, "If the design and construction were such that the structure had only small damping during elastic vibrations, the spectrum curves show that during strong ground motion the vibrations of such a structure could become worse than the equivalent 25% g load and some member would then show distress." The third line from the top of page 128 should read, ". . .lateral loads much larger than are now prescribed by building codes." The fourth sentence from the end of the paper on page 128 should read, "One of these projects is a study of how to compute the ultimate lateral strength of structures; another, being done at Stanford University, is a study of the damping characteristics of structures; a third, . . ."

BEHAVIOR OF BUCKLED RECTANGULAR PLATES[a]

Discussion by Morris Ojalvo and Ahmet Cakmak

MORRIS OJALVO,[18] M. ASCE and AHMET CAKMAK.[19]—Mr. Stein has provided an illuminating paper on the behavior of flat plates in edge compression, and has supplied, as well, a novel approach to the solution of the large deflection plate equations.

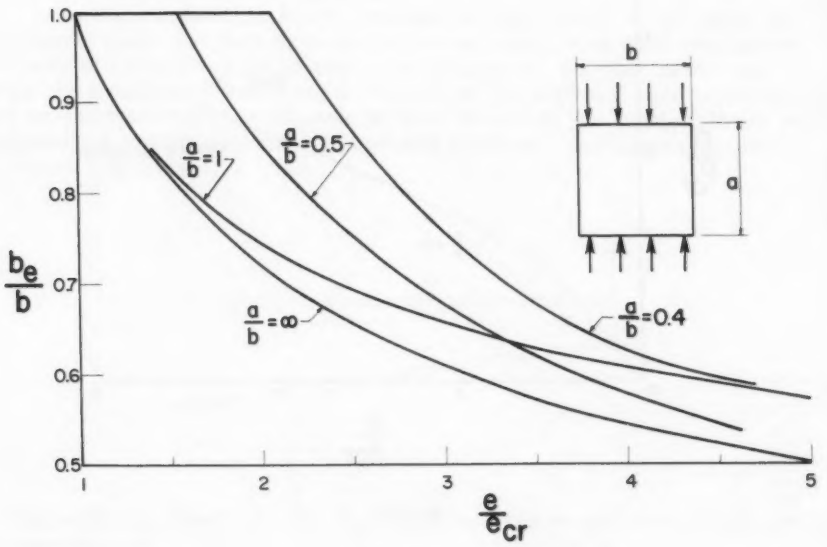

FIG. 15

This discussion will compare the results obtained by the author for the infinitely long plate with the results of a similar investigation, in which S. Levy's[10] method of solving the large deflection plate equations was used.[20] In

[a] April, 1960, by Manuel Stein.
[18] Assoc. Prof., Dept. of Civ. Engrg., Ohio State Univ., Columbus, Ohio.
[19] Graduate Student, Columbia Univ., New York, N. Y.
[20] "Bending of Rectangular Plates Under Compression, in One Direction Only, With Large Deflections," by Ahmet Cakmak, thesis presented to Princeton Univ., Princeton, N. J., in 1958, in partial fulfilment of the requirements for the degree of Master of Science.

the comparative investigation, the effective width was plotted against average unit shortening in the direction of the load for plates having length-width ratios between 0.4 and 1.0. The effective width curves for rectangular plates of length-width ratio below 0.8 do not appear in the reference cited.[20] These were computed after the first computations demonstrated that the envelope of the effective width curves could give the solution for the infinitely long plate. These results consider the first three terms of the series for the deflections of the buckled plate, that is,

$$w = a_{11} \sin \frac{\pi x}{a} \sin \frac{\pi y}{b} + a_{13} \sin \frac{\pi x}{a} \sin \frac{3\pi y}{b} + a_{31} \sin \frac{3\pi x}{a} \sin \frac{\pi y}{b} \quad ..(21)$$

Fig. 15 shows several of the effective width versus shortening curves and the envelope curve for the infinitely long plate. In Fig. 16 the envelope curve is

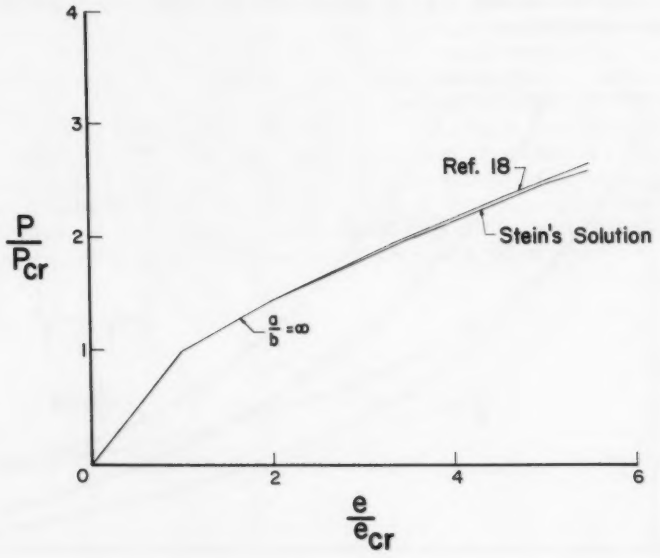

FIG. 16

transformed to one of load versus shortening so that it can be compared with the results of Mr. Stein's "second approximation" (Fig. 5). In these figures P is the total compressive load supported by the plate in edge compression, P_{cr} refers to the buckling load of a square plate, e denotes the shortening divided by the length of the compressed plate, e_{cr} is the unit shortening of a square plate at P_{cr}, and b_e refers to the effective width. As can be seen, there is very little difference and it may be concluded that Mr. Stein's perturbation method is as accurate as Mr. Levy's method, which requires the use of the digital computer.

COMMENTARY ON PLASTIC DESIGN IN STEEL: CONNECTIONS[a]

Discussion by Hashim H. Hamzawi

HASHIM H. HAMZAWI.[1]—While discussing tapered haunches, it is stated that "It has been shown that if the plastic moment of resistance is adequate at the rolled section (section 1 Fig. 8.6) and at the re-entrant corner (section 2 Fig. 8.6), there will be no necessity of checking at other sections along the haunch." This statement, which was made when only bending of the haunch was considered, is questioned by this writer.

For the haunch shown in Fig. 1, between sections 1 and 2, the same assumption is made that the original paper makes, namely, that the cross section is symmetrical and that the centroid is at mid depth. The haunch then can be treated as a cantilever beam (Fig. 2) fixed at A (relative to B) and acted upon by a concentrated load Q and a moment M at the end B. The moment M can be clockwise or counterclockwise and assumed positive in the direction shown in the figure (clockwise).

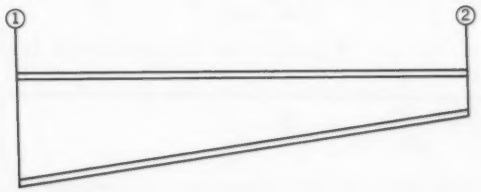

FIG. 1

The resisting plastic moment M_{px} of the member at any cross section can be expressed as

$$M_{px} = \frac{\sigma_{yp}\, w}{4}\left(d_{wA} - 2\,n\,x\right)^2 + \sigma_{yp}\, b\, t\left(d_A - t - 2\,n\,x\right) \ldots\ldots (1)$$

where σ_{yp} is the yield point stress. The external moment M_{qx} at any cross section x is

$$M_{qx} = Q(L - x) + M \ldots\ldots\ldots\ldots\ldots (2)$$

Equating Eqs. 1 and 2 and solving for x (the point of tangency between the two curves of Fig. 2), which will be equal to p (the distance of the plastic hinge

[a] April, 1960, Progress Report No. 6 of the Joint WRC-ASCE Committee on Plasticity Related to Design.

[1] Asst. Dean, College of Engrg., Univ. of Baghdad, Iraq.

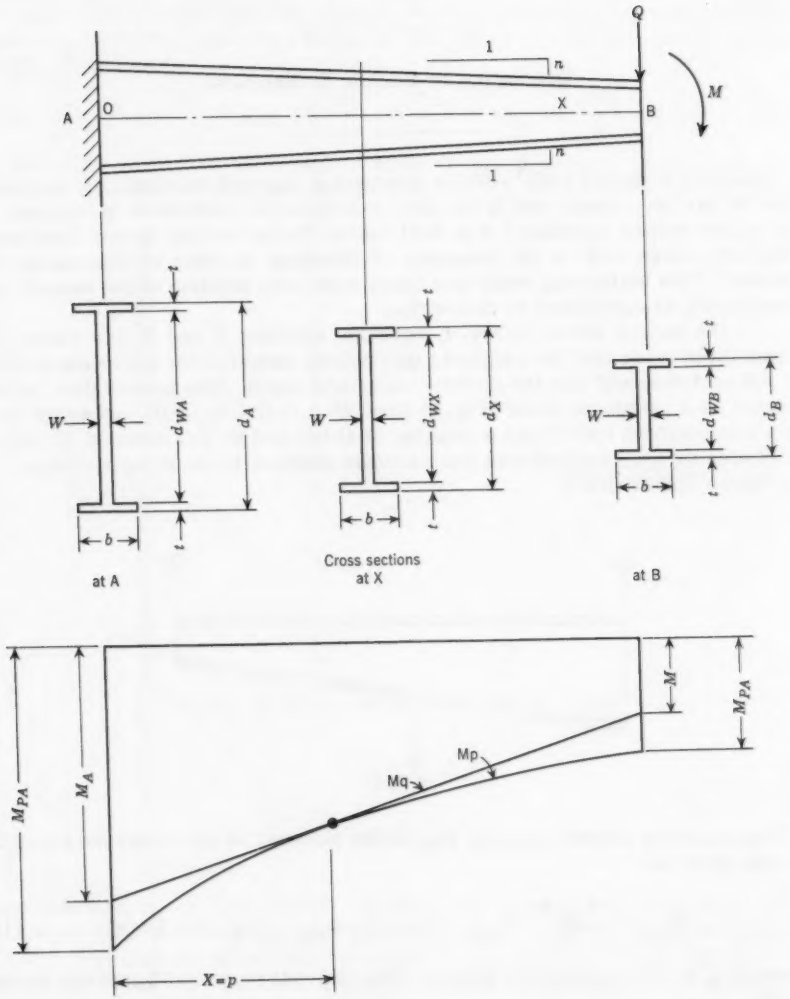
Q
1
n
M
A
O
X
B
n
1
t
W
d_{WA}
d_A
b
t
at A
t
W
d_{WX}
d_X
b
t
Cross sections
at X
t
W
d_{WB}
d_B
b
t
at B
M_{PA}
M_A
Mq
Mp
M
M_{PA}
X=p

FIG. 2

from the end A) it is found that

$$x = p = \frac{\rho n d_{wA} + 2 n t - \frac{Q}{\sigma_{yp} b}}{2 \rho n^2} \quad \ldots\ldots\ldots\ldots (3)$$

and

$$Q = \sigma_{yp} b n \rho d_{wA} + 2t - 2 \rho n L + \sqrt{\rho^2 d^2_{wB} + 4 t \rho d_{wB} + 4 t^2 \rho - \frac{4M}{\sigma_{yp} b}} \ldots (4)$$

in which $\rho = \frac{w}{b}$ substituting $\frac{1-k}{k} \frac{d_B}{2L}$ for n where $k = \frac{d_B}{d_A}$, $d_B - 2t$ for d_{wB}, β_B for $\frac{t}{d_B}$ and the value of Q given by Eq. 4 in Eq. 3 gives

$$p = L \left\{ 1 - \frac{k}{1-k} \sqrt{\left[4 \beta_B (1 - \beta_B) \left(\frac{1}{\rho} - 1 \right) + 1 \right]} - \frac{4 M}{\sigma_{yp} w d_B^2} \right\} \ldots (5a)$$

or

$$p = \frac{1 - \left[1 + (C_B - 1) \left(1 - \sqrt{\frac{M}{M_{pB}}} \right) \right] k}{1 - k} L \ldots\ldots\ldots (5b)$$

where

$$C_B = 4 \beta_B \left(1 - \beta_B \left(\frac{1}{\rho} - 1 \right) \right) + 1 \quad \ldots\ldots\ldots\ldots (6)$$

Examining Eq. 5(b) it is found that for values of

$$0 \leq k \leq \frac{1}{1 + (C_B - 1) \left(1 - \sqrt{\frac{M}{M_{pB}}} \right)} \quad \ldots\ldots\ldots\ldots (7)$$

the value of p lies between L and O indicating that the plastic hinge develops at an intermediate section between the ends A and B due to the applied moment M and the corresponding Q (Eq. 4). Therefore, it is evident that even though the member is safe for bending at the ends, it may fail at any other intermediate section where the plastic hinge develops.

COMMENTARY ON PLASTIC DESIGN IN STEEL: DEFLECTIONS[a]

Discussion by R. J. P. Garden

R. J. P. GARDEN.[1]—The report gives a concise explanation of the plastic hinge method of computing deflections, and states that the other four methods provide a small increase in accuracy at the expense of considerable increase in complexity.

The plastic hinge method achieves its practical validity because it obtains deflections that would be correct for loading, slightly different from the stipulated loading. However, these deflections are often many times less than the true deflections at full stipulated load.

A method will be described of making truer computations of deflection with little increase in complexity. This is, there is little complexity in making the actual computation for deflection if the designer is provided beforehand with properties applicable to the shape of section and the nature of the material. The work involved in providing the prerequisite properties is not great for simple shapes of section with simple stress-strain relations; it is greater for materials with stress-strain relations, such as exhibited by concrete. Apart from mention that the method is applicable to other types of stress-strain relation, the illustrations given will be confined to plain rectangular sections of material assumed to accord with the simple plastic theory. This holds for spread plasticity.

Basically, the method relies on the fact that a property, called by the writer, commuted plastic curvature, can be so determined that the deflection of a structure in the elastic-plastic range is to be determined by considering the structure to remain in a wholly elastic state under the influence of the actual elastic-plastic moments, and under the influence of applied rotations equal to the commuted curvatures.

Some description of the method has been published elsewhere.[2,3] For the present discussion, it is sufficient to state two key values relating to commuted curvature for rectangular sections behaving in accordance with the simple plastic theory. Thus, for any member having imposed on it moments that rise linearly through M_y to M_p over a length of member called l, the amount of commuted curvature due to the spread plasticity will always be equal to $\frac{1}{2}\frac{M_p}{EI}$ in

[a] April, 1960, Project Report No. 7 the Joint WRC-ASCE Committee on Plasticity Related to Design.

[1] E. R. Garden, and Assoc., Dunedin, New Zealand.

[2] "Analysis for Moments and Deflexions in the Elastic Plastic Range," by R. J. P. Garden, Proceedings, Inst. Civ. Engrs., Vol. 16, pp. 157-170.

[3] "Notes on Inelastic Deflections," by R. J. P. Garden, New Zealand Engineering, August, 1960.

radians. Also, the center of gravity of the commuted curvature, l_g will always be at 1/9 from the point where $M = M_p$ (See Fig. 1). As $M_p = 1.5\ M_y$ for a rectangular section, l will be 1/3 of the length x on Fig. 1, and l_g will be 1/27 x.

The frame considered in 9.4 of the report is shown in Fig. 2. Lengths of spread plasticity and lengths to points of zero moment are shown on this figure. Fig. 3 indicates, by open circles, the locations of the centers of gravity of commuted plastic curvatures, and a solid circle shows the location of the only point of concentrated hinging.

The location of the point of concentrated hinging may be determined by the method of trial as used in the report, with additional terms used to take account of the commuted plastic curvature. To illustrate the use of the additional terms in the slope deflection equations, the working for the second trial only, for continuity at 4, will be given herein.

First, to illustrate how these commuted curvatures are included in the slope deflection equations, Fig. 4 (a modification of Fig. 9.3 of the report) is given. The full circles indicate localized hinging θ'_A and θ''_B, and the open circles indicate centers of gravity of commuted curvatures due to spread plasticity of values $\theta''_A = \theta''_B$.

$$\theta_A = \theta'_A + \frac{\Delta}{L} + \frac{L}{3EI}\left[M_{AB} - \frac{M_{BA}}{2}\right] + \left(\theta''_A\right)\left(\frac{L - l_{gA}}{L} - \theta''_B\right)\left(\frac{l_{gB}}{L}\right) \quad . . \quad (1)$$

The solution given in the report will be repeated on this basis.

Trial at Section 4.— $(\theta_{43} = \theta_{45})$

$$\theta_{43} = 0 - \frac{V_4}{L/2} + \frac{L/2}{3EI}\left(M_p - 1/2\ M_p\right)$$

$$+\left(\theta''_{43}\right)\left[\frac{(L/2 - L/108)}{L/2} - \theta''_{34}\right]\left(\frac{L/108}{L/2}\right) \quad . . . . . \quad (2)$$

and as

$$\theta''_{43} = \theta''_{34} = \left(1/2\,\frac{M_p}{EI}\right)\left(\frac{L}{12}\right) = \frac{M_p\,L}{24\,EI} \quad . . . . . \quad (3)$$

$$\theta_{43} = -\frac{2\delta_{V4}}{L} + \frac{10}{81}\,\frac{M_p\,L}{EI} \quad . . . . . \quad (4)$$

and

$$\theta_{45} = 0 + \frac{\delta_{H4}}{L/2} + \frac{L/2}{3EI}\left(-M_p - 0\right) - \theta''_{45}\ x\ \frac{L/2 - \frac{L}{54}}{L/2} \quad . . . . . \quad (5)$$

and

$$\theta''_{45} = \left(1/2\,\frac{M_p}{EI}\right)\left(\frac{L}{6}\right) = \frac{M_p\,L}{12\,EI} \quad . . . . . \quad (6)$$

then

$$\theta_{45} = \frac{2\,\delta_{H4}}{L} - \frac{20}{81}\,\frac{M_p\,L}{EI} \quad . . . . . \quad (7)$$

By similar means, the revised version of Eq. 9.4 is obtained as

$$\delta_V = \delta_H + \left(\frac{17}{264} - \frac{11^2}{81^2\ 32}\right)\frac{M_p\,L^2}{EI} \quad . . . . . \quad (8)$$

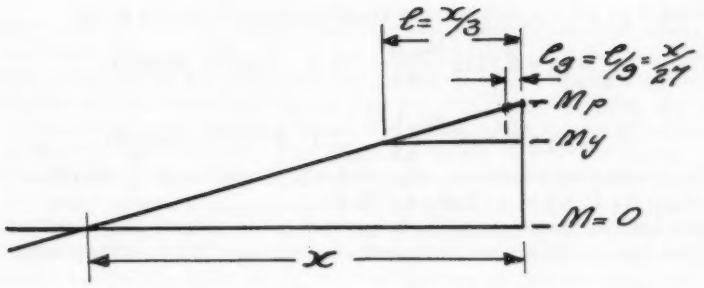

FIG. 1

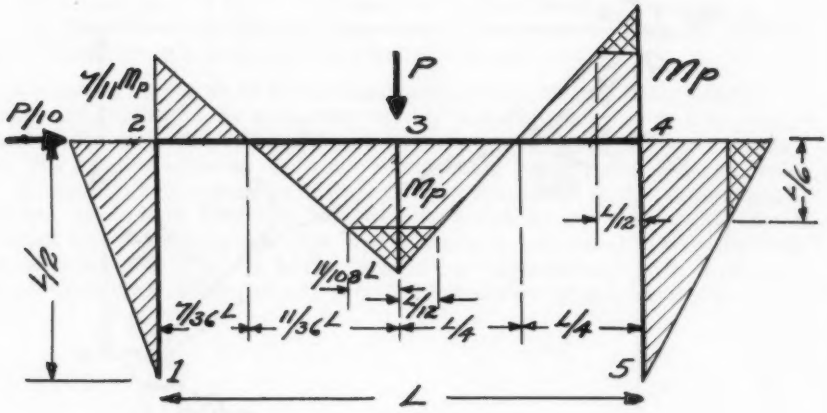

FIG. 2.—EXTENT OF PLASTICITY APPROPRIATE TO RECTANGULAR SECTION IS SHOWN BY CROSSHATCHING

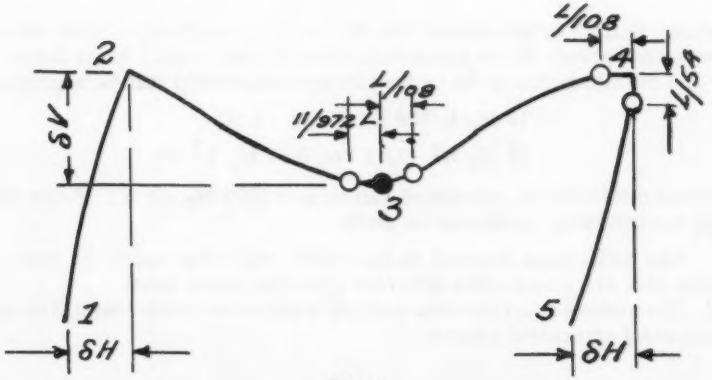

FIG. 3

Equating θ_{43} and θ_{45} and solving simultaneously with this gives

$$\delta_{V4} = 0.1245 \frac{M_p L^2}{EI} \quad \text{(C.f 0.095 in Report)} \quad \ldots\ldots\ldots (9)$$

$$\delta_{H4} = 0.0607 \frac{M_p L^2}{EI} \quad \text{(C.f 0.0303 in Report)} \quad \ldots\ldots\ldots (10)$$

The commuted rotations, ϕ''_{45} and ϕ''_{43}, amount to $\left[-13/(12 \times 27) - 13/(6 \times 27)\right] M_p L/EI = -13 M_p L/108 EI$.

This spread plastic rotation is ignored in the plastic hinge method; it follows that this method must tacitly have undervalued the positive plastic rotation

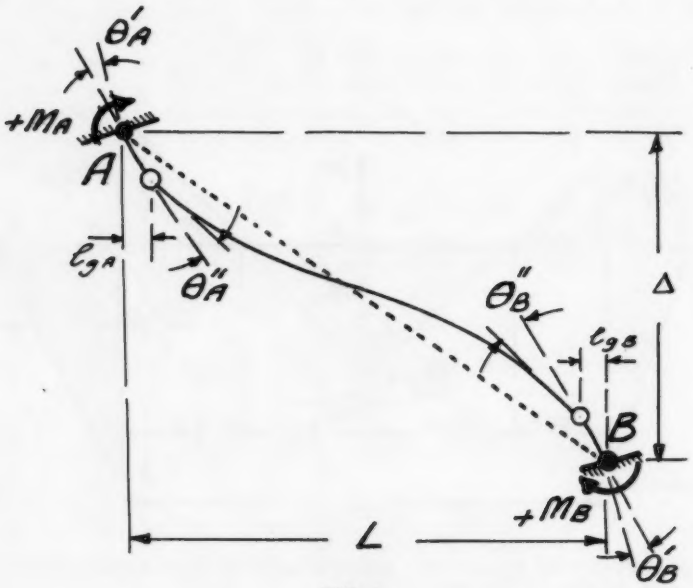

FIG. 4

at and near point 3 by an amount that will be very nearly equal when expressed in commuted values. Extra commuted rotation near point 3 has a direct effect on δ_V and the difference in δ_V by the two methods should then be approximately

$$13 M_p L/108 EI \; (1/2) \; (L/2)$$

$$= 13 M_p L^2/432 EI \text{ or } 0.03 M_p L^2/EI \quad \ldots\ldots\ldots (11)$$

The actual difference of calculated values is $0.0295 M_p L^2/EI$. From the preceding, the following points can be made:

(1) The deflections derived in the report will very nearly be true values for loads that are only a little different from the stated loads.

(2) The results from the two methods would show much less difference for common steel structural shapes.

For this example, then, the plastic hinge method is good enough in practice. However, as referred to in Table 9.1 of the report, this simple method yields large errors in curvature and deflection for members whose moment values of M_p are constant along a finite length, and also for members that have, at hinge points, a curvature moment diagram where the tangent to the curve, at the hinge point, is parallel to the member. For instance, in Fig. 9.4 of the report, the curvature near point C in the rafter, is very great at full collapse load. Indeed, a rough calculation shows that, again for members of rectangular section, the rotation due to spread plasticity near C that would occur with M_c at only 0.9 M_p, is sufficient of itself to cause a vertical deflection at D of about the same magnitude as the quantity given in Eq. 9.17 of the report for the total deflection at D for full collapse load. The following comments can be made:

(1) The simple plastic theory would give a very great deflection of D for full nominal collapse load even for members of usual structural sections.

(2) Occurrence of strain-hardening will reduce the discrepancy.

(3) The deflection derived in the report will be true for loadings appreciably, but not grossly less than full nominal collapse load.

Constants, such as used in this discussion, can be derived for any structural shape and applied in the same way for any material assumed to have simple plastic behavior. The effect of upper and lower yield point can be incorporated. For strain-hardening and other continuously varying stress-strain relations, the parameters have values that vary with values of M, but again, similar use can be made of constants that are appropriate to any value of M_u chosen to limit the desirable strain. The writer would be interested to hear the opinion of committee members on the value of the commuted curvature method for breaking through the complexity ascribed to the other precise methods.

BEHAVIOR OF VISCOELASTIC PLATES IN BENDING[a]

Discussion by O. C. Zienkiewicz

O. C. ZIENKIEWICZ,[12] F. ASCE.—The author presents a detailed analysis of a problem for which visco-elastic solutions are of considerable interest. The general terms in which the analysis is carried out and the admirably clear introduction will serve as a starting point for other similar investigations. It is the object of this discussion to comment on some minor points omitted in the paper and to suggest a possible alternative approach to this class of problem.

The first of the points concerns the question of boundary conditions of the plate. For a complete separation of the variables used in Eqs. 14 through 18, it is necessary for the boundary conditions to be similarly separate. This certainly is achieved in the case of a clamped plate on the boundary of which, if n is the normal,

$$w = \frac{\partial w}{\partial n} = 0 \quad \ldots\ldots\ldots\ldots\ldots\ldots \quad (59)$$

which in terms of the separated variables will correspond to

$$W = \frac{\partial W}{\partial n} = 0 \quad \ldots\ldots\ldots\ldots\ldots\ldots \quad (60)$$

It will be noted that a similar separation is possible along simply supported edges of a plate in which the conditions

$$w = \frac{\partial^2 w}{\partial n^2} = 0 \quad \ldots\ldots\ldots\ldots\ldots\ldots (61)$$

translate immediately into

$$W = \frac{\partial^2 W}{\partial n^2} = 0 \quad \ldots\ldots\ldots\ldots\ldots\ldots \quad (62)$$

If, however, a plate with a free edge is considered or a plate in which the edge is given some predetermined slope or deformation (which itself can be an independent function of time), then the assumptions of the suggested procedure are not applicable.

A further point concerning the expressions for the bending moments is simply a question of notation. Some explanation of the meaning of the suffices $\alpha\beta$ and $\gamma\gamma$ would be desirable.

With reference to an alternative solution of this class of problem, the following procedure is at times advantageous. This, in essence, is a well-known application of the method of integral operators. Considering Eq. 18, in which

---

[a] June, 1960, by George E. Mase.

[12] Prof. of Civ. Engr., Northwestern Univ., Evanston, Ill.

B_1 is a differential operator, it is possible to solve this for a unit step function "input" of $d\theta$ applied at a time τ from which results

$$d\phi = D\lambda_c(t-\tau)\, d\theta \quad \ldots\ldots\ldots\ldots \quad (63)$$

It is easily recognized that λ_c is in fact the "creep function" of the plate under constant load and, in the particular example discussed by the author with a plate of Kelvin material, corresponds with the bracketed term of Eq. 24. For any particular form of $\theta(\tau)$ defining the load-time variation, the Duhamel integral results in

$$\phi = D\int_0^t \lambda_c\,(t-\tau)\,\frac{d\theta}{d\tau}\,d\tau \quad \ldots\ldots\ldots\ldots \quad (64)$$

This is essentially similar to the author's Eq. 21 but has this advantage that, whereas it is often difficult to approximate the behavior of a visco-elastic material by a simple mechanical model, it is a relatively simple matter to arrive at the creep function formula by an experiment. The integrations can then be performed numerically if desired.

The integral approach is not limited to the "proportional loading" case. It is possible to tackle with its use problems of the moving load type or, in fact, any in which the loading distribution is not of the simple type defined by Eq. 14. To approach this type of problem let us consider the deflections caused by an incremental step function of load.

$$df = \frac{\partial f}{\partial \tau}\,d\tau;\quad f = f(x, y, \tau) \quad \ldots\ldots\ldots\ldots \quad (65)$$

placed at time instant, τ, on the plate. As this increment by itself does in fact obey the proportionality relationship, it is noted that the deflections can be obtained by an elastic solution of the plate with rigidity, D, loaded with a distributed loading of magnitude df ($\theta(\tau)$ is a unit step function now), multiplied by a factor $D\lambda_c\,(t-\tau)$.

The preceding statement is clearly true for all the increments of which the load, f, is composed, and the final solution can be synthesized by superposition, as the sum of such deflections.

This appears to require a series of solutions of the elastic problem for differently distributed forms of load at different times. If however the deflections at some specified time, t, are required, it is apparent that the same deflection would be achieved by loading the elastic plate of rigidity D with a loading df $D\lambda_c\,(t-\tau)$ at the instant, t, and that the total deflection could be obtained simply by solving the elastic plate problem subjected to a distributed loading of magnitude p(x, y, t), with

$$p(x, y, t.) = D\int_0^t \lambda_c\,(t-\tau)\,\frac{\partial f}{\partial}\,d\tau \quad \ldots\ldots \quad (66)$$

or by solving the biharmonic equation

$$\nabla^4 w\,(x, y, t) = \frac{P\,(x, y, t)}{D} \quad \ldots\ldots\ldots\ldots \quad (67)$$

at any desired instant of time. This latter form shows indeed that any of the known elastic techniques of solving flat plates can be easily adapted to the treatment of plates made from visco-elastic materials provided that a suitably equivalent form of the loading given previously, is used. It is for instance possible to apply numerical methods of solution in exactly the same way as done in elas-

tic plate deflection after the preliminary step of evaluating p has been carried out. The application of this to the moving load type of problem is evident.

It is interesting to note that in the examples cited by the author the distribution of bending moments in the plate varies in time in a different manner from the assumed variation in load. In fact, for the case of a constant load distribution applied at time zero the moments are time dependent for the assumed Kelvin and Maxwell types of bodies. With many visco-elastic materials the compressibility is negligible while in others, such as concrete for instance, it appears that the equivalent Poisson's ratio is constant. This in effect means that the operators Q/P and K of Eq. 3 are of a form differing by a constant multiplier only. It is easy to show that in such cases with a constant load the distribution of moments is also constant with time and, in fact, is indentical with the appropriate elastic solution.

ERRATA

Journal of the Engineering Mechanics Division

Proceedings of the American Society of Civil Engineers

January, 1960

p. 169. In line 7 of the second paragraph, change "paste that exist" to "paste there exist."

April, 1960

p. 173. In item 5 the material in parentheses at the end of this item should be changed to the following:

> The Polytechnical School in Mexico City appeared, as a result of a perusal of an article in CIVIL ENGINEERING, October, 1957, p. 79, to have been designed by the dynamic theory. Further study reveals, however, that this building had a relatively short period, that engineers did not observe any foundation failure, and that it did not reflect a proper test of an aseismically designed building.

August, 1960

p. 93. In Eq. 17 add a final parentheses.

p. 93. In Eq. 18b insert a parentheses just prior to the first number one.